Extreme Sub-daily Rainfall in Europe: Climatology and Dynamical Drivers

Anna C. Whitford

School of Engineering

Newcastle University

A thesis presented for the degree of Doctor of Philosophy

September 2023

Abstract

This thesis explores the large-scale dynamical drivers of sub-daily rainfall extremes in western Europe. Initially a sub-daily extreme rainfall climatology for the region is developed using a set of extreme indices for short duration rainfall. The spatiotemporal connections between synoptic-scale atmospheric circulation and summer (JJA) 3-hour extremes are then assessed, using a set of 30 weather patterns developed by the UK Met Office (MO30) and composites of geopotential height at 500hPa (z500). Finally, the relationships between Rossby wave patterns and extreme 3-hour rainfall are examined, using the local finite amplitude wave activity metric (LWA), and composites of 300hPa meridional wind (v300) anomalies.

The results reveal sub-daily extremes are more intense and more frequent in southern and Alpine areas of western Europe, with greatest intensity and frequency of extremes in autumn in the Iberian Peninsula and in summer across the rest of the region. Other index results indicate these events are produced by very short or peaked storms which occur preferentially in the afternoon or evening.

The spatiotemporal correlations between MO30 weather patterns (WP) and extreme sub-daily events show a strong preference for extremes to occur under just 5 or 6 of the 30 patterns. Comparing the composite z500 anomalies for all WP days against only WP days with an extreme rainfall event indicates there is significant intra-WP variability on the event days. WPs favouring sub-daily extremes are generally associated with a southerly or south-westerly flow over western Europe, along the leading edge of a trough. There is often also a blocking anomaly present over the Baltic Sea. Rossby wave patterns on the days of the most extreme 3-hour events in the UK and Germany (used as case study regions) show a clear wave train stretching westwards from Europe, with a positive anticyclonic anomaly over Scandinavia and a positive cyclonic anomaly to the west of the UK, echoing the patterns seen in the z500 analysis. While the group velocity (energy) of the wave train moves downstream over time, the phase speed appears to be very low, suggesting there is a level of stationarity to the wave train on days preceding the extreme events.

Overall, the results show strong links between large-scale atmospheric dynamics and the occurrence of sub-daily extremes. As large-scale atmospheric variables are much better represented in both forecast and climate models than individual extreme rainfall events, the relationships identified here could be used to increase the lead time of probabilistic forecasts of periods with higher risk of sub-daily rainfall extremes. The UK Met Office Decider system calculates the daily WP probability from an ensemble prediction system and uses this to generate probabilistic forecasts of periods with higher risk of extreme daily rainfall. A similar system for forecasting periods with increased risk of sub-daily extremes could be developed from these results.

Acknowledgements

Firstly, I would like to thank my supervisors Hayley Fowler and Stephen Blenkinsop, for their continuing support and guidance over the past four years. Aside from contributions to this thesis, their encouragement in all aspects of the PhD, from attending conferences, to undertaking placements and writing papers has been invaluable and is very much appreciated. I am also incredibly grateful to Rachel White, who has been an excellent unofficial supervisor on both sides of the Atlantic. Thank you for reminding me of why I wanted to be a researcher in the first place and for filling our meetings with endless optimism.

Thanks also go to colleagues and friends in Cassie building, not least for providing a source of normality throughout the Covid lockdowns via our virtual coffee mornings.

Beyond the walls of Cassie, a special mention must go to friends who have contributed in many ways to me actually making it to the end of this PhD. In particular, to Fergus for the outdoor activities and sage wisdom; To Lindsey and Johannes for the adventures; to Roberto for the coding advice and obscure Discworld references; to Leaf for the calming garden visits and reality checks; and to Katie, for the maintenance of my sanity during the final weeks. To my Cornish friends, who have spent the last few years having to pretend to be interested in weather, thank you for the patience and much-needed reminders of the world outside academia.

Finally, a huge thank you must also go to my family, for their continued support in countless ways over the last four years. To my Grandma, for your pride in me throughout this PhD endeavour, despite having no clue what I was actually doing – it's definitely the thought that counts. To my mum for the endless supply of freezer meals and checks that I remembered to do things outside of the PhD, especially in the final few months, which are the main reason I am still here in one piece; and to dad, for the many many 'walking home chats' over my whole university career. I hope this thesis is finally proof that I did not in fact spend four years counting raindrops.

Contents

List of Publications

Chapter 3 of this thesis has been published as a journal article:

Whitford, A.C., Blenkinsop, S.B., Pritchard, D., Fowler, H.J. (2023). A gauge-based sub-daily extreme rainfall climatology for western Europe. *Weather and Climate Extremes*, 41, 100585.

Chapter 4 has been accepted for publication in Climate Dynamics.

In both cases I took the lead in development of the articles and was responsible for Conceptualization, Data curation, Formal Analysis, Writing – original draft, Writing review & editing. The co-authors contributed to research ideas and manuscript review.

I have also contributed to the following publication which is relevant to this thesis:

Pritchard, D., Lewis, E., Blenkinsop, S., Velasquez, L., Whitford, A.C., Fowler, H. J. (2023) 'GSDR-I: An Observation-Based Dataset of Global Sub-Daily Precipitation Indices', *Scientific Data*. Springer US, pp. 1–13. doi: 10.1038/s41597-023-02238-4.
In this article I was involved in testing the indices, including determining which would be most useful to include in the dataset and contributed to manuscript review.

List of Figures

List of Tables

Common Abbreviations

AMAX	Annual Maximum rainfall
AR	Atmospheric river
CC	Clausius Clapeyron
COL	Cut-off low
CPM	Convection permitting model
DWD	Deutscher Wetterdienst (German Weather Service)
ECMWF	European Centre for Medium Range Weather Forecasting
ETCCDI	Expert Team on Climate Change Detection and Indices
FAWA	Finite amplitude wave activity metric
FFC	Flood forecasting centre
GWL	Grosswetterlagen weather patterns classification
GSDR	Global sub-daily rainfall dataset
GSDR-I	GSDR indices dataset
IVT	Integrated water vapour transport
JJA	June, July, August
LWA	Local finite amplitude wave activity metric
LWT	Lamb weather type
MSLP	Mean sea level pressure
MO30	Met Office set of 30 WPs
MO8	Met Office set of 8 WPs
NAO	North Atlantic Oscillation
POT	Peaks over threshold
PV	Potential vorticity
PVA	Positive vorticity advection
QSW	Quasistationary wave
RCM	Regional climate model
SLP	Sea level pressure
v300	Meridional wind at 300hPa
WP	Weather pattern
z500	Geopotential height at 500hPa

Chapter 1
Introduction

1.1 Flooding

Floods are one of the most common natural hazards and can have severe economic and social impacts (Barredo, 2007; Alderman *et al.*, 2012). The risks and costs associated with flooding are expected to increase in the coming decades, due to both global warming and the increase in populations living in vulnerable areas (Trenberth *et al.*, 2003; Lenderink and Fowler, 2017a; IPCC, 2022).

There are several different categories of flood; fluvial flooding results from rivers overflowing their channel boundaries, pluvial or surface water flooding occurs when the rainfall volume exceeds the infiltration capacity of the surrounding area and groundwater flooding which happens when the water table rises above the ground surface (Pitt, 2008). These different types of flooding arise from the complex interactions between extreme rainfall characteristics and those of the catchment, including antecedent conditions such as soil moisture (Sharma *et al.*, 2018) and human interventions such as the level of urbanisation and storm drainage systems (Dale, 2021).

Pluvial flooding is often referred to as flash flooding due to the rapid onset nature of these floods. This type of flooding is most common in urban settings, where the high level of impermeability impedes the natural infiltration processes that may moderate floods in rural settings (Archer and Fowler, 2018; Dale, 2021; Fowler *et al.*, 2021b). Flash floods also occur in steep, narrow catchments in rural areas, such as in both Boscastle (2004) and Coverack (2017) in Cornwall (Doe, 2004; Essex, 2018). Flash flooding is especially dangerous to life due to the speed with which the flood waters can develop and move, often with very little advance warning given to affected communities due to the difficulties of forecasting such events (Archer and Fowler, 2018; Flack *et al.*, 2019). They can also cause huge amounts of economic damage due to their propensity to occur in cities, away from areas which typically have flood protections in place (e.g. along river banks). The Copenhagen floods in July 2011 resulted in 800 million euros worth of insurance claims (Arnbjerg-Nielsen *et al.*, 2015) while flash floods in London in July 2021 caused extensive disruption with over 1000 properties and 30 underground stations being flooded, due to over a month's worth of rain falling in under an hour (Flood Forecasting Centre, 2022). Given the aforementioned increase in populations living in cities, combined with the expected increase in intense rainfall in a warmer climate, these quoted damage values are therefore likely to increase, as is the risk to life (Sharma *et al.*, 2018; Sayers *et al.*, 2020; Kam *et al.*, 2021).

There have been several attempts, using different methods, to develop a more detailed understanding of future sub-daily extreme rainfall changes in Europe. These have included developing climate change factors from RCM outputs (Larsen *et al.*, 2009) and development of extreme event statistics from GCMs (Scoccimarro *et al.*, 2015). These studies have shown increasing intensity and frequency of sub-daily extremes in future scenarios. The more recent development of convection-permitting climate models has allowed a significant increase in the ability to model how sub-daily rainfall extremes may change in the future (Kendon *et al.*, 2014; Fowler *et al.*, 2021b). Model experiments have shown how the km-scale motions within convective storms may change in a warmer climate, with a predicted increase in sub-daily rainfall intensity and frequency (Chan *et al.*, 2014; Kendon *et al.*, 2014; Chan *et al.*, 2020a). Results from simulations using a 1.5km resolution CPM and a 12km resolution RCM show intensification of winter and summer (although only in the 1.5km simulation for summer) sub-daily rainfall extremes over the UK by the end of the 21st century (Chan *et al.*, 2018a). For the wider European area, the 2.2km Unified Model convection permitting model simulations provide slightly contrasting results, with an apparent decrease in frequency of summer extremes over central Europe while northern Europe shows an increase (although the very highest intensity percentiles see an increase everywhere). Autumn extremes are projected to become more frequent in southern Europe (Chan *et al.*, 2020b). These studies provide strong evidence of relative future increase in the frequency and intensity of extreme short-duration rainfall in Europe. To mitigate the impacts from these changes, several factors need to be addressed, including in-place flood defences and storm drainage systems, population awareness of the hazard and, crucially, the skill of forecasting of the kind of intense rainfall that may result in flash flooding (Pappenberger *et al.*, 2015; Dale, 2021; IPCC, 2022).

1.2 Sub-daily Rainfall Extremes

Sub-daily extreme rainfall refers to rainfall which lasts for less than 24-hours, with studies generally focussing on rainfall of 1-, 3- and 6-hr durations. This type of short-duration, high intensity rainfall is the main cause of flash flooding in Europe (Marchi *et al.*, 2010) and can also lead to landslides and debris flows (Gaume *et al.*, 2009; Borga *et al.*, 2014; Archer and Fowler, 2018). These types of rainfall events are generally associated with warm season processes and so the most intense events tend to occur during the summer (JJA) and autumn (SON) months in Europe (Blenkinsop *et al.*, 2015; Whitford *et al.*, 2023).

Sub-daily rainfall in Europe, and particularly extreme sub-daily rainfall has so far been examined less intensively than daily rainfall (Westra *et al.*, 2014). This is largely due to the scarcity of homogenous sub-daily data of suitable quality and record length (Blenkinsop *et al.*, 2018; Darwish *et al.*, 2018; Alexander *et al.*, 2019). However, recent developments in the collection, quality control and sharing of such data have allowed research in this area to progress. Of particular significance for this thesis is the development of the Global Sub-daily Rainfall Dataset (GSDR) by the INTENSE (INTElligent use of climate models for adaptation to Non-Stationary hydrological Extremes) project following the collection and assessment of sub-daily rainfall observations from around the globe (Blenkinsop *et al.*, 2018). This is the first comprehensive global-scale sub-daily rainfall dataset, with all gauges quality-controlled to the same standard using a homogeneous procedure (GSDR; Lewis *et al.*, 2019, 2021). This dataset is used throughout the thesis, with the area of focus being Europe, with the scope limited by the data available from different countries and regions in the GSDR dataset. The use of the gauge-based data over other datasets of sub-daily rainfall, such as satellite or reanalysis data was motivated by several factors. This includes the lack of freely available, long duration radar datasets (Lengfeld *et al.*, 2020), the relatively low ability of satellite datasets to capture sub-daily rainfall extremes (Jiang *et al.*, 2019) and the finding that reanalysis data underestimates extreme (99th percentile) rainfall in many regions, likely due to the poor performance in simulating extreme convective rainfall (Ali *et al.*, 2021b). Additionally, rain gauge datasets provide the longest records of short duration rainfall and produce more reliable estimates of extreme event intensity compared to gridded or reanalysis data (Reder *et al.*, 2022), both important aspects of the analysis in this thesis given the focus on long term trends (Chapters 3 and 4) and high intensity events (Chapter 5). To provide a more comprehensive analysis of continental-scale extremes, a set of indices for extreme sub-daily rainfall (GSDR-I) has been derived from the GSDR dataset (Pritchard *et al.*, 2023). The GSDR-I dataset is used in Chapter 3 of this thesis.

The analysis of sub-daily rainfall is important given the fact that using daily rainfall totals can easily mask the periods with strongest intensity rainfall, meaning assessments of flood risk or storm drainage requirements may not be using the most pertinent information (Alexander *et al.*, 2006; Dale, 2021). Thus, despite the difficulties associated with such analysis, investigation of sub-daily rainfall events, including their intensity and frequency, is vital to ensure models and infrastructure design do not underestimate the associated rainfall characteristics and therefore impacts (Dale, 2021). It has been shown that flood estimation methods based solely on daily rainfall totals can significantly underestimate the true intensity of storm temporal profiles and therefore perhaps result in the misinformation of storm drainage design (Villalobos-Herrera *et al.*, 2024). Additionally, both model experiments and observational studies have indicated that signals of climate change on extreme rainfall emerge earlier for sub-daily (hourly) than for daily rainfall extremes (Barbero *et al.*, 2017; Kendon *et al.*, 2018).

The classification of sub-daily rainfall as extreme or not-extreme has used many different methods, including a block-maxima approach, the peak-over-thresholds method (Coles, 2001) and general extreme value (GEV) estimations (Coles, 2001). The use of multiple different methods can make comparing results between geographical regions difficult. Therefore, the analysis of extremes in this thesis uses only the peak-over-thresholds method and the statistical *n*-largest approach, where the largest *n.m* events are selected where *m* is the length of the record in years (so if n=1 then the number of events selected is equal to the number of years) (Blenkinsop *et al.*, 2017), to make comparison between different geographical regions possible by using a standard methodology.

1.3 Drivers of sub-daily rainfall extremes

Sub-daily rainfall extremes have two main classes of drivers; thermodynamic and dynamic (Oueslati *et al.*, 2019). Thermodynamic drivers are linked to temperature changes, such as the dew-point temperature while dynamical drivers are those linked to atmospheric circulations, such as vertical wind velocity and lifting. In this thesis, 'dynamical drivers' refers to features on a spatial scale above the mesoscale (~10-1000km). This includes synoptic scale features (~1000-2500km) such as troughs and ridges but does not include local scale enhancement of convection. This distinction in dynamical drivers is made in order to focus on the larger-scale features which can be more readily identified in forecast models (Baker *et al.*, 2018; Lavers *et al.*, 2018; Dorrington *et al.*, 2023), given the desire to produce operationally useful output from this thesis.

Most research into sub-daily rainfall so far has concentrated on the thermodynamic drivers, particularly the scaling relationship between temperature and rainfall intensity (Lenderink et al., 2017; Pfahl, O'Gorman and Fischer, 2017; Drobinski et al., 2018). While the influence of thermodynamics on regional variations in sub-daily extreme precipitation has been successfully linked to local variations in (dew point) temperature (Lenderink and Van Meijgaard, 2010; Barbero *et al.*, 2018; Ali *et al.*, 2021a, 2021b), there remains a lower understanding of the influence of dynamical drivers on extreme events.

The dynamical drivers of daily rainfall extremes have been investigated at a range of spatial scales extending from global teleconnections (Boers *et al.*, 2019) and hemispheric wave patterns (Schubert *et al.*, 2011; Barton *et al.*, 2016; Hirata and Grimm, 2016; Wolf *et al.*, 2018; Kornhuber *et al.*, 2019), to multidecadal oscillating atmospheric circulations (e.g. the NAO and ENSO) (Grimm and Tedeschi, 2009; Krichak *et al.*, 2014; Cioffi *et al.*, 2015; Guimares Nobre *et al.*, 2017) and individual synoptic scale features (e.g. Pfahl and Wernli, 2012; Catto and Pfahl, 2013; Lavers and Villarini, 2013; Pfahl, 2014; Ruff and Pfahl, 2022). These studies have revealed the strong linkage between the spatiotemporal occurrence of the extreme rainfall and the various dynamical drivers, with cyclonic features (troughs and cyclones) found to be especially important for longer-duration extremes over Europe. While several studies have investigated the dynamical drivers of sub-daily rainfall (e.g. Luo *et al.*, 2016; Weder *et al.*, 2017; Chan *et al.*, 2018a, 2023; Barbero *et al.*, 2019b; Moron *et al.*, 2019; Darwish *et al.*, 2020). these have generally focussed on a single country, or only utilised data from a small sample of rain gauges. For example, so far in Europe only the drivers of extreme sub-daily rainfall in Germany (Weder *et al.*, 2017; Brieber and Hoy, 2019; Haacke and Paton, 2021) and the UK (Blenkinsop *et al.*, 2017; Allan *et al.*, 2019; Champion *et al.*, 2019; Darwish *et al.*, 2020) have been investigated in detail. Therefore, a more comprehensive understanding of these drivers is still missing for the wider European region. Understanding the mechanisms behind sub-daily extreme rainfall events is key to improving the forecasting of such events and for projecting changes in their frequency and intensity under future climates (Pfahl and Wernli, 2012b; Breugem *et al.*, 2020). This is especially important given the recent findings that atmospheric circulation changes may be a significant driver of the greater intensification of extreme events compared to more moderate events in a warmer climate (Li *et al.*, 2019; Chan *et al.*, 2023).

The dynamical drivers of sub-daily rainfall are examined in this thesis at two different spatial scales; the synoptic scale (using weather patterns) and the hemispheric scale (using Rossby wave proxies). Weather pattern classifications are often used as a simplified method to look at atmospheric circulations, as they characterise the key patterns of large-scale meteorological variables over a synoptic time-scale (daily to 2-3 days) and for a set domain. The use of weather patterns (WP) allows for easier identification of the atmospheric conditions associated with a particular type of weather event (Huth *et al.*, 2008) as they provide a discrete set of conditions rather than a noisy picture of all possible influences. There are several weather pattern classifications which have been used in the investigation of dynamical drivers of (sub-daily) rainfall extremes in Europe and these are discussed further in Section 2.4. The weather pattern classification used in this thesis is the set of 30 WPs (MO30) created at the UK Met Office in 2016 (Neal *et al.*, 2016). This classification is based on the objective identification of mean sea level pressure (MSLP) patterns across a domain covering western Europe and the eastern North Atlantic and then assigning the daily MSLP pattern to the closest matching pre-defined WP.

Rossby waves are planetary-scale atmospheric waves, which often appear as meanders in the jet stream (Platzman, 1968). These waves control the positioning of large-scale flow patterns (such as troughs and ridges) within the atmosphere and as such have been shown to contribute to extreme weather events globally (e.g. Schubert *et al.*, 2011; Hirata and Grimm, 2016; Kornhuber *et al.*, 2019, 2020; de Vries, 2021; Xu *et al.*, 2021; White *et al.*, 2022). Rossby waves therefore provide a much larger-scale assessment of dynamical drivers associated with extreme weather than the synoptic-scale WPs. These large-scale drivers have previously been associated with longer-duration extreme rainfall events in Europe (Martius *et al.*, 2008; Barton *et al.*, 2016; Wolf *et al.*, 2018; Kornhuber *et al.*, 2019; de Vries, 2021). In this thesis two metrics for analysing Rossby waves are used; the Local Finite Amplitude Wave Activity metric (LWA) (Huang and Nakamura, 2016) and meridional wind at 300hPa (v300).

1.4 Forecasting of sub-daily rainfall extremes

The medium to long range forecast skill of rainfall outside of the tropics is low (Smith *et al.*, 2012) , however, the forecast skill of atmospheric variables can be much higher (Lavers *et al.*, 2016; Baker *et al.*, 2018; Ferranti *et al.*, 2018; Dorrington *et al.*, 2023). Additionally, the local-scale features associated with convective rainfall initiation can only be established a few hours in advance, whereas the large-scale atmospheric processes can be identified a few days ahead (Flack *et al.*, 2019). Therefore, it is feasible that longer-lead time forecast skill for rainfall can be improved by instead predicting atmospheric patterns and then deriving the predicted precipitation from these forecasts (Lavers *et al.*, 2016; Flack *et al.*, 2019; Dorrington *et al.*, 2023). The UK Met Office already use probabilistic forecasts of daily WPs to identify periods with a higher likelihood of extreme daily rainfall (based on the probability of threshold exceedance associated with each WP), up to two weeks in advance (Richardson *et al.*, 2020). The UK Met Office Decider system calculates the daily WP probability from an ensemble prediction system and uses this to generate the probabilistic forecasts of periods with higher risk of extreme daily rainfall. This information then feeds into a probabilistic fluvial flood forecasting model, Fluvial Decider. This forecast model supports the operations of the Flood Forecast Centre (a joint operation between the Met Office and Environment Agency), who issue warnings of flood risk over a 5-day lead time for England and Wales.

One of the key challenges of forecasting flooding from intense rainfall is the short lead time between identifying a convective feature in the forecast model that could lead to flooding, and the flooding occurring (Flack *et al.*, 2019). While continental-scale flood forecasting systems with longer lead times do exist (such as the European Flood Awareness System) (Smith *et al.*, 2016), these models require large amounts of data, are time-consuming to run and focus on events with larger-scale impacts. Therefore, simpler models which involve the identification of atmospheric features which have a probabilistic link to flooding, such as the MO WP based method, are of benefit to the FFC and the wider impact-based forecasting community (Richardson *et al.*, 2020).

Increasing the accuracy and also the lead-time of forecasts of extreme rainfall is one of the key ways in which impacts from the associated flooding may be reduced (Pappenberger *et al.*, 2015). Being able to identify weather systems further in advance that have the potential to result in flooding from intense rainfall is therefore one way to increase this lead time (Flack *et al.*, 2019; Dorrington *et al.*, 2023). Having an increased warning time of impending (flash) flooding would raise the awareness of a potential event to flood forecasters and provide time to run more computationally demanding urban flood models (Flack *et al.*, 2019). This in turn would allow more time for increased protection of infrastructure to be put in place, minimising the disruption and damage to key services and would also provide individuals with extra time to evacuate to a safe location if necessary. The extension of the extreme rainfall forecast lead-time, even via a probabilistic forecast, to ~5 days would therefore be enormously helpful.

1.5 Research Aims and Objectives

The overall aim of this thesis is to identify dynamical drivers of sub-daily rainfall extremes in western Europe, in a context which is useful for operational forecasting. This aim is addressed by utilising a new series of indices created specifically for sub-daily rainfall extremes to develop a climatology of these events in Europe and assessing the relationships between the sub-daily extremes and dynamical drivers at both the synoptic and hemispheric scale.

The following research objectives are addressed in this thesis:

- Conduct a thorough review of the literature surrounding sub-daily rainfall extremes, including their identification and measurement, current knowledge of climatological occurrence of sub-daily extremes, the relationship between dynamical drivers and rainfall extremes at both daily and sub-daily timescales, the use of WPs in assessing the drivers of these events, and connections between Rossby waves and rainfall extremes.
- Develop a climatology of sub-daily rainfall extremes in western Europe, based on GSDR-I index analysis.
- Assess the relationships between the MO30 weather patterns and sub-daily extremes, including the frequency of extreme events under each WP and the probability of extremes.
- Analyse how the upper-level atmospheric circulation changes on days with extreme rainfall compared to days without extremes.
- Investigate the connections between sub-daily rainfall extremes and very large-scale atmospheric circulations in the form of Rossby wave activity.
- Discuss opportunities for the identified circulation-rainfall relationships to be used operationally for longer-lead time forecasts of sub-daily rainfall extremes.

1.6 Thesis Structure

A literature review of the key topics investigated in this thesis is presented in Chapter 2. Chapter 3 provides a climatology of sub-daily rainfall extremes in Europe, created from the GSDR-I dataset, with the frequency, intensity and timing of extreme events investigated. The work in this chapter has been published in Whitford *et al.,* (2023). In Chapter 4 the MO30 WPs are formally introduced and the relationships between these WPs and 3hr extremes are examined. This investigation of dynamical drivers is further extended by assessing the geopotential height at 500hPa (z500) anomalies present on days with the WPs, with a comparison of the anomalies between days with and without extreme rainfall. This chapter provides an understanding of synoptic-scale dynamical drivers associated with sub-daily extremes in Europe. Chapter 5 looks at dynamical drivers on a hemispheric scale, assessing the spatiotemporal relationships between Rossby wave patterns and sub-daily extremes. This structure of looking at the synoptic-scale and then hemispheric scale introduces a more holistic view of the drivers, with connections found between the features identified in Chapter 4 and the wave patterns identified in Chapter 5. In both Chapters 4 and 5 the potential forecast utility of the identified relationships is assessed in relation to published literature. Finally, the conclusions are presented in Chapter 6, with a review of the results in the thesis, their relevance within the wider research field and opportunities for future work, including the operational potential of the identified driver-rainfall relationships.

Chapter 2
Literature Review

2.1 Sub-daily rainfall extremes

Extreme rainfall events on a sub-daily scale are recognised as causing significant socioeconomic damage and loss of life, as they frequently occur with little warning and generate dangerous pluvial (flash) floods and debris flows (Doe, 2004; Marchi *et al.*, 2010; Borga *et al.*, 2014; Gaume *et al.*, 2016; Archer and Fowler, 2018). This is particularly the case in small steep catchments and in urban areas. Due to outdated drainage infrastructure and high levels of impermeable surfaces, extreme pluvial events can quickly exceed the capacity of urban storm-drainage systems, leading to flash flooding in urban areas (Westra *et al.*, 2014; Blenkinsop *et al.*, 2015; Dale *et al.*, 2017; Dale, 2021; Fowler *et al.*, 2021c). The Boscastle floods in 2004 are an example of flash flooding in small rural catchment (Doe, 2004) while the 'Toon monsoon' in 2012 is a classic example of urban pluvial flooding after storm drainage systems were overwhelmed (Clark and Webb, 2013). Until recently, there was significantly less research into sub-daily rainfall compared to longer duration events due to the lack of availability of long, quality-controlled and homogeneous datasets (Westra *et al.*, 2014; Blenkinsop *et al.*, 2017). However, the development of new quality controlled observational datasets (Lewis *et al.*, 2019) and much higher resolution climate models (Kendon *et al.*, 2014; Chan *et al.*, 2018b; Rybka *et al.*, 2022) has helped fuel the recent surge in research in this area.

Sub-daily rainfall extremes can occur as individual short-duration events or as part of a longer storm event. The development of extremes in short-duration storms is more commonly the case in the warm season, when local- to meso-scale convective systems can generate short, intense events (Hoy *et al.*, 2014; Champion *et al.*, 2019; Chan *et al.*, 2023). The generation of extreme rainfall by convective processes requires three key ingredients: moisture, instability and lifting which can be provided by a combination of large- and mesoscale processes (Doswell, 1987; Doswell *et al.*, 1996). Sub-hourly to sub-daily extremes are more typically associated with these convective cells (Westra *et al.*, 2014; Kahraman *et al.*, 2021; Formetta *et al.*, 2022), however, they have also been linked to larger synoptic-scale patterns (Allan *et al.*, 2019; Barbero *et al.*, 2019b; Champion *et al.*, 2019) and can be associated with stratiform processes (Formetta *et al.*, 2022). The sub-daily extremes are driven by a combination of thermodynamic (linked to temperature changes) and dynamic (linked to atmospheric circulation) processes, which are both affected by changes in the local and global climate (Oueslati *et al.*, 2019). While the thermodynamic drivers are now relatively well understood, with multiple studies providing information on the relationship between temperature, humidity and sub-daily extremes (Hardwick Jones *et al.*, 2010; Barbero *et* *al.*, 2018; Ali *et al.*, 2021a, 2021b), less is known about the dynamical drivers. Therefore, how these synoptic-scale processes initiate sub-daily rainfall extremes under the present day climate, and subsequently how the relationship will evolve under future climate, remains an important research question (Pfahl *et al.*, 2017; Barbero *et al.*, 2019b; Fowler *et al.*, 2021b).

2.1.1 Climatology of sub-daily rainfall extremes in Europe

To date there have been only a few studies investigating the climatology of sub-daily rainfall extremes in globally. This leaves a gap in our understanding of when and where these events occur in the current climate and how their magnitude varies in different regions. Several of these aforementioned studies have used the GSDR dataset to investigate regional and continental patterns in the frequency and intensity of sub-daily extremes, particularly in Australia (Guerreiro *et al.*, 2018) and North America (Barbero *et al.*, 2017). Beck *et al.* (2020) used the GSDR data and other sources to develop a 0.1° gridded global rainfall probability dataset based on climatologies of a suite of occurrence and intensity indices for daily and 3-hourly rainfall. The occurrence indices were based on threshold values and the intensity indices on return periods and were calculated from observational data using neural networks. Their results showed a 15-year return-period intensity for 3-hour rainfall of ~16 mm in northern Europe and ~30-40 mm in southern and central Europe. In the only global-scale assessment of sub-daily climatology, Barbero *et al.* (2019a) used the GSDR dataset to look at the seasonal and diurnal distribution of 1-hour annual maximum rainfall intensity and frequency for the US, Australia, the British Isles, Japan, India and Malaysia to compare regions of varying climate which have good data availability. For the British Isles, the authors found the majority of 1hr annual maxima (AMAX) were associated with short duration storms (1-5 hours) and occurred in summer. There was a strong preference for the 1hr AMAX to occur in the late afternoon, coinciding with the peak convective activity timing.

Blenkinsop *et al.* (2017) and Darwish *et al.* (2018) also both investigated sub-daily rainfall extremes in the UK (using early versions of the GSDR data), focussing on the spatial and temporal distribution of the events. Both these studies identified a peak in both intensity and frequency of events in summer, with a diurnal cycle showing a peak in the late afternoon/early evening. Darwish *et al.* (2018) also found that 3hr AMAX had a wider seasonal distribution than 1hr AMAX and were less strongly tied into the convective cycle. For the rest of Europe outside of the UK, the climatology of sub-daily extremes has mostly received attention in Germany and Switzerland. Examining 10-minute and 60-minute extreme storms in urban areas of Germany, Haacke and Paton (2021) found the majority of storms occurred in the afternoon and evening and 58% (10-min) and 83% (60-min) of the events occurred in summer (JJA). Radar data was used by Lengfeld *et al.* (2019) to develop a climatology for daily and hourly rainfall in Germany, although this record was only 16 years long. Combined radar and rain gauge datasets have been utilised to investigate sub-daily rainfall in Germany (Paulat *et al.*, 2008; Panziera *et al.*, 2018), although these records are generally quite short <12 years. Panziera *et al.* (2018) used 12-years of data for the Swiss Alps. They found the largest 1 hr seasonal maxima values occur in summer, along the southerly and northerly alpine slopes and over the Jura mountains. The maxima values were significantly lower in the inner alps, indicating that at higher altitudes convection is inhibited by the lower moisture availability. These authors also found that in general, storms producing 1hr extreme rainfall were shorter in summer than autumn (due to summer extremes being caused mainly by short convective thunderstorms) and summer 1hr extremes contributed up to 30% of the total seasonal rainfall (along the southern Alpine slopes and Po valley). Finally, Olsson *et al.* (2022) used a gauge-based dataset to examine the intensity and timing of 1-, 3-, 6- and 12-hr rainfall in the Nordic-Baltic regions. The highest 1hr intensities were generally found in Denmark, southern Sweden and the Baltic states with highest frequency in summer. At longer durations there was a transition towards the higher values being found along western coasts and later in the year (more in September). The GSDR-I indices (Pritchard *et al.*, 2023) were used by Lakatos *et al.* (2021) to generate a dataset of 1-, 3- and 6-hourly extreme rainfall indices in the Pannonian Basin of eastern and central Europe. This data was then used to assess the basic climatological properties of sub-daily rainfall in this area. Their analysis revealed strong spatial patterns to the intensity of annual maxima and the most intense rainfall occurring in summer with a strong late afternoon to evening peak in the diurnal cycle. Additionally, they found that the occurrence of 3hr periods with >20mm rainfall was most frequent in the regions with a Mediterranean climate.

The studies mentioned here all provide a useful insight into the characteristics of sub-daily extreme rainfall in Europe, indicating the most intense events generally occur in summer, in more southerly or continental regions, with a strong afternoon or evening diurnal peak. However, a wide variety of different methods have been used in the calculation of the climatologies, which are mostly focussed on individual countries. The different methods and time periods used in analyses of extreme events make it difficult to accurately and consistently assess the variations in characteristics of extremes (across Europe) based on information currently available in the literature (Fowler *et al.*, 2021a). Therefore, a climatology of sub-daily extremes in western Europe as a whole, created using a consistent methodology, will generate a better understanding of the seasonality and spatial distribution of sub-daily extreme events across this region.

2.1.2 Rainfall extremes under climate change

In recent years it has become apparent that an increase in the frequency and intensity of extreme rainfall events is one of the consequences of a warmer climate (Trenberth *et al.*, 2003; O'Gorman, 2015; Lenderink and Fowler, 2017b; Fowler *et al.*, 2021c). The Clausius-Clapeyron (CC) equation governs the saturation specific humidity of the atmosphere as a function of temperature and increases at a rate of ~6-7% per degree increase in temperature (K) near the surface. Assuming other conditions such as relative humidity remain constant with warming, the specific humidity of the air will therefore also increase at approximately the same rate. As rainfall extremes are limited by the available atmospheric moisture, changes in rainfall intensity are therefore expected to scale approximately with the CC rate (Fowler *et al.*, 2021a). However, there is evidence that extreme rainfall, particularly short-duration (<6hr) extremes, may increase at a rate even higher than this locally (Westra et al., 2014), while global precipitation and evaporation are constrained by Earth's energy balance to increase at ~2-3% per degree (Allan and Liu, 2021). This higher scaling rate in hourly peak rainfall intensities has been noted in both observations (Lenderink *et al.*, 2017b; Guerreiro *et al.*, 2018; Ali *et al.*, 2021a) and in climate models (Chan et al., 2014; Lenderink et al., 2019; Förster and Thiele, 2020). There are several possible physical explanations for this higher scaling rate in sub-daily rainfall extremes, including dynamical feedbacks in cloud-core updrafts (Trenberth *et al.*, 2003; Lenderink *et al.*, 2017b) and quasi-geostrophic large-scale vertical lifting (Lenderink *et al.*, 2017a; Nie *et al.*, 2018). This potential for greater increases in sub-daily compared to daily rainfall extremes is another reason to urgently improve our understanding of the drivers and characteristics of sub-daily extreme events given their already significant impacts.

Future changes in extreme rainfall events have been extensively investigated using climate models (Seneviratne *et al.*, 2021).Uncertainties in the projections of changes in future rainfall are, however, much larger than those for temperature projections and there remains large ambiguity over the spatial distribution, timing and causes of this change (Larsen *et al.*, 2009; Lenderink and Fowler, 2017b). A key cause of this uncertainty is model uncertainty (whereby different models produce different results for the same forcing) (Hawkins and Sutton, 2011). The ambiguity in the models' forced responses can be reduced by improving the model representation of atmospheric dynamics and understanding the contribution from circulation-related components to the variable under investigation (Fereday *et al.*, 2018). Therefore, improving model simulations of future rainfall requires improving our understanding of atmospheric dynamics, on global to regional scales, and their relationships to rainfall (Lenderink and Fowler, 2017b; Pfahl *et al.*, 2017).

Regional-scale variations in extreme rainfall under global warming can show very different patterns to the changes on a global scale, due to natural variability and the influence of regional atmospheric circulations and thermodynamics (Phfal, et al., 2017). The impact of future atmospheric circulation changes on rainfall in Europe has received some attention (Lorenzo *et al.*, 2011; Murphy *et al.*, 2018; Cotterill *et al.*, 2023). Pope *et al.* (2022) examined future changes in the MO30 weather patterns to identify end-of-century changes in UK climate. Their results indicate an increase in anticyclonic weather types in summer with an accompanying decrease in frequency of cyclonic types, indicating a decrease in patterns associated with strong anomaly pressure gradients, thereby leading to reductions in rainfall overall and particularly large-scale frontal rainfall events in summer. Chan *et al.* (2023) found future large-scale circulation changes to be a key driver of changes in mesoscale convective systems (often responsible for sub-daily rainfall extremes) over Europe. Using a physical scaling diagnostic, Pfahl *et al.* (2017) separated the forced regional change in future global daily extreme rainfall into the thermodynamic and dynamic contribution. Their results showed the thermodynamic signal was responsible for a globally consistent rainfall response of CC scaling. The dynamic contribution, largely through variations in vertical pressure velocity, was shown to play a crucial role in moderating the spatial pattern and intensity of extreme rainfall (away from C-C scaling). This experiment highlights the importance of atmospheric dynamics in altering future rainfall extremes.

2.1.3 Impacts of Extreme Sub-daily Rainfall

Flooding resulting from extreme rainfall depends on many factors including rainfall intensity and duration and drainage basin conditions. River (fluvial) floods most commonly occur due to extreme, longer-lasting rainfall in large river basins (Kundzewicz *et al.*, 2014). Daily extreme rainfall events have been responsible for several large flood events in Europe in recent decades, such as the August 2002 floods in Germany and Austria along the Vltava, Elbe and Danube rivers which were generated by two separate 24-hour extreme events and caused 100 fatalities and €12 billion in economic losses (Ulbrich *et al.*, 2003). In contrast to the large fluvial floods generated by long-term extreme rainfall events, short-duration intense events more commonly generate sudden, localised 'flash' floods in steep rural catchments and urban areas (Marchi *et al.*, 2010; Archer and Fowler, 2018; Dale, 2021). Despite their smaller spatial extent, these pluvial floods can still cause significant impacts. A cloudburst over Copenhagen in July 2011 generated >125 mm rainfall in just a few hours and caused damages exceeding EUR 800 million (Arnbjerg-Nielsen *et al.*, 2015). The July floods in western-Europe in 2021 resulted in pluvial and river floods across large parts of Germany and Belgium, with accumulated 24-hour rainfall sums reaching 150 mm in some areas (Kreienkamp *et al.*, 2021). These floods caused 220 fatalities and cost over 8billion euros in Germany alone ((GDV), 2021). Barredo (2007) noted that flash flooding caused 40% of the flood-related casualties in Europe during 1950-2006. The response time of floods due to intense short duration rainfall appears to be considerably shorter than for other flood events, with the water rising much faster, which is a serious threat to life as the time to escape rising waters is reduced (Archer and Fowler, 2018). This rapid onset and ability to cause extensive disruption to a range of environments, combined with the difficulties in forecasting such events resulting in short warning times, make flash floods one of the most dangerous natural hazards (Flack *et al.*, 2019). The short period intensity of the rainfall inducing a flood is a key factor in determining its severity, while the damage caused by a flash flood also depends on the local geomorphological factors and human influences (Marchi *et al.*, 2010; Špitalar *et al.*, 2014; Dale, 2021). In rural areas flash floods can cause significant erosion, scouring fields of soil and crops and carrying these for a considerable distance and potentially causing damage to infrastructure (Martínez-Casasnovas *et al.*, 2002). In urban areas the smooth, impermeable surfaces allow the rainwater to gather velocity very rapidly, forming a sheet of fast moving water that may be deep enough to sweep people off their feet (Archer and Fowler, 2018) e.g. the 'Toon Monsoon' event in Newcastle upon Tyne (Clark and Webb, 2013).

With the projected increase in extreme rainfall events in a future warmer climate, it is reasonable to infer that the associated negative impacts will also increase (Sharma *et al.*, 2018), endangering infrastructure, economy and lives on a more regular basis. The risk in the UK alone is projected to double under a 4ºC warming future scenario, resulting in an expected annual damages increase from the current ~£0.6bn to ~£1.2bn by the 2080s (Sayers *et al.*, 2020). It is therefore, of great importance to better understand the drivers and characteristics of these extreme rainfall events, to enhance our understanding of their occurrence and improve projections of future change (Beniston *et al.*, 2007; Westra *et al.*, 2014; Fereday *et al.*, 2018; Allan *et al.*, 2019; Champion *et al.*, 2019). Improving flood adaptation strategies requires a detailed understanding of where and when extreme sub-daily rainfall events and associated floods occur in the current climate, in order to develop robust models for how these events may evolve in the future (Alexander *et al.*, 2019). However, there are currently few studies of flood trends on sub-daily timescales and little assessment of the regional-scale future changes in occurrence of flash flooding, due largely to the lack of sub-daily streamflow (and coordinating sub-daily rainfall) data (Hosseinzadehtalaei *et al.*, 2020; Fowler *et al.*, 2021a).

2.2 Quantifying extreme rainfall

The definition of an 'extreme' rainfall event varies greatly – it can be based on several different statistical methods and an event which is considered extreme in one geographical region may not be extreme in another region. Extreme events can be defined as the maximum rainfall (intensity) for a given duration (Larsen *et al.*, 2009; Darwish *et al.*, 2018). Alternatively they can be based on statistical percentiles or indices, rendering them geographically variable (Łupikasza *et al.*, 2011; Alexander *et al.*, 2019). Recently the use of a peaks-over-threshold (POT) method has become more common, whereby the extreme events are identified as being above a threshold value chosen by the investigator as indicative of potential impacts (Toreti *et al.*, 2010).

Indices are one of the simplest ways to investigate climatic extremes due to their comparability across geographical regions and with each other (Donat *et al.*, 2013b; Alexander *et al.*, 2019). They have been used to examine rainfall characteristics for several decades, since the development of standardised definitions of daily climate indices at the beginning of the 21st century (Klein Tank *et al.*, 2002; Peterson and Manton, 2008). Work by the Expert Team on Climate Change Detection and Indices (ETCCDI) led to the generation of a set of standard indices, 10 of which can be used to assess daily rainfall extremes (Alexander *et al.*, 2019). These indices include the annual maximum 1-day rainfall amount, heavy (>10 mm) and very heavy (>20 mm) rainfall days and the number of days with rainfall greater than the 99th percentile of daily amounts. Several studies have used selections of these indices to investigate daily extreme rainfall, especially since the development of the European Climate Assessment & Dataset (ECA&D) (Klein Tank *et al.*, 2002) and HADEX/HADEX2 datasets (Alexander *et al.*, 2006; Donat *et al.*, 2013b), although these studies have mostly focussed on identifying trends (e.g. Moberg *et al.* (2006); Donat *et al.* (2013); Cioffi *et al.* (2015)), rather than developing climatologies. One example of an indices-based rainfall climatology is the study by Dietzsch *et al.* (2017). Using the Daily Rainfall Analysis for Climate Prediction (DAPACLIP) dataset created from a combination of interpolated and gridded gauge-based measurements, the authors used several ETCCDI indices to investigate the climatology of rainfall globally for the period 1988 - 2008, with a focus on Europe. Their results showed the European regions with most frequent heavy rainfall were the western coasts of Norway, the British Isles, the northern coasts of Spain and Portugal and the Alps. However, indices based solely on daily (gauge-based) data may mask some of the most intense short-duration events that can lead to flash flooding, especially in the case of convective extremes (Schroeer *et al.*, 2018; Alexander *et al.*, 2019; Lengfeld *et al.*, 2020). A lack of long-term records of high quality observations has so far prevented similar analyses at the sub-daily scale (Zhang *et al.*, 2017; Alexander *et al.*, 2019) and there remains an incomplete understanding of the variability of these events under the current climate (Westra *et al.*, 2014; Barbero *et al.*, 2019a; Lewis *et al.*, 2019; Fowler *et al.*, 2021b). The development of the GSDR dataset, and other tools such as CPMs as discussed above, is leading towards an increase in research outputs focussing on quantification of sub-daily extremes. The rainfall probability distribution climatology produced by Beck *et al.* (2020) using the GSDR dataset is the first example of a global sub-daily rainfall climatology based on indices. Despite these advances, there remain few studies investigating sub-daily rainfall (indices) in detail over the wider European region, despite the significant impacts associated with flash floods across Europe (Gaume *et al.*, 2009; Marchi *et al.*, 2010). To provide a more comprehensive analysis of continental-scale extremes, a set of indices for extreme sub-daily rainfall (GSDR-I) has been derived from the GSDR dataset (Pritchard *et al.*, 2023). The Pannonian

Basin study of Lakatos *et al.* (2021) uses these indices to develop a sub-daily extreme rainfall climatology. The GSDR-I indices are listed in Table 3.1 and further details on the methods used to calculate them are provided in Section 3.2.

2.3 Relationship between dynamical drivers and extreme rainfall events

The dynamical drivers of rainfall extremes are being increasingly recognised as important factors in improving the skill of forecasts of extreme events and subsequent potential (flash) flooding (Lavers *et al.*, 2018; Flack *et al.*, 2019; Mastrantonas *et al.*, 2022b). There is currently a relatively good understanding of the dynamical drivers of daily (and longer) extreme rainfall, however, a similar level of understanding of the dynamical drivers of sub-daily extremes is lacking (Pfahl, 2014; Barbero *et al.*, 2019b; Fowler *et al.*, 2021b). Additionally, the response of atmospheric dynamics to global warming, and how this will in turn affect extreme weather events is still unclear, with the potential changes in large-scale circulations and resulting impacts on extreme weather a topic of ongoing research and debate (Shepherd, 2014; Blackport and Screen, 2020). Therefore, improvement of our understanding of the relationship between atmospheric drivers and sub-daily rainfall extremes would benefit both forecasting applications and projections of future changes in these events.

2.3.1 Dynamical Drivers of Daily Extreme Rainfall in Europe

Dynamical drivers of rainfall are atmospheric features which influence the intensity, location and timing of the events. Several key atmospheric variables have been shown to be dynamical drivers of extreme rainfall on daily timescales, including water vapour transport (IVT), vertical instability, potential vorticity (PV), geopotential height and mean sea level pressure (e.g. Doswell, 1987; Martius *et al.*, 2008; Lavers and Villarini, 2013; Barton *et al.*, 2016; Toreti *et al.*, 2016; Mastrantonas *et al.*, 2021; de Vries, 2021; Tuel and Martius, 2022). These variables control weather systems such as cyclones, fronts and atmospheric rivers which are associated with extreme daily rainfall in midlatitudes (Toreti *et al.*, 2010; Pfahl and Wernli, 2012b; Catto and Pfahl, 2013; Lavers and Villarini, 2013; Ruff and Pfahl, 2022). The importance of the geographical relationship between extreme rainfall and the dynamical drivers and the strong influence of local orography on the generation of extremes has been shown by several studies (Maraun *et al.*, 2011; Pfahl, 2014; Barton *et al.*, 2016; Giannakaki and Martius, 2016).

Investigation of the relationship between individual atmospheric variables and rainfall extremes can reveal more detail about the extent to which the specific driver influences extremes. For example, Lavers and Villarini (2013) used the vertically integrated water vapour transport to identify atmospheric rivers (ARs) associated with daily annual maxima events across Europe. This analysis revealed that ARs had a strong influence on events in the winter half year, with a high proportion (up to 80%) of the most intense daily extremes along the western seaboard being caused by ARs. However, this relationship does not continue into the summer half year, with ARs specifically found to not be connected with daily extremes in the UK in summer (Champion *et al.*, 2015). Allan *et al.* (2016) utilised the specific humidity and vapour transport at 850hPa to investigate moisture characteristics associated with extreme daily rainfall in the UK, identifying a propensity for the events to be associated with elevated levels of both these variables. Events in the north and west of the UK generally occurred in the winter half year and were associated with narrow bands of increased moisture content and transport (essentially ARs) extending from the southwest, while the south east experienced a higher proportion of daily extremes in the summer half year, with weaker moisture transport fields with a more southerly orientation. These findings indicate distinct differences in the atmospheric moisture conditions leading to daily rainfall extremes in different regions of the UK. Blenkinsop *et al.* (2015) examined the relationship between daily summertime rainfall extremes and a series of airflow indices, finding the highest intensities for events in southern England were associated with anticyclonic flow while in the north the most intense events occurred under cyclonic flow. These studies highlight how the impact different dynamical drivers have on rainfall extremes can vary between different seasons and how the response of rainfall to these drivers can be geographically dependent.

Investigation of individual features in this manner is eminently useful for diagnosing individual influences on generation of extreme events, however this is not the only method of investigating dynamical drivers. The overall synoptic patterns which are present in association with extremes provide an overview of the large-scale atmospheric features which may be influencing the event, through providing large-scale lifting or moisture advection (Mastrantonas *et al.*, 2021). Many studies therefore use the synoptic patterns based on mid-tropospheric or surface features as indicators of the larger-scale conditions driving extreme rainfall, rather than focussing on individual features (e.g. Toreti *et al.*, 2010; Richardson *et al.*, 2020; Mastrantonas *et al.*, 2021). These will be discussed further in Section 2.4.

A final dynamical driver to mention here is Rossby waves. These are planetary-scale waves which circle the globe, often in the form of undulations on the atmospheric jet streams (Platzman, 1968). There are multiple examples of daily and longer rainfall extremes being linked to Rossby waves through the occurrence of smaller-scale Rossby wave packets over a certain region (Martius *et al.*, 2008; Barton *et al.*, 2022) and Rossby wave breaking (Grams *et al.*, 2014; Giannakaki and Martius, 2016; Tuel and Martius, 2022). De Vries (2021) investigated the relationship between daily rainfall extremes and intense moisture transport (IVT) and Rossby wave breaking (through identification of PV streamers), finding that extreme rainfall events over the Mediterranean in particular were associated with Rossby wave breaking while coastal regions experienced extremes under high IVT values. The strength of these features was also found to have an influence, with deeper PV streamers and higher IVT maxima leading to larger rainfall volumes. The links between Rossy waves and extreme rainfall are discussed in more detail in Section 2.5.

2.3.2 Dynamical Drivers of Sub-Daily Extreme Rainfall in Europe

The most substantial analysis of the influence of atmospheric features on sub-daily extreme rainfall events in Europe has been undertaken for the UK and Germany. Champion *et al.* (2019) looked at the influence of an array of atmospheric variables on 3-hourly summer extreme rainfall in the NW and SE UK. Analysis of these variables showed that extreme rainfall events in the NW region were strongly affected by larger-scale orographically enhanced processes while in the SE more localised sources of moisture and relatively unstable air masses were more important. Similar to the results of Pfahl (2014), the authors' demonstrated the importance of considering both the large-scale conditions and thermodynamic effects when developing projections of changes in extreme short-duration events. Subsequently to Champion *et al*. (2019), regional-scale atmospheric precursors of intense sub-daily rainfall across the whole UK were investigated by Allan *et al.* (2019). The 200 most extreme 3hr events in several UK regions were matched with daily mean atmospheric conditions on days prior to the events, revealing multiple dynamical precursors to the 3hr extremes could be identified in the days leading up to the events. These included negative anomalies in SLP and 200hPa geopotential height to the west or southwest of the UK, anomalous southerly airflow and associated northwards moisture transport and elevated dewpoint temperature and moisture across NW Europe. All these anomalies were visible from 4 days prior to the extreme rainfall events. Investigations of dynamical drivers of sub-daily rainfall events in Germany have generally used weather patterns to investigate the atmospheric circulations and are therefore discussed in Section 2.4.2

It has also been shown that cut-off lows (COLs) and progressive jet stream disturbances in the US have a strong influence on the seasonality and spatial distribution of hourly rainfall extremes (Barbero *et al.*, 2019b). Both phenomena were shown to contribute disproportionately to the occurrence of hourly rainfall extremes relative to their overall frequency across the US, with the COLs shown to be responsible for a significant proportion of extreme events in spring and autumn while jet stream disturbances were associated with more extremes in winter. Synoptic events of this type also occur across Europe (Nieto *et al.*, 2006), however, their influence on sub-daily rainfall extremes in this region has not yet been examined.

2.4 Weather Pattern Classifications

Weather patterns typically characterise one or more large-scale meteorological variables over a particular geographical domain and time-scale. They are generally defined by an atmospheric variable, such as (mean) sea level pressure (MSLP) or a geopotential height, within the lower-to mid-troposphere (eg. z500). They therefore represent the broad scale atmospheric circulation over a given region and timescale (typically daily) (Huth *et al.*, 2008). A weather pattern classification is a group of weather patterns (WPs) which may also be referred to as weather types, circulation patterns or circulation types. Any classification of circulation patterns should be viewed as a purposefully developed simplification of the circulation conditions rather than as a physical reality of the conditions. However, they are a very useful way of reducing complex meteorological data into a few discrete states, which can then be linked to a 'weather' impact (Huth *et al.*, 2008).

The categorisation of large-scale circulation patterns into weather patterns has been used for many decades in weather forecasting or to assess the climatology of mesoscale atmospheric events (Pope *et al.*, 2022). While improved computing power meant pattern classifications fell out of use for forecasting over time, they became increasingly favoured by climatologists, who used the patterns initially to understand and explain observed climatologies and later in climate models as indicators of how circulations might change in future climates (Otero *et al.*, 2018; Pope *et al.*, 2022). More recently however, the usefulness of weather patterns in making ensemble forecast outputs easier to understand has led to a renaissance in their usage in forecasting (Huth *et al.*, 2008). The development of automated classification systems has further enabled the use of weather patterns both in ensemble forecasting to indicate periods of change in the synoptic circulation (Huth *et al.*, 2008) and in identifying periods with increased risk of (coastal and fluvial) flooding up to two weeks ahead (Neal *et al.*, 2016; Richardson *et al.*, 2020). The WPs can also be used to develop a probabilistic forecast by objectively assigning ensemble members from an ensemble prediction system to the nearest weather pattern type. These forecasts can be verified, providing an understanding of the level of predictability of different circulation types when forecast through numerical weather prediction models (Ferranti *et al.*, 2015; Neal *et al.*, 2016).

WP classifications can be developed using subjective or objective methods. Earlier WP classifications are typically subjective, where WPs are defined prior to the assignment procedure using either expert knowledge or physical parameters such as airflow direction (Huth *et al.*, 2008; Hoy *et al.*, 2014). Time series of the classifications are also subjectively derived by visual attribution of daily pressure fields to the closest WP. The original Lamb Weather Types (LWT) (Lamb, 1972) and Grosswetterlagen (GWL) catalogue (Werner and Gerstengarbe, 2010) are the most well-known subjective classifications and will be described in more detail in the following section. Objectively-defined WP classifications are now more common, largely due to the increase in computing power in recent decades allowing researchers to design classifications more suited to their own purposes. Many different methods are used in creating objective classifications, including correlation techniques, cluster analysis, principal component analysis and neural networks (Huth *et al.*, 2008). With the development of suitable computer software and datasets the original LWT and GWL catalogues have been updated and turned into objective classifications (Jenkinson and Collison, 1977; Werner and Gerstengarbe, 2010). All of these techniques still do involve some level of subjectivity, such as the choosing of the number of clusters and there is a level of uncertainty around the individual WP due to intra-WP variability (Neal *et al.*, 2016).

The literature on the applications of WP classifications is largely focussed around climatological studies, in particular the observed recent changes in the frequency of occurrence of WPs. This has generally been investigated using the changes in atmospheric circulation over time on their own (Jenkinson and Collison, 1977; Bárdossy and Caspary, 1990; Stefanicki *et al.*, 1998; Kučerová *et al.*, 2017). However, the variety of classifications used and the lack of a common time period make it difficult to draw any Europe-wide conclusions, except perhaps for an increase in frequency of circulation types with a zonal flow in winter (Kučerová *et al.*, 2017).

WPs have been used in future climate projections as they help to reduce the complexity of climate model output, making results clearer. It is easier to identify changes in future conditions by comparing projected changes in large-scale WP frequencies between the present day and future periods than individual atmospheric/meteorological variables that require fine spatial scales (Pope *et al.*, 2022). In particular Fereday *et al.* (2018) noted uncertainty in future atmospheric circulation accounted for more than half the intermodal variance of twenty-first century rainfall trends for winter months over Europe. These changes in WP frequency are then often related to local-scale meteorological variables (Cassano *et al.*, 2006; Donat *et al.*, 2010; Hoffmann and Schlünzen, 2013; Fereday *et al.*, 2018; Pope *et al.*, 2022).

WPs are now becoming utilised again in weather forecasting and analysis of trends/variability in weather conditions. Several studies have investigated the relationships between weather patterns and particular meteorological features including rainfall (e.g. Planchon *et al.*, 2009; Richardson *et al.*, 2020; Mastrantonas *et al.*, 2021), thunderstorms (Wilkinson and Neal, 2021), drought (Richardson *et al.*, 2018) and temperature (Hoffmann and Schlünzen, 2013) in the present day. A more detailed discussion of WP classifications being used in the study of rainfall is provided in the next section.

2.4.1 Using weather patterns with daily rainfall

The most commonly used weather pattern classification systems for investigating rainfall in Europe are the Lamb Weather Type (LWT) and Grosswetterlagen (GWL) classifications. The LWT scheme was initially based on manual identification of basic daily WPS (Lamb, 1972) until the scheme was updated by Jenkinson and Collison (1977) and developed into an objective version based on daily mean sea level pressure, before finally developed into a new daily objective classification series using reanalysis data by Jones *et al.* (2013). This classification system is centred on the UK. The GWL regimes are 29 subjectively derived large-scale circulations, centred over Germany but covering the wider Central European area (Werner and Gerstengarbe, 2010). They represent regimes which persist for at least three days before transitioning. Recently a new set of 30 weather patterns have been developed by the UK Met Office (Neal *et al.*, 2016). These patterns are based on clustering of daily mean sea level pressure fields across the western Europe/eastern North Atlantic region and are therefore representative of the general atmospheric circulation over the UK and surrounding European area. This large area of definition gives the MO30 patterns an advantage over other classification systems such as the LWT, as they are applicable for other European regions, not just the region of origin (Richardson *et al.*, 2018).

There have been a number of investigations of the links between the GWL and rainfall in central Europe. These have covered Germany (Brieber and Hoy, 2019), the Elbe catchment (Werner *et al.*, 2008), the Meuse basin (Tu *et al.*, 2005), the Netherlands (Adri Buishand and Brandsma, 1997), the Baltic states (Jaagus *et al.*, 2010), the Ore mountains (Minářová *et al.*, 2017) and Brittany (Planchon *et al.*, 2009) as examples. Hoy *et al.* (2014) used a combination of the GWL and the Vangengeim-Girs classification to determine the synoptic features associated with daily rainfall anomalies on a continental scale for Europe. The LWTs have also been used to determine correlations between rainfall and circulation patterns, mostly for the UK as this is where the LWTs are defined (Fowler and Kilsby, 2002; Malby *et al.*, 2007; Pattison and Lane, 2012).

Individual studies have also created their own weather patterns using clustering procedures on atmospheric variables to identify large-scale circulation patterns associated with rainfall in Europe. Clustering of variables including sea level pressure (SLP), geopotential height at 500hPa (z500) and precipitable water using k-means clustering, principal component analysis and simulated annealing techniques have been utilised in several studies (Wibig, 1999; Jacobeit *et al.*, 2009; Toreti *et al.*, 2010; Hidalgo-Muñoz *et al.*, 2011; Giannakaki and Martius, 2016; Merino *et al.*, 2016; Santos *et al.*, 2017; Mastrantonas *et al.*, 2021).

2.4.2 WPs and extreme daily rainfall

Given the topic of this thesis, we focus here on the links identified between WPs and extreme rainfall. Multiple WP classifications have been used to identify correlations between atmospheric conditions and extreme daily rainfall in Europe, especially the GWL classification and individual classifications based on specific variables. For example, Minářová *et al.* (2017) used the GWL to determine the weather type most frequently associated with extreme rainfall over the Ore Mountains (on the Czech-German border) as being a trough over central Europe, while Planchon *et al.* (2009) identified the synoptic conditions associated with winter daily extreme (>20 mm) rainfall in NW France as being predominantly westerly and southerly cyclonic circulations.

Regardless of the classification system or variables used, it is often possible to identify just a handful of circulation types related to extreme rainfall (or floods) in Europe. Using self-organising maps and modified k-means clustering Toreti *et al.* (2010) developed circulation clusters based on SLP and z500 which were associated with extreme daily winter rainfall in the Mediterranean. They identified 3 clusters each for the East and West Mediterranean which could explain the atmospheric conditions associated with the extreme rainfall. Mastrantonas *et al.* (2021) similarly used k-means clustering of SLP and z500 anomalies to develop a set of weather patterns associated with extreme daily rainfall across the Mediterranean. Their analysis indicated that the conditional probability of the extreme events increased by a factor of 3 for most locations when the most strongly correlated weather pattern was present. Six atmospheric circulation patterns based on a range of atmospheric variables including SLP and z500 were developed by Merino *et al.* (2016) to explain the conditions present during extreme daily rainfall in Spain. Jacobeit *et al.,* (2009) created WPs through simulated annealing of MSLP to show there were clear links between a handful of the circulation types and occurrence of heavy daily rainfall with the circulation type having a strong influence on the frequency of events. A range of variables including PV and total precipitable water were used in k-means clustering by Giannakaki and Martius (2016) to develop ten upper-level flow classes for conditions associated with daily extreme rainfall events over northern Switzerland. Finally, Santos *et al.* (2017) used a set of WPs defined on clustering of daily MSLP fields to identify the conditions associated with flash flooding in a set of drainage basins in Portugal. Their results showed just 3 WPs were strongly associated with flash flooding and anomalous features within the WPs were identified on the flash flood days, highlighting their difference to the normal circulation. It is clear that MSLP and an atmospheric pressure variable such as z500 are commonly used in assessment of atmospheric circulation links to extreme rainfall, with the use of variables at various tropospheric levels required to identify details in the atmospheric situations under which extreme rainfall events occur (Merino et al., 2016). This thereby supports the decision to use both MSLP-based WPs and the z500 variable in the analysis presented in Chapter 4. These studies also each highlight the operational potential for using large-scale atmospheric circulation patterns to provide advance warning of periods with a higher risk of extreme rainfall impacts, allowing communities to prepare for events with longer warning times and also the uses in climate modelling of future rainfall (Jacobeit et al., 2009; Merino et al., 2016; Santos et al., 2017; Richardson et al., 2020; Mastrantonas et al., 2021).

In a recent study, Richardson *et al.* (2020) assessed the links between the MO30 patterns and regional daily extreme rainfall in the UK, with results showing clear differences in the rainfall percentile exceedance probabilities between individual WPs and regional rainfall. This indicated a clear connection between the MO30 WPs and conditions leading to enhanced likelihood of extreme rainfall for the UK. The information was subsequently used by the authors to develop a probabilistic fluvial flood forecasting tool (Fluvial Decider) based on the UK Met Office's Decider tool. This investigation shows an assessment of this type for Europe could be very productive and a similar study of other regions of Europe and for sub-daily extremes is therefore evidently feasible and a suitable extension of this work.

2.4.3 WPs and sub-daily extreme rainfall

While daily extreme rainfall across Europe has been extensively linked to various weather pattern classification schemes, sub-daily rainfall extremes have not received the same level of attention so far. The GWL WPs have been used to examine atmospheric conditions associated with sub-daily extremes in Germany (Brieber and Hoy, 2019; Haacke and Paton, 2021) and a set of objective WPs created by the Deutscher Wetterdienst (DWD) were used to investigate the dynamical drivers of sub-daily extremes in Hamburg (Weder *et al.*, 2017). These DWD WPs were also used to assess the circulation patterns associated with extreme (>99th percentile) hourly rainfall in Amsterdam (Manola *et al.*, 2019). These central Europe studies all found the sub-daily extremes were most frequently associated with a south-westerly flow regime. The MO8 WPs were used in an investigation of the atmospheric circulation associated with sub-daily annual maxima in Sicily (Cipolla *et al.*, 2020) although the use of these WPs instead of MO30 results in assessment of only broad scale patterns e.g. North Atlantic Oscillation phase rather than more localised atmospheric conditions. There are several studies investigating large-scale circulation patterns associated with summertime thunderstorms in central and western Europe (Sibley, 2012; Piper *et al.*, 2016, 2019; Mohr *et al.*, 2020; Wilkinson and Neal, 2021), although only Wilkinson and Neal (2021) explicitly use WPs (the MO30 classification). However, these studies generally use lightning data as indicators of the presence of thunderstorms and do not explicitly investigate the associated rainfall. There is therefore a paucity of literature investigating the large-scale weather patterns linked to summertime sub-daily rainfall extremes across the European region, which may occur without any lightning.

2.5 Rossby Waves and extreme weather events

Rossby waves contribute to multiple extreme weather events globally, including temperature extremes (Schubert *et al.*, 2011; Röthlisberger *et al.*, 2019; Kornhuber *et al.*, 2020; Xu *et al.*, 2021; White *et al.*, 2022) and rainfall extremes (Martius *et al.*, 2008; Schubert *et al.*, 2011; Hirata and Grimm, 2016; Baker *et al.*, 2018; Kornhuber *et al.*, 2019; de Vries, 2021; Barton *et al.*, 2022; Tuel *et al.*, 2022), on differing timescales, making them an important component of investigations into dynamical drivers of extreme weather.

Recently White *et al.,* (2022) produced a review of how Rossby waves can lead to extreme midlatitude weather which was an important source of information in this section. Rossby waves form as a result of the conservation of the dynamical property potential vorticity (PV). PV is a function of both relative and planetary vorticity, and static stability. Planetary vorticity increases towards the poles, therefore, a parcel of air moving poleward must, in order to conserve PV, decrease its relative vorticity by rotating anticyclonically. The resulting pattern of atmospheric motion is what gives rise to Rossby waves, consisting of consecutive regions of anomalous cyclonic and anticyclonic vorticity (White *et al.*, 2022). Rossby waves occur continuously in the atmosphere and are forced by the upper-level divergence of air due to diabatic heating, interactions with orography or growth of baroclinic instability (White *et al.*, 2021, 2022). There are essentially two forms of Rossby waves; very slow moving, long wavelength waves referred to as 'stationary waves' due to their persistence in a geographical location over entire seasons, and faster moving, smaller wavelength waves referred to as 'transient waves'. Stationary waves develop from zonal asymmetries in orography, land-sea thermal contrast and atmospheric diabatic heating, while transient waves are generated by disturbances in the large-scale flow that travel downstream. This second type of wave is of interest for weather extremes as they can persist for several day (and up to several weeks) over an area before moving on (Wills *et al.*, 2019; White *et al.*, 2022).

Rossby waves can initiate extreme weather events either through the presence of anomalously high stationarity/persistence (Schubert *et al.*, 2011; Gelbrecht *et al.*, 2018; Wolf *et al.*, 2018; Röthlisberger *et al.*, 2019) or through anomalously high wave amplitude (Petoukhov *et al.*, 2013; Screen and Simmonds, 2014; Röthlisberger *et al.*, 2016b; Kornhuber *et al.*, 2020) or a combination of both. The specific case of Rossby wave breaking has been linked to several extreme rainfall events through the production of potential vorticity streamers (Martius *et al.*, 2008; Barton *et al.*, 2016; de Vries, 2021), however, this is not investigated further in this thesis. When Rossby waves that are usually transient become anomalously persistent they are described as being 'quasi-stationary'. These quasi-stationary waves (QSW) can remain in the same location with roughly the same phase for several days to weeks, leading to extreme weather events due to the long duration of rainfall or high temperatures (Wolf *et al.*, 2018). However, it can be hard to undertake a precise assessment of the impact Rossby waves have on an extreme weather event. Defining and diagnosing the waves is difficult, especially when nonlinear effects are present, an issue that has been unresolved since the 1950s (White *et al.*, 2022). This is largely due to the difficulties of separating waves from the background flow, and to the fact vorticity anomalies in the atmosphere can occur on a size scale anywhere from individual blocks (Rex, 1950; Nakamura and Huang, 2018; Kautz *et al.*, 2022) to localised Rossby wave packets (Huang and Nakamura, 2016; Fragkoulidis *et al.*, 2018) to circumglobal Rossby waves (Branstator, 2002; Xu *et al.*, 2021). Circumglobal waves are those which extend around most of a latitude band, and they have been linked to extreme events (Boers *et al.*, 2019) and are particularly relevant for weather extremes occurring concurrently across a hemisphere (Kornhuber *et al.*, 2019, 2020).

European temperature extremes have been associated with blocking anticyclones which form at the exit of the north Atlantic storm track (Kautz *et al.*, 2022). Strong localised blocking anticyclones over Europe can be part of a larger wave pattern, associated with a slowly evolving, latitudinally extended quasi-stationary wave (QSW) (Wolf *et al.*, 2018). Summertime heatwaves and droughts can therefore be linked to strong blocking anticyclones that are part of a larger wave signal (Kornhuber *et al.*, 2017). Additionally, anomalously persistent, high-amplitude Rossby waves were identified as being present in several cases of extreme weather during summer months in recent years, including the July 2003 heatwaves in Europe, the July 2018 heatwaves in Scandinavia and Iberia and the June 2021 heatwave in western Canada (White *et al.*, 2022). Of particular interest in this study is the identification of a second, high latitude Rossby wave in each of these months which is not present in the climatology. The presence of a double wave structure over Eurasia (one in midlatitudes and one in high latitudes) is consistent with other work which suggests a double jet structure is important for extratropical extreme weather events (Kornhuber *et al.*, 2017; Xu *et al.*, 2021; Rousi *et al.*, 2022). It has also been shown that the waveguide effect of the polar front jet (PFJ) is strongest in summer and the presence of amplified planetary wave activity along the PFJ has been linked to the occurrence of summer heatwaves over Eurasia (Xu *et al.*, 2021). While waveguides are not specifically investigated in this thesis it is worth noting that they are present and may have an influence on the wave amplitude over Eurasia.

It has been suggested that periods with increased QSW activity lead to more extreme weather conditions, while periods with attenuated QSW activity tend to have average weather conditions (Screen and Simmonds, 2014). Wolf *et al.* (2018) examined the amplitudes of QSWs for periods when extreme 7-day temperature anomalies occurred in western Europe. For all seasons they find the temperature extremes are connected to very strong, high-amplitude QSWs. The extreme hot anomalies in particular were associated with zonally elongated regions of enhanced QSW amplitudes, indicating the extreme events were also connected to a long-lived, extended wave pattern as well as a strong local block. In most of their event composites, the QSW does not form a complete zonal wave, indicating a local amplification of the QSW occurs during the extreme events. The authors also examined the QSW links to extreme rainfall events, using the 7-day running mean of total rainfall for the western Europe region. In this case, all seasons except winter were shown to have a highly statistically significant QSW and a large-scale trough over the region associated with the rainfall extremes. QSW patterns can therefore feasibly increase the prediction skill for weather extremes in regions that are remote from the wave source (Wolf *et al.*, 2018)

While it has been shown that high-amplitude quasi-stationary Rossby waves can lead to extreme events, the mechanisms through which this occurs are still unclear (White *et al.*, 2022). Current ideas include quasi-resonance, whereby waveguide-trapped waves can resonate with stationary forcing from orography (Petoukhov *et al.*, 2013), and phase locking of the waves whereby there is an observed preference for the wave ridges and troughs to reoccur over the same regions as the disturbance of mid-altitude flow by large-scale orography and land-ocean boundaries can have an effect on the preferred phases of Rossby waves (Kornhuber *et al.*, 2020). A handful of studies have identified that Rossby waves with certain zonal wavenumbers appear to be related to extreme weather conditions (Fragkoulidis *et al.*, 2018; Kornhuber *et al.*, 2019, 2020; Tuel *et al.*, 2022). These are generally higher wavenumbers within the synoptic-scale range of 5-8 (White, 2019). Waves with these wavenumbers tend to have preferred phase locations and can often form circumglobal teleconnections (Petoukhov *et al.*, 2013; Kornhuber *et al.*, 2019; Di Capua *et al.*, 2020). This can lead to an increased likelihood of amplified waves occurring in the same global position repeatedly, with subsequent impacts on extreme weather events such as temperature anomalies.

Studies investigating ways in which Rossby waves can influence extreme rainfall events in the midlatitudes have so far focused on longer term events (Hirata and Grimm, 2016; Wolf *et al.*, 2018; Kornhuber *et al.*, 2019, 2020) with a few studies looking at daily rainfall events (Barton *et al.*, 2016; Röthlisberger *et al.*, 2016b; de Vries, 2021; Barton *et al.*, 2022) and none looking at sub-daily events. This is understandable given the large-scale nature of Rossby waves and the small-scale of (sub-daily) rainfall events, however, as previous studies have shown, there are identifiable connections between large-scale atmospheric circulations and sub-daily rainfall extremes (Weder *et al.*, 2017; Allan *et al.*, 2019; Barbero *et al.*, 2019b; Champion *et al.*, 2019; Moron *et al.*, 2019;

Haacke and Paton, 2021) and therefore it is not impossible for there to exist a link between certain Rossby wave configurations and the occurrence of sub-daily rainfall extremes. A strong link between the breakdown of heatwaves and short-duration rainfall extremes has also recently been identified for mid-latitude regions (Sauter *et al.*, 2023). Given the previously mentioned links between heatwaves and (quasi-stationary) Rossby waves, there is feasibility for a connection between the sub-daily rainfall extremes and Rossby waves via heatwaves.

2.5.1 Local Finite Amplitude Wave Activity Metric

There are a multitude of different methods used to detect and characterise Rossby waves. These include looking at potential vorticity contours (Röthlisberger *et al.*, 2016a; de Vries, 2021), geopotential height (Gelbrecht *et al.*, 2018) and meridional wind (Fragkoulidis and Wirth, 2020). The majority of these methods involve using specific metrics such as sinuosity, or reconstruction of the envelope of the meridional wind field, or specific forms of wave activity flux to detect Rossby wave activity within the atmospheric variable being studied (Ghinassi *et al.*, 2018). While these methods are useful to evaluate global or regional changes in wave activity or meanders in the jet stream, it is not possible to use them to identify true local features due to assumptions made within these methods that waves must be linear and/or small amplitude. Most observed waves do not conform to these assumptions, having large amplitude or showing strongly non-linear behaviour such as wave breaking or cutoff formation (Ghinassi *et al.*, 2018). Additionally, it could be misleading to use measures based on contour elongation alone as proxies of extreme weather events that depend on the intensity of local anomalies (Martineau *et al.*, 2017). The finite amplitude wave activity (FAWA) index created by Nakamura and Zhu (2010) was developed as a solution to this problem as it obeys exact conservation relations even for large-amplitude waves. However, the FAWA index is defined by zonally averaged quantities and as such is not well suited for diagnosing the dynamics of transient synoptic-scale Rossby waves. Therefore, Huang and Nakamura (2016) created an extension of FAWA, the Local Finite Amplitude Wave Activity (LWA) metric, which is capable of quantifying regional disturbances in the atmospheric circulation (Martineau *et al.*, 2017).

The LWA is a function of both latitude and longitude and recovers FAWA upon zonal averaging. This diagnostic provides information on the local waviness of the flow whilst remaining valid for finite-amplitude eddies (Huang and Nakamura, 2016; Ghinassi *et al.*, 2018). While FAWA links the patterns of atmospheric circulation to large-scale wave dynamics mathematically, the LWA can better capture local wave amplification (Chen *et al.*, 2015) and also has the advantage of having a dynamical basis, rather than being based on mathematical diagnostics of blocking or jet meanders (Martineau *et al.*, 2017). The LWA does not only take into account the meridional displacement of

(PV) contours as other waviness diagnostics do but also examines the strength of enclosed anomalies, remaining valid for both large and small displacements and providing a more robust measure of waviness (Chen *et al.*, 2015; Martineau *et al.*, 2017). This feature is particularly relevant for examining conditions associated with extreme weather events, which may depend on the strength of the circulation anomalies instead of/as well as their extent. Further details on the LWA and its calculation are given in Chapter 5.

2.5.2 Using LWA as a diagnostic of mid-latitude weather

Since its conception, the LWA has been used in several studies investigating the relationship between wave activity and extreme midlatitude weather events. The first of these was in the original Huang and Nakamura (2016) study introducing the LWA. Here the LWA was used to study the blocking episode which steered Superstorm Sandy into the US in October 2012. For the days surrounding the event, the LWA showed a quasi-stationary feature which remained in place for ~2 days and eventually split into two vortices. This closely reflected the location and magnitude of the block which was associated with Superstorm Sandy, indicating the LWA was capable of detecting blocking.

The LWA was subsequently used by Chen *et al.*, (2015) with z500 (instead of the PV used by Huang and Nakamura (2016)) as this variable is linearly related to PV at 500 hPa and it is widely used to characterise synoptic weather events, making the results more easily comparable with previous studies. They investigate the LWA associated with 4 high-impact, temperature related weather events. Their results show the LWA is a natural diagnostic of the blocking highs and cutoff low associated with temperature extremes in Paris, Moscow and Chicago.

Martineau *et al.* (2017) also used LWA with z500 to quantify wave activity. They state that the LWA used in this way 'can be thought of as a hybrid method bridging the gap between wave amplitudes measured as departures from zonal symmetry and methods investigating the meridional displacement of contours'. These authors split the LWA into its cyclonic (LWA-c) and anticyclonic (LWA-a) components to investigate the nature of local anomalies in the form of extreme 'wave events'. Regional temperature extremes were found to be more likely under the large-amplitude troughs and ridges of the extreme wave events.

2.6 Forecasting of sub-daily extremes based on large scale dynamics

Extreme rainfall is one of the most challenging variables to forecast (Sukovich *et al.*, 2014). Even in state-of-the-art forecast systems, skill in predictions of extreme rainfall rarely extend more than 5 days ahead (Lledo *et al.*, 2023). The most obvious benefit to using large-scale dynamics in the forecasting of sub-daily rainfall extremes is the advance warning this can provide for pluvial and flash flooding events. The description of the atmospheric patterns associated with extreme rainfall can help in their early identification by operational forecasters, by recognizing analogs alongside output fields predicted by forecast models (Merino *et al.*, 2016). This contextual information of atmospheric precursors to sub-daily extremes could also be of benefit for forecasts of flash flooding (Allan *et al.*, 2019). Skill in forecasting of large-scale atmospheric circulation is generally higher than for rainfall, thereby allowing identification of circulation conditions leading to potential extreme rainfall up to 10-days in advance (Lavers *et al.*, 2014, 2018; Baker *et al.*, 2018; Dorrington *et al.*, 2023). Richardson *et al.,* (2020) have shown how probabilistic forecasts of the MO30 patterns can be used to provide warning of periods with increased risk of fluvial flooding in the UK with lead times of over 5-days. Similarly, using weather patterns previously identified to be related to localised extreme rainfall events over the Mediterranean for indirect predictability of extreme daily rainfall was shown to result in skilful predictions for up to ~10 days lead time for many locations (Mastrantonas *et al.*, 2022b). Mastrantonas *et al.* (2022a) further assessed the skill of extreme 3-day rainfall forecasts from different forecasting strategies, identifying the use of pre-defined circulation patterns combined with the extremity state of local moisture predictors (e.g. water vapour flux) to be the most skilful for lead times beyond 7 days. These studies all indicate the utility of atmospheric circulation patterns in providing longer-lead time forecasts of extreme daily rainfall from models which are relatively simple and computationally cheap to run (Richardson *et al.*, 2020). There is therefore potential for a similar methodology to be applied to sub-daily rainfall.

Mohr *et al.,* (2020) argue that an increased understanding of the relationship between atmospheric blocking and deep moist convection could enhance the forecast horizon of thunderstorms on sub-seasonal timescales beyond the classical weather forecast timescale of a few days, due to the persistence associated with the block. However, this link is only helpful if the blocking is correctly predicted, which remains a challenge for numerical weather prediction models (and climate models) (Ferranti *et al.*, 2015) which often underestimate the blocking frequency in the Euro-Atlantic sector (Quinting and Vitart, 2019). The importance of capturing the sequence of atmospheric events leading up to an extreme weather event was highlighted by Oertel *et al.* (2023) in their study of factors limiting the predictability of the strength of the blocking anomaly and subsequent extreme heatwave in the Pacific Northwest in June 2021. The authors found dynamical processes on a range of spatiotemporal scales (from extreme rainfall over SE Asia to diabatic amplification of upper-level Rossby waves) formed a linked system of precursors to the heatwave. It is therefore necessary for long to medium-range forecasts to take into account the larger picture of atmospheric dynamics, rather than focussing on individual features. This necessity of examining the atmospheric drivers of extreme weather events at a larger spatial scale is also noted by Allan *et al.* (2019).

Despite much investment in flood protection methods, flooding remains a significant hazard throughout Europe (Kundzewicz *et al.*, 2014). The projected increase in frequency and intensity of extreme sub-daily rainfall over much of Europe (Chan *et al.*, 2020) is likely to lead to an increase in probability of pluvial and flash flooding in regions where floods are often triggered by intense summer rainfall (Kundzewicz *et al.*, 2006, 2014). Early warning information on floods is vital to allow national and international civil protection authorities to make decisions on how to prepare for the upcoming floods (Pappenberger *et al.*, 2015). An example of this is the Howard Hanson Dam flood risk management crisis in Seattle in 2009. The Dam showed signs of failure, thereby necessitating improved forecasts (including longer lead times) of extreme rainfall by the American National Weather Service to allow evacuations to be carried out if necessary (Sukovich *et al.*, 2014). Early flood warning therefore has multiple benefits, including of course the reduction in loss of life, but also economic and infrastructure benefits. It may be possible, with advance warning providing the time to run urban flood models, to enable identification and protection of high-value infrastructure which may be at risk from flash floods (Flack *et al.*, 2019). The benefits of delivering early warnings using the European Flood Awareness System were estimated to save 400 euros for every 1 euro invested, with improved forecast performance alone increasing the cost benefit ratio of preventative action to 1:202 (Pappenberger *et al.*, 2015). Incorporating large-scale dynamics in forecasts could contribute to such improvements.

2.7 Summary

Previous climatological investigations of rainfall in Europe have been introduced, with the need for a climatology of sub-daily extremes specifically emphasized. This clear research gap is filled in Chapter 3. This chapter has also highlighted the substantial body of research on dynamical drivers of extreme rainfall, yet only a handful of these have focussed on sub-daily extremes (Allan et al., 2019; Barbero et al., 2019b; Champion et al., 2019; Manola et al., 2019; Cipolla et al., 2020). Given the focus in this thesis on using WPs as indicators of the atmospheric circulation occurring in connection with extreme events, this chapter concentrated on reviewing other studies which utilise these features. The vast majority of these looked at daily or longer rainfall, with those that do investigate WP-sub-daily rainfall links in Europe being focussed on Germany (Weder et al., 2017; Brieber and Hoy, 2019; Haacke and Paton, 2021). This scarcity of attention so far on the large-scale drivers of sub-daily rainfall extremes in Europe is motivation to investigate this relationship using new rainfall data and a recently developed set of WPs, for a wider geographical region than previously considered. Additionally, there is a clear opportunity for assessing the connections of sub-daily rainfall with hemispheric scale circulations in the form of Rossby waves, which have previously been found to influence extreme rainfall events at daily and longer time scales (e.g. Martius et al., 2008; Barton et al., 2016; Kornhuber et al., 2019; de Vries, 2021). This connection between sub-daily weather extremes and atmospheric circulation at the scale of Rossby waves represents a new line of research. The utility of identifying links between large-scale atmospheric dynamics and sub-daily extremes for operational forecasting has been shown, with strong potential for improving the lead-time of short-duration extreme rainfall forecasts and the added benefit of advanced warning of pluvial flooding.

Chapter 3

A gauge-based sub-daily extreme rainfall climatology for western Europe

The material in this chapter has been published in the following article:

Whitford, A.C., Blenkinsop, S.B., Pritchard, D., Fowler, H.J. (2023). A gauge-based sub-daily extreme rainfall climatology for western Europe. *Weather and Climate Extremes*, 41, 100585.

Part of the introduction of this journal article has been moved to Chapter 2 of this thesis. Minor changes have been made to make the article more coherent in the context of this thesis.

3.1 Introduction

Sub-daily extreme rainfall events can cause significant socioeconomic and physical damage, alongside loss of life, due to their ability to generate destructive flash floods and debris flows (Doe, 2004; Marchi *et al.*, 2010; Borga *et al.*, 2014; Gaume *et al.*, 2016; Archer and Fowler, 2018). Urban areas are particularly vulnerable to flash flood events due to outdated drainage infrastructure and high levels of impermeable surfaces, leading to surface water flooding (Westra *et al.*, 2014; Dale, 2021; Fowler *et al.*, 2021b).

With this expected increase in extreme sub-daily rainfall intensities in a future warmer climate, it is reasonable to infer that the associated negative impacts will also increase (Sharma *et al.*, 2018). For example, surface water flooding has been identified as one of the most significant climate change risks to infrastructure in the UK (Dawson *et al.*, 2016; Jaroszweski *et al.*, 2021), with the risk projected to double under a 4°C warming future scenario, resulting in an expected annual damages increase from the current ~£0.6bn to ~£1.2bn by the 2080s (Sayers *et al.*, 2020). Improving flood adaptation strategies requires a detailed understanding of where and when extreme sub-daily rainfall events occur in the current climate, in order to develop robust models for how these events may evolve in the future (Alexander *et al.*, 2019).

3.1.1 Rainfall Indices

Indices are one of the simplest ways to investigate climatic extremes due to their comparability across geographical regions and with each other (Donat *et al.*, 2013b; Alexander *et al.*, 2019). They have been used to examine rainfall characteristics for several decades, since the development of standardised definitions of daily climate extremes at the beginning of the 21st century (Klein Tank *et al.*, 2002; Peterson and Manton, 2008). The use of indices has facilitated the characterisation of daily rainfall extremes and the monitoring of their long-term changes over large areas of the globe, providing useful information for climate modellers and hydrologists (Alexander *et al.*, 2006; Donat *et al.*, 2013b; Lewis *et al.*, 2019). Work by the Expert Team on Climate Change Detection and Indices (ETCCDI) led to the generation of a set of standard indices, 10 of which can be used to assess daily rainfall extremes (Alexander *et al.*, 2019). Several studies have used selections of these indices to investigate daily extreme rainfall, especially since the development of the European Climate Assessment & Dataset (ECA&D) (Klein Tank *et al.*, 2002) and HADEX/HADEX2 datasets (Alexander *et al.*, 2006; Donat *et al.*, 2013b), although these studies have mostly focussed on identifying trends (e.g. Moberg *et al.* (2006); Donat *et al.* (2013); Cioffi *et al.* (2015)), rather than developing climatologies.

However, indices based solely on daily data may mask some of the most intense short-duration events that can lead to flash flooding, especially in the case of convective extremes, which have been found to be significantly underestimated by operational rain gauge networks (Schroeer *et al.*, 2018; Alexander *et al.*, 2019; Lengfeld *et al.*, 2020). A lack of long-term records of high quality observations has so far prevented similar analyses at the sub-daily scale (Zhang *et al.*, 2017; Alexander *et al.*, 2019) and there remains an incomplete understanding of the variability of these events under the current climate (Westra *et al.*, 2014; Barbero *et al.*, 2019a; Lewis *et al.*, 2019; Fowler *et al.*, 2021b). However, the INTENSE (INTElligent use of climate models for adaptation to non-Stationary hydrological Extremes) project has led the collection and assessment of sub-daily rainfall observations from around the globe, forming the first comprehensive global-scale sub-daily rainfall dataset (GSDR; Lewis *et al.*, 2019, 2021).

Several studies have already used the GSDR dataset to investigate regional and continental changes to the frequency and intensity of sub-daily extremes, particularly in Australia (Guerreiro *et al.*, 2018) and North America (Barbero *et al.*, 2017). Barbero *et al.* (2019a) used the GSDR dataset to look at the seasonal and diurnal distribution of an index of 1-hour annual maximum rainfall (AMP-1hr) for the US, Australia, the British Isles, Japan, India and Malaysia to compare regions of varying climate which have good data availability. Beck *et al.* (2020) used the GSDR data and other sources to develop a global climatology dataset based on a suite of occurrence and intensity indices for daily and sub-daily rainfall. The occurrence indices were based on threshold values and the intensity indices on return periods and were calculated using neural networks. On a more local scale, Blenkinsop *et al.* (2017) and Darwish *et al.* (2018) both investigated sub-daily rainfall extremes in the UK, focussing on the spatial and temporal distribution of the events. However, there remain very few studies investigating sub-daily rainfall in detail over the wider European region, despite the significant impacts associated with flash floods across Europe (Gaume *et al.*, 2009; Marchi *et al.*, 2010).

To provide a more comprehensive analysis of continental-scale extremes, a set of indices for extreme sub-daily rainfall (GSDR-I) has been derived from the GSDR dataset (Pritchard *et al.*, 2023). These indices are listed in Table 3.1 and further details on the methods used to calculate them are provided in Section 3.2 and in Pritchard *et al.* (2023).

Index Group	Abbreviation	Explanation	Units
		GSDR-I indices and summary statistics	
Intensity (Maxima)	Rx*H*hr H can be 1, 3 or 24 to denote the time aggregation of the index e.g. Rx3hr	Annual maxima based on rolling window aggregations. Provided here as the mean of the annual maxima timeseries for each gauge.	mm
Intensity Summary (Maxima)	Rmed	The median value of the seasonal Rx*H*hr series at each gauge.	mm
Intensity Summary (Percentile)	R*Q*p*H*hr Q indicates the percentile (99^{th} or 99.9^{th}) e.g. RR99.9p3hr	Wet hour percentiles (99^{th} and 99.9^{th}). The specified percentile value based on the full record period for wet hours only (hours with >0.1mm).	mm
Contribution (Percentile)	R*Q*p*H*hrP e.g. R99.9p3hrP	Percentage contribution to seasonal or annual rainfall totals by *H*-hour intervals exceeding the *Q*th (99^{th}/99.9^{th}) wet-hour percentile. E.g. if the sum of rainfall in Jan 2000 for hours exceeding the (Jan) 99th percentile is 20 mm and the Jan 2000 month total is 200 mm, this index would have a value of 10%. While this index is a time series, the wet hour percentile thresholds are calculated based on the full record period.	%
Contribution (Percentile)	Rx*H*hrP e.g. Rx3hrP	Percentage contribution of Rx*H*hr to the total rainfall on that day.	%
Frequency	R*H*r*T*mm T indicates the threshold value e.g. R3hr20mm	Count of hours (or multi-hour intervals) greater than the chosen threshold. Provided here as the mean count in each year/season.	Hours
General	NWH	Number of wet hours. Annual or seasonal count of the hours with >0.1 mm rainfall	Hours
		Summary statistics developed for this paper	
Diurnal Cycle Summary	Rx*H*hrDC e.g. Rx3hrDC	Proportional frequency of occurrence of the time window associated with the *H*-hour annual maxima at each gauge. The time associated with Rx*H*hr annual maxima marks the end of the *H* hour accumulation interval.	Hours
Contribution Summary (Percentile)	Rd*T*mm*H*hrP e.g. Rd20mm3hrP	Contribution to days with rainfall >*T* mm from the maximum *H*-hour period on that day. If the daily total is 24mm and the maximum 3-hour rainfall on that day is 12mm then this index has a value of 50%. The contribution values are averaged across the period being examined.	%

Table 3.1: descriptions of the GSDR-I indices and summary statistics analysed in this paper. Details of the diurnal cycle and contribution summary statistics developed specifically for this work are also provided.

The code to calculate these sub-daily indices was developed as part of the INTENSE project and performs quality-control checks on the data before calculating the index values (The code is available at https://doi.org/10.5281/zenodo.7492877). The GSDR-I python library has already been used by Lakatos *et al.* (2021) to calculate sub-daily indices for the Pannonian Basin region between central and southeast Europe. Their results reveal large spatial variability across the region for both the mean and maximum annual 1-hour rainfall maxima, with the highest maxima values occurring mostly towards the centre of the region, while the most intense rainfall occurred in summer.

While the above studies all provide valuable information on sub-daily rainfall (extremes), they mostly focus on individual countries or regions and on trends rather than climatology. In this paper, we provide the first extreme sub-daily rainfall climatology for large regions within western Europe, generated from a new set of rainfall indices (Pritchard *et al.*, 2023). In doing so we provide information for a region that has so far (with the exception of the UK) been largely neglected by sub-daily rainfall analyses, despite having a good coverage of observational data, and we demonstrate the kind of detailed analysis that can be undertaken with the high-quality GSDR-I data. The rest of this chapter is structured as follows: section 3.2 describes the data and methods used in the analysis while section 3.3 provides the climatology results followed by the discussion and conclusions in section 3.4.

3.2 Data and Methods

The GSDR dataset is the first single repository of global sub-daily rainfall data with the same units of measurement and temporal resolution, with all data quality-controlled to the same standard (Lewis *et al.*, 2019, 2021). This dataset goes a long way towards resolving the issues of rainfall data availability and processing differences between different countries and meteorological agencies. However, there is significant variation in record length and completeness between participating countries and the number of gauges varies over time. These limitations mean that while the climatology presented here covers a substantial part of western Europe, it does not cover the whole region and data-sharing restrictions prevent the involvement of some countries completely, resulting in several areas lacking data. However, with the code to calculate the indices freely available we are hopeful that these gaps could be filled by data licence holders. It should also be noted that there are several inherent shortcomings associated with observation based rainfall datasets, from systematic rain gauge under-catch due to wind (especially in winter) to evaporation losses (especially in summer) (Paulat *et al.*, 2008). The GSDR data has been used to develop a set of global rainfall indices – GSDR-I. Full details on the development and calculation of the GSDR-I dataset is available in (Pritchard *et al.*, 2023). The indices in the GSDR-I dataset were chosen following discussions with climate observation and modelling experts, to provide a suite of the most useful indices for the community (Pritchard *et al.*, 2023). Of the GSDR data available for Europe, only a small percentage of the gauge records are of a suitable length for trend analysis (>30 years), with the majority of gauges having record lengths of 10-20 years (Table 3.2).

Therefore, we do not investigate trends in the indices. A final point to be made here is the difficulty of developing a traditional climatology from sub-daily rainfall records which are almost all shorter than the 30-years minimum length usually required. To have the spatial coverage required for a useful climatology of rainfall we have retained gauges with short records, but this invokes the caveat of using records of varying length in this analysis, which may cause biases at individual gauges. Consequently, whilst the overall picture drawn from this data is a credible representation of the climatological distribution of extreme events in western Europe, the available sub-daily data cannot provide as precise a climatology as one created from daily rainfall data.

The geographical coverage of this data is extensive; however, the variation in density of gauges between regions makes inferring spatial patterns for some regions much easier than others. For example, whilst the data presented covers large parts of central and western Europe, the dense gauge coverage in the UK makes identifying spatial patterns here more effective than for the sparse coverage in France. A map of the locations of GSDR gauges in Europe is presented in Figure 3.1. Data sharing restrictions differ between European nations, resulting in different levels of participation in the INTENSE project. However, the development of the indices using open-access code means it is possible for meteorological agencies to run the code on their data themselves and share the index results e.g. Lakatos *et al.* (2021).

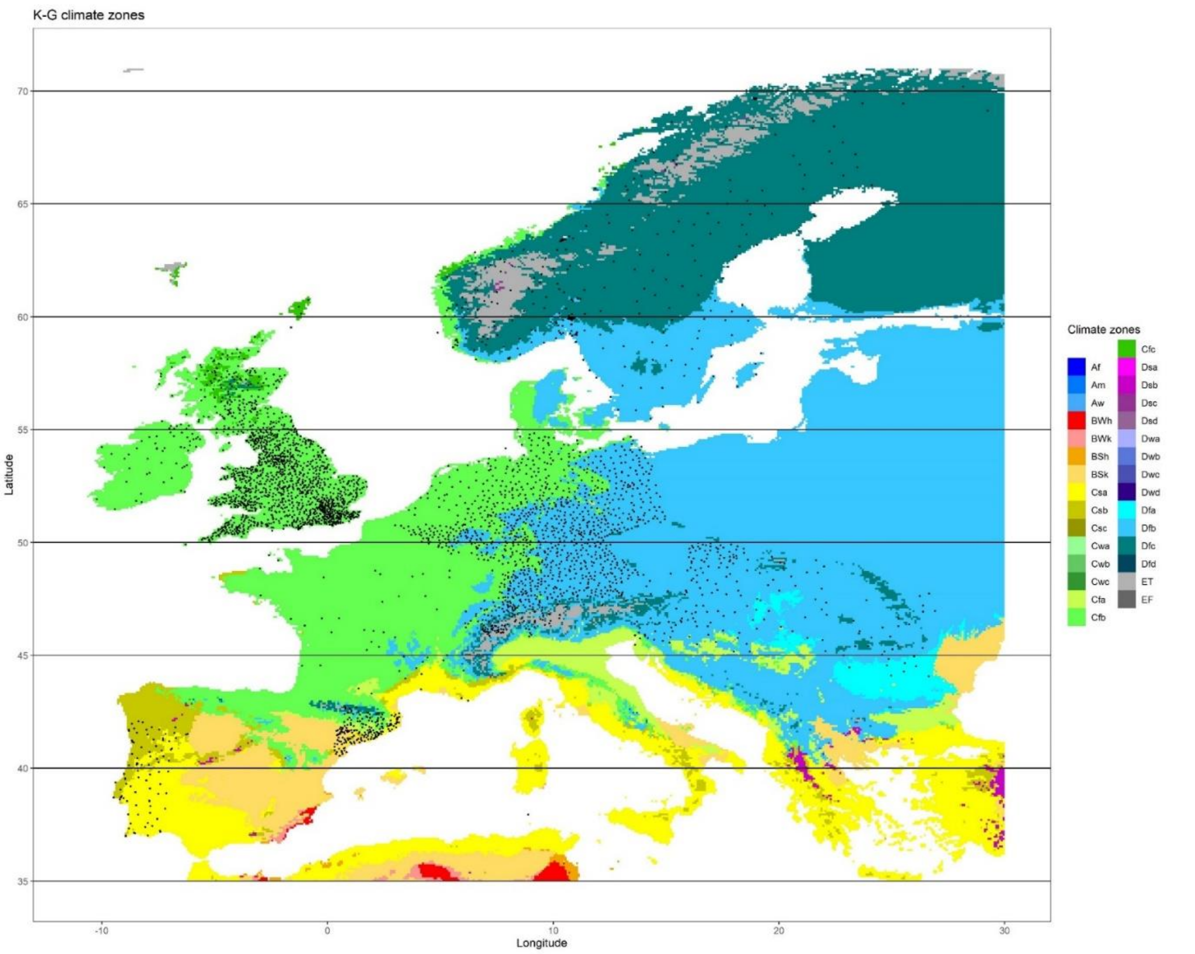

Figure 3.1: Map of GSDR gauge locations in Europe (black dots). Koppen-Geiger climate zones (colours) are also shown.

The GSDR dataset provides hourly data, which is then aggregated to 3-hours and 24-hours, using rolling windows for calculating annual/seasonal maxima indices and fixed windows for the remaining indices. The indices are available at monthly, seasonal and annual resolution, with publicly available gauge data accessible at https://doi.org/10.5281/zenodo.7492812. Seasons are defined as winter (December to February), spring (March to May), summer (June to August) and autumn (September to November). Most indices are available as a timeseries, e.g. annual maxima (Rx*H*hr, Table 3.1); however, for some statistics it is only possible to calculate a single summary climatological value from the entire record period, e.g. wet hour percentiles (R*Y*p*H*hr, Table 3.1), referred to as a supplementary statistic in Pritchard *et al.* (2023). For simplicity all values are referred to as indices here, but the summary statistics are specified in Table 3.1. For the time-series indices, a percentage completeness is calculated for the index values at each timestep. In this case the 80% completeness threshold (i.e. less than 20% missing data per temporal resolution) is used to filter gauge records that are suitable to use for index analysis. This strikes a balance between retaining enough data to develop a reliable index assessment and having consistent records, whilst matching the completeness level of the supplementary statistics (only available as calculated from either all available data or only data where 80% completeness is reached). When analysing the results, only gauges with more than 2 complete years of record are included. Relevant indices are available for both all-hour (including hours with 0 mm rain) and wet-hour only (hours with >= 0.1 mm rain, acknowledging that not all instruments measure to this precision) intervals, but only the wet-hour results are shown here in order to highlight the magnitude of extreme rainfall values that can be reached. Here, the 3-hour intervals are defined as wet if the total rainfall over the period is >=0.1 mm. As our aim is to produce a present-day climatology, using wet-hour indices will not incur the problems associated with changes in the frequency of wet days when analysing trends in heavy rainfall events over time, as discussed in Schär *et al.* (2016) . The diurnal cycle based on the timing of the RxHhr event has been calculated specifically for this paper, to provide greater understanding of the extreme rainfall climatology (and is not available as part of the GSDR-I dataset). The full list of indices used in this paper is provided in Table 3.1.

Country	**Time period covered by gauge records**	**Number of gauges with >2 complete years of data**	**Region the country is in**
Austria	1998-2019	35	Central
Belgium	2002-2015	83	Central
Catalonia	1990-2015	205	Southern
France	1991-2010	45	Southern
Germany	1996-2015	993	Central
Ireland	1940-2018	36	Northern
Netherlands	1951-2016	33	Central
Norway	1979-2016	200	Northern
Portugal	1958-2015	100	Southern
Sweden	1987-2016	120	Northern
Switzerland	1981-2015	149	Central
UK	1949-2014	1706	Northern
Pannonian Basin Region			
Czechia	1995-2020	51	Pannonian
Slovakia	1998-2019	17	Pannonian
Slovenia	1948-2018	29	Pannonian
Croatia	1981-2018	12	Pannonian
Hungary	1998-2020	29	Pannonian
Romania	2008-2020	44	Pannonian

Table 3.2: Data available for each country from the GSDR-I dataset, including countries that are part of the PannEx Region Project (Lakatos et al., 2021). Complete years have 80% of data for that year available. The locations of these gauges are shown in Figure 1

Each index in GSDR-I dataset has been developed to relate as closely to the ETCCDI indices as possible, providing sub-daily equivalents to the existing daily indices. It is worth noting however, that the ETCCDI indices describe the R10mm index (daily rainfall of 10 mm) as being a heavy rainfall day, whereas the GSDR indices identify hourly events with the same rainfall totals (e.g. R1hr10mm). The GSDR-I dataset therefore provides a climatology of much more intense events than the ETCCDI indices permit.

Assessing extreme weather events naturally generates the difficulty of obtaining a sufficient event sample as the detection probability decreases as the events become rarer (Klein Tank and Können, 2003; Moberg *et al.*, 2006). To ensure we have enough data to develop a consistent and spatially coherent extreme event climatology, all available gauge records are used regardless of the time-period they cover, provided they meet the data completeness and length criteria discussed above. The results of analysis of the indices are presented here on annual and seasonal timescales.

3.3 Results

While it would be possible to carry out smaller scale assessments with the GSDR-I data, the purpose of this paper is to provide an overview of the climatology of extreme sub-daily rainfall across western Europe. Therefore, for brevity and to reduce the effect of arbitrary country boundaries, the results are discussed within the context of a simplified geography consisting of four regions. Sweden, Norway, the UK and Ireland form the ‘Northern region’; Belgium, the Netherlands, Germany, Switzerland and Austria form the ‘Central region’ and Portugal, Catalonia and France form the ‘Southern region’. These three regions were designated based on areas that had similar rainfall characteristics during initial analysis of the indices. The fourth ‘Pannonian Basin region’ (comprising parts of the Czech Republic, Slovakia, Slovenia, Croatia, Hungary and Romania) is included where possible, as data for this region are not available for all the indices presented here and only on an annual rather than seasonal level. A detailed analysis of sub-daily indices for the Pannonian Basin region has already been carried out by Lakatos *et al.* (2021). The countries associated with each region defined above are outlined in Figure 3.2.

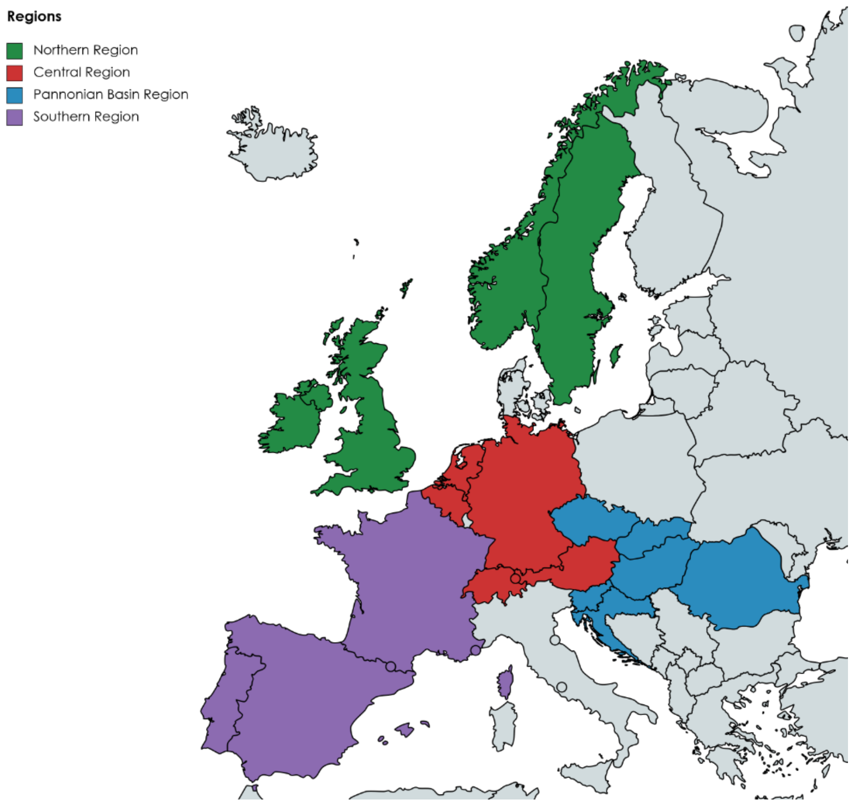

Figure 3.2: The four regions used for analysis of the GSDR-I results in this chapter.

Initial analysis of the number of wet hours (NWH) index was carried out to determine the general characteristics of sub-daily rainfall in Europe, with clear spatial and temporal patterns identified across the region. The mean annual NWH index (not shown) indicates the most frequent wet hours occur in the Northern region, particularly along western coastlines (up to 3000 hours per year) and in the Central region, particularly in Alpine areas. This agrees with the findings of Dietzsch *et al.* (2017) for consecutive wet days in Europe. The least frequent wet hours occur in the Southern region (just 500 hours per year in Southern Portugal) and the eastern Pannonian Basin. The seasonal NWH index (Figure 3.3) shows the lowest number of wet hours occurs in all regions in summer, while the highest values occur in winter in the Northern region (up to 1000 hours) and over the Alps.

The extreme indices were examined at both 1hr, 3hr and 24hr durations, although only 3hr and 24hr results are shown here as the spatial and temporal patterns between the 1hr and 3hr durations are very similar. This similarity between durations was also noted by Darwish *et al.* (2018) for the UK. In central western Europe, for events with rainfall intensities >40mm h^{-1}, (Meyer *et al.*, 2022) showed the duration of events which subsequently caused flash floods was around 90-120 minutes. The authors also point out that events above the 40mm h^{-1} threshold which caused flash flooding were generally longer duration than those which did not cause flooding.

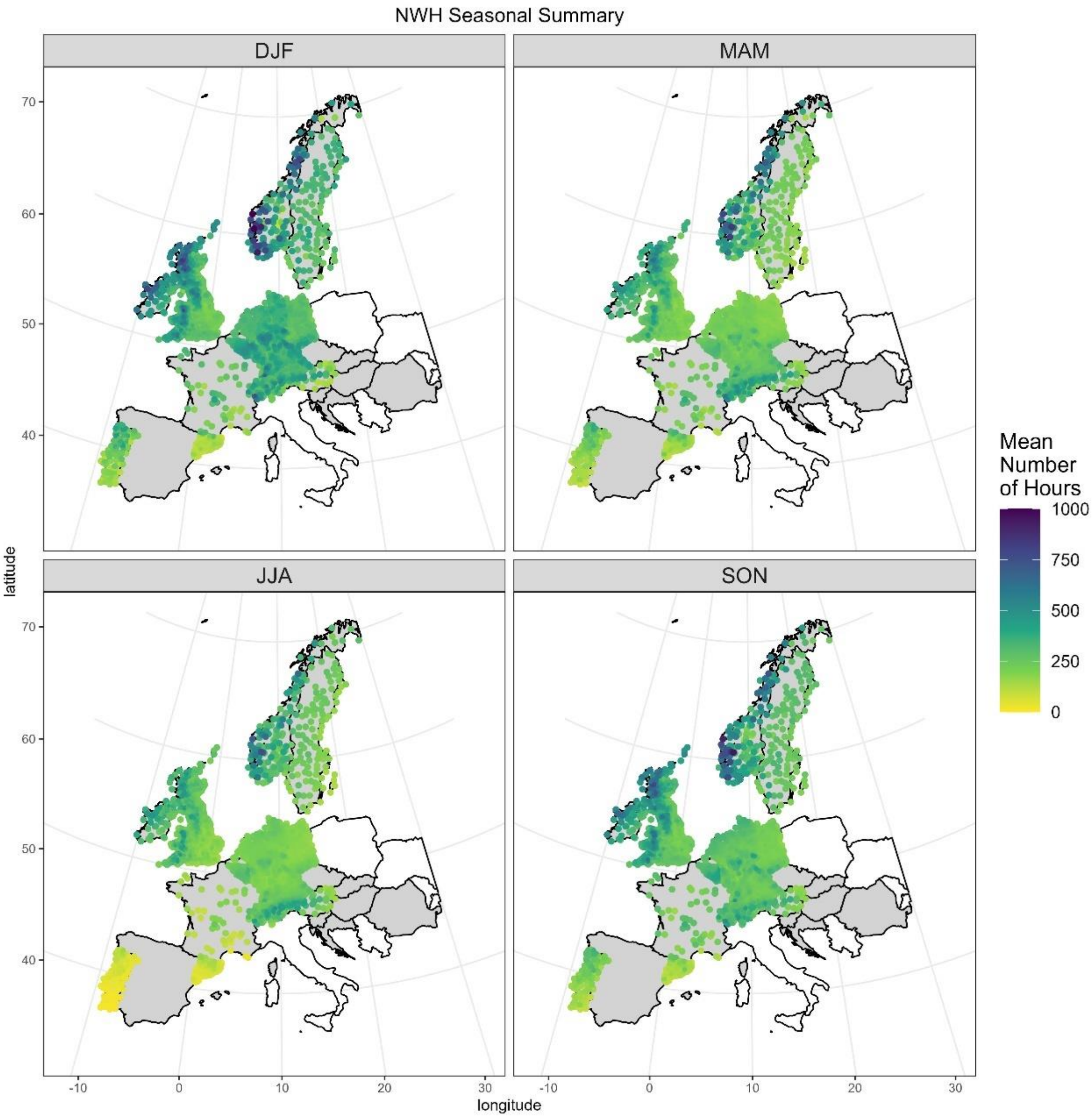

Figure 3.3: Number of wet hours (NWH) index seasonal mean values. Grey background denotes countries contributing data to the GSDR-I dataset (data for the Pannonian Basin region is only available at annual level).

3.3.1 Intensity Indices

Overall, the most intense 3hr annual maxima (Rx3hr) occur in the Southern region (Figure 3.4), with mean values of 20-40 mm, while the most extreme individual events occur in locations around the North-West Mediterranean and the Southern Alps. There are also notably high values in the Pannonian Basin region, while the Central and Northern regions generally have lower intensities, just 10-20 mm in 3 hours in the Northern regions (although with high individual outlier values, Appendix Figure A1).

Seasonal 3hr Rmed (median seasonal maxima, Appendix Figure A2) values are lowest across Europe in winter and spring and highest in summer and autumn. Northern and Central regions have highest median intensities (10-30 mm, up to 40 mm in a few locations) in the summer, while the Southern region shows highest intensities (up to 50 mm) in the autumn. There is a general west to east pattern of orographic influence to the 3hr Rmed results in the UK and Norway in winter and spring (Appendix Figure A2). This is consistent with the patterns identified for UK 1hr Rmed by Blenkinsop *et al.* (2017). The 3hr 99.9th percentile (R99.9p3hr) seasonal index shows similar spatial patterns to the 3hr Rmed index, with the highest threshold intensities in summer in Northern and Central regions (40-60 mm) and in autumn in the Southern region (up to 100 mm in areas around the NW Mediterranean) (Figure 3.5).

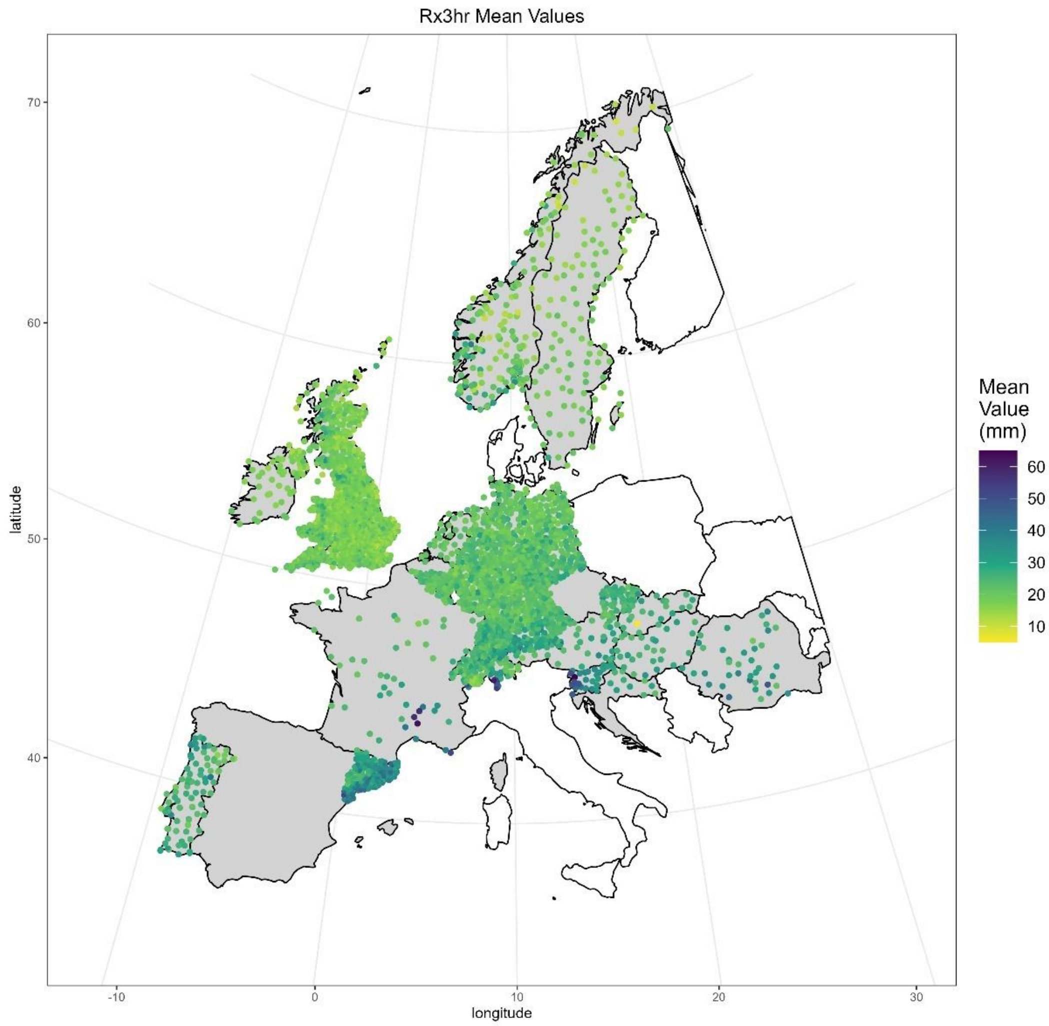

Figure 3.4: Annual maxima (Rx3hr) mean value at each gauge.

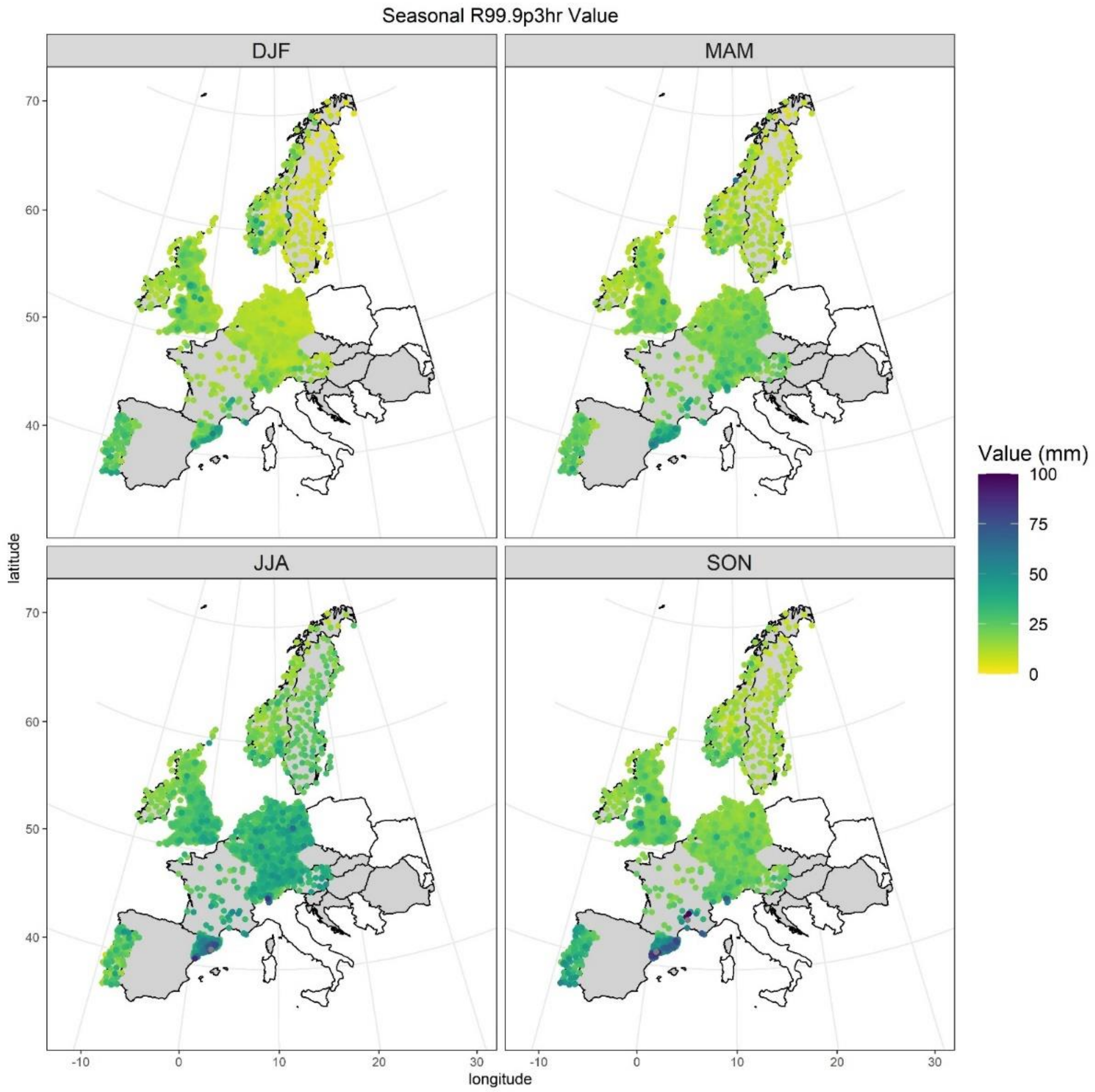

Figure 3.5: 3-hour 99.9th percentile seasonal values for each gauge (R99.9p3hr)

3.3.2 Frequency Index

The frequency of 3hr durations with rainfall exceeding 20 mm (R3hr20mm) is highest in summer in the Northern and Central regions and in autumn in the Southern region (Figure 3.6). In summer particularly high frequencies occur over the Alps (mean of 3-5 events), while in autumn high frequencies occur over the NW Mediterranean (up to mean of 6 events). The UK west coast also shows high frequencies in autumn, likely due to orographic enhancement of longer duration storms (Blenkinsop *et al.*, 2017). Across all regions there are very few 3hr events above the 20 mm threshold in winter and spring. The 30 mm threshold (not shown) has very similar temporal and spatial patterns albeit with lower frequencies, with highest mean values of 2 events (per season) in the Southern region in autumn. Comparison with the Rx3hr results in Figure 3.4 shows the fixed threshold value (20 mm) represents different portions of the rainfall distribution in different regions; hence we would expect higher R3hr20mm frequencies in the Southern region. The generally low values for the frequency index are in part due to the small chance that individual gauges will be within the footprint of an extreme event of this intensity, given the rarity of such an event and the small surface coverage of the gauge networks.

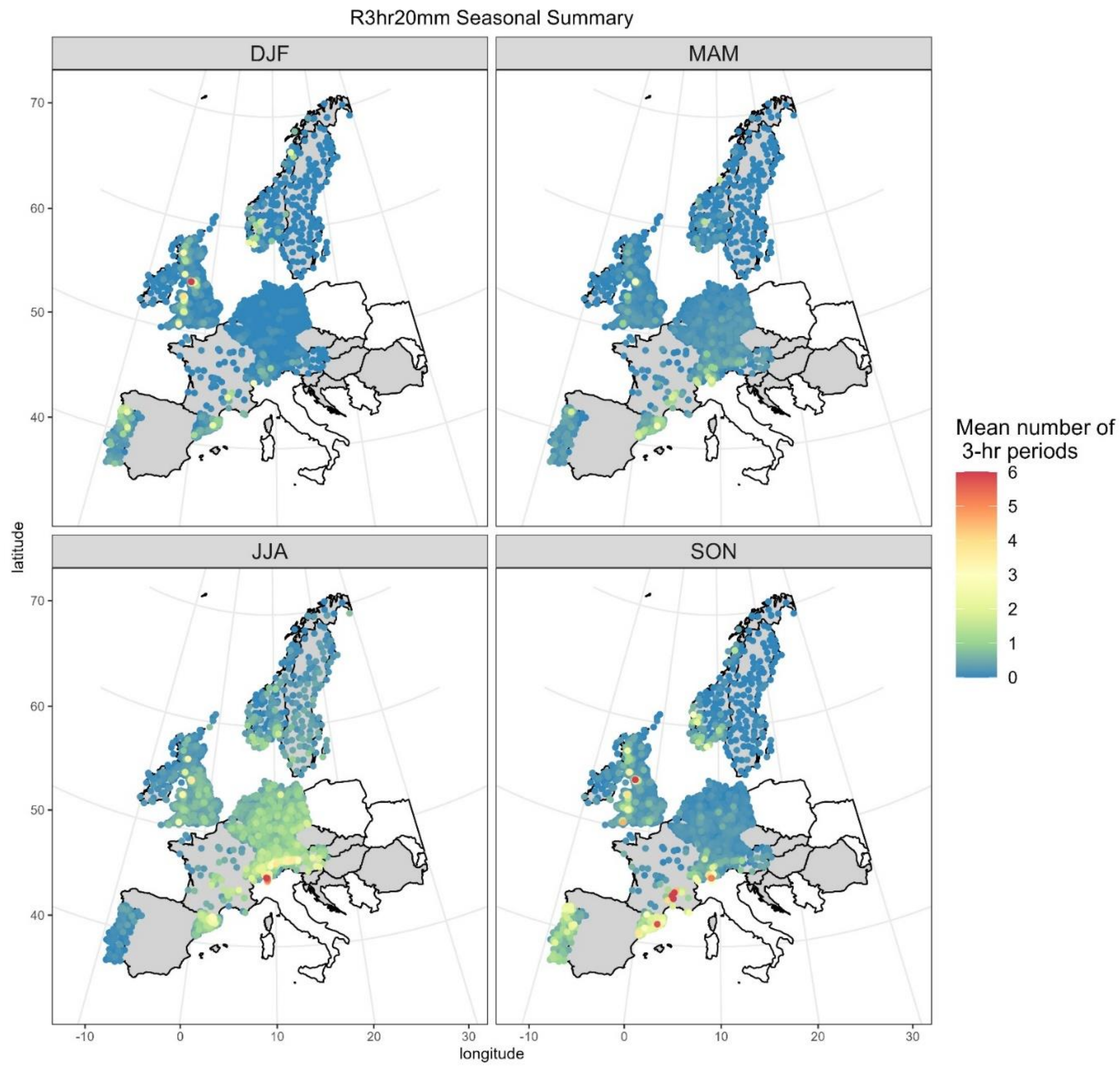

Figure 3.6: Seasonal mean frequency of 3-hour events above 20 mm (R3hr30mm)

3.3.3 Contribution Indices

The mean percentage of the daily rainfall total contributed by the 3hr annual maximum event (Rx3hrP) is highest in Central Europe and the Pannonian Basin, with values up to 95%, and lowest in the Northern region (and Portugal) with contributions of 50-60% (Figure 3.7).

Seasonally, the R99.9p3hrP index (Appendix Figure A3) shows the highest contribution in all regions in summer, with a mean contribution of around 5% in the Northern and Central regions and up to 8% in the Southern region. The other seasons (especially winter) have significantly lower contribution values in all regions. The contribution to the daily total from the maximum 3hr rainfall on days with >20 mm total rainfall (Rd20mm3hrP, not shown) is also highest in all regions in summer, with the greatest mean contributions reaching 60-70% in Central and Southern regions (albeit Portugal has highest values in autumn).

The different contribution index values in different regions and seasons are due to a variety of factors. The very low values in most of the Northern and Central regions in autumn and winter is largely due to the high NWH index values and lower intensities in these seasons, meaning the majority of rainfall is delivered in longer lasting, low intensity events. In contrast, the high contribution values in summer in all regions are due to the lower NWH values combined with higher intensities, indicating a few hours with high intensity rainfall can provide a large proportion of the daily (or even monthly) rainfall.

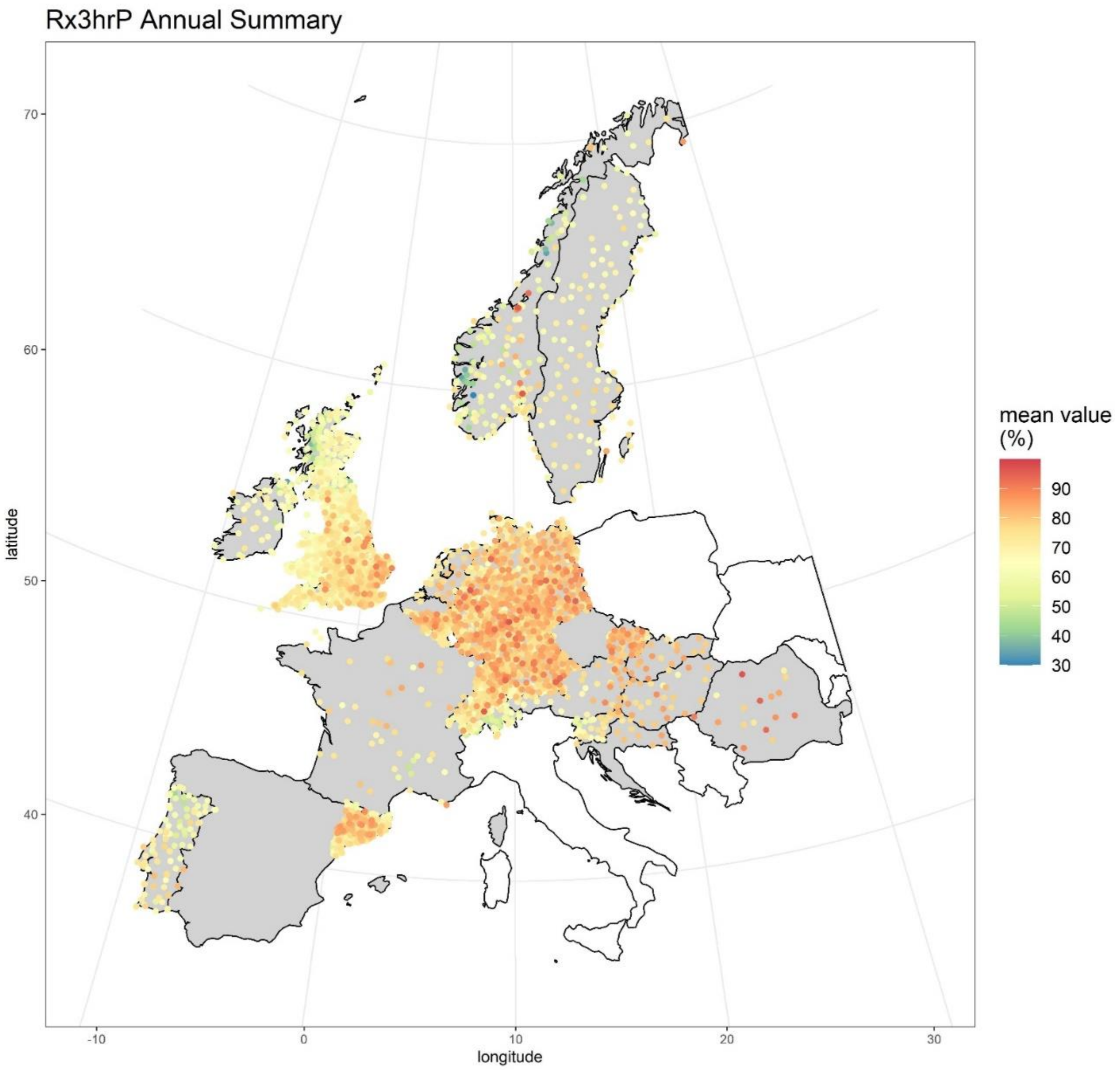

Figure 3.7: The mean percentage of the corresponding daily rainfall total contributed by the 3-hour annual maxima event (Rx3hrP)

3.3.4 Diurnal cycle index

We developed a diurnal cycle index for extremes by taking the time window of the Rx3hr events in each year of record at each gauge in the region and calculating the proportional frequency of occurrence for each 3hr period per season. Figure 3.8 shows a strong seasonal signal in the diurnal cycle in all regions. The Northern and Southern region both show a strong afternoon peak in event timing in summer, while the Central region has a slightly later peak. In spring there is a main late afternoon peak in all regions, with an additional evening peak in the Central region. None of the regions have a strong diurnal cycle in 3hr extremes in autumn or winter. Interestingly, despite the highest intensities occurring in autumn in the Southern region this is not accompanied by a strong diurnal cycle.

The general late afternoon to late evening peak found for all regions in summer agrees with the results of the global study of Barbero *et al*. (2019a). The seasonally-varying diurnal cycle observed here for the Northern region is consistent with the findings of Blenkinsop *et al.* (2017) and Darwish *et al.* (2018) for the UK, while the early evening peak in summer in the Central region agrees with previous results for the Czech Republic (Beranová *et al.*, 2018) and for continental European stations in general (Jeong *et al.*, 2011; Xiao *et al.*, 2018; Barbero *et al.*, 2019a).

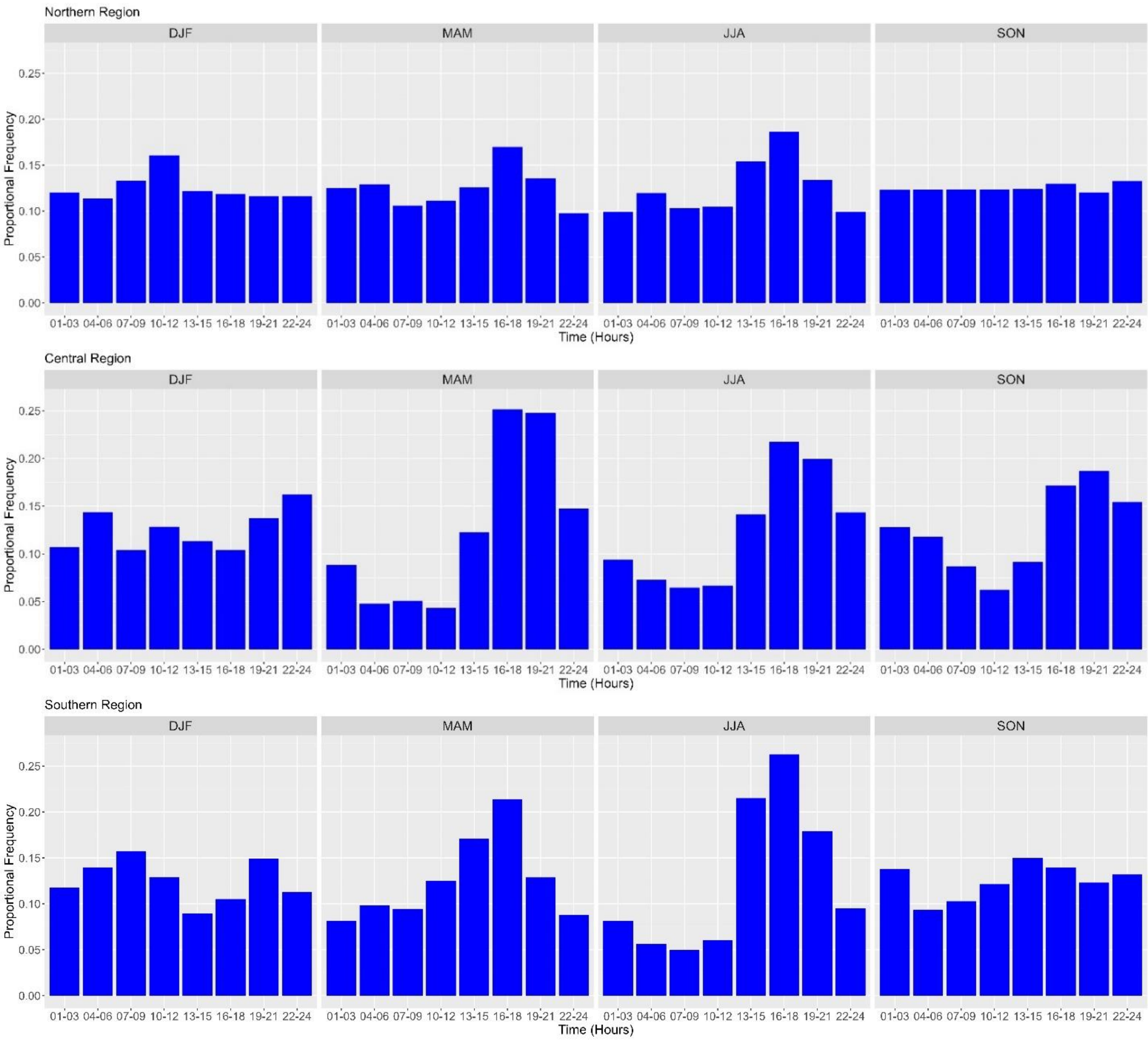

Figure 3.8: The seasonal diurnal cycle for the 3-hour annual maxima events in each region

3.3.5 *24-hour indices comparison*

To investigate the differences between daily and sub-daily indices, we now compare the 3-hour and 24-hour indices. While the same general spatial and temporal patterns remain, the R99.9p24hr index shows much weaker seasonality than the R99.9p3hr index, displaying similar values between the seasons with only a slight increase in summer (Figure 3.9). The R24hr30mm index shows a stronger seasonality than the intensity index, with a clear peak in summer in most regions, indicating an increased frequency of heavy events over 30 mm (Appendix Figure A4).

There is a strong signal of higher intensity and frequency of 24hr events along the western coastlines of the UK and Norway and over the Alps in autumn and winter (and to a lesser extent spring). This orographic effect is less obvious in the 3hr indices. This difference in orographic influence at different durations is also observed by (Barbero *et al.*, 2019a), who propose this indicates that the short duration extremes are mostly influenced by the moisture content of storms and are less susceptible to orographic enhancement effects. However, as seen from Figure 9, there remains some orographic influence of 3hr accumulations, likely part of longer duration storms, especially in the western UK and over the Alps in autumn and winter. An orographic influence on sub-daily extremes in the UK during these seasons was also identified by both Blenkinsop *et al.* (2017) and Darwish *et al.* (2018). Marra *et al.* (2021) identified an increasing intensity with duration for accumulations of longer than 1-hour over the SE Mediterranean mountains. This enhancement is likely due to the triggering and modification of convection by the local topography, due to rapid height variations over small horizontal scales resulting in atmospheric instability and the lifting of moist air (Wilkinson and Neal, 2021), which at these durations can evolve towards sequences of convective and stratiform-like processes, causing the well-known orographic enhancement (Marra *et al.*, 2021). However, the role of orography in the enhancement or generation of sub-daily extremes cannot be taken as a given. As shown in other studies on the Italian peninsula and Italian Alps there is not always a consistent relationship between topography and sub-daily rainfall intensity and local factors play a large role in varying this relationship (Formetta *et al.*, 2022; Mazzoglio *et al.*, 2022). At durations below 1-hour a reverse-orographic effect of decreasing intensity with elevation is well documented (Avanzi *et al.*, 2015; Marra *et al.*, 2021) but for durations between 2 and 6-hours the effect is less clear, with intensity sometimes enhanced but not consistently (Formetta *et al.*, 2022; Mazzoglio *et al.*, 2022). Coastal effects may also be important for short-duration extremes (Marra *et al.*, 2022) but this effect is not obvious here. This may be due to the sparse coverage of the rain gauge network relative to these effects.

The strong seasonality of the short-duration extremes compared to the weaker seasonal cycle in the 24-hour extremes reflects the difference in mechanisms causing the extreme rainfall. The short-duration extremes are strongly locked into the seasonal convective cycle while the longer-duration extremes are more strongly tied to large-scale circulations which occur throughout the year but particularly in autumn and winter (Blenkinsop *et al.*, 2017; Beranová *et al.*, 2018; Darwish *et al.*, 2018; Barbero *et al.*, 2019a). The Northern region, along with the western coastlines of France and Portugal, are areas where extreme rainfall in winter can often be influenced by atmospheric rivers, which could explain the high 24-hour winter index values in these areas (Lavers and Villarini, 2013; Champion *et al.*, 2015).

Figure 3.9: Seasonal 99.9th percentile values (R99.9pHhr) for a) 3-hour and b) 24-hour durations. For each duration the R99.9pHhr values for all gauges are ranked to give a distribution of all the values. The colour scales represent where each gauge lies within five equally distributed percentile bins for that season, enabling comparison of the relative intensity between different regions. For example, dark blue indicates that the index value at that gauge lies between the 80th and 100th percentile of all results across the study region for that season. Seasonal rainfall values associated with selected percentiles are provided (values in mm).

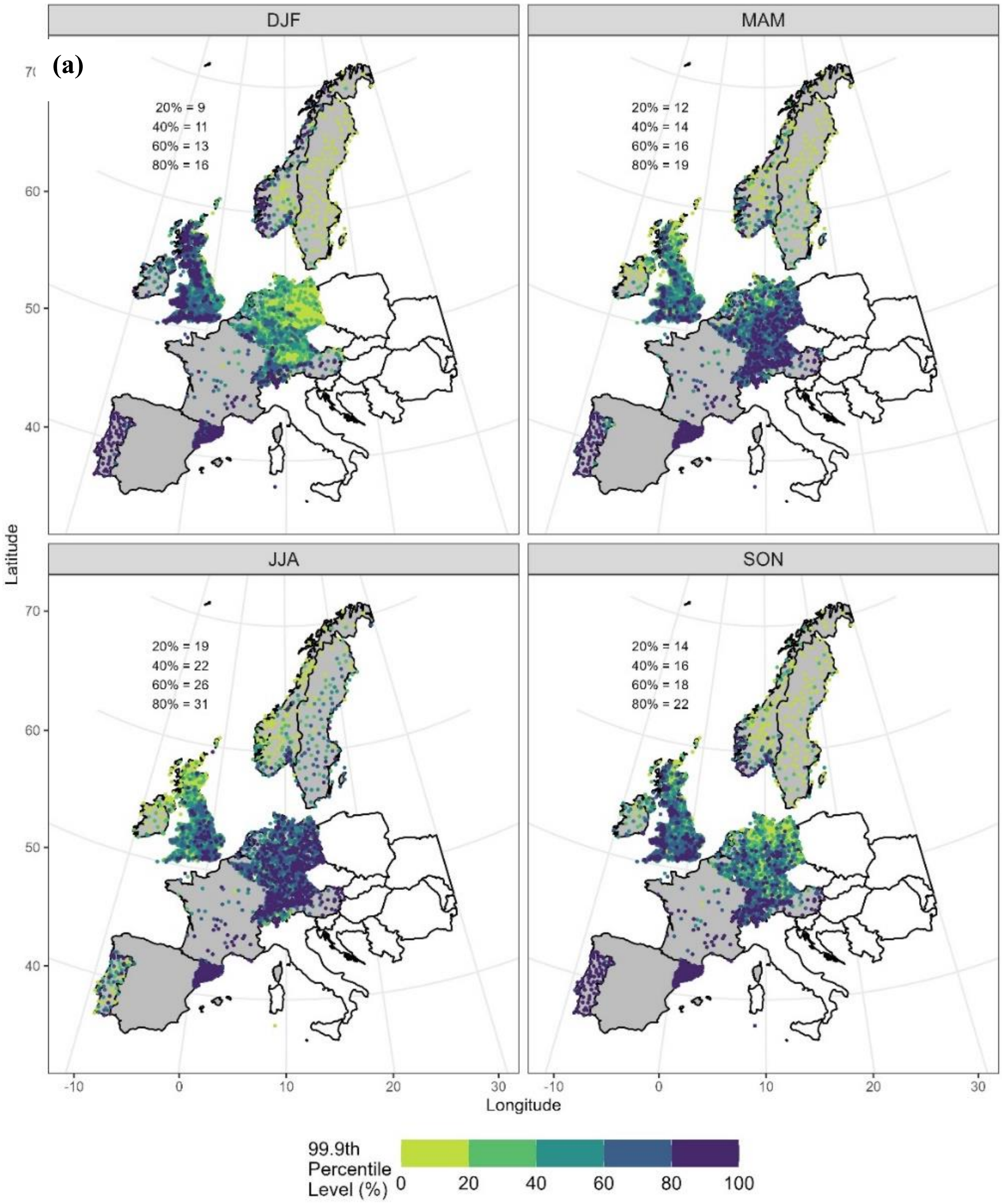

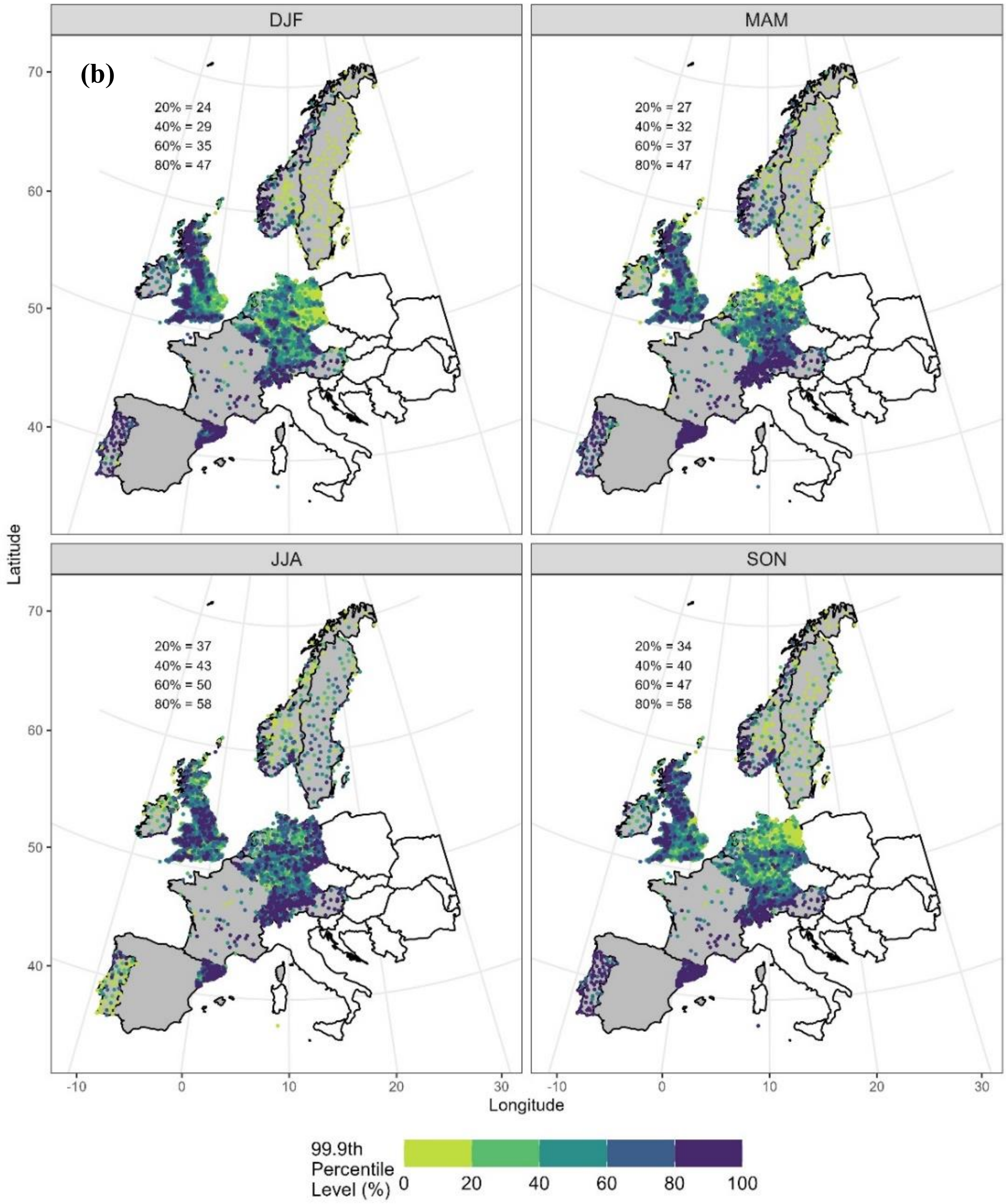

3.3.6 Influence of Latitude Band and Climate Zone

Given the influence temperature has on short duration rainfall extremes through convection and the Clausius-Clapeyron relationship (e.g. Trenberth *et al.*, 2003; Westra *et al.*, 2014; Fowler *et al.*, 2021b) we initially chose to analyse the influence of latitude on the GSDR-I. As the mean temperature decreases with increasing latitude, this provides some quantification of the extent to which the change in temperature through Europe affects the sub-daily rainfall climatology. Additionally, changes in the mean elevation at different latitudes can also contribute to the change in rainfall climatology, with areas of higher elevation expected to receive more rainfall (Jaagus *et al.*, 2010; Formetta *et al.*, 2022). A summary of annual results for the R3hr99.9p and R3hr20mm indices plotted in latitude bins is provided in Figure 3.10 (see Figure 1 for detail on the gauge locations within the latitude bands). Our analysis indicates that the highest intensities and frequencies of extreme events occur in more southerly latitudes, corresponding to the areas with the highest temperatures and lower numbers of wet hours. However, both the intensity and frequency index mean values are highest in the 40-45° latitude band (Figure 3.10 A&B) rather than the 35-40° band. This is likely due to the lack of rainfall in the Iberian Peninsula in summer (gauges in the 35-40° latitude band are limited to Southern Portugal here), which reduces the overall annual intensity and frequency of extremes. Northwards of 45°N there is a consistent decrease in both the intensity and frequency indices, although long tails in some latitude bands reflect individual locations with much higher intensities than the average for that latitude. The contribution index (Rx3hrP) also peaks in the 45-50° band then decreases beyond this (Appendix Figure A5).

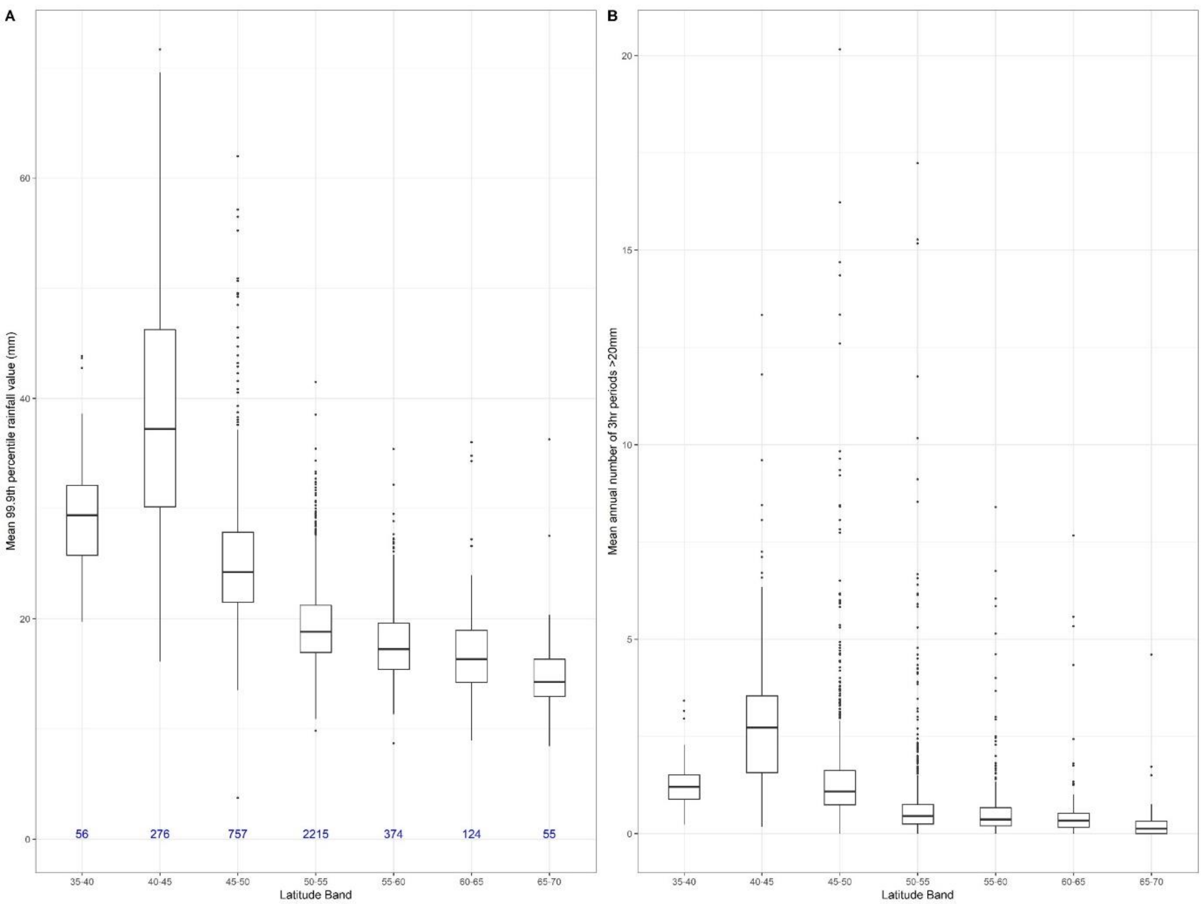

Figure 3.10: A) R99.9p3hr mean values by latitude band. B) R3hr20mm annual mean values by latitude band. Blue numbers in A are the number of gauges in each latitude band.

While latitude is only a rough proxy for temperature, the correlation between increase in latitude and decrease in extreme rainfall intensity and frequency reflects the strong air temperature influence on sub-daily rainfall extremes, with the generally higher temperatures in the lower latitudes leading to higher intensity rainfall, due to the increased atmospheric water holding capacity (Trenberth *et al.*, 2003; Fowler *et al.*, 2021c). However, the long tails to the distributions show that other factors, such as orography, atmospheric dynamics, and moisture availability still have a substantial effect on the individual gauge climatology (Pizarro *et al.*, 2012; Champion *et al.*, 2019).

To further investigate potential drivers of the spatial patterns and long distribution tails seen in our analysis of the indices we examined the influence of local climate on sub-daily extreme events using the Köppen-Geiger (K-G) climate zone classification system. The K-G climate classification is based on seasonal rainfall and temperature patterns (Beck *et al.*, 2018). We used the 1-km scale K-G climate zone map created by Beck *et al.* (2018) to assign each gauge to a climate zone with a high degree of accuracy.

The GSDR data available for Europe have a range of different climate zones (Figure 3.2) and for each zone the mean value of the intensity and frequency indices was calculated (Table 3.3). The BSk, Cfa, Csa and Csb zones are Mediterranean zones, the Cfb and Dfb are Temperate zones and Dfc and ET are Sub-polar zones. Note that although there is large variation in the number of gauges within each climate zone, all zones have at least 50 gauges providing results.

Climate Zone	***No. of Gauges***	***Rx3hr mean (Intensity)***	***Rx3hr maximum (Intensity)***	***R99.9p3hr mean (Intensity)***	***R3hr20mm mean (Frequency)***	***R99.9p3hrP mean (Contributi-on)***
BSk *cold semi-arid*	65	32.2mm	169.6mm	39.8mm	2.1hrs	2.8%
Cfa *humid sub-tropical*	52	34.4mm	155.5mm	40.7mm	2.8hrs	2.3%
Cfb *temperate oceanic*	2270	19.5mm	145mm	19mm	0.6hrs	1.7%
Csa *hot-summer Mediterranean*	105	30.4mm	144.6mm	36.2mm	2.2hrs	2.2%
Csb *warm-summer Mediterranean*	50	28.6mm	108.8mm	30.4mm	2.3hrs	1.9%
Dfb *humid continental mild summer*	1045	24.3mm	186.4mm	24mm	1.2hrs	2.1%
Dfc *subarctic with cool summers*	201	19.5mm	146.3mm	18mm	0.8hrs	1.9%
ET *tundra climate*	57	20.5mm	70.2mm	19.8mm	1.4hrs	1.6%

Table 3.3: Summary of GSDR-I indices by climate zone, including the number of gauges in each zone and the annual mean index values for each zone. The climate zone names follow the convention of the first letter indicating the main group, the second letter the seasonal precipitation category and the third letter the temperature category.

We find that the lowest intensities (Rx3hr, R99.9p3hr) and frequencies (R3hr20mm) of 3hr rainfall extremes occur in the Northern subarctic (Dfc) and temperate (Cfb) zones (Figure 3.11 & Table 3.3). The low intensities in the Cfb zone suggest the temperature buffering effect of the oceanic influence helps prevent the generation of strong summertime convection compared to continental climate regions (UK Met Office, 2022), while cool temperatures even in summer in the Dfc regions likely reduce the convective rainfall intensities here. The tundra (ET) zone shows higher intensities and frequencies than the Dfc zone despite being a polar climate classification (Figure 3.11, Table 3.3). This may be due to orographic enhancement of rainfall by the Alps and highland areas of Norway. The Dfb zone (covering a significant proportion of the Central and Pannonian Basin regions) has high Rx3hr intensities with a long positive tail, indicating outlier gauges with values much higher than the main distribution (Figure 3.11). Being a warm-summer humid continental climate, this zone is predisposed towards having strong convection during summer months when high temperatures can be reached, resulting in more intense rainfall due to higher convective available potential energy (CAPE) (Riemann-Campe *et al.*, 2009; Barbero *et al.*, 2019a). The Mediterranean climate zones (BSk, Cfa, Csa, Csb) show the highest mean values for all 3hr indices, supporting previous results for the Southern region. This also agrees with Lakatos *et al.* (2021) who determined that areas of the Pannonian Basin with a Mediterranean climate had higher frequency of extreme events (R3hr20mm) than in areas with Continental climate. Pizarro *et al.* (2012) also found the highest intensities of 1hr rainfall occurred in Mediterranean climate zones in a study of sub-daily rainfall in Chile.

The seasonal patterns seen in the Mediterranean climate zones of the Southern region, with the highest intensity and frequency of 3hr extremes being in autumn, is typical of this climate type (Insua-Costa *et al.*, 2021; Mastrantonas *et al.*, 2021). Additionally, the higher intensities of 3hr extremes seen in SE France are likely influenced by this area having a Mediterranean (Csa) climate compared to the oceanic Cfb climate in the rest of Southern France. However, the slight difference in timing and intensities of 3hr extremes between Portugal and the rest of the Southern region must be due to other influences outside of the climate zone, e.g. the influence of the Azores high inhibiting summertime thunderstorm activity over the Iberian peninsula (Taszarek *et al.*, 2019). Although there is a clear difference in the average intensity of 3hr extremes between the Mediterranean and all other climate zones, Figure 3.11 shows individual gauges within different zones can still reach similar values of maximum rainfall intensity despite climatic differences. Similar results of gauges in different climate zones reaching comparable maximum sub-daily rainfall intensities were also obtained by Pizarro *et al.* (2012) in Chile. The outlier values in each zone may partly be due to the method of dividing land areas into K-G zones. This division is based on monthly threshold values for temperature and rainfall, with the aim to map biome distributions (Beck et al., 2018), so it is to be expected that these pre-defined climate zones will not provide perfectly homogenous sub-daily extreme rainfall zones. However, the clear pattern of higher intensity and frequency of 3hr extreme events in the climate zones around the Mediterranean and the lower intensity and frequency of the extremes in the more northerly climate zones echoes the patterns already seen in the regional analysis.

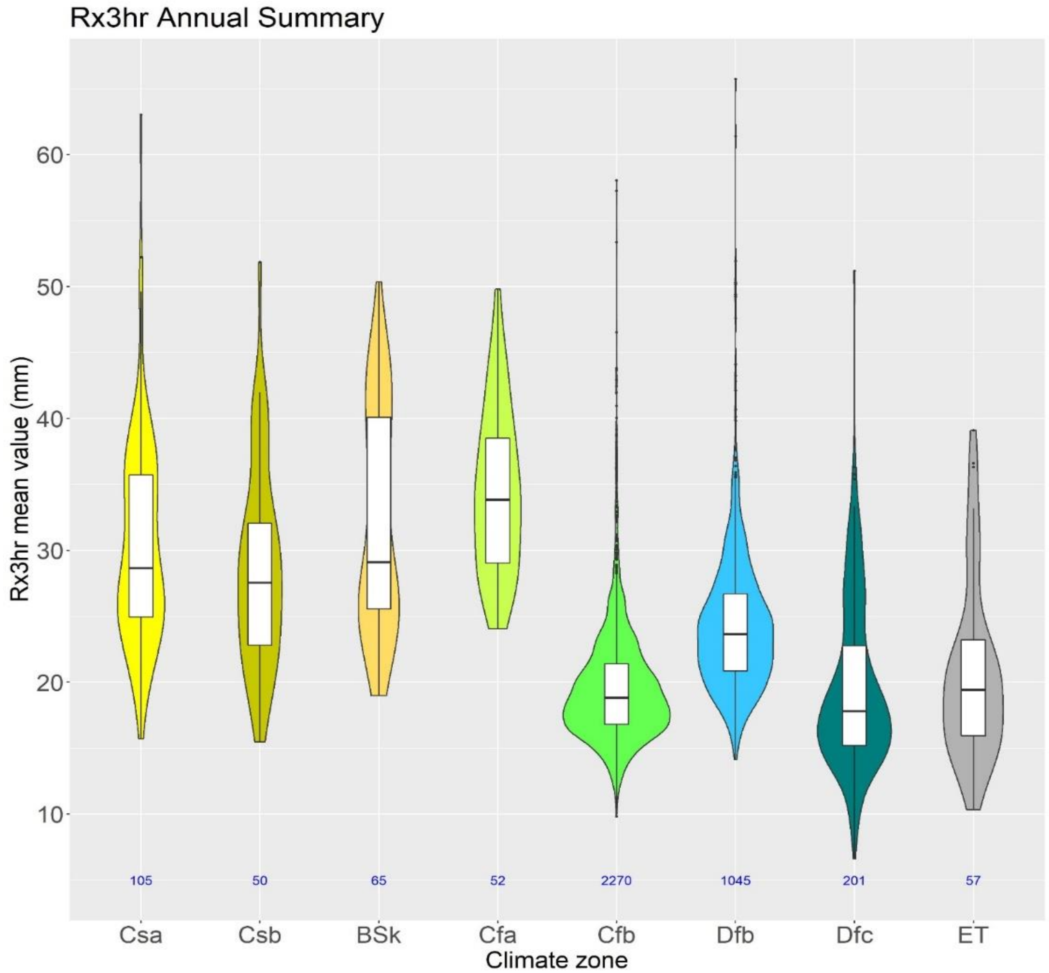

Figure 3.11: Distribution of 3-hour annual maxima (Rx3hr) gauge values by climate zone. The number of gauges in each zone is given in blue.

3.4 Discussion and Conclusions

This study has provided the first large-scale climatology of sub-daily rainfall extremes in Europe, taking advantage of a newly created indices dataset (GSDR-I) to examine the intensity, frequency and diurnal cycle of 3-hour extremes, as well as their contribution to the overall rainfall received by each region. The influence of latitudinal and climatic variations across Europe on the extremes has also been considered.

The timing of peak intensity and frequency of extreme events both occur in the same season in each region (Figures 3.5 & 3.6), indicating these aspects are affected by similar processes. The high proportion of intense sub-daily events occurring in summer across most of western Europe is in line with other sub-daily rainfall studies (Lenderink and Van Meijgaard, 2008; Blenkinsop *et al.*, 2017; Darwish *et al.*, 2018; Barbero *et al.*, 2019a). Barbero *et al.* (2019a) showed that 1-hour annual maxima are correlated to CAPE, with the event intensity increasing with CAPE until a threshold of 1500 Jkg^{-1}, above which the event intensity plateaus. The annual cycle of CAPE peaks in summer in the Northern hemisphere (Riemann-Campe *et al.*, 2009), hence the peak in sub-daily events in summer shown in the index results for most regions.

The predominance of extreme rainfall events in autumn around the western Mediterranean and Portugal agrees with findings from previous studies at daily timescales (Taszarek *et al.*, 2019; Insua-Costa *et al.*, 2021; Mastrantonas *et al.*, 2021). Annual thunderstorm activity peaks in July and August in northern, eastern and central Europe whereas in the western and central parts of the Mediterranean, thunderstorms occur mostly in October and November (Taszarek *et al.*, 2019). Taszarek *et al.* (2019) also noted the strong influence of the Azores High on the Iberian peninsula, reducing summertime convective activity in this region. These findings suggest the later seasonal peak in extreme events in the Southern region is due to both a later peak in the annual convective cycle and the influence of large-scale circulation drivers. In a study of flash flood events in Europe, Gaume *et al.* (2009) identified the most extreme flash floods in Catalonia and Mediterranean France occurred without exception in autumn, while in central Europe extreme floods occurred only in spring and summer. This seasonality in flash flood events was also noted by Marchi *et al.* (2010) who additionally identified the flash flood regime was more intense in Mediterranean regions than in inland continental areas. This indicates there is a strong link between the climatological timing and intensity of sub-daily rainfall and the risk of flash flooding, demonstrating the benefit of this kind of climatological analysis for impact assessments. Deviations from these large-scale temporal and spatial patterns across Europe are generally due to local influences such as a coastal location and orography (Darwish *et al.*, 2018; Champion *et al.*, 2019; Marra *et al.*, 2021). Additionally, climate oscillations, such as the North Atlantic Oscillation and Azores-Scandinavia Oscillation, can cause decadal cycles within the rainfall regimes; hence individual extremes could be much stronger or weaker than the mean values (Willems, 2013; Förster and Thiele, 2020). Some of this variability can be seen in Appendix Figure A1.

There are two possible explanations for the high contributions from 3hr annual maxima events to the daily rainfall total (Figure 3.7). Firstly, that when these intense events occur they are often isolated short-duration events and thus contribute the majority of the rainfall recorded on that day. Barbero *et al*. (2019a) noted that a majority of 1hr annual maxima occur during short-duration storms with convective origins. Secondly, they are part of longer storms with a very 'peaked' profile (the majority of rain falls in a small proportion of the storm) (Villalobos-Herrera *et al.*, 2024). This agrees with the findings of Barbero *et al.* (2019a) that 1hr extremes can provide a large proportion of daily extremes. The lower percentage contribution of 3hr annual maxima in the Northern region suggests that these events are more often embedded within longer-duration storms. Overall, these results indicate that intense short-duration events could be a major source of flash flood risk, especially in summer in the Central region and in autumn in the Southern region.

The strong late afternoon to early evening peak for spring and summer Rx3hr events in all regions provides further evidence for these events being strongly tied to the convective cycle (Figure 3.8) and agrees with the findings by Barbero *et al*. (2019a) for several regions globally. Moist convection generally begins in the mid-afternoon due to solar heating creating atmospheric instability, and the resultant convective systems reach their peak a few hours later (Barbero *et al.*, 2019a). The smaller amplitude of the autumn and winter diurnal cycle is likely related to differences in the generating mechanism between seasons; in cooler seasons more mixed processes occur and convection becomes less dominant, so the diurnal cycle becomes weaker (Trenberth *et al.*, 2003; Darwish *et al.*, 2018; Barbero *et al.*, 2019a).

The difference in seasonal timing and location of 3hr and 24hr extremes indicates this should be an important consideration for flood management design, as the different types of flooding these events produce (especially in urban areas) require different management systems (Hurford *et al.*, 2012; Dale, 2021). Figure 3.9 indicates some locations have high rainfall intensities regardless of the duration and season, for example Catalonia, SE France and southern Austria have high values year-round for both 3hr and 24hr intensities. However, much of the Central region has intensities in the upper quantiles in summer for 3hr intensities but is in the lower quantiles in summer for 24hr intensities. This highlights another useful aspect of this index-based analysis, enabling direct comparison between long- and short-duration extreme events, which can provide further information as to which type of flooding (fluvial or pluvial) a particular area is most at risk of during each season.

While latitude provides a broad indication of the expected extreme rainfall characteristics due to the temperature influence, other factors also play a role. For example, the 45-50^{o} latitude band contains Cfb, Dfc and ET climate zones, which have different index characteristics when plotted separately, indicating different driving influences within each climate zone. When examined as a group, the Mediterranean-type climate zones experience the most intense and most frequent sub-daily extremes, while the cooler zones have lower intensities and the extreme events are largely restricted to summer months, as expected from the regional analysis. There are also clear differences in the rainfall characteristics between the climate zones. Therefore, we propose that climate zones provide a readily-available first-order determination of the intensity and frequency of extreme sub-daily events a particular location can expect. Thus providing information useable for high-level flood hazard preparation and mitigation activities, especially for regions with sparse historical rain gauge coverage. Additionally, this information could provide a proxy for how the sub-daily rainfall characteristics of a region may change under global warming. If an area is known to be transitioning from one climate zone to another, an understanding of the characteristics of extreme events in the new climate zone could help in providing an indication of the flood/drought challenges the region may face in the future (Beck *et al.*, 2018). Finally, the similar maximum rainfall intensities that are reached in each climate zone are a further indicator of the important role local conditions play in influencing extreme rainfall intensities.

The main conclusions of this analysis are:

- The highest intensities and frequencies of sub-daily extreme events occur in the Southern region, with lower intensities and frequencies in the Central and Northern regions.
- The most intense and frequent 3hr rainfall extremes occur in summer in most of Europe (Figure 3.5 and 3.6) and in autumn in Mediterranean regions and Portugal.
- High contributions from 3hr extreme events to the daily rainfall total, particularly in the Central and Southern regions, indicate these extremes are often either isolated short-duration events, or are part of longer duration storms with a very 'peaked' profile.
- There are clear seasonal patterns in the diurnal cycle of sub-daily extremes in all regions, with a dominant late afternoon to early evening peak in summer.
- Comparing extreme event indices of different duration (3hr versus 24hr) reveals different spatial and temporal patterns, which should be taken into consideration when designing larger scale water management systems. The 24hr indices show a stronger orographic influence but lower seasonal variability than the 3hr indices.
- KG climate zones are a relatively good indicator of the general extreme sub-daily rainfall characteristics that can be expected at a particular location, potentially providing information for ungauged areas and a proxy for future changes in extremes in regions transitioning from one climate zone to another.

The climatology presented in this paper provides the first detailed sub-daily rainfall climatology for western Europe and demonstrates the information that indices of extreme sub-daily rainfall can provide, including insight into the spatial and temporal distribution of these events and their potential driving mechanisms. As much of the data and code used to generate the GSDR-I indices is open access, constant expansion of the dataset as new gauges are added is eminently feasible. There is also strong potential for the application of these sub-daily indices in validation of

European-scale simulations of convection-permitting climate models, such as in the recent study by Ban *et al.* (2021) where hourly indices of observational data were used to assess the performance of a set of high-resolution (3 km) climate simulations. The GSDR-I dataset will go a long way towards helping to improve understanding of the extreme event generation processes on these timescales and provide a clear benchmark against which to validate climate model outputs.

Chapter 4
Atmospheric patterns associated with sub-daily rainfall extremes in western Europe

4.1 Introduction

Sub-daily rainfall extremes are responsible for many pluvial and flash floods in Europe, resulting in significant damage and fatalities (Westra *et al.*, 2014; Archer and Fowler, 2018). These extreme events are driven by both thermodynamic and dynamic processes (Pfahl *et al.*, 2017). Recent studies focussed on thermodynamical drivers have greatly improved understanding of these processes (Hardwick Jones *et al.*, 2010; Lenderink and Van Meijgaard, 2010; Wasko *et al.*, 2018; Ali *et al.*, 2021a). However, the same effort has only recently been extended to dynamical drivers (e.g. Allan *et al.*, 2019; Barbero *et al.*, 2019b; Brieber and Hoy, 2019; Champion *et al.*, 2019) due in large part to lack of available high-quality sub-daily data; this, in most cases, has focussed on individual countries or regions. Thus, the influence of large-scale dynamical drivers on sub-daily rainfall extremes is less well understood (Westra *et al.*, 2014; Fowler *et al.*, 2021b). Nonetheless, as dynamical drivers occur on a wide range of spatial scales and are an essential component in operational forecasts of extreme rainfall and flooding, improving forecasts of floods by improving our understanding of these dynamical drivers may provide the most cost-beneficial way of reducing economic losses from flooding (Pappenberger *et al.*, 2015).

Weather patterns (WPs) characterise one or more large-scale meteorological variables over a particular geographical domain and time-scale and are derived from average conditions of atmospheric circulations. Several synoptic-scale WP classifications have been used to investigate dynamical drivers of daily and longer rainfall events over Europe, with the most commonly-used being the Lamb Weather Type (LWT) and Grosswetterlagen (GWL) schemes. The LWT scheme was based on manual identification of basic daily WPs (Lamb, 1972), but was extended into a new objective classification scheme using reanalysis data, producing 27 WPs centred on the UK (Jones *et al.* 2013). The GWL scheme has 29 subjectively-derived large-scale WPs, centred over Germany but covering Europe (Werner and Gerstengarbe, 2010). They represent regimes which persist for at least three days before transitioning. These schemes have been used in several studies investigating links between WPs and extreme rainfall in Europe (e.g., Tu *et al.*, 2005; Planchon *et al.*, 2009; Jaagus *et al.*, 2010; Pattison and Lane, 2012; Hoy *et al.*, 2014; Minářová *et al.*, 2017). More recently, the development of automated classification systems has enabled WPs to be used to identify periods with increased risk of fluvial flooding up to two weeks ahead (Neal *et al.*, 2016; Richardson *et al.*, 2020).

Some studies have created their own WPs using clustering procedures on atmospheric variables including mean sea level pressure (MSLP) and geopotential height at 500hPa (z500) (Toreti *et al.*, 2010; Merino *et al.*, 2016; Mastrantonas *et al.*, 2021). Several variables, including potential vorticity (PV) and total precipitable water, were used by Giannakaki and Martius (2016) to develop ten upper-level flow classes for conditions associated with daily extreme rainfall events over northern Switzerland. Additionally, Santos *et al.* (2017) used a set of WPs defined on clustering of daily MSLP fields to identify that just 3 WPs were strongly associated with flash flooding for a set of drainage basins in Portugal, highlighting anomalous features within the WPs on flash flood days. Similarly, Pattison and Lane (2012) identified that just 5 of the 27 LWTs accounted for 80% of extreme floods in Carlisle in northwest England. Minářová *et al.* (2017) used the GWL classification to determine the WP most frequently associated with multi-day extreme precipitation over the Ore Mountains (on the Czech-German border) as a trough over central Europe. Also using GWL, Planchon *et al.* (2009) identified that winter daily extreme (>20 mm) rainfall in NW France was predominantly associated with westerly and southerly cyclonic circulations. These examples demonstrate that regardless of classification system or variable used, only a few circulation types are associated with extreme rainfall (or floods). This highlights the operational potential for using large-scale atmospheric circulation patterns to provide advance warning of periods with a higher risk of extreme rainfall impacts, as forecasters can identify analogs in model predicted fields, allowing communities to prepare for events with longer warning times (Merino *et al.*, 2016; Richardson *et al.*, 2020; Wilkinson and Neal, 2021; Flack *et al.*, 2019).

Recently a new set of 30 WPs have been developed by the UK Met Office (MO30) (Neal *et al.*, 2016). These patterns are based on clustering of daily MSLP fields across western Europe/eastern North Atlantic and are therefore representative of large-scale MSLP patterns over the British Isles and Europe. In a recent study, Richardson *et al.* (2020) assessed links between the MO30 WPs and UK regional daily rainfall extremes; results showed clear differences in the regional precipitation percentile exceedance probabilities between individual WPs. This indicates a tangible connection between the MO30 WPs and conditions leading to enhanced likelihood of extreme precipitation (on daily timescales) for the UK. This information was subsequently used by the authors to develop a fluvial forecasting tool based on the UK Flood Forecasting Centre's Coastal Decider tool (Neal *et al.*, 2018).

However, there are limited studies assessing links between WPs and sub-daily rainfall extremes. Although there are several studies investigating atmospheric conditions associated with summertime thunderstorms in central and western Europe (Sibley, 2012; Piper *et al.*, 2016, 2019; Mohr *et al.*, 2019, 2020; Wilkinson and Neal, 2021), these generally use lightning data as indicators of thunderstorm presence and do not investigate the associated rainfall. There have been a handful of investigations where composites of atmospheric variables are linked to sub-daily rainfall extremes in Europe (e.g., Pfahl, 2014; Allan *et al.*, 2019; Champion *et al.*, 2019). Most studies on the links between WPs and sub-daily rainfall in Europe are for Germany; Haacke and Paton (2021) and Brieber and Hoy (2019) used the GWL WPs to examine the conditions associated with sub-daily extremes. Both these studies identified a link between the influx of warm, moist air from the south or east and sub-daily rainfall extremes, with Brieber and Hoy (2019) also identifying the presence of an upper-level trough over western Europe as important. Similar results were obtained by Weder *et al.* (2017) for Hamburg (Germany), using the objective WPs from the Deutscher Wetterdienst (DWD). The DWD WPs have also been used to assess the circulation patterns associated with extreme (>99th percentile) hourly rainfall in Amsterdam (Manola et al., 2019), again indicating the dominance of south-westerly flow in coincidence with the extreme events. Mohr *et al.* (2020) also found that interactions between a persistent Scandinavian block and several cut-off lows contributed to a 3-week period of exceptional thunderstorm activity over central Europe in May-June 2018. There is a single study looking at the relationship between sub-daily extremes in Sicily and a set of 8 WPs developed by the UK Met Office (Cipolla *et al.*, 2020), with results showing an NAO negative pattern associated with summer 1-rh and 3hr maxima. However, to our knowledge there are no studies investigating WPs linked to summertime sub-daily rainfall extremes over the wider western Europe region.

We use the gauge-based Global Sub-daily Rainfall (GSDR) dataset (Lewis *et al.*, 2019) and the MO30 WPs to provide the first assessment of links between WPs and summertime sub-daily rainfall extremes in western Europe. The MO30 WPs were recently used to examine relationships between the WPs and lightning activity over the UK (Wilkinson and Neal, 2021), demonstrating the utility of these WPs in diagnosing conditions associated with small-scale weather features. We focus here on processes that can be readily identified in forecast models and climate models. WPs provide insights into the atmospheric conditions favourable for convection to occur. Mesoscale processes are then required for triggering convective activity (Doswell, 1987). We do not examine small-scale convective processes that often trigger sub-daily rainfall extremes in this chapter. This analysis is extended by using z500 reanalysis data to identify variations within the WP circulation that are conducive to the development of extreme events. The chapter is organised as follows: Section 4.2 describes the data and methods used, Section 4.3 presents the results, followed by discussion in Section 4.4 and conclusions in Section 4.5.

4.2 Data and Methods

We focus our analysis on the summer season (JJA) only as the highest frequency of 3-hour events above 40-mm occur during summer in western Europe (Whitford *et al.*, 2023).

4.2.1 Weather Patterns

We use the MO30 WPs (as described in Neal *et al.* 2016) due to their large spatial domain which covers the majority of western Europe and the fact these patterns can vary daily; we believe that the 3-day persistence of GWL WPs may not be appropriate for sub-daily rainfall events. In brief, the MO30 WPs were produced by K-means clustering of daily MSLP anomaly fields taken from the European and North Atlantic daily to multi-decadal climate variability data set (EMULATE), for 1850 to 2003, over 30°W–20°E; 35°–70°N. This large domain gives the MO30 WPs an advantage over other classification systems such as LWT, as they are applicable for other European regions (Richardson *et al.*, 2018). However, each WP will deliver different meteorological conditions to each geographical region, for example WP2 would bring strong westerly winds and low pressure to Scotland but weak winds and higher pressure to Portugal. For regions on the edge of the area of definition of the MO30 patterns, e.g. the southern Iberian peninsula or northern Norway, the WPs are likely to be less informative and more information on patterns centred over these regions would be required to definitively link the WPs to rainfall here. These differences are discussed later on in this chapter. The MO30 WPs have a coarse resolution of 5° latitude and longitude meaning local-scale features are not captured. Daily WP classifications have been extended from 2004 to present using the ECMWF ERA-Interim dataset (Dee *et al.*, 2011). Before MSLP fields were clustered, the seasonal cycle was removed by subtracting a smoothed climatology from each field. The resulting WPs are representative of the long-term climatology and capture broad-scale circulation types. The final set of 30 WPs (Figure 4.1) was evaluated by operational meteorologists to ensure a full range of circulation types affecting the UK and Europe were represented and are designed to be used in medium-range forecasting, out to 15 days (Neal *et al.*, 2016; Richardson *et al.*, 2020).

The MO30 WPs are ordered based on their historic occurrence from 1850 to 2003, with WP1 having the highest annual frequency and WP30 the lowest. The clustering procedure results in grouping the days with stronger anomalies together resulting in lower numbered WPs having smaller magnitude MSLP anomalies and occurring more frequently in summer (Figure 4.2), while higher numbered WPs have larger magnitude anomalies and occur more often in winter (Neal *et al.*, 2016; Richardson *et al.*, 2018, 2020).

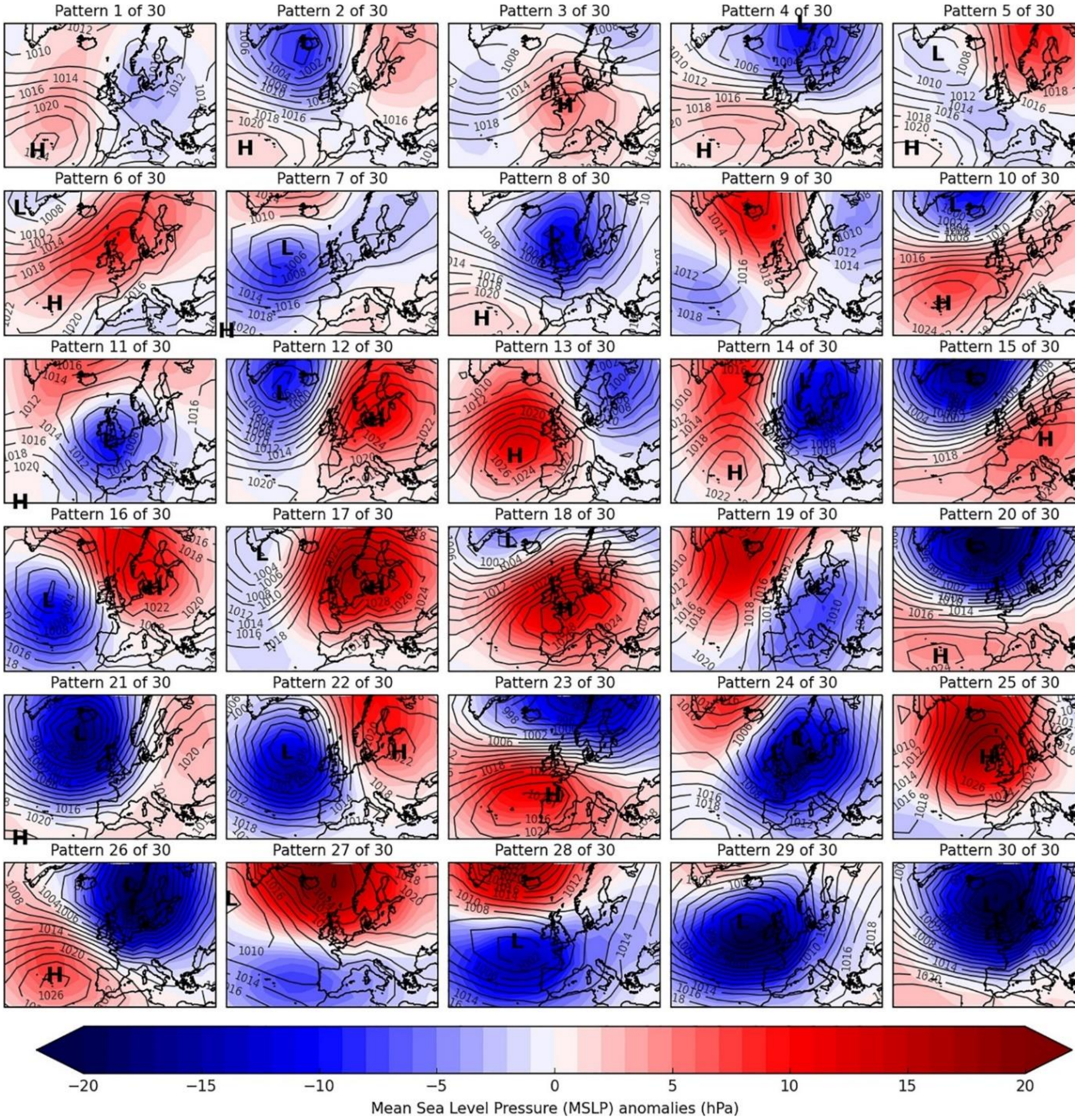

Figure 4.1: The set of 30 Met Office weather patterns (MO30), showing mean sea level pressure (MSLP) anomalies plotted as filled contours (hPa) and MSLP mean values plotted in foreground (2 hPa intervals). Figure source: reproduced from Neal et al. (2016) Fig. 1.

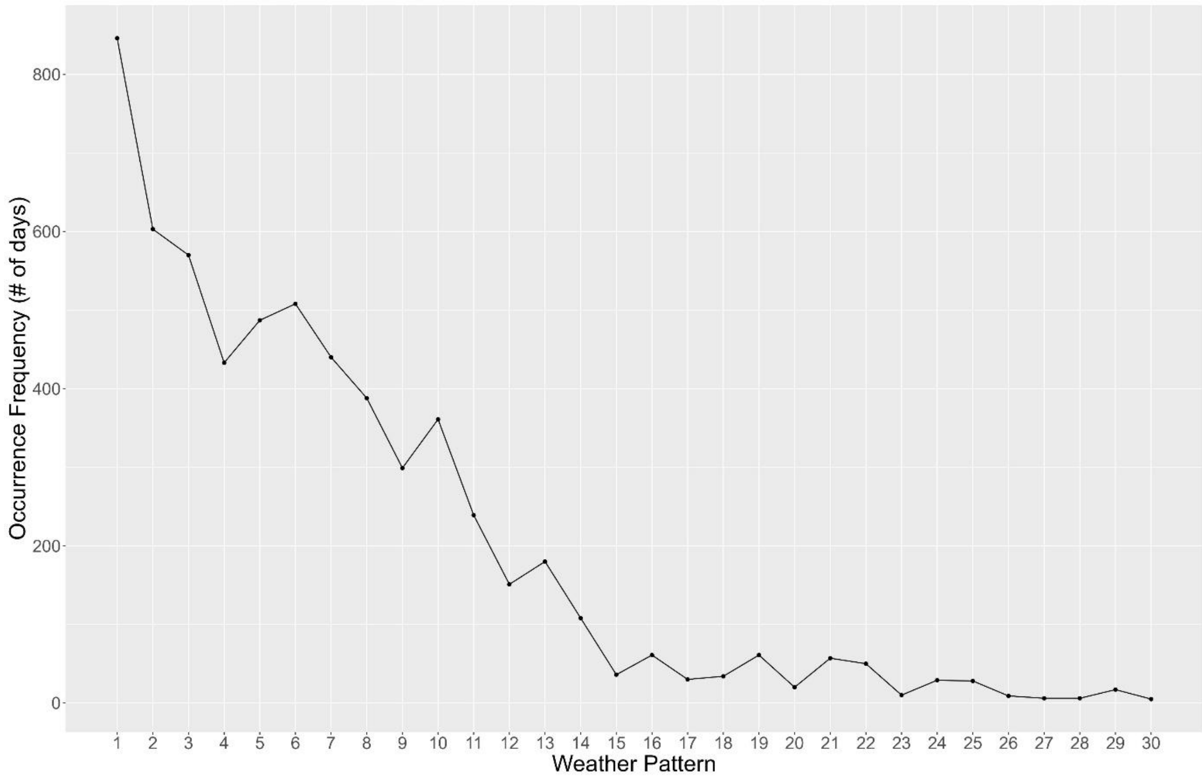

Figure 4.2: The MO30 patterns frequency of occurrence in all summer months from 1950 - 2015.

4.2.2 Rainfall data

We use hourly rainfall data from the GSDR (Global Sub-Daily Rainfall) dataset (Lewis *et al.*, 2019); this is gauge-based and has been subjected to strict quality-control measures (Lewis *et al.*, 2021) (Lewis et al., 2021). Gauge data available in Europe are shown in Figure 4.3. There is a much higher gauge coverage in the UK and Germany than for the rest of Europe, a factor that may influence some results as discussed later. There are also variations in record length and completeness. While completeness has been accounted for in the data creation steps, variation in record length means some countries have >50 years gauge data while others have only 15 years. To maximise data availability we have used all gauges rather than restricting our analysis to only those which cover a standard period. This caveat should be kept in mind when examining the results presented here.

We used a peaks-over-threshold (POT) analysis and extracted 3hr events above a 40 mm threshold from a rolling window timeseries where months with >15% missing data were removed. The 40 mm threshold was chosen as a compromise, to allow inclusion of only the more extreme events and to maintain a consistent threshold across the region. This threshold was also chosen based on results from published literature indicating 40 mm represents an ~10 year return level for 3hr rainfall across central Europe and a >10 year return level in northern Europe. Beck *et al.* (2020) showed a 15-year return-period intensity for 3-hour rainfall of ~16 mm in northern Europe and ~30-40 mm in southern and central Europe, while Poschlod *et al*. (2021) found 10-yr return levels for 3hr rainfall of ~35-45 mm in central Europe and ~20-30 mm in the UK and Scandinavia, using a high-resolution single-model large ensemble climate model. Figure 3.9 shows that 40mm in 3hrs is above the 99.9th percentile level of 3hr rainfall in all of western Europe except Catalonia. Therefore, this 40 mm threshold represents potentially impactful events across the region under investigation.

The Flood Forecasting Centre in the UK uses extreme rainfall alert thresholds of 30 mm in 1hr and 40 mm in 3hr. Given the very rare occurrence of 30 mm rainfall in 1hr in most of northern Europe (see Appendix B.1) using the 3hr totals provides a larger dataset to use for this analysis and is still an indicator of potential flash flood inducing rainfall. Additionally, extreme 3hr rainfall events can often include a 1hr extreme, therefore using 3hr rainfall here is also ensuring a large proportion of 1hr extreme events are captured (Barbero *et al.,* 2019; Villalobos-Herrera *et al.,* 2023). Short duration (<3hr) rainfall events tend to be front loaded and therefore using a full 3hr duration allows for 1hr and 2hr extremes to be included in the dataset (Villalobos-Herrera *et al*., 2024). Several studies including Darwish *et al.* (2018) and Barbero et al. (2019) have noted the strong similarity in behaviour between 1hr and 3hr extremes, but 1hr extremes are more strongly tied into the diurnal convective cycle, indicating their reliance on local (small-scale) drivers, while 3hr extremes are more influenced by larger-scale drivers. Finally, 3hr totals are most commonly used as indicators for flash flooding by practitioners (in the UK) (Hurford *et al.*, 2012). The variation in rainfall distribution between northern and southern Europe (Whitford *et al.*, 2023) means some regions have many more events over the threshold than others, a factor which should also be taken into consideration when examining the results. Finally, events above the threshold are declustered by keeping only the largest 3hr event per gauge per day. There may be more than one threshold exceedance in a region in a day, as multiple gauges may have recorded an event in the same storm. Multiple events per day were retained as an indicator of the influence of each WP, showing how many extreme rainfall events can be attributed to each WP.

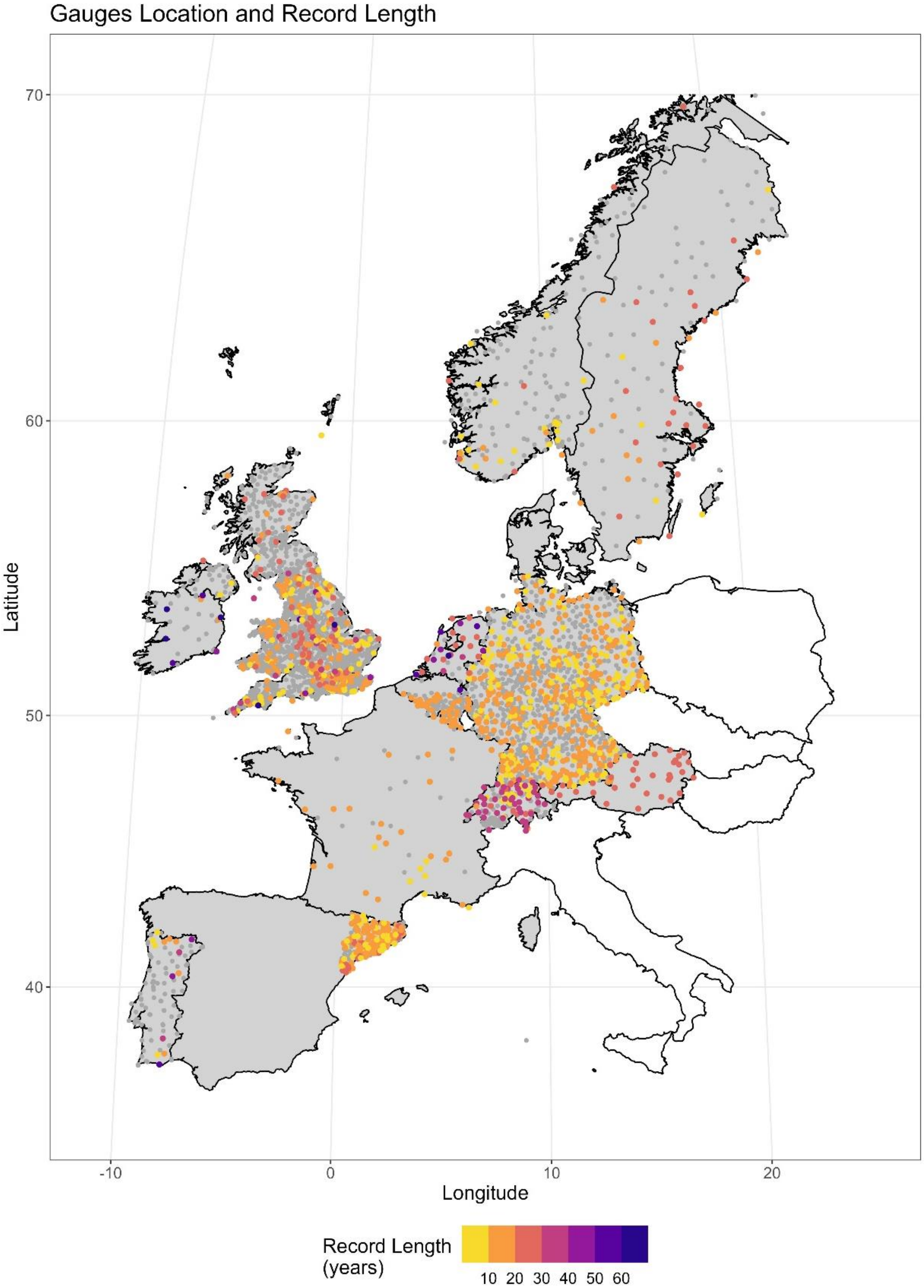

Figure 4.3: The location and record length of gauges from the GSDR dataset in Europe that have at least one 3hr ≥40mm event in summer. Gauges which are part of the dataset but do not have a recorded 3hr ≥40mm event shown in grey.

4.2.3 Atmospheric Data

To characterise upper-level atmospheric conditions, we used ERA5 daily-averaged geopotential height data at 500 hPa (z500), with a resolution of 0.25° x 0.25° for the period 1970-2016 over 20 to 80ºN and -180 to 180ºE. The z500 variable was chosen for this analysis as it represents the level of non-divergence (level in the atmosphere at which horizontal divergence of air is near zero), where vertical ascent can be largest, thereby indicating regions where dynamical ascent may occur. The importance of z500 in defining the synoptic environment connected to extreme rainfall events has been shown in several investigations (e.g. Hidalgo-Muñoz *et al.*, 2011; Mastrantonas *et al.*, 2021; Dorrington *et al.*, 2023) The large domain size was chosen to enable investigation of large-scale circulations upstream of extreme rainfall locations. z500 anomalies were calculated in several steps. Firstly, a climatology of daily z500 was calculated using a 45-day rolling mean. This rolling window length was chosen as it removed noise and provided a smooth climatology, meaning further smoothing was not required. Then, for each day, the climatology is subtracted from the z500 value to calculate the anomaly at each grid point. Daily data is used rather than 6-hourly to maintain temporal consistency with the MO30 patterns as this study focusses on atmospheric conditions on the day of, rather than in the hours before, sub-daily rainfall extremes. We aim to identify synoptic-scale situations that generate conditions conducive to mesoscale convective processes being triggered.

4.2.4 Methods

To examine the links between weather patterns and extreme sub-daily events, we calculated the percentage of 3hr ≥40 mm events which coincide with each WP, where $f = 100(N_{WP}^{ext}/N^{ext})$ where N_{WP}^{ext} denotes the number of 3hr ≥40 mm events which occur on the same days as the selected WP, and N^{ext} is the total number of extremes. This calculation was performed for each country separately, to allow for the varying number of extreme events and record lengths in each country. To account for the influence of WP relative frequencies on the coincidence results, the probability of having a 3hr event ≥40 mm given a certain WP was calculated, for each WP and each country. In this case $p = N_{WP}^{ext}/N^{WP}$, where N^{WP} represents the total number of summer (JJA) days with the WP. This was determined for the common time period covered by the gauge records in each country (1996-2015).

Composites of the z500 anomalies present on days with each WP and extreme rainfall are generated by taking the mean of the anomalies at each gridpoint on these days. The difference between days with a certain WP without extreme rainfall and days with the WP and an extreme event is calculated by subtracting the mean z500 anomaly on all days with the WP and no 3hr extreme event from the mean z500 anomaly on all days with the WP and a 3hr extreme event. The statistical signficiance of the z500 anomalies on event days is also assessed. The 5th and 95th percentile confidence intervals were determined for each WP using seasonal bootstrap resampling 500 times on all summer dates with the WP (and no 3hr extreme event) for the given country. Areas with mean z500 anomaly on event days which are above or below these confidence intervals are then identified as regions with anomalies which are statistically significant at the 90th percentile level.

4.3 Results

4.3.1 WPs associated with 3hr rainfall events over 40 mm threshold

For southern and Mediterranean regions of western Europe (France, Catalonia and Portugal), most 3hr 40 mm events coincide with WPs 1, 2, 5 and 6, while Catalonia and Portugal have a high proportion from WP10 (Figure 4.4); over 55% of the 40 mm events come from these 5 WPs (see Table 4.1). Portugal shows a very strong peak for WP29 however, this is likely influenced by the low number of events over the 40-mm threshold recorded in Portugal in summer. The percentage of events under each WP in autumn in Portugal is shown in Appendix Figure B1 and this also shows the strong peak in WP29. Given the strong low pressure anomaly over Ireland in WP29, the westerly winds reaching Portugal from the Atlantic likely provide the source of moisture for extremes to occur. The significantly higher number of events recorded in Catalonia is partly due to the fact 40 mm represents a lower part of the distribution here (Whitford *et al.*, 2023) and also that the denser gauge network enables more events to be captured.

For central and Alpine regions (Belgium, the Netherlands, Germany, Switzerland, Austria), a limited number of WPs (1, 2, 5, 6 and 11) are associated with 3hr rainfall extremes (Figure 4.5), although Belgium also has a high proportion of events under WP7. Each country (except Switzerland) has >15 % of events above 40 mm coinciding with WP5 and WP6, indicating these WPs are associated with conditions favouring extreme rainfall development across central Europe. Interestingly, for Switzerland and Austria the top 5 WPs account for only 56.9% and 48.2% of 3hr events over 40 mm respectively, whereas for Germany, Belgium and the Netherlands it is near to or over 60% (60.9%, 69% and 70% respectively – Table 4.1). This suggests that 3hr extreme rainfalls occur under a wider range of large-scale atmospheric conditions in the Alps than in the Low Countries, possibly due to the potential for convection initiation through the 'Alpine pumping' mechanism (Graf *et al.*, 2016; Kahraman *et al.*, 2022). This mechanism aids in the triggering of thunderstorms over mountainous regions where local winds converge (due to mountain-valley circulations), leading to low-level rising motions and enhanced probability of convection-driven rainfall, especially during periods where large-scale circulation is weak and moisture is already present (Giorgi *et al.*, 2016; Kahraman *et al.*, 2022). The high number of events in Germany is influenced by the much higher gauge density here, allowing for more occurrences of threshold exceedance to be recorded.

Country	*1st*	%	*2nd*	%	*3rd*	%	*4th*	%	*5th*	%	Total (%)
Austria	*6*	14.8	*1*	9.3	*2*	9.3	*5*	8.3	*8*	6.5	48.2
Belgium	*2*	23	*7*	21	*6*	9.6	*5*	7.7	*11*	7.7	69
Catalonia	*5*	15.9	*1*	15.7	*6*	9.6	*10*	7.6	*2*	7.4	56.2
France	*1*	21	*2*	15.8	*11*	10.5	*7*	8.7	*5*	7	63
Germany	*1*	15.7	*2*	13.8	*5*	11.6	*6*	10.1	*11*	9.7	60.9
Ireland	*5*	27.3	*3*	18.2	*8*	18.2	*11*	18.2	*7*	9	90.9
Netherlands	*11*	22	*1*	18	*6*	14	*2*	8	*5*	8	70
Norway	*7*	18	*3*	16	*5*	16	*8*	14	*2*	10	74
Portugal	*29*	21	*4*	15.7	*1*	10.5	*6*	10.5	*10*	10.5	68.2
Sweden	*1*	18	*3*	13.1	*5*	13.1	*2*	8.2	*11*	8.2	60.6
Switzerland	*1*	16.6	*11*	12	*5*	10.2	*2*	9.9	*8*	8.2	56.9
UK	*6*	20	*11*	17.4	*1*	9.7	*5*	9.5	*2*	6.5	63.1

Table 4.1: The top 5 ranked weather patterns with the highest percentage of 3hr periods with ≥40 mm rainfall in each country and the total proportion of the events that occur under these weather patterns.

In northern Europe (Ireland, the UK, Norway and Sweden) there is a geographical divide in WPs associated with extreme 3hr rainfall (Figure 4.6). For the UK, Ireland and Sweden a high percentage of events occur under WP11 but this strong event coincidence does not appear in Norway. WP11 shows a west or south-westerly flow, where moisture from the Irish sea is forced to rise over the Pennines in England and Highlands in Scotland (Wilkinson and Neal, 2021). In Norway, Sweden, and Ireland WP3 is important in generating 3hr extreme rainfall, but this is not the case for the UK. WP5 is important across the whole region, while WP6 is most strongly associated with UK 3hr rainfall but is not important elsewhere in northern Europe (see discussion on Spanish Plumes in section 4.3.2). Disparity in results between the UK and Ireland is likely due to only 11 events above the 40 mm threshold being recorded in Ireland. Northern European countries all have over 60% of recorded 3hr 40 mm events occurring under the top 5 WPs (Table 4.1).

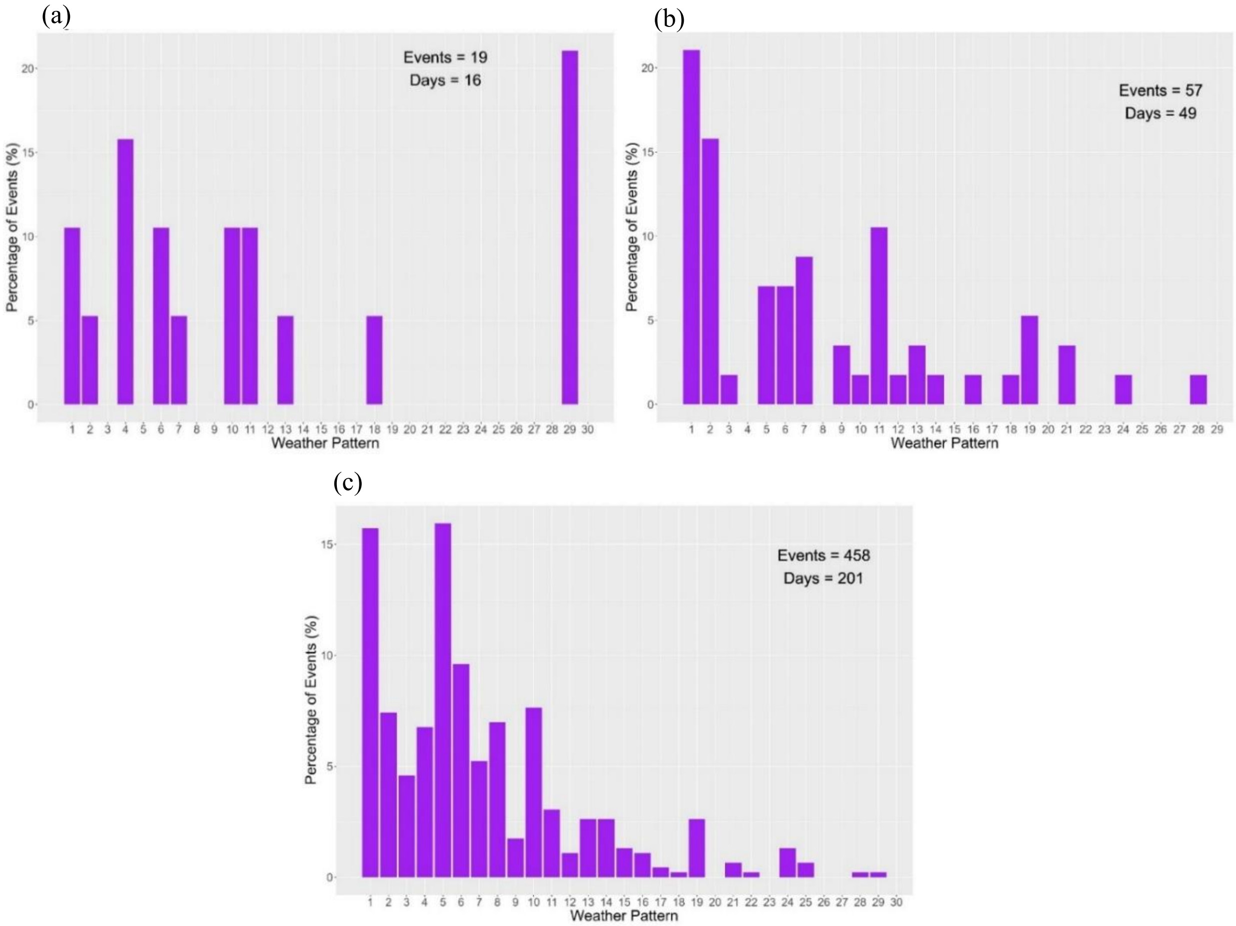

Figure 4.4: The frequency f (%) of 3hr ≥40 mm events coinciding with each of the MO30 weather patterns in southern European regions; a) Portugal, b) France, and c) Catalonia. The number of events and the number of days with events over the threshold are given in the top right corner of each panel.

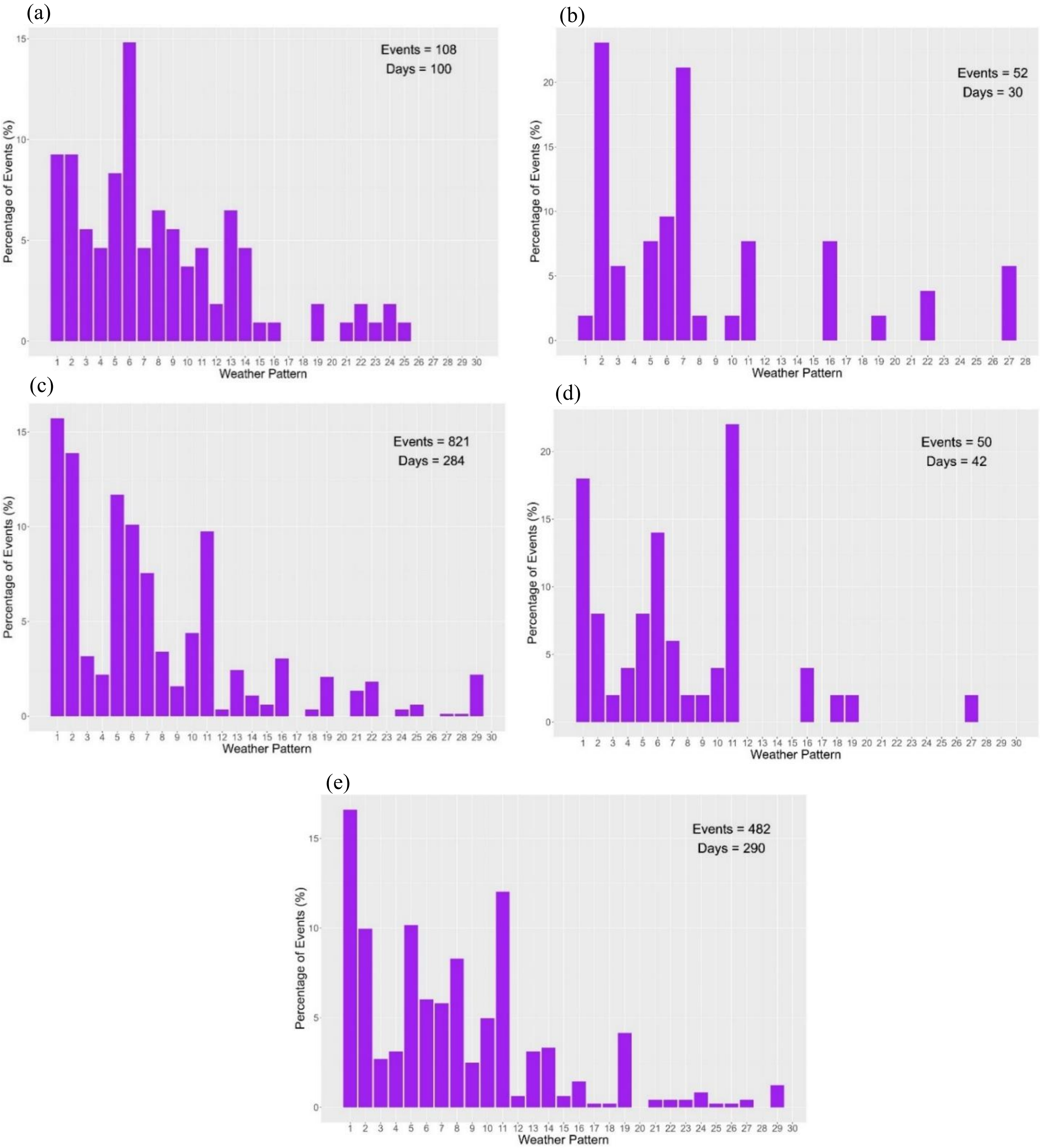

Figure 4.5: The frequency f (%) of 3hr ≥40 mm events coinciding with each of the MO30 weather patterns in central European regions; a) Austria, b) Belgium, c) Germany, d) Netherlands, e) Switzerland. The number of events and the number of days with events over the threshold are given in the top right corner of each panel.

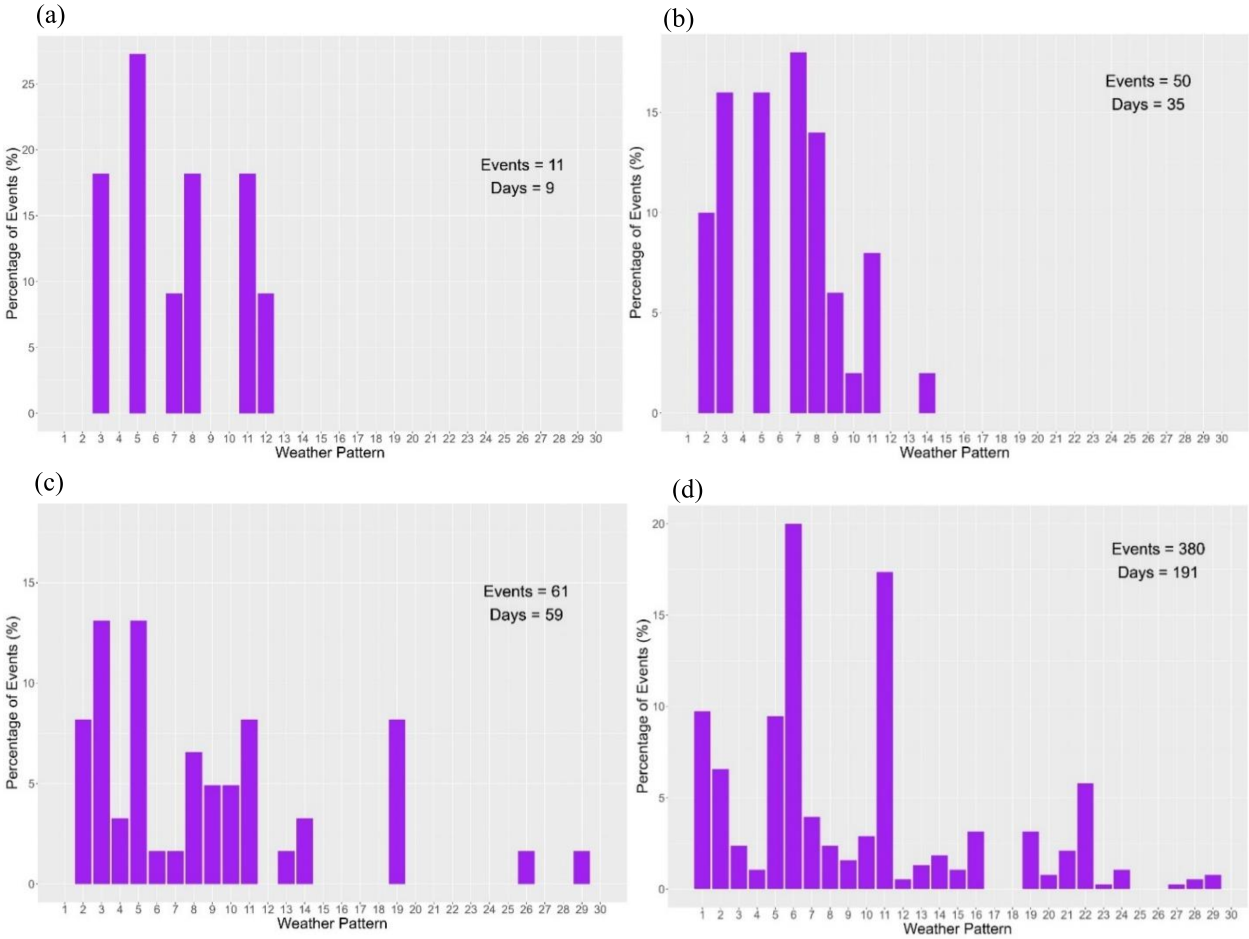

Figure 4.6: The frequency f (%) of 3hr ≥40 mm events coinciding with each of the MO30 weather patterns in northern European regions; a) Ireland, b) Norway, c) Sweden, d) UK. The number of events and the number of days with events over the threshold are given in the top right corner of each panel.

For all regions examined, some WPs never contribute substantially to the occurrence of summer 3hr extreme rainfall events. These include WP4 and WP9, and most of the patterns between WP12 and WP30. The small number of WPs responsible for most 3hr extreme rainfall events in each country indicates that a relatively small set of synoptic-scale atmospheric conditions cause summer sub-daily rainfall extremes in western Europe. Table 4.1 shows that in all countries, 25% of all 3hr, 40 mm events occur in just two WPs, and up to 35% in several cases. WPs associated with summertime 3hr rainfall extremes here are nearly all lower numbered patterns, which as discussed in Section 2 and shown in Figure 2, means they occur more frequently in summer. There is a significant decrease in the frequency of events associated with the WPs beyond pattern 13, which would be expected based on WP frequencies in summer.

To account for the influence of WP relative frequencies on the results, the probability p of having a 3hr event ≥ 40 mm given a certain WP was calculated, for each WP and each country. This also provides useful information for forecasting, providing the probability of a certain region experiencing at least one extreme event for any given WP (Wilkinson and Neal, 2021). Figure 4.7

shows the probability of a 3hr ≥40 mm event for each WP for a selection of countries within western Europe (Germany, Switzerland, UK, Catalonia). The binomial proportion confidence intervals of the probabilities (black lines) were calculated using the method of Wilson (1927). The dashed line in each plot represents the probability of an event over the threshold, regardless of the WP (number of days with events/number of days in record). The confidence intervals in each case become much larger towards the higher numbered weather patterns. This is due to the low frequency of these patterns, which increases the uncertainty in probability estimates due to the very small sample size, meaning the probability is strongly influenced by just one or two days with an event under the WP. Therefore, in this analysis we focus on the WPs with a probability of ≥0.1 and confidence interval ≤0.2, shown in red in Figure 4.7.

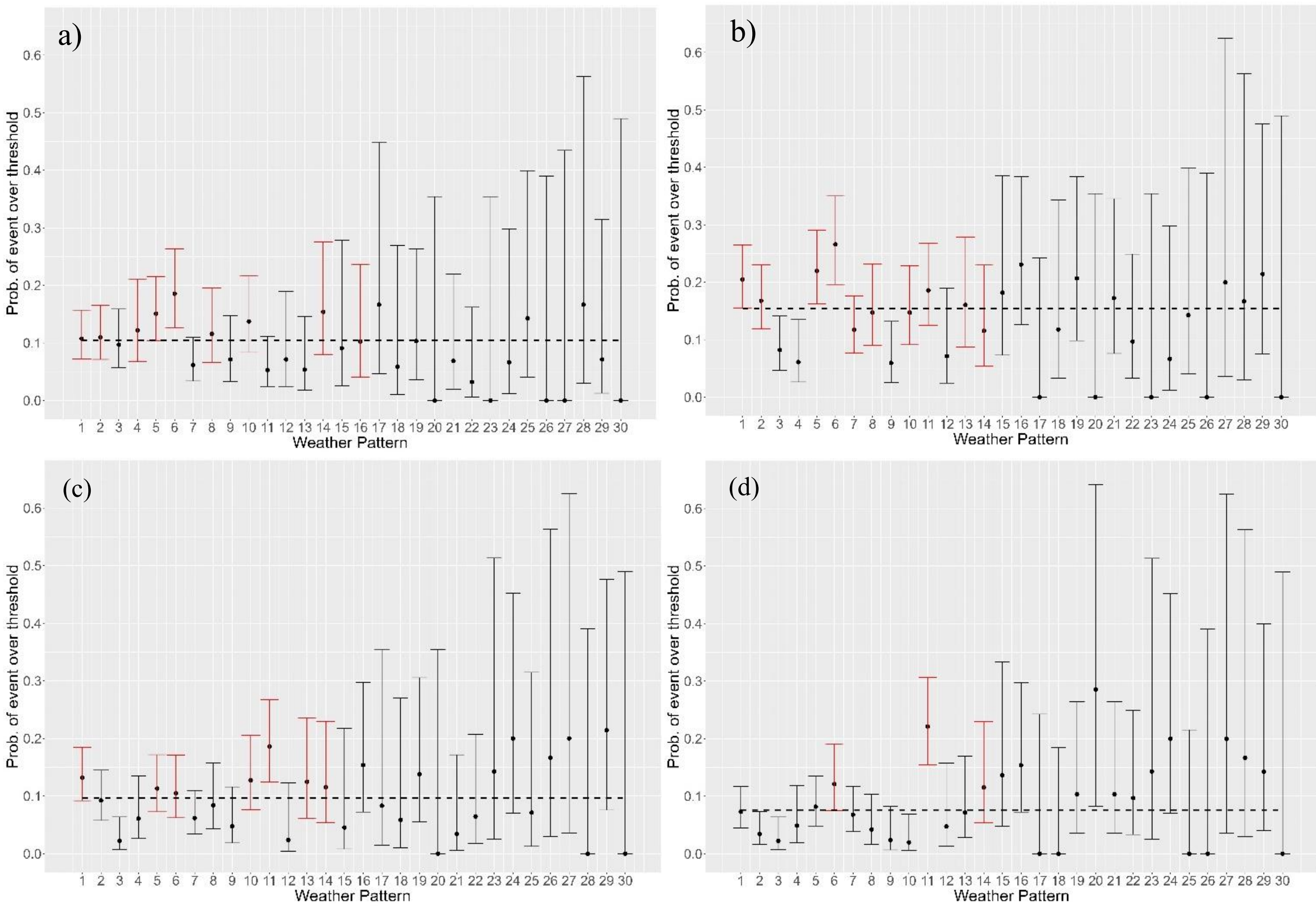

Figure 4.7: Probability (p) of experiencing a 3hr ≥40 mm rainfall event under each WP for a) Catalonia, b) Germany, c) Switzerland and d) UK. Lines indicate the Wilson confidence interval score. Red lines for WP that meet criteria of probability > 0.1 and confidence interval <0. Dashed line indicates probability of having a 3hr ≥40 mm event regardless of the WP.

Figure 4.7 shows that the WPs most strongly associated with 3hr ≥40 mm events (Figs. 4-6) nearly all have a probability higher than would be expected if the events were evenly distributed across all WPs, as shown by the dashed line (Figure 4.7). In Germany, Switzerland and Catalonia, WPs 1, 5, 6 and 11 all have a probability above the ‘random chance’ line, with the same for Catalonia except with WP10 instead of WP11. This indicates that despite the relatively frequent occurrence of these WPs there is still an unusually high associated probability of experiencing a 3hr extreme rainfall event. For the UK and Switzerland, WP11 has the highest probability of 3hr rainfall extremes with a probability of around 0.2. In Germany and Catalonia, WP6 has the highest probability of 3hr extreme rainfall (0.26 and 0.19 respectively). These results indicate that WPs associated with the highest proportions of extreme events also (except WP2) have the highest probability of an event occurring under that WP. This result holds for the rest of the countries analysed (not shown). The probabilities of 3hr events under the most important WPs are very high considering these are local-scale, short-duration rainfall events. In a similar study investigating the relationship between the MO30 WPs and significant thunderstorm days in the UK, Wilkinson and Neal (2021) found probabilities of 0.7-0.8 for the most strongly correlated WPs in summer. To have a 20% chance of an extreme sub-daily rainfall event in a given region under a specific WP is high, given the likelihood of missing individual extremes in the dataset. Especially considering the difficulties of measuring and forecasting relationships between the extreme rainfall events and atmospheric circulations, this is a significant result (Pfahl and Wernli, 2012b; Pfahl, 2014). Looking at the WP present on the day before the extreme event occurred may increase the probabilities of extreme event occurrence, as it may be the conditions from the day before, or even the longer term persistence of particular WPs, that influence the development of extreme rainfall in the following 24 hours. This would be an interesting feature for future research to investigate.

However, for lower numbered WPs, there is still only a small fraction of days on which WPs occur that have extreme rainfall. In most cases, over 80% of WP days do not have extreme rain events (Figure 4.7). Therefore, there must be a mesoscale feature(s) on days with extreme 3hr events that favours the triggering of convective processes, or at least processes where a high rainfall rate may be sustained for a significant amount of time (Doswell *et al.*, 1996). This theory is examined further in the next section using composites of z500 anomaly patterns on days with extreme 3hr events.

4.3.2 Comparison of z500 anomalies to WPs on days with 3hr ≥40 mm event

To examine the large-scale conditions associated with 3hr rainfall extreme in more detail, we examine the geopotential height anomalies at 500hPa (z500) for summer days with a given WP and 3hr events >40 mm in each region. These results are then compared to the z500 anomaly pattern composite for all days with the given WP. This enables a comparison between WP climatological atmospheric conditions and WP atmospheric conditions on days with a 3hr rainfall extreme, allowing identification of variations in large-scale flow potentially related to the occurrence of extremes. For brevity only the WPs most strongly associated with extreme 3hr events over western Europe are examined here –WPs 1, 2, 5, 6 and 11.

The z500 anomaly composites for all JJA days with each WP (Appendix Figure B.3) are very similar to the MSLP patterns (Figure 4.1). The anomalies appear stronger in the z500 patterns but otherwise the same features are highlighted in the same locations as they appear in the MO30 patterns.

For days with WP1 and 3hr events > 40 mm, each region shows the same pattern of a negative z500 anomaly over the UK to Bay of Biscay, accompanied by a positive z500 anomaly to the east and another to the west (Figure 4.8). The orientation axis of this trough varies from N-S to NE-SW to NW-SE depending on the region examined, but each would enable southerly or south-westerly flow over most of western Europe. On the forward side of an upper-level trough, positive vorticity advection (PVA) can occur, which in this case would lead to PVA enhancing divergence at 500hPa or higher. This upper level divergence would subsequently lead to convergence at low levels, with ascent on the forward side of the trough leading to conditions prone to triggering of convective activity (Weder *et al.*, 2017). This low-level convergence could also lead to an increase in moisture near to the surface and increase the chance of triggering thunderstorms where there is instability aloft. The 'ingredients' theory of Doswell *et al.*(1996) indicates that flash-flood producing storms require a combination of three key ingredients, namely; a conditionally unstable air parcel, sufficient low-level moisture and a process to lift the moist air parcel to its level of free convection. The PVA enhanced divergence associated with an upper level trough could therefore help to trigger ascent that leads to rainfall extremes through horizontal convergence in the lower troposphere increasing available moisture and lifting motion in the mid-troposphere (Champion *et al.*, 2019). Therefore, there appears to be a combination of factors driving the extremes on days with WP1. For Germany, Switzerland, and inland Catalonia the aforementioned Alpine pumping mechanism may play a role (due to weaker z500 gradients here), alongside increased PVA in front of the trough, while the UK lies under a strong negative anomaly which may be connected to a shortwave trough.

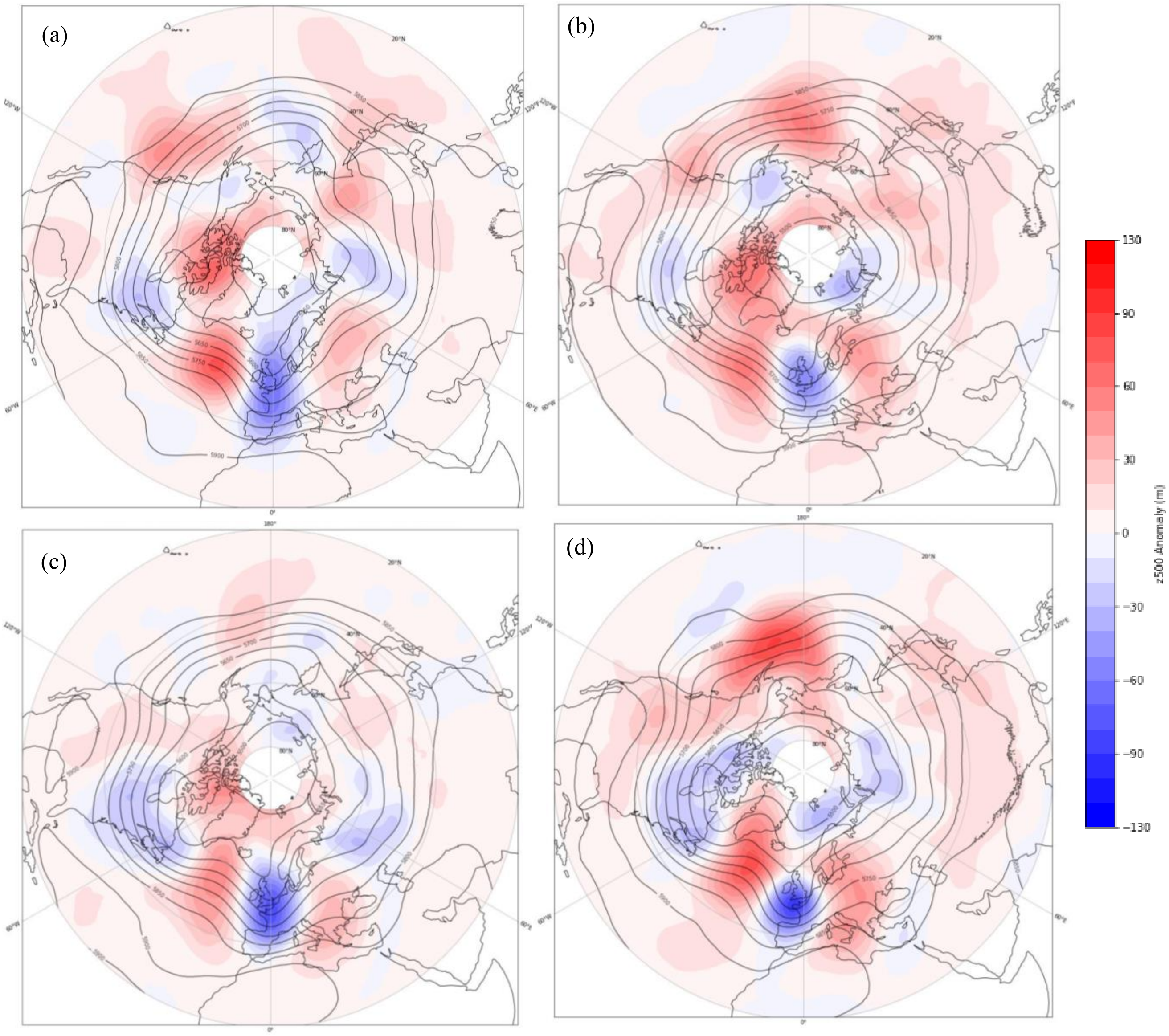

Figure 4.8: z500 composite anomaly maps on days with WP1 and 3hr ≥40 mm rainfall in a) Catalonia, b) Germany, c) Switzerland and d) UK. The z500 anomalies are shown on colour scale and mean z500 in black contours (m).

For days with WP2 and 3hr extreme rainfall events, the z500 anomaly composites are more varied between regions. Whilst still roughly resembling the standard WP2 configuration, the negative anomaly to the NW of Ireland is stronger, as is the positive anomaly over Scandinavia (Figure 4.9). The orientation of the ridge and trough are aligned in each case, with an approximately NW-SE orientation (N-S in the UK) which would favour southerly or south-westerly flow over each of the study regions. This negatively-tilted trough orientation is relatively rare and is often associated with severe weather due to the deepening low pressure at the surface and increasing vertical wind shear (Clark and Webb, 2013). Large-scale forcing for ascent can also occur ahead of a strong upper-level trough, triggering deep convection (Grams and Blumer, 2015; Giannakaki and Martius, 2016).

The N-S orientation of the trough in most cases suggests it may potentially be conducive to the development of a 'Spanish plume', where unstable, moist air is drawn up from the Iberian Peninsula along the leading edge of the trough, towards the UK (Morris, 1986; Wilkinson and Neal, 2021). Lewis and Gray (2010) describe a N-S oriented trough in this location as a 'classical' Spanish plume, allowing the transport of unstable, moist air from France/Iberia capped by warm, dry air from the Spanish plateau towards more northerly or north-eastern regions. This transport of an elevated mixed-layer northwards from Iberia leads to a large-scale environment favourable to thunderstorm development by mesoscale processes (Lewis and Gray, 2010). For Catalonia, the localised negative anomaly over the region suggests the extreme 3hr rainfall is associated with this feature, as an extension of the larger trough to the north. On reaching the highland areas of Catalonia, lifting of unstable, moist airmasses around the low's centre could result in extreme precipitation (Doswell *et al.*, 1996; Merino *et al.*, 2016).

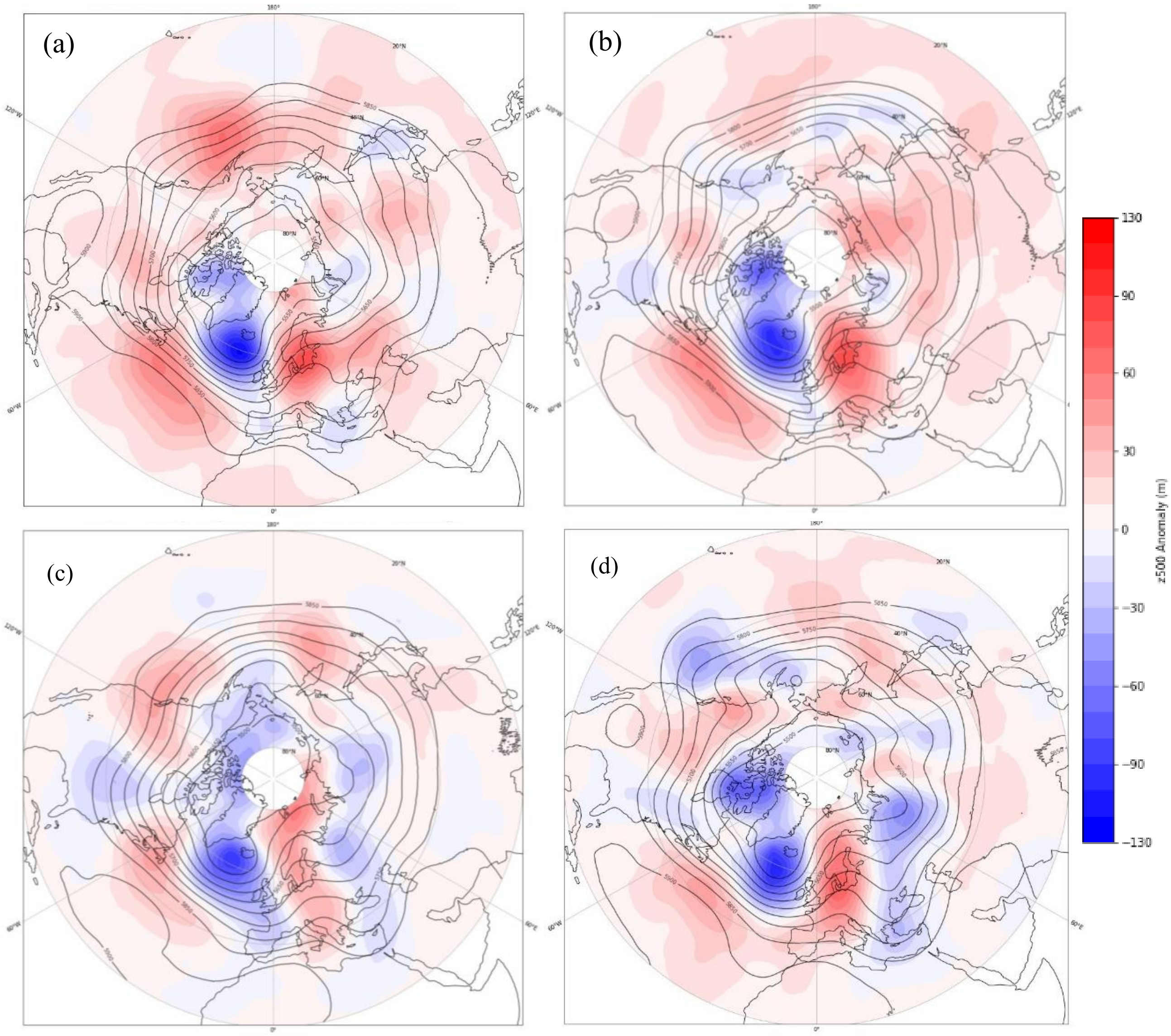

Figure 4.9:z500 composite anomaly maps on days with WP2 and 3hr ≥40 mm rainfall in a) Catalonia, b) Germany, c) Switzerland and d) UK. The z500 anomalies in colours and the mean z500 in black contours (m).

For days with WP5 and extremes, the z500 anomaly composites for each region are similar to the standard WP5 day, except for Catalonia which shows a much stronger and smaller negative anomaly over the western Mediterranean. For other regions the main change is an increase in high pressure area over Scandinavia and a shift in trough location to the west of this (Figure 4.10). The trough to the north-west again has a negatively (NW-SE) tilted orientation in each case and may extend as far south as Iberia, leading to south or south-easterly flow over much of western Europe. The forward-tilted trough (NW-SE) here, and cut-off formation in the case of Catalonia, indicates a 'modified' Spanish plume type (as defined by Lewis and Gray 2010). This synoptic setup has been linked to severe convective storms across many parts of western and central Europe (Delden, 2001; Piper and Kunz, 2017; Wilkinson and Neal, 2021). Relatively weak upper-level circulation in the composites for Germany and Switzerland suggest the Alpine pumping mechanism may also contribute to rainfall extremes here. Additionally, the increased strength of the ridge over Scandinavia may result in blocking of the low to the west, particularly for the UK and Catalonia, resulting in longer lasting rainfall events in these regions.

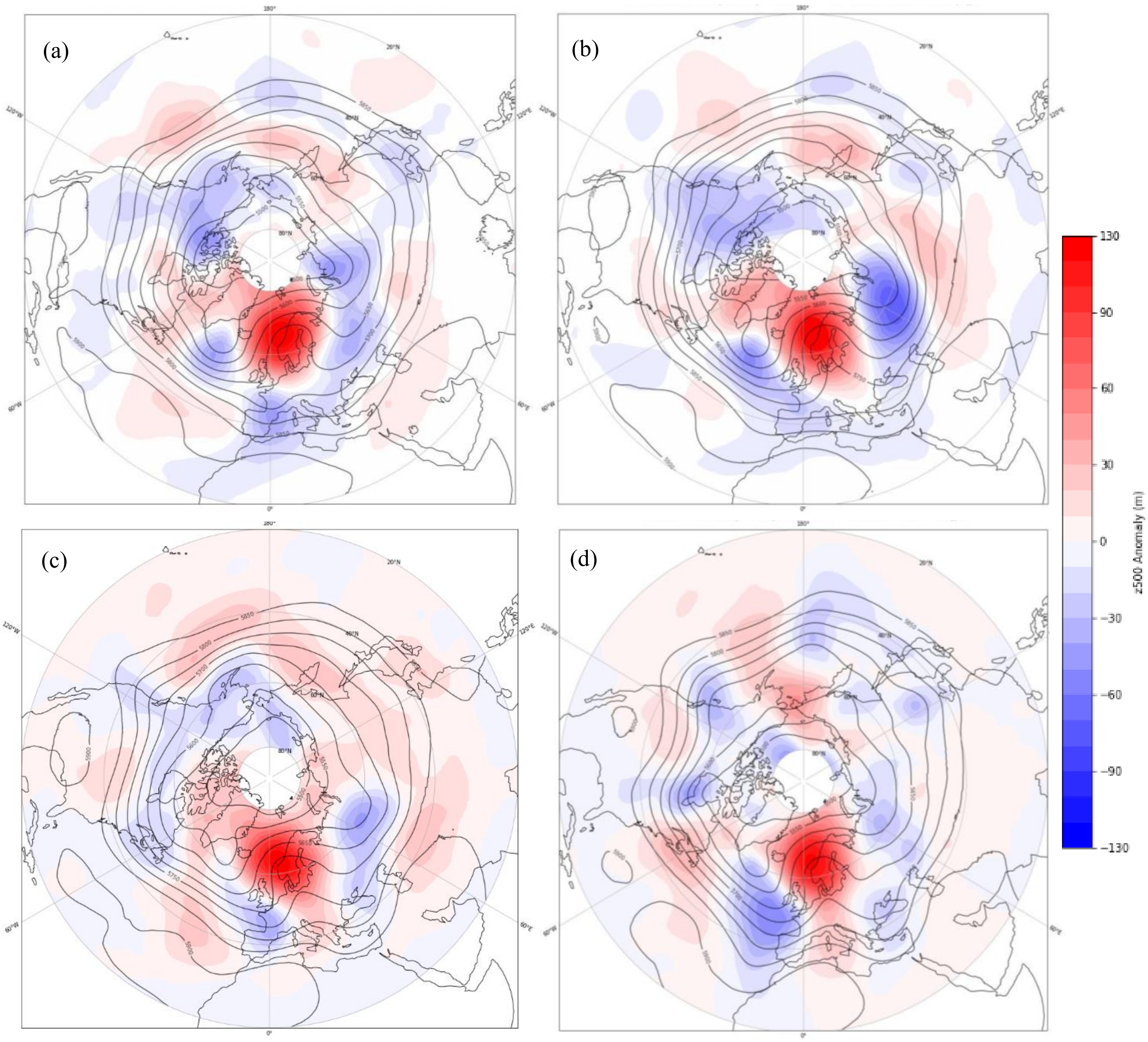

Figure 4.10: z500 composite anomaly maps on days with WP5 and 3hr ≥40 mm rainfall in a) Catalonia, b) Germany, c) Switzerland and d) UK. The z500 anomalies in colours and the mean z500 in black contours (m).

On days with WP6 and extreme events, for all regions where this WP is important, the most significant difference to the standard WP6 z500 anomaly pattern is the development of a spatially restricted, strong negative anomaly over Iberia/southern France, located to the south of a strong, zonally elongated ridge across the UK and southern Scandinavia (Figure 4.11). The negative z500 anomaly over, or to the east of, Iberia has the appearance of a cut-off low (COL). COLs are often associated with extreme rainfall along their north-east flank and the presence of the strong ridge to the north would reduce the movement of the COL, potentially stalling it over a region for some time, allowing substantial rainfall to occur over the affected area (Mohr *et al.*, 2020; Prein *et al.*, submitted). Ascent along the fronts associated with the cyclone can also induce lifting, leading to heavy rainfall (Pfahl, 2014). A strong connection between COLs and sub-daily extreme rainfall has already been identified for the US (Barbero *et al.*, 2019b). The high proportion of 3hr extremes associated with WP6 suggests this may also be the case in western Europe; however, further investigation of this connection is outside the scope of this study.

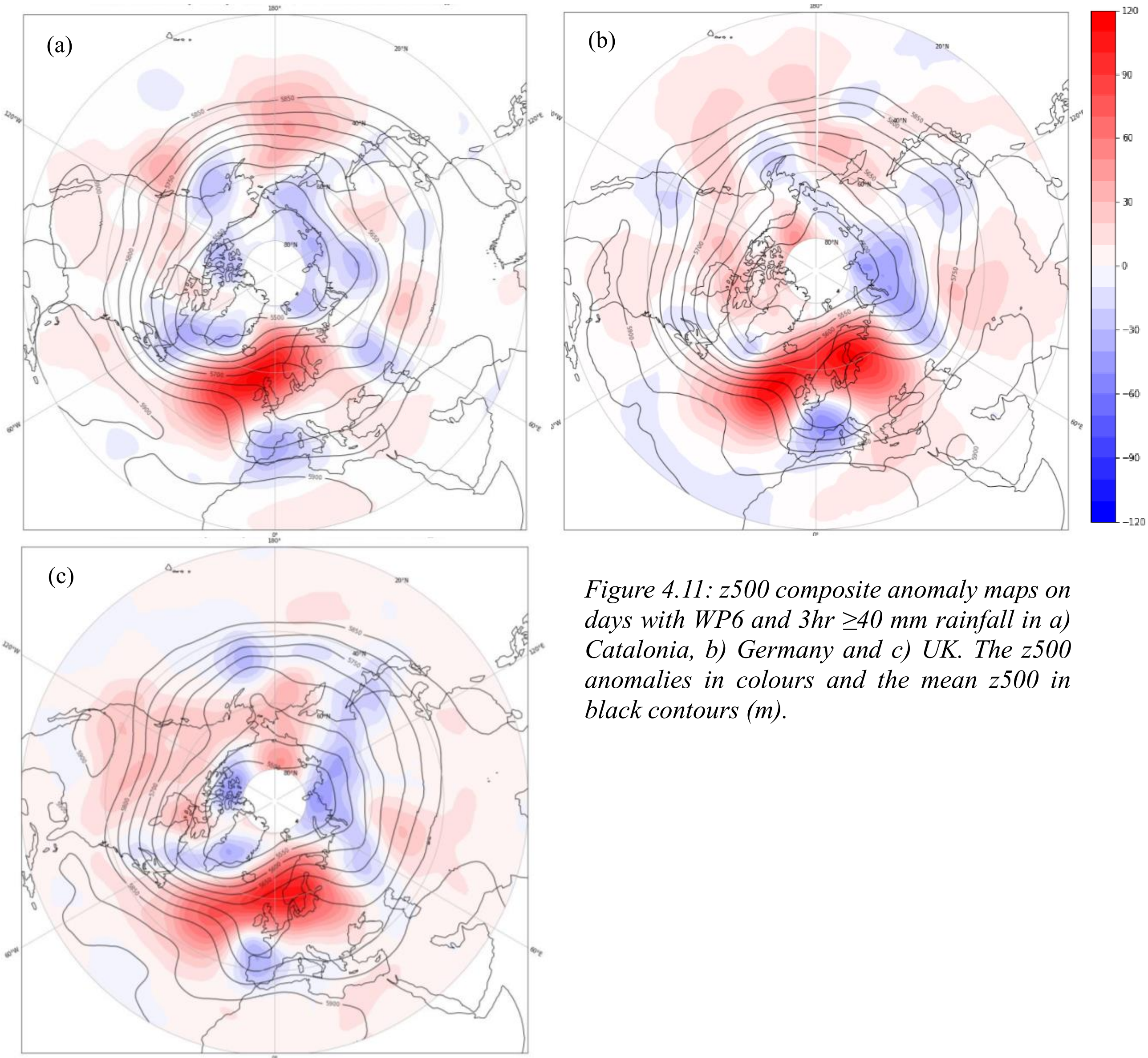

Figure 4.11: z500 composite anomaly maps on days with WP6 and 3hr ≥40 mm rainfall in a) Catalonia, b) Germany and c) UK. The z500 anomalies in colours and the mean z500 in black contours (m).

Finally, the z500 anomaly spatial pattern on days with WP11 and extreme events is spatially very similar to the standard WP11 z500 pattern (Figure 4.12). There is a strong increase in the intensity of the negative anomaly, but the positioning remains consistently to the NW of Brittany. An intense low pressure centre in this location would lead to strong southerly flow, with the potential to bring unstable, moist air up from Iberia/Bay of Biscay over the study region with divergence aloft, resulting in deep moist convection where local features cause lifting to occur (Doswell *et al.*, 1996). For Switzerland the orientation of these features results in a strong southerly flow towards the Alps, indicating lifting of moist, warm air could occur here (Giannakaki and Martius, 2016). It is interesting to note the slight change in orientation of the low and resultant flow for each country, with a change to a position allowing more southerly or south-westerly flow over the affected area each time.

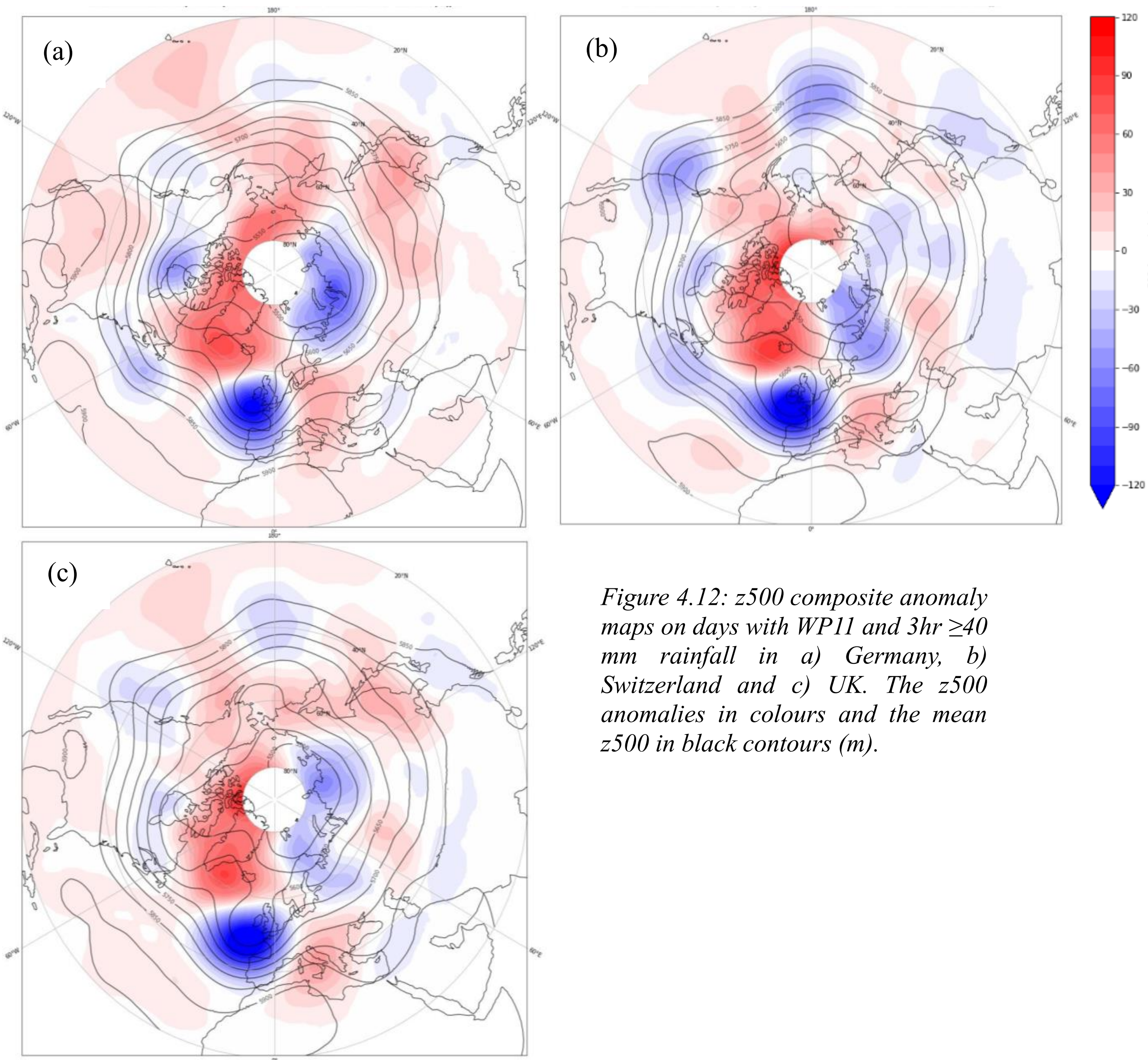

Figure 4.12: z500 composite anomaly maps on days with WP11 and 3hr ≥40 mm rainfall in a) Germany, b) Switzerland and c) UK. The z500 anomalies in colours and the mean z500 in black contours (m).

The difference in z500 anomalies between WP + event days and WP non-event days and the statistical significance of the anomalies on WP + event days were investigated for each country for each of the 5 WPs. This is useful information from a forecasting perspective as it provides insight on how the intra-WP conditions associated with extremes differ from those not associated with the extremes. The results of this analysis for WP6 in the UK are shown in Figure 4.13 and for the remaining WPs in Appendix B. These results clearly indicate the differences in the z500 anomalies on WP6 days with a 3hr extreme event compared to days without a 3hr extreme (Figure 4.13a, b) and shows the z500 anomalies on event days are statistically significant at the 90th percentile level (Figure 4.13c). This therefore supports the previous discussion of WP6 by showing how the development of the low pressure anomaly over Iberia is significantly different to a standard WP6 day, indicating this is connected to the occurrence of extreme rainfall events.

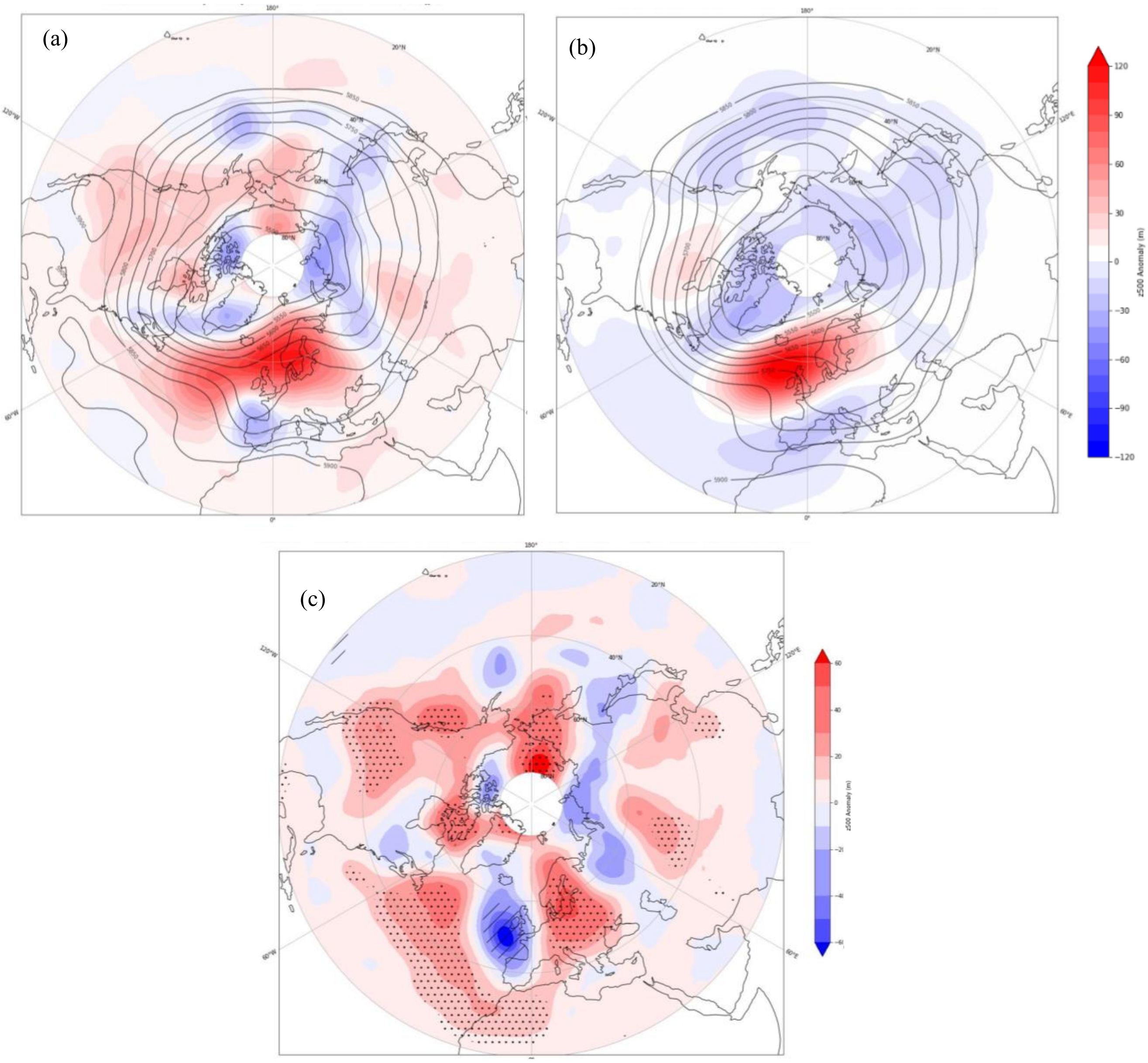

Figure 4.13: Results of significance testing of the z500 anomalies on event days. a) the mean z500 anomalies on days with WP6 + 3hr ≥40 mm event in the UK. B) mean z500 anomalies on days with WP6 and no extreme even in the UK. The colours are z500 anomaly (m) and black contours mean z500 (m). c) The difference between a) and b). Colours are the mean z500 anomaly difference between (a) and (b) and the stippling shows areas where the mean z500 anomaly on event days (from (a)) are above the 95th percentile (dots) and below the 5th percentile (hashes) limits from the bootstrap of all WP6 days without an event (b).

4.4 Discussion

We have examined 3hr rainfall extremes at rain gauges across western Europe and determined spatio-temporal relationships between these and large-scale WPs. Variations in available gauge density mean results for some regions are more robust than others (e.g. the UK compared to France) and the localised nature of 3hr rainfall extremes, being mainly from convective systems, means many events will be unrecorded by gauges (see, e.g. Lengfeld *et al.*, 2020, Flack *et al.,* 2019), meaning there may be more events associated with each WP than we are able to show here.

The analysis of WPs associated with 3hr rainfall events above a 40 mm threshold has shown that from 30 WPs, just 5 account for the vast majority of 3hr extremes across western Europe. These are all low-numbered WPs which occur more frequently in summer and have generally weak MSLP anomalies. The high proportion of 3hr events occurring under a small number of WPs suggests strong links between particular large-scale atmospheric circulations and triggering of sub-daily rainfall extremes. Richardson *et al.* (2020) also identified a small number of lower-numbered WPs as important for UK extreme daily rainfall events in summer. They found that typical winter WPs 19, 21, 22 and 29 had the highest probability of being associated with an extreme daily event in summer, while WPs 7, 8 and 11 were also strongly associated with daily extremes above the 90th and 95th percentile. However, as noted earlier and in Richardson et al. (2020), these winter patterns occur very rarely in summer and so the high probabilities associated with these patterns should be treated with caution. Richardson et al. (2020) agree with our assessment that WP11 is important for summer daily rainfall extremes; but not WPs 1, 2, 5 and 6, which are shown to be very important for the UK for 3hr extremes here. This suggests the 3hr extremes occurring under WP11 may be part of longer rainfall events, while the extremes under the lower numbered patterns are likely shorter, convection-driven events, highlighting the importance of investigating the drivers of sub-daily extreme rainfall events separately from driers of longer-duration extremes. A final specific point of interest is that WP6 is here shown to be associated with a high frequency of sub-daily rainfall extremes in the UK, while Richardson *et al.* (2018) found this WP to be associated with droughts in the UK.

Wilkinson and Neal (2021) investigated relationships between MO30 WPs and thunderstorm days over the UK. They found WPs 5, 8, 11, 16, 21 and 22 had high thunderstorm probability in summer. While WP5 and WP11 also have high extreme rainfall probability here, the other patterns are not strongly associated with 3hr extremes in the UK, although WP8 has high proportions of events in Norway and Ireland, which may be linked to thunderstorm occurrence under WP8. The Wilkinson and Neal (2021) study did not identify WP6 as being important for thunderstorms over the UK. This may be related to the convective available potential energy (CAPE) and upper-level wind conditions associated with the weather patterns. While strong CAPE and strong winds aloft (associated with the higher numbered patterns 16-22) are conducive to lighting/hail these conditions may then propagate quickly, reducing the rain falling at a specific location. The lower numbered patterns (5-11) with weaker MSLP gradients are more likely to be associated with weaker winds aloft, with the resulting slower propagation allowing more rain to fall over a specific location leading to increased rainfall depth (Doswell *et al.*, 1996; Púčik *et al.*, 2015; Mohr *et al.*, 2020). This comparison indicates that different WPs are associated with different hazards, and therefore investigation of the relationship between individual hazards and WPs is beneficial to improving understanding of the large-scale conditions that may lead to different types of extremes (Púčik *et al.*, 2015).

The investigation of the z500 anomalies associated with extreme sub-daily rainfall days for each WP has revealed the presence of distinct variations in the large-scale flow on these days. The WPs represent a mean state of a multitude of possible atmospheric configurations, so it is expected that within each WP there is variability in the intensity and location of features and in their spatial extent (Neal *et al.*, 2016; Wilkinson and Neal, 2021). However, despite this, we find that triggering of 3hr extreme rainfall under each WP is linked to a distinct z500 anomaly pattern. The presence of an anomalous southerly or south-westerly flow along the eastern side of a trough positioned over the western European coast is particularly prevalent in connection with 3hr rainfall extremes across much of western Europe. This pattern has been observed in numerous studies investigating thunderstorm activity (Sibley, 2012; Piper *et al.*, 2016, 2019; Mohr *et al.*, 2019; Wilkinson and Neal, 2021) and extreme rainfall in central and western Europe (Pfahl, 2014; Giannakaki and Martius, 2016; Merino *et al.*, 2016; Brieber and Hoy, 2019). This flow pattern supports the advection of convection-favouring (and often conditionally unstable) air masses originating in the subtropics into Europe along the eastern flank of an upper level trough (Mohr *et al.*, 2019; Piper *et al.*, 2019). The shifts in the positioning of the upper-level trough when examining the z500 composites for different countries highlights the importance of this southerly or south-westerly flow, with (potential) lifting along the leading edge of the trough (or low-pressure centre) to generate conditions favourable to 3hr rainfall extremes. As the short-duration rainfall events investigated here are mostly convective in origin, the similarity between large-scale conditions associated with thunderstorms is expected. However, these thunderstorm studies generally focus on identifying periods of enhanced lightning activity and thus storms resulting in heavy rainfall without accompanying lightning are not included in these datasets. Therefore, our study provides more comprehensive understanding of large-scale atmospheric conditions associated with summertime extreme rainfall and subsequently has greater relevance for flash flood forecasting.

While most studies of summertime convective phenomena in Europe have focussed on thunderstorms, a few have explicitly examined daily and shorter (e.g. 1-hour) rainfall extremes. Champion *et al.* (2019) found 3hr extremes in SE England were associated with a negative MSLP anomaly over Iberia and France and a positive MSLP anomaly over the northern UK, reminiscent of MO30 WP5. For extremes in NW England, a positive MSLP anomaly was present over the UK accompanied by a negative anomaly in relative humidity and westerly winds, a situation the authors took as being indicative of orographically-enhanced rainfall occurring – this resembles MO30 WP6. Similarly, Allan *et al.* (2019) found that one to four days day prior to the heaviest 200 3hr events in 6 regions across the UK, a negative MSLP and z200 anomaly was present to the west or southwest of the UK. These anomalies were associated with anomalous cyclonic southerly airflow, transporting moisture from the south/southwest, as seen in many cases in this study. The study of hourly rainfall extremes in 22 cities in German by Haacke and Paton (2021) also found a high proportion of events (34%) were associated with southerly flow related to a trough over western Europe, with a further 14% associated with south-westerly airflow. Brieber and Hoy (2019) found, for a region in central Germany, 15-min rainfall extremes were most common under southerly or easterly inflow from warm continental air and when there was a trough over western Europe. Weder *et al.* (2017) looked at the MSLP and z500 composites for the days with DWD weather types most frequently associated with summertime hourly extreme rainfall at the Hamburg weather mast. Their results indicated an upper-air trough just to the west of Hamburg, with southerly airflow and vertical lifting occurring ahead of the trough. On many days there is also a ridge over Scandinavia leading to increased upper-level cyclonic motions above northern Germany. The authors also mention that a strong jet stream over Germany, with weak near surface wind on these days, could result in even stronger convective activity. Finally, Mohr *et al.* (2020) show that the flash flood producing extreme thunderstorms in the May-June 2018 period occurred under a synoptic situation very similar to the WP6 z500 analysis shown here. In their case, the high-pressure ridge over Scandinavia blocked the passage of successive COLs that formed on its upstream edge, resulting in a 'locally enclosed geopotential minimum over the Bay of Biscay'. These results all indicate that our findings of WPs with an upper-level trough over western Europe, causing large-scale flow transporting moist air masses from the south or southwest (WP1, 2, 5, 6 and 11), being strongly associated with extreme sub-daily events in western Europe are robust and agree with previous, smaller-scale studies. Additionally the results from Weder *et al*. (2017) and Mohr *et al.* (2020) support the apparent importance of the high pressure anomaly over Scandinavia in WP2, WP5 and WP6 causing 3hr rainfall extremes, while the COLs in Mohr *et al.* (2020) are reminiscent of the z500 minima seen in days with 3hr extremes under WP6.

These large-scale flow patterns induce the advection of warm and moist air masses from west and southwest of the study region, often over the Iberian Peninsula and when this occurs in combination with an elevated mixed layer, a Spanish plume can develop (Morris, 1986; Lewis and Gray, 2010), resulting in conditions favourable to development of convective storms across much of north-western Europe. Lewis and Gray (2010) state their 'modified' Spanish plume can often result in the formation of a cut-off low. Here we have identified that z500 anomalies on days with

WP6 and extreme events feature a COL over Iberia. It is therefore feasible that in some situations the modified Spanish plume of WP5 may transition into the ridge and COL of WP6. Barbero *et al.*, (2019b) found that COLs contributed disproportionately (relative to their frequency) to the occurrence of hourly annual and seasonal maxima in the US. The high proportion of 3-hour events across Europe associated with WP6 suggests such a connection may also be present in this region. Indeed, the fatal flash flooding in Germany in July 2021 has been associated with a strong COL in the region (Kreienkamp *et al.*, 2021) and the extended period of flash flooding related to thunderstorms in early summer 2018 has been linked to multiple transitory COLs (Mohr *et al.*, 2020).

The presence of a wave pattern in the geopotential height anomalies under WP1 and WP2 for many of the regions studied here indicates a more meandering jet (less zonal), potentially associated with blocking of the westerly flow. If such blocking occurs in the days before a rainfall event, it could allow heat to build up in the regions under the high pressure, especially in summer when dry soils mean the solar radiation is heating the ground rather than evaporating surface water (Allan *et al.*, 2019; Mohr *et al.*, 2019) The subsequent introduction of warm, moist airflow can create conditions conducive to the generation of intense rainfall (high energy unstable atmosphere and moisture) (Allan *et al.*, 2019). Blocking systems have been shown to increase the odds of heavy 1-day and 3-day precipitation in the areas to the southwest and southeast of the blocking anticyclone (Lenggenhager and Martius, 2019) and Mohr *et al.* (2019) identified blocking over southern Sweden and the Baltic Sea in particular leads to an increase in the probability of thunderstorms over western and central Europe. This is thought to be due to decreased stability and increased moisture in the area from transport of warm, moist air masses from the southwest along the western flank of the blocking system, resulting in convection-favouring conditions. Additionally, Sauter *et al.* (2023) found extreme hourly rainfall was more likely to occur after a heatwave than for climatology in mid-latitude regions including Europe. Therefore, this could also be a factor in the relationship between 3 hour extremes and WPs with a blocking component over Europe.

4.5 Conclusions

We examined the relationship between large-scale atmospheric circulation and summertime 3hr rainfall events above 40 mm across large parts of western Europe. Large-scale circulation variability is represented by weather patterns (WPs) based on MSLP and composites of geopotential height at 500hPa. We found that during summer, a small number of WPs are repeatedly associated with 3hr extreme rainfall events across western Europe. These WPs typically occur in summer, according to the ordering system used in their development (Neal *et al.*, 2016). WPs 1, 2, 5, 6 and 11 were found to cause extreme 3hr rainfall events across most of Europe while

WPs 7 and 8 are also associated with 3hr extremes in Belgium, France, Norway and Ireland. Whilst MSLP patterns on their own do not provide an obvious mechanism for sub-daily extreme rainfall, examining their z500 anomalies reveals more information on the large-scale drivers. All WPs important for 3hr rainfall extremes have a southerly or south-westerly flow component across western Europe, bringing warm and moist air from regions to the south. In many cases this occurs along the leading edge of a trough, resulting in increased dynamical ascent due to PVA (Pfahl, 2014). There is often also a blocking ridge present over the Scandinavia/Baltic Sea region. In summary, 3hr extreme rainfall events in western Europe are connected with WPs that provide at least two of the three key ingredients for convective rainfall triggering (lifting, instability or moisture), with the final ingredient being delivered by mesoscale processes (Doswell, 1987; Doswell *et al.*, 1996). The presence of blocking (e.g. the Baltic sea) may enhance conditions conducive to development of convective activity as observed by Mohr *et al.* (2019, 2020). There is also a propensity for extremes to be associated with patterns which indicate a Spanish plume moving over western Europe (Morris, 1986; Lewis and Gray, 2010; Wilkinson and Neal, 2021).

Knowing which WPs are likely to be associated with extreme sub-daily rainfall has potentially beneficial applications for forecasting, as having an initial indication for early-warning of these events would help to identify periods with increased risk of (flash) flooding (Flack *et al.*, 2019; Richardson *et al.*, 2020; Wilkinson and Neal, 2021; Mastrantonas *et al.*, 2022b). While the WPs alone may not be sufficient as a predictor of extremes, the addition of the z500 anomalies greatly increases the ability to statistically identify extreme rainfall-producing WPs from non-extreme patterns. This benefit of the z500 parameter was also identified by Weder *et al.* (2017) for sub-daily extremes in Germany. As the current forecast warning time for sub-daily extremes is so short, a method to extend this lead time using forecasts of large-scale dynamics would be highly beneficial, enabling greater preparedness and helping to reduce the risk to infrastructure and lives from associated flash flooding (Flack *et al.*, 2019).

Richardson *et al.* (2020) have already shown the feasibility of using the MO30 patterns to forecast periods with higher risk of fluvial flooding several weeks ahead using the 30 WPs. Similarly, Wilkinson and Neal (2021) used ensemble outputs to create forecasts of UK thunderstorm probability based on the projected probabilities of MO30 WP occurrence. Their single case study result showed a signal for thunderstorms several days in advance, with the predicted location of the storms matching the observed occurrence. Based on the relationships found here, a similar method of forecasting periods with increased risk of sub-daily rainfall extremes (and therefore flash flooding) would be feasible. While the 3hr 40 mm threshold chosen here may not be representative of flash flood inducing rainfall everywhere within western Europe, it would be possible use local thresholds. This would provide increased confidence in forecasting of sub-daily rainfall extremes several days ahead, a large improvement on the current several hours ahead (Flack *et al.*, 2019). Including the z500 anomalies in these forecasts would allow even greater confidence in the results, as they can provide greater detail on the potential location of the extremes. As the z500 variable is already included in forecast models this would be an easy step to take. The inclusion of further variables such as integrated water vapour transport could provide even greater confidence in the forecasts (Lavers *et al.*, 2016; Wilkinson and Neal, 2021).

Links identified here between MSLP-based WPs (and z500) and sub-daily rainfall extremes could be used in climate modelling of future changes in these extremes. Climate models are much better at representing large-scale atmospheric patterns than small-scale rainfall and so these relationships could be used as a proxy for how the frequency and distribution of rainfall extremes may change in future climate (Chan *et al.*, 2018a, 2023). An investigation of future changes in the frequency of MO30 patterns and associated changes in climatological temperature and rainfall in the UK has already been performed by Pope *et al.* (2022), finding an increase in dry and calm weather types in summer, while Cotterill *et al.* (2023) examined the change in frequency of the weather patterns in autumn, linking this to a reduction in the number of extreme daily rainfall events. The actual weather patterns themselves will likely change in the future, due to changes in circulation such as extension of the Azores high driven by global warming (Cresswell-Clay et al., 2022). This would lead to future changes in the relationships between the weather patterns and extreme rainfall, however, this phenomenon (within-pattern changes) has not yet been investigated. The quantification of these relationships between WPs and extreme rainfall could also be used to improve the statistical downscaling of sub-daily hydrological impacts from future climate scenarios (Weder *et al.*, 2017; Rau *et al.*, 2020).

Chapter 5

Rossby Wave Connections to Sub-daily Rainfall Extremes

5.1 Introduction

Having identified in Chapter 4 that links between large-scale dynamical drivers and sub-daily rainfall extremes in Europe are possible to identify in weather patterns used in forecast models, this chapter investigates whether these links exist for even larger scale dynamics. As discussed in Section 1.6, Rossby waves are planetary-scale waves which can be identified through a variety of different methods and have been shown to contribute to multiple types of extreme weather events globally (Platzman, 1968; Röthlisberger *et al.*, 2019; Ali *et al.*, 2021; de Vries, 2021; Xu *et al.*, 2021). Previous analyses of connections between Rossby waves and extreme weather have predominantly focussed on the connections with temperature extremes. While several studies have identified clear links between Rossby wave or jet stream activity and extreme heat or cold events (Schubert *et al.*, 2011; Petoukhov *et al.*, 2013; Röthlisberger *et al.*, 2016b, 2019; Fragkoulidis *et al.*, 2018; Kornhuber *et al.*, 2020; Xu *et al.*, 2021), only a handful have examined the same connections for extreme rainfall events. Those that have looked at rainfall have only looked at daily or longer events and have generally focussed on winter rather than summer events (Röthlisberger *et al.*, 2016b; Kornhuber *et al.*, 2019; Ali *et al.*, 2021; de Vries, 2021; Barton *et al.*, 2022).

Most of the methods used to identify Rossby waves make an assumption that the waves must be small amplitude and linear. However most observed waves do not conform to these assumptions, having large amplitude or showing strongly non-linear behaviour such as wave breaking or cutoff formation (Ghinassi *et al.*, 2018). The finite amplitude wave activity (FAWA) index created by Nakamura and Zhu (2010) was developed as a solution to this problem as it obeys exact conservation relations even for large-amplitude waves. The FAWA index can be calculated from atmospheric data and is defined in terms of the meridional displacement of a potential vorticity (PV) contour from a suitably defined, zonally symmetric reference contour; it possesses an exact conservation relation alongside an exact non-acceleration theorem (Nakamura and Zhu, 2010; Ghinassi *et al.*, 2018). However, the FAWA index is defined by zonally averaged quantities and as such is not well suited for diagnosing the dynamics of transient synoptic-scale Rossby waves. Therefore, Huang and Nakamura (2016) created an extension of FAWA, the Local Finite Amplitude Wave Activity (LWA) metric, which is capable of quantifying regional disturbances in the atmospheric circulation (Martineau *et al.*, 2017). The LWA is a function of both latitude and longitude and recovers FAWA upon zonal averaging. This diagnostic provides information on the local waviness of the flow whilst remaining valid for finite-amplitude eddies (Huang and Nakamura, 2016; Ghinassi *et al.*, 2018).

The LWA has a benefit over previous metrics of waviness in that it can be calculated at each latitude and longitude, allowing regional trends to be examined without having to make arbitrary regional definitions (Blackport and Screen, 2020). It also takes into account both the meridional displacement of contours and the strength of the zonal anomalies, providing a more robust measure of waviness than methods investigating the meridional displacement of contours or measuring the departures from zonal symmetry (Martineau *et al.*, 2017). Since Huang and Nakamura (2016), several studies have used LWA on 500hPa geopotential height contours instead of on PV contours. These include Chen *et al.* (2015) who used the LWA calculated on z500 to describe four midlatitude extreme temperature events. Their results indicated that the LWA was a natural diagnostic of the atmospheric features (namely blocking) associated with these extreme events. Blackport and Screen (2020) used LWA on z500 to measure the response of waviness in the mid-latitude circulation to Arctic amplification. Martineau *et al.* (2017) used the LWA based on z500 to diagnose extreme wave activity events in the troposphere. The wave events were identified as contiguous areas where the grid points had LWA > median LWA and the maximum value of LWA over the event and its geographical coordinates were kept, with the LWA divided into its cyclonic and anticyclonic components. Regional temperature extremes were found to be more likely under the large-amplitude troughs and ridges of the wave events.

The LWA can be split into cyclonic (LWA-c) and anticyclonic (LWA-a) components, which highlight regions of anomalous troughs and ridges. Martineau *et al.* (2017) found that these components have different climatological behaviour, with anticyclonic LWA having a bigger effect on wave activity in winter (DJF). The locations of the LWA-a and LWA-c winter activity correspond to the winter location of stationary waves with a maximum in LWA-a found over the UK and Alaska and the LWA-c maximum over northern Canada and the Sea of Okhotsk. The anticyclonic and cyclonic components of Rossby wave activity thus have climatological locations at longitudes corresponding to the jet stream exit and entrance regions respectively (Martineau *et al.*, 2017). Both components of wave activity weaken in summer months in the mid-latitudes and undergo an eastward shift in the location of maximum activity in this season. This overall weaker wave activity in summer may, in part, be explained by the reduced amplitude of planetary-scale waves and their weaker baroclinicity (Randel, 1988; Martineau *et al.*, 2017). Martineau *et al.* (2017) also investigate the LWA climatology for z500 in both winter (DJF) and summer (JJA). For winter, they find a European LWA maximum dominated by anticyclonic wave activity, while in the northwest Atlantic the LWA maximum represents cyclonic wave activity. In summer the LWA amplitude is reduced over the Atlantic and Europe, while the European LWA maximum shifts to the north following the poleward shift of the North Atlantic jet. Similar to Chen *et al.* (2015), the authors find cold and hot extremes are more likely to occur under the large-amplitude troughs and ridges associated with wave events, suggesting large-scale wave trains may play an important role in the frequency of these extremes in the northern hemisphere.

The meridional wind at 300 hPa (v300) is also used as a proxy for Rossby waves and has been utilised in several studies investigating links with extreme weather events. Wolf *et al.* (2018) used the v300 to assess the connections between quasi-stationary waves (QSW) and extreme temperature events in Europe. Using a 7-day running mean to identify more persistent extreme events, they showed the extremes are connected to very strong contemporaneous QSW amplitudes, which are zonally elongated, indicating the extremes are connected not just to a local block but also a strong, zonally extended and long-lived wave train. They also found similar results for extreme precipitation events which are discussed further in section 5.4. Composites of v300 were also used by Kornhuber *et al.* (2020) to diagnose the presence of Rossby wave patterns with wavenumbers 5 and 7 in the midlatitude circulation. They found that waves with these wavenumbers exhibit preferred phase positions. High-amplitude waves with these wavenumbers were also strongly associated with extreme heat events, particularly for the co-occurrence of these events simultaneously in multiple regions. Kornhuber *et al.* (2019) used spectral decomposition of v300 to identify the phase and amplitude of Rossby waves, revealing a wavenumber 7 pattern associated with persistent temperature and rainfall anomalies in the northern hemisphere in summer 2018.

Quasi-stationary waves are waves with a phase speed close to zero. Such waves have been identified as being connected to extreme weather events in recent investigations (Hoskins and Woollings, 2015; Wolf *et al.*, 2018; Kornhuber *et al.*, 2019, 2020). Atmospheric QSWs that influence extreme weather typically have anomalously high amplitudes that persist for longer than synoptic timescales and are detectable in e.g. 14-day low-pass filtered data (Wills *et al.*, 2019). Wolf *et al.* (2018) use a 15-day lowpass filter to identify slowly propagating waves in the v300 parameter. These filters mean the wave phase only needs to remain the same for ~7 days. However, there is no official time related definition of QSW. In this thesis we examine the Rossby wave activity over the 7 days before and 3 days after an extreme event - given the short timescale of the rainfall events and the restricted ability of forecast models to provide a skillful forecast beyond 5-7 days, this provides a time period within which a relationship between sub-daily rainfall and a relatively slow-moving wave can be identified. Therefore, here we refer to waves which have a phase speed close to zero for ~5 days as quasi-stationary.

This chapter investigates the potential relationships between very large-scale dynamical drivers (in the form of Rossby waves) and sub-daily rainfall extremes. This is done by examining the large-scale circulation present on days with the 20 strongest 3hr rainfall events in Germany and the UK using the LWA, z500 and v300 metrics. The data and methods used are in section 5.2, the results in 5.3 and discussions in 5.4 with conclusions in 5.5.

5.2 Data and Methods

5.2.1 Local Finite Amplitude Wave Activity

While the LWA diagnostic was originally developed for use with PV (Huang and Nakamura, 2016) it has since been used in association with the 500-hPa geopotential height (z500); as z500 is an easily obtainable atmospheric metric that has already been widely used to investigate weather extremes (Chen *et al.*, 2015; Martineau *et al.*, 2017). This allows comparison with other studies of extreme weather using geopotential height. The code used to calculate the LWA values used here was kindly provided by R. Blackport from Blackport and Screen (2020). These values were calculated following the methods of Chen *et al.,* (2015) and Martineau *et al.,* (2017).

The calculation of wave activity relies on the determination of the equivalent latitude (ϕ_e) for a given line of constant geopotential height (z_c) (Eqn 1.)

$$\phi_e(z_c) = sin^{-1}\left(1 - \frac{\iint_{z \leq z_c} cos\phi \; d\lambda d\phi}{2\pi}\right)$$

Equation 1: Calculation of equivalent latitude

Here, z is the geopotential height, ϕ is the latitude and λ represents the longitude. This equation provides the latitude for which the total area enclosed between the latitude and the pole is equivalent to the area where z is smaller than z_c. The equivalent latitudes were calculated separately each day to avoid any effects from the northward migration of geopotential heights due to seasonal changes or global warming. The cyclonic (LWA-c) and anticyclonic (LWA-a) components of LWA were then calculated for each latitude and longitude, where $\hat{z} = z - z_c$ and a is the radius of the Earth (Eqn 2 and 3). The total LWA is then the sum of the cyclonic and anticyclonic components. The total length of the line integrals of LWA-a and LWA-c are equal when integrated around the northern hemisphere (Chen *et al.*, 2015; Huang and Nakamura, 2016; Martineau *et al.*, 2017; Blackport and Screen, 2020). An illustration of the calculation of LWA is provided in Figure 5.1.

$$LWAa(\lambda, \phi_e) = \frac{a}{cos\phi_e} \int_{\hat{z} \geq 0, \phi \geq \phi_e(z_c)} \hat{z}(\lambda, \phi) cos\phi d\phi$$

Equation 2: Calculation of anticyclonic LWA

$$LWAc(\lambda, \phi_e) = -\frac{a}{cos\phi_e} \int_{\hat{z} \leq 0, \phi \leq \phi_e(z_c)} \hat{z}(\lambda, \phi) cos\phi d\phi$$

Equation 3: Calculation of cyclonic LWA

a)

b)

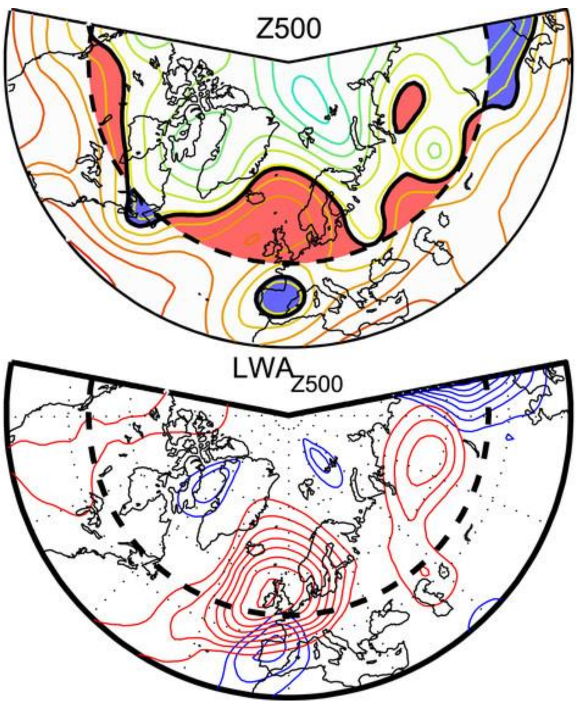

Figure 5.1: a) The displacement of a wavy z500 contour (z_c) with respect to its equivalent latitude (ϕ_e) (dashed line). In this case the contour $z_c(\phi_e$ = 50oN) is shown for 13 Feb 1983. The wavy contour z_c encloses an area z500 $\leq z_c$ that is equal to the area found to the north of the equivalent latitude. By definition, the regions shaded in red and blue, used for the computation of LWA-a and LWA-c components of LWA, respectively, are also of equal surface area.

b) Values of LWA-a and LWA-c calculated at all equivalent latitudes, with the ϕ_e for 50oN shown again.

Figure reproduced from Figure 1 in Martineau et al. (2017).

The LWA data used in this study was calculated for each day from daily averaged 500-hPa geopotential height data and is available as daily values at 1°x1° resolution for the period 1979-2018 (Blackport and Screen, 2020). Here only the data for grid points between 20°N and 80°N were used as the focus is on extratropical regions. Data above 80°N were excluded to avoid spurious results due to the spherical nature of the Earth. The LWA at each grid point measures the extent and magnitude of excursions of geopotential height to the north (ridges) and south (troughs), including any cutoff lows and highs; this gives the extent/amplitude of waviness within the large-scale flow (Blackport and Screen, 2020). In this thesis, we consider the LWA-a and LWA-c separately to investigate the anticyclonic or cyclonic activity of the local anomalies; these highlight local variations in activity (as Martineau *et al.* 2017). Large values of LWA-a correspond to prominent atmospheric ridges while large LWA-c values are associated with troughs or cutoff lows.

A seasonal JJA climatology for the LWA components was calculated by averaging all JJA days across all years (Figure 5.1). This is very similar to the climatology shown in Martineau *et al.*

(2017) (their Figure 5) and therefore we are confident that the method used to calculate the LWA here is robust. To account for intra-seasonal variation of the LWA climatology a daily climatology was calculated and smoothed using a 45-day rolling mean. Several different rolling-mean lengths were tested and 45 days was found to produce the smoothest climatology whilst still capturing significant variations over time. This climatology is influenced by both the stationary waves and transient waves. The smoothed LWA climatology was then used to calculate daily anomalies for LWA-a and LWA-c at each grid point. Composites of the mean anomaly for each LWA component on days with extreme rainfall events were then created, enabling the average wave activity on these days to be examined. A climatology of the LWA calculated on the z500 climatology was also plotted to show the location of stationary waves without the influence of transient waves.

5.2.2 Rainfall data

The rainfall data used in this analysis was taken from the observational gauge-based GSDR dataset (Lewis *et al.*, 2019, 2021). Only gauges with <15% missing data in the calendar year and at least 2 complete years of record are included. This missing data threshold was used to ensure only gauges with less than 2 months of data missing were included, so there is a higher chance of having relatively complete records over the summer months (the focus of this analysis). The 3hr data was calculated from rolling window aggregations of 1hr data. The 3hr rainfall extremes are examined using the *n*-largest approach (Blenkinsop *et al.*, 2017). In this approach the top $n.y$ events are selected from the gauge record where *n* is the desired number of events and *y* is the number of years. Therefore, if the gauge has a record length of 20 years and an *n* value of 1 is chosen then the top 1 x 20 = 20 events will be selected. This removes an issue of the block maxima approach where the maximum event in one year may be lower than several events in another year, but these larger events are excluded from the analysis. Hence, the n-largest approach produces a more comprehensive series of extreme events than may be achieved with the block maxima approach (Blenkinsop *et al.*, 2017). The analysis here uses an *n*=1 method and focusses on summer, so only events occurring in June, July or August are selected (giving the largest seasonal events rather than the largest annual events). The *n*-largest events were declustered in time to ensure their independence from each other. Identifying independent rainfall events relies on determining the minimum time required between events (*tb*) for them to be considered independent. To this end the declustering procedure was carried out following the methods from Restrepo-Posada and Eagleson (1982), who created a statistical method to calculate *tb* based on the assumption that independent rainstorms follow a Poisson arrival process. To identify independent 3hr events, the critical interarrival time (*tb*) required between wet periods for them to be considered independent was calculated for each gauge, using the Restrepo-Posada and Eagleson (1982) algorithm. To obtain independent events, all rainfall that is separated by $tb < tb_{min}$ is considered to belong to a single storm. The value for tb_{min} was iteratively increased until rainfall arrival times follow an exponential distribution and are therefore independently distributed. The value of *tb* where this condition is met was then used as the time period required between events for them to be considered independent. For each gauge the maximum continuous dry day (CDD) index value for the closest grid cell of the GHCNDEX (Donat *et al.*, 2013a) and HadEX2 (Donat *et al.*, 2013b) Climdex datasets was used as the upper bound on the duration of the dry spell between events. We note here that longer periods without recorded rainfall may be present in the dataset due to missing data or the removal of suspect data during the QC procedure (Lewis *et al.*, 2021) and their presence may bias the *tb* estimates (Villalobos-Herrera *et al.*, 2023). The *tb* value was then used to ensure that the 3hr *n*-largest events were temporally independent events.

The *n*1-largest events were identified and the top 20 largest 3hr events for each country (Germany and the UK) were then selected from this timeseries. These events are selected from the time period from 1979-2015 to match the start date of the LWA data, although for Germany data is only available from 1995, and in both countries GSDR gauge records end in 2015. Only events on separate days were kept, *i.e.* if 2 events within the top 20 occur on the same day at different gauges then only the largest event is kept and the 21st largest event is then chosen. Removing events occurring on the same day ensures that the atmospheric conditions associated with events affecting multiple gauges on a single day are not given extra weighting when the atmospheric composites are computed over multiple events (Allan *et al.*, 2019). The locations and intensity of these events are shown in Figure 5.2. While examining rainfall by country does not necessarily provide the best hydrological division, the gauge data is provided by country and trying to determine homogeneous rainfall regions for several countries was outside the scope of this study. The countries chosen as case studies are the UK and Germany due to the density and quality of hourly rain gauge coverage and their representation of two different rainfall regimes – with the UK having a maritime influenced regime and Germany a continental regime.

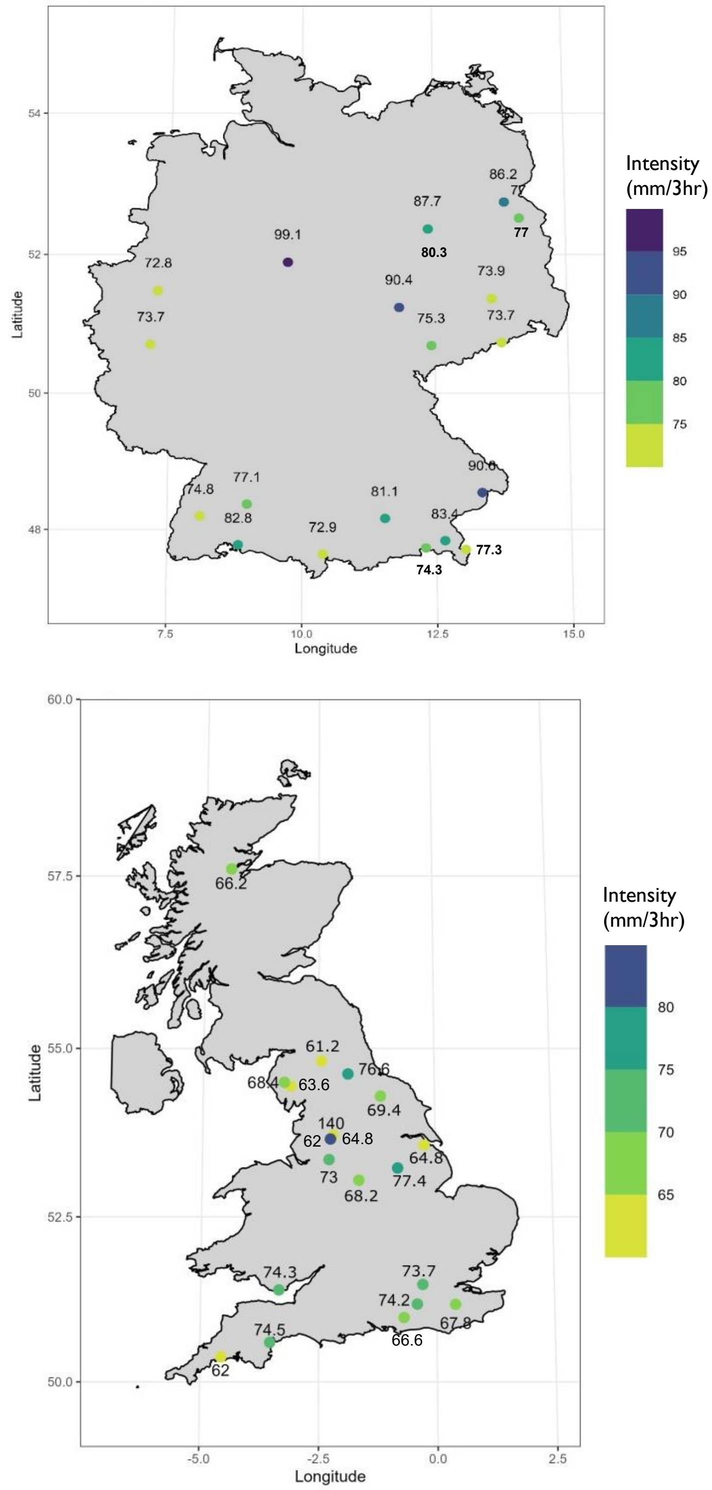

Figure 5.2: The location and intensity of the top 20 3hr rainfall events in Germany and the UK. The individual event intensity is given in mm next to the gauge recording the event (coloured dot). Note in both cases there is one gauge which recorded two of the top 20 events so only 19 gauges are shown.

5.2.3 Geopotential Height Data

As in Chapter 4 we use ERA5 geopotential height data at 500 hPa (z500) with a resolution of 0.25° x 0.25° and 6-hourly timestamps. Here, the data were converted into daily data by averaging 6-hourly data across the 24 hour period (0-6hr, 6-12hr, 12-24hr, 18-24hr) . Using the daily average of 6-hourly data for the z500 maintains temporal consistency of these data with the LWA data. The z500 anomalies were then calculated in several steps. Firstly, a climatology of the daily z500 was determined using a 45-day rolling mean (with the geopotential at 500hPa values divided by 9.80665 to get z500). Then for each day the climatology was subtracted from the z500 value to get the anomaly at each grid point. This anomaly was then plotted for the desired days. The standardised z500 anomalies were calculated by taking the standard deviation of the anomalies in time and then dividing the z500 anomaly on desired days by this standard deviation. This enabled the identification of areas with very small anomalies in regions which typically have very small variability, which may otherwise be missed in plotting.

5.2.4 Meridional Wind Data

We used daily mean meridional wind at 300hPa data from ERA5 for 1979-2016, to match the LWA time period, with a resolution of 0.25^{o} x 0.25^{o}. A 45-day rolling mean climatology was calculated and daily anomalies from this climatology determined. The anomalies on the days of the top 20 3hr rainfall events were extracted and composites of these days were created. The evolution of the v300 in the days leading up to the extreme rainfall events were then examined using these composites.

5.2.5 Temperature Data

We used the maximum daily 2m temperature hourly data from ERA5 at 1^{o} x 1^{o} resolution. The climatology of these data was calculated using a 30-day rolling mean and the daily anomalies determined from this climatology. A shorter rolling mean was used for the temperature data than for the atmospheric data given the lower variability of the former. To identify and compare the temperature change at each rain gauge on the days surrounding the extreme rainfall event, the temperature anomalies from the ERA5 grid cell closest to the gauge were extracted. In each case the composite anomalies were then normalised against the temperature climatology for this grid cell, by subtracting the mean and dividing by the standard deviation. This allows the temperature variation at gauges in different parts of Germany/the UK to be compared in anomaly space.

5.3 Results

Results are shown only for summer months, the same as Chapter 4.

5.3.1 Climatology

The climatologies for LWA cyclonic and anticyclonic components are shown in Figure 5.3. The LWA anticyclonic climatology shows a peak over Scandinavia and much of northern Russia and Alaska. There is also an extended region of high values over northern Africa. The cyclonic climatology shows peaks over Greenland and Baffin Bay and also over the Bering Strait. These climatologies are very similar to those shown in Figure 5 of Martineau *et al.* (2017). A second climatology for the LWA was calculated using the climatological z500 values as described in Section 5.2. This shows the location of the stationary waves only, as it is a LWA climatology of the mean z500 (stationary waves), essentially removing the transient waves in this climatology. These figures show a similar pattern to the cyclonic LWA, but the anticyclonic LWA shows a much weaker peak over eastern Russia and no extended peak towards Alaska. These differences indicate that the large peak seen over Scandinavia in Figure 5.3 is mostly driven by transient waves, suggesting that this is a preferred pathway for the waves.

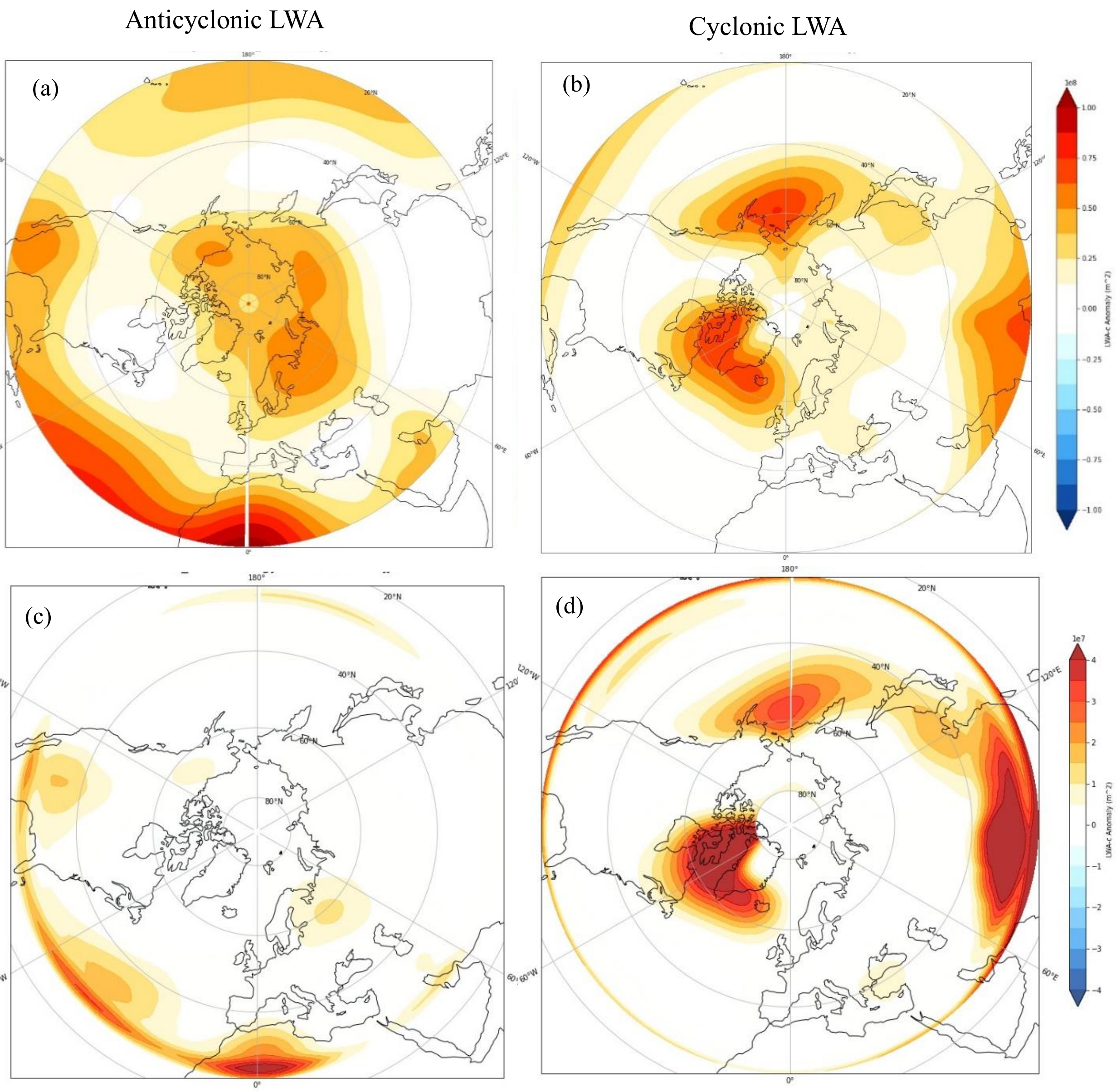

Figure 5.3: Climatologies of anticyclonic (column 1) and cyclonic (column 2) components of LWA. a) and b) climatology of LWA based on daily z500 values (Stationary waves + transient waves). c) and d) climatology of LWA based on climatological z500 (Stationary waves only).

5.3.2 Top 20 3hr Event Composites

The LWA component anomalies for each day with a top 20 3hr event were extracted and a composite of the anomalies on these days created for each country (Figure 5.4). For Germany the composite of the 20 most intense 3hr events in summer has a positive LWA-c anomaly extending from the UK northwest towards Greenland, indicating anomalous cyclonic activity in this region, with a negative anomaly over the Labrador Sea. Notably there is also a very strong positive anomaly over Alaska, and this anomaly is present on most days included in the composite (Figure 5.7). The LWA-a exerts a strong positive anomaly over Scandinavia and a negative anomaly over the Bay of Biscay with another positive anomaly further south. These results indicate that during extreme 3hr rainfall events in Germany, the large-scale atmospheric conditions feature anticyclonic activity to the northeast of Germany and cyclonic activity to the west, potentially resulting in the transport of moisture from the Mediterranean over Germany. There appears to be a wave pattern in the LWA-a at lower latitudes, stretching from the Pacific across to the middle of the Atlantic, where there is another wave stretching north over the UK and Scandinavia.

For events in the UK there is a strong signal of a positive LWA-c anomaly to the west of the UK and a negative anomaly over the Labrador Sea and over the Bering Strait. The LWA-a shows a strong positive anomaly over the Low countries and southern Scandinavia and another positive anomaly over Alaska, with negative anomalies over northern Russia. This large-scale circulation pattern would potentially lead to transport of moisture from the Bay of Biscay and the English Channel over the UK. There is an identifiable wave pattern in the LWA-a at lower latitudes, stretching from the eastern Pacific around to the coast of Portugal.

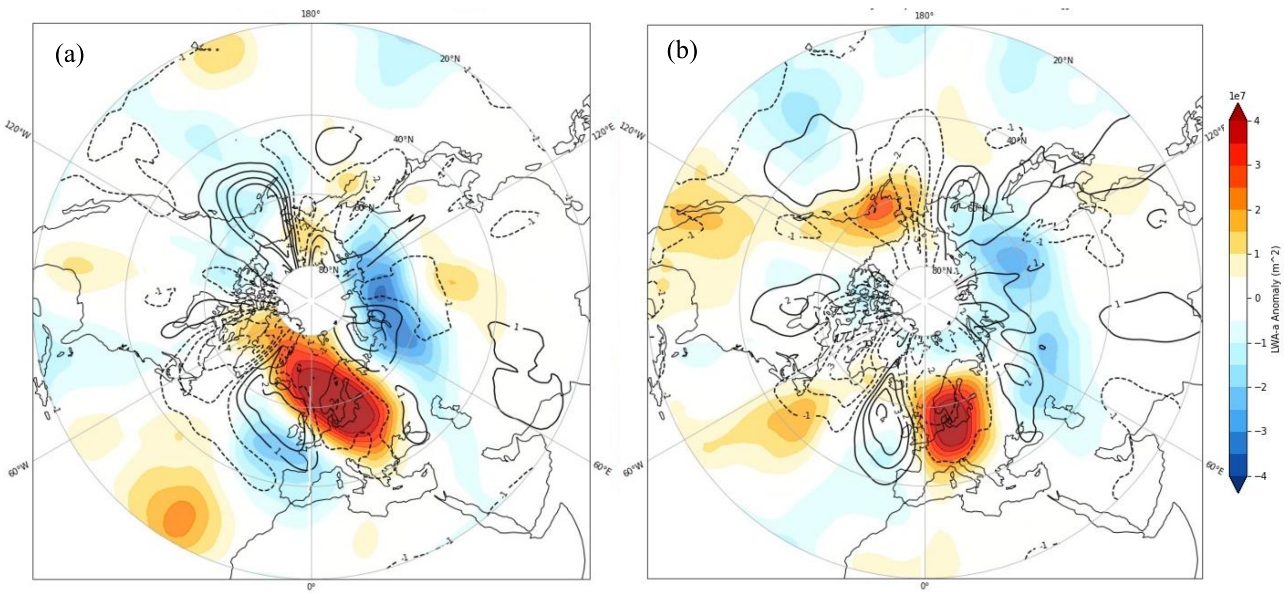

Figure 5.4: Composites of the mean LWA cyclonic and anticyclonic component anomalies on days with top 20 3hr rainfall events in a) Germany and b) the UK. LWA-a shown in colour and LWA-c as black contours.

The LWA anomalies from the LWA climatology based on the z500 climatology (Figure 5.3 c&d) were also calculated. This removes the stationary waves from the everyday flow, with the resulting anomalies representing the transitory waves present on each day. Composites of LWA anomalies from the z500-based LWA climatology for the top 20 3hr events were produced and the results show some small differences (See Appendix Figure C.1). In both case studies the LWA-c shows much larger anomalies (spatially) and a wave pattern. A positive LWA-a anomaly over the

Scandinavian region indicates blocking occurs here above the stationary wave effect. The LWA-a still shows the low latitude wave train, although this is a weaker signal. The composites in Figure 5.4 and Figure C.1 all indicate strong associations between particular Rossby wave patterns and the location and occurrence of extreme sub-daily rainfall events, with some similarities between the patterns for the UK and Germany.

5.3.3 Top 20 3hr vs Top 20 24hr Event Composites

To assess the differences between the observed composite wave patterns associated with the 3hr events and the conditions for longer-duration events, the LWA anomalies for the top 20 24hr events were also calculated and used to create a composite plot (Figure 5.5). For both the UK and Germany this reveals a Rossby wave pattern very different to the 3hr event composite pattern.

For Germany 24hr events (Figure 5.5a) there is a very strong, contained negative LWA-c anomaly over Germany with a small positive LWA-a anomaly to the north. The negative anomaly here indicates a strong cyclone associated with the events. The strong positive LWA-c anomaly over Alaska is not present and the low latitude wave pattern while still present is much weaker. Similarly for the UK (Figure 5.5b) there is a strong positive LWA-c anomaly directly over the UK and Ireland and unlike for the 3hr events, there is no accompanying strong positive LWA-a anomaly over Scandinavia. There is also a positive LWA-c anomaly over Alaska. The wave pattern in the LWA-a at lower latitudes in the 3hr composite is still present but much weaker in the 24hr composite.

These results indicate that both the UK and Germany 24hr rainfall extremes are reliant on a large cyclonic anomaly being present, indicating a large-scale trough in the area, whereas 3hr rainfall extremes originate from a positive anticyclonic anomaly adjacent to a smaller cyclonic anomaly.

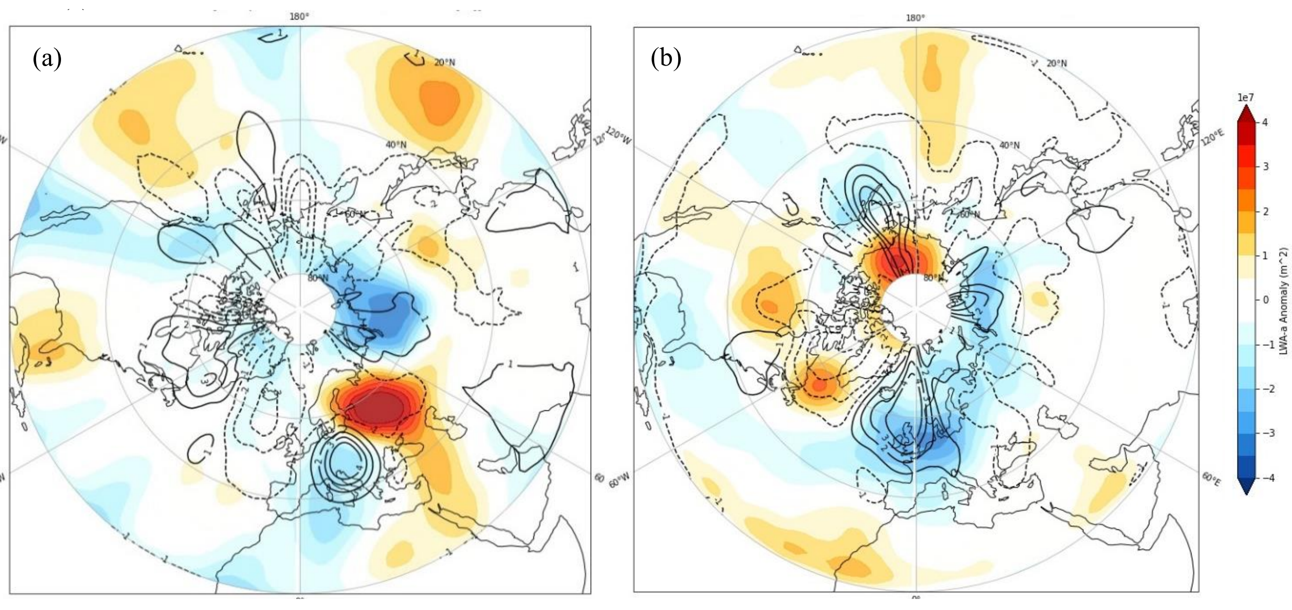

Figure 5.5: Composites of mean LWA cyclonic and anticyclonic component anomalies on days with top 20 24hr events in a) Germany and b) the UK. LWA-a shown in colour and LWA-c in black contours.

These results indicate a difference in the large-scale atmospheric (Rossby wave) patterns associated with sub-daily and daily extremes in the UK and Germany, which highlights the need to examine the dynamical drivers of different duration rainfall events separately. While the LWA is only capable of showing the large-scale features of midlatitude flow (Martineau *et al.,* 2017), these results suggest that it can identify variability between the atmospheric patterns associated with sub-daily extreme rainfall events and those associated with daily extremes, suggesting a large-scale dynamical influence for both.

5.3.4 Top 20 3hr vs Top 21-40 3h Event Composites

To assess whether the identified LWA patterns are only present for the most intense events, the LWA anomaly on each of the top 21-40 most intense 3hr events was calculated to create the composites in Figure 5.6.

For Germany, the top 21-40 3hr events have a visually similar LWA anomaly pattern to the top 20 events (see Figure 5.4a), with a positive LWA-a anomaly over Scandinavia and a positive LWA-c anomaly over Germany and France. The positive LWA-c anomaly over Alaska disappears for the weaker extremes but the wave pattern in both the cyclonic and anticyclonic components is still present, although much weaker. The very strong positive values at low latitudes are likely an artefact of the methodology and not a physical signal. For weaker 3hr events in the UK, the positive LWA-c anomaly becomes more centred over the UK and the positive LAW-a anomaly over Scandinavia disappears, with the pattern more resembling the 24hr event composite. There is still a wave pattern to the LWA-c components, with a positive anomaly over eastern Canada and Alaska as well as the UK. However, the wave pattern within the LWA-a is no longer clearly visible. The lack of positive LWA-a over Alaska and the change in position of the positive LWA-c over the UK suggests these weaker events are perhaps not as strongly associated with Rossby wave forcing.

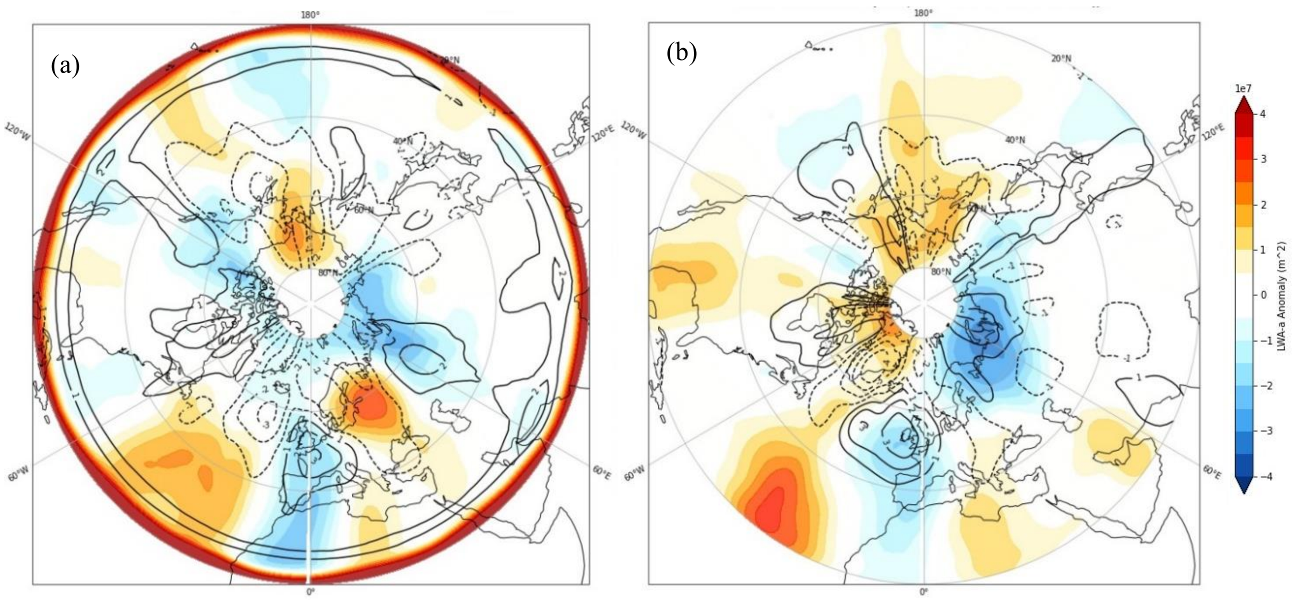

Figure 5.6: Composites of the LWA component anomalies on the top 21-40 3hr rainfall events in a) Germany and b) the UK

5.3.5 Individual Day LWA Anomalies

To further examine the LWA anomalies present on the days with 3hr extreme rainfall, the anomalies for each extreme event day were plotted, with results shown in Figure 5.7a and 5.7b. These show that most days with an extreme event in Germany (Figure 5.7a) have a similar pattern to the composite, indicating the composite is not heavily dominated by a small number of the days. Visually, 15 of the days have a positive cyclonic anomaly to the west of the UK and 15 days have a positive anticyclonic anomaly over Scandinavia (although a few of these days do not have both). Additionally, 15 of the 20 days have a positive cyclonic anomaly over or close to Alaska, which appears to be part of a wave train at high latitudes. Some of the individual days also have a wave train reaching from the Atlantic up to Europe, although this is only clear in ~9 or 10 of the days.

For the UK (Figure 5.7b), a smaller proportion of the individual days show a pattern clearly similar to the composite plot. Only 11 of the 20 days have both a positive anticyclonic anomaly over Scandinavia and a positive cyclonic anomaly to the west of the UK. 10 of the days show a positive anticyclonic anomaly over Alaska and 12 days appear to have a wave train around the pole from Russia towards Europe. The fact these patterns show up in the composite is therefore an indication that when these patterns are present, they are particularly high magnitude.

We note that these individual day plots are relatively noisy and we do not expect every extreme event to be related to a particular large-scale pattern. Some will certainly be triggered simply by mesoscale processes. However, the individual day plots provide evidence that the wave patterns seen in the composites are genuine and are not artefacts from taking the composite mean.

To further investigate the level of variability across the composites from Fig 5.4, the standard deviation across the 20 days was calculated for each country. These plots are in Appendix Figure C.2 (a, b) and show there is greater variation across the composite in the LWA-c anomalies, which is likely due to the fact the smaller (spatially) cyclonic anomaly can occur in different locations to produce the conditions for extreme rainfall. There is less variability in the LWA-a anomalies as the blocking anticyclonic anomaly occurs more consistently over the Baltic region. This is true of the results for both countries. The standard error on the mean for each composite was also determined with the results shown in Figure C.3 (a, b). This again shows the largest signals occur over Scandinavia for the anticyclonic anomalies indicating this mean anomaly is significant, while the cyclonic anomalies have large signals in a variety of locations indicating despite the variable location of the mean cyclonic anomalies associated with the extreme events they are still significant.

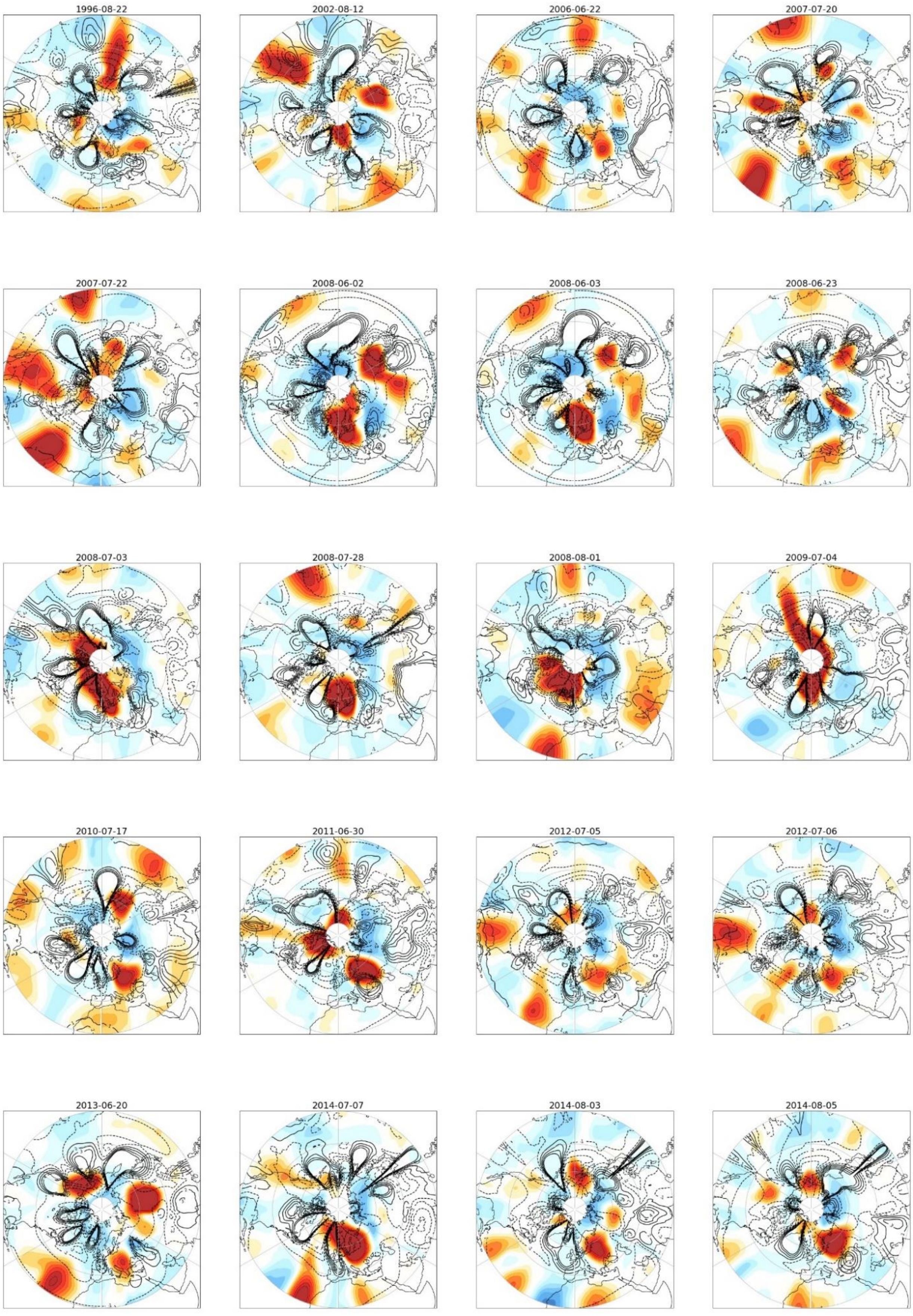

Figure 5.7a: LWA component anomalies on each of the top 20 3hr rainfall event days, Germany.

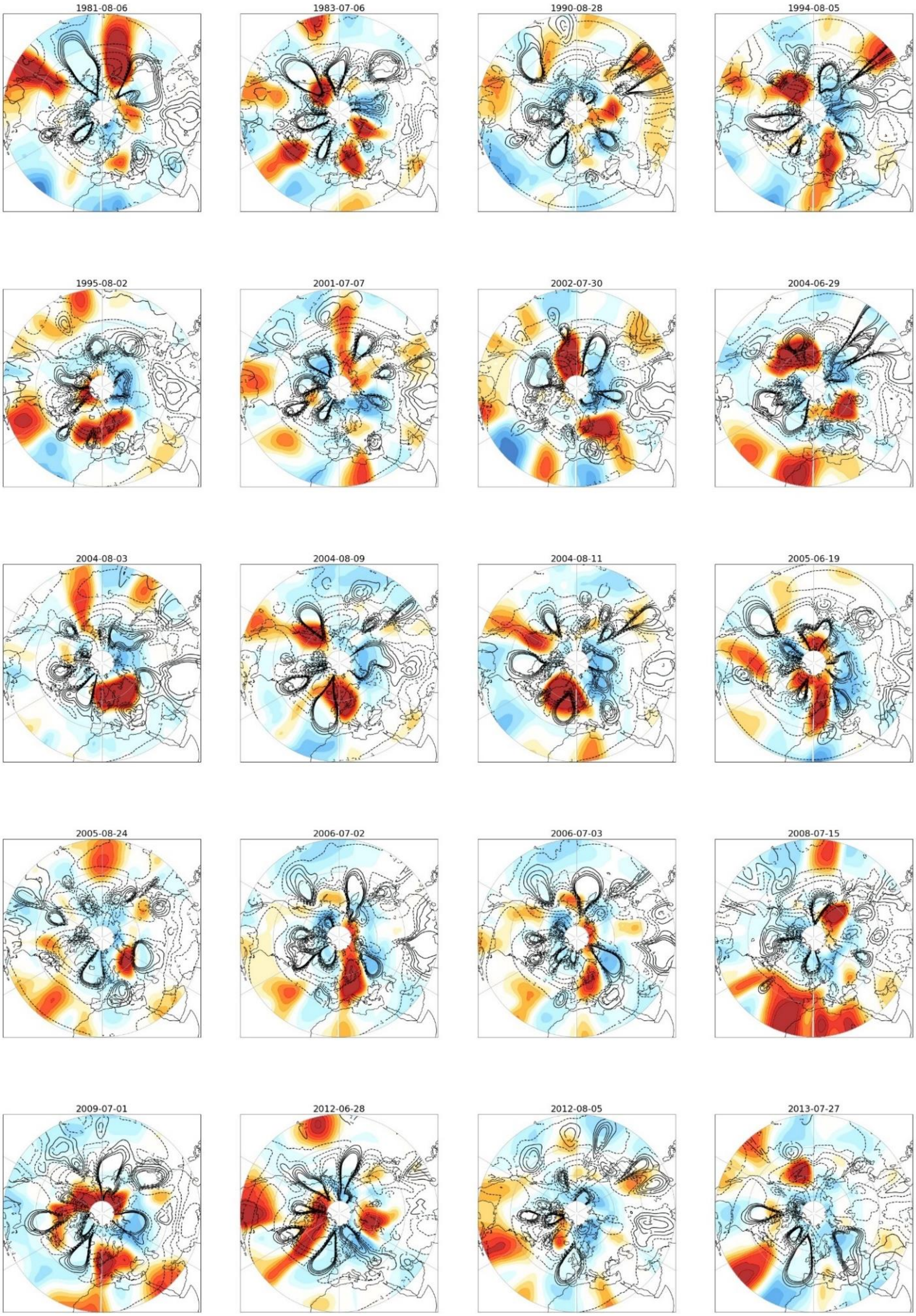

Figure 5.7b: LWA component anomalies on each of the top 20 3hr rainfall event days, UK

5.3.6 *Significance of LWA Anomalies*

To assess whether large-scale patterns seen in the top 20 3hr event composites are robust, we now assess the statistical significance of the anomalies using bootstrapping. This indicates whether the observed composite anomaly patterns are significantly different in their spatial location and amplitude compared to a bootstrapped composite of 20 randomly selected 'standard' days. We bootstrap resample 500 times for JJA days with randomised years to determine the 5^{th} and 95^{th} percentiles of the LWA-a and LWA-c anomaly composites on summer days, with the mean of 20 random days taken each time. In the bootstrapped composites, we keep the day-of-year of the 20 extreme events to account for any effects due to the seasonal cycle and randomise only the years. The results of this analysis are shown in Figure 5.8.

The results for the UK show the positive LWA-a anomaly over Scandinavia on these days is above the bootstrap 95^{th} percentile, as is the anomaly over Alaska. The LWA-c positive anomaly to the west of the UK is also above the 95^{th} percentile. Therefore, the anomalies associated with the 3hr extreme events are significant at the 90% confidence interval. The results for Germany indicate the positive LWA-a anomaly over Scandinavia is significant, as are the negative anomalies on either side of this and the positive LWA-c anomaly over the UK. These results suggest that the wave pattern is not noise and that the anomalies linked to rainfall are significant as the stippling occurs in the regions which have 3hr rainfall extremes, as well as in much of the upstream Rossby wave pattern.

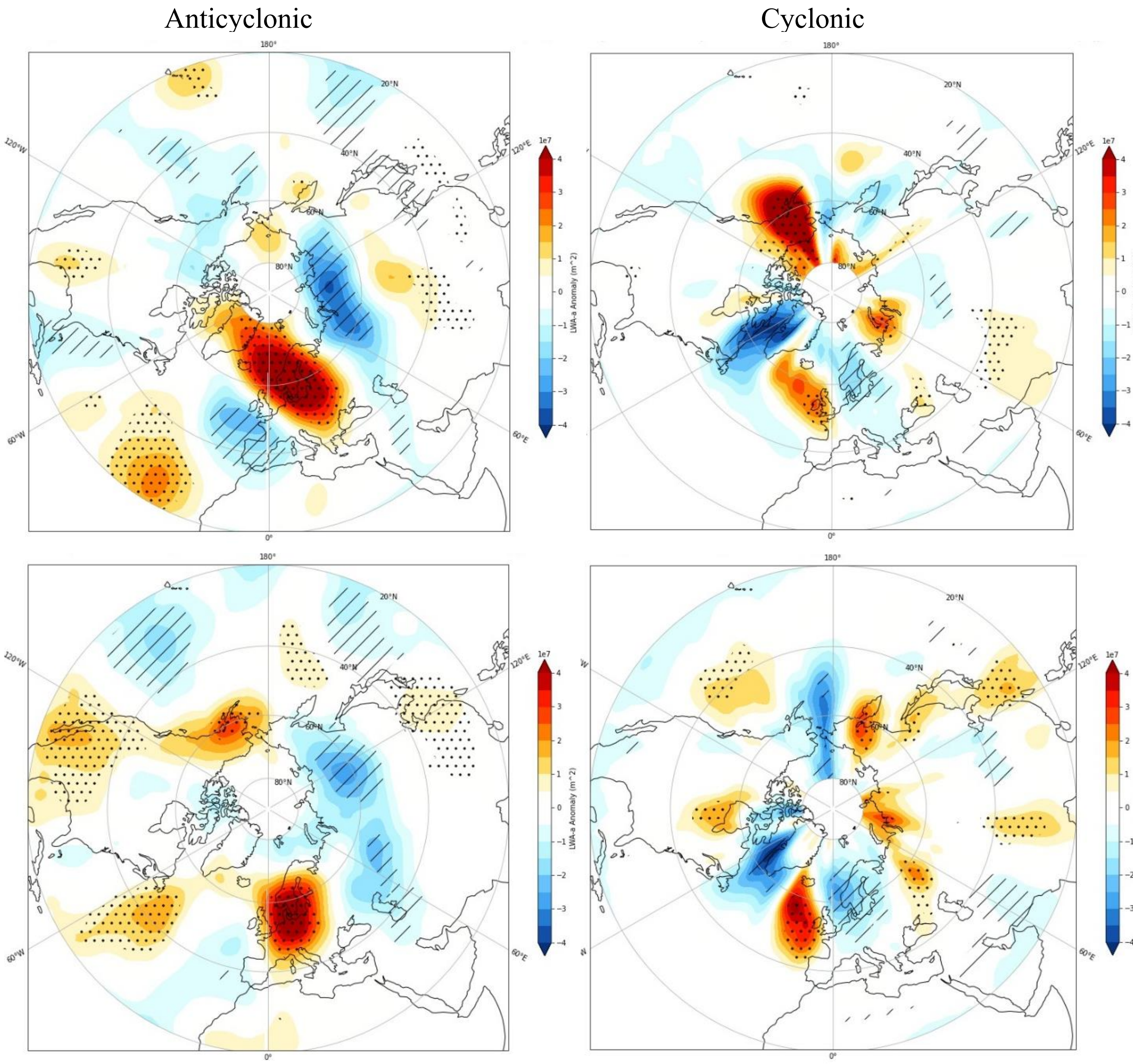

Figure 5.2: Bootstrapped significance of the mean LWA anomalies on top 20 3hr event days in Germany (top row) and the UK (bottom row). The first column shows anticyclonic anomalies, the second column cyclonic anomalies. Stippling shows regions with anomalies above the 95th percentile level. Hashes show regions with anomalies below the 5th percentile.

To further investigate whether the magnitude of LWA anomalies on the 3hr extreme event days were unusual, histograms of the daily mean LWA anomalies at certain locations were constructed. Bounding boxes were determined, which covered regions of one whole wavelength where the LWA component anomalies on the top 20 days were particularly strong. Then for each JJA day of the LWA record (1979 – 2020) the mean absolute cyclonic and anticyclonic anomalies within these boxes was calculated. The results of this analysis for Germany are shown as a 2d histogram in Figure 5.9 (See Appendix Figure C.4 for UK results). The individual anomaly values for the top 20 event days are also shown (red crosses), as is the mean value for all JJA days (pink circle) and the top 20 days (red circle). Figure 5.9 indicates that anomalies on the top 20 3hr rainfall days are not generally any higher in amplitude than anomalies on non-extreme days. Therefore, the driver for extreme rainfall is unlikely to be the increased amplitude of the LWA anomalies alone.

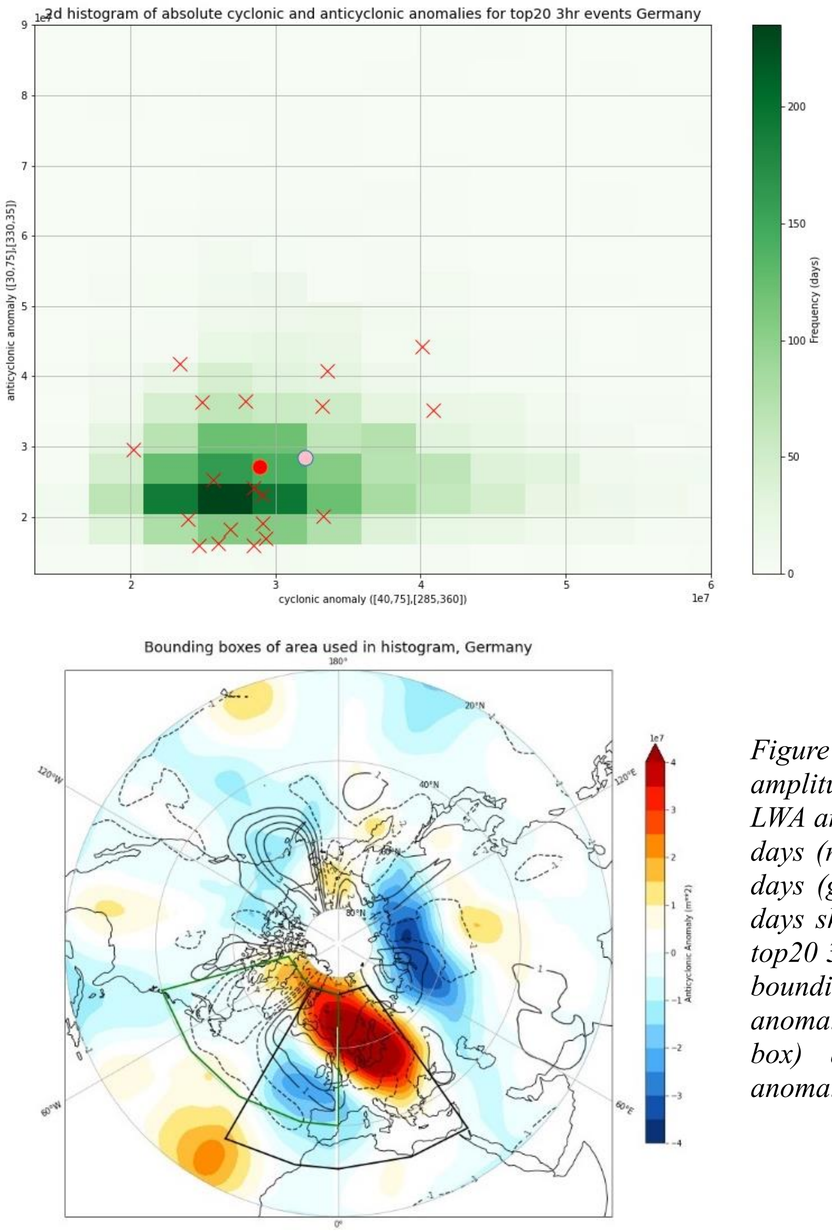

Figure 5.3: Histogram of the absolute amplitude of anticyclonic and cyclonic LWA anomalies for Germany top 20 3hr days (red crosses) compared to all JJA days (green shading). Mean of all JJA days shown by pink circle, mean of all top20 3hr days shown by red circle. The bounding area boxes for calculating anomalies over are for cyclonic (green box) and anticyclonic (black box) anomalies.

5.3.7 Development of LWA on Days Prior to Extreme Events

The results from the previous sections demonstrate that the phase of the Rossby wave over Europe is important for extreme events, and much more so than the amplitude. Thus, we now investigate the timescale of the waves, by analysing development of the LWA anomalies in days before the extreme 3hr events. We calculate the mean of the LWA-a and LWA-c values on each of the 5 days prior to the 3hr events to provide a single composite of LWA-a and LWA-c for preceding day.

LWA anomaly evolution on days leading up to the top 20 3h events over Germany are presented in Figure 5.10. The composite indicates that from 5 days before a 3hr event, a high-latitude wave train is present in the LWA-c, while a wave train from the central Atlantic is visible in the LWA-a.

By 3 days prior to the event, the positive LWA-c anomaly to the west of the UK is present and there is a strong positive LWA-a anomaly over central Europe. At 1 day prior to the event, the positive LWA-c anomaly over Alaska has appeared and the anomaly to the west of the UK has strengthened. The positive LWA-a anomaly in Europe has moved north over Scandinavia and has increased in size and strength. Over the 5 days before the 3hr event, wave energy appears to move through the LWA-a wave; initially (at 5 days before), the positive anomaly in the central Atlantic is strongest; by 3 days before, this has decreased slightly and the positive anomaly over Europe has increased; by 1 day before, the Atlantic anomaly has greatly decreased in strength and size, while the anomaly over Scandinavia is much larger. This evolution indicates an element of stationarity in the wave, with the phase speed remaining at approximately 0, while the group velocity moves downstream. This is consistent with the concept of the downstream development of Rossby waves (Wirth *et al.*, 2018).

The evolution of LWA anomalies in the 5-days leading up to the top 20 3hr events in the UK is shown in Figure 5.11. Five days before the 3hr event, the signal is quite noisy with no clear pattern, except for the spatially-extended positive LWA-a anomaly over Scandinavia and a positive LWA-c anomaly over southern Greenland. At 4 days before, the wave patterns visible on the day of 3hr event composite start to appear, with higher latitude LWA-c anomalies forming a wave train from eastern Canada to the north of the UK. The LWA-a anomaly over Scandinavia has become more concentrated and there appears to be a wave train reaching up from the central Atlantic. From 4 days before until the day of 3hr event, the positive LWA-c to the west of the UK and the positive LWA-a over Scandinavia are present, as is the higher latitude wave train associated with LWA-c and the lower latitude wave in the LWA-a. This indicates there is again an element of stationarity to waves causing these 3hr events over the UK, with the anomalies remaining in roughly the same locations from 4 days before the 3hr extreme event. In both Figures 5.10 and 5.11 there appear to be two wave trains, one in the anticyclonic anomalies at a lower latitude and another in the cyclonic anomalies at a higher latitude. This possible 'double wave' is investigated further in the next section.

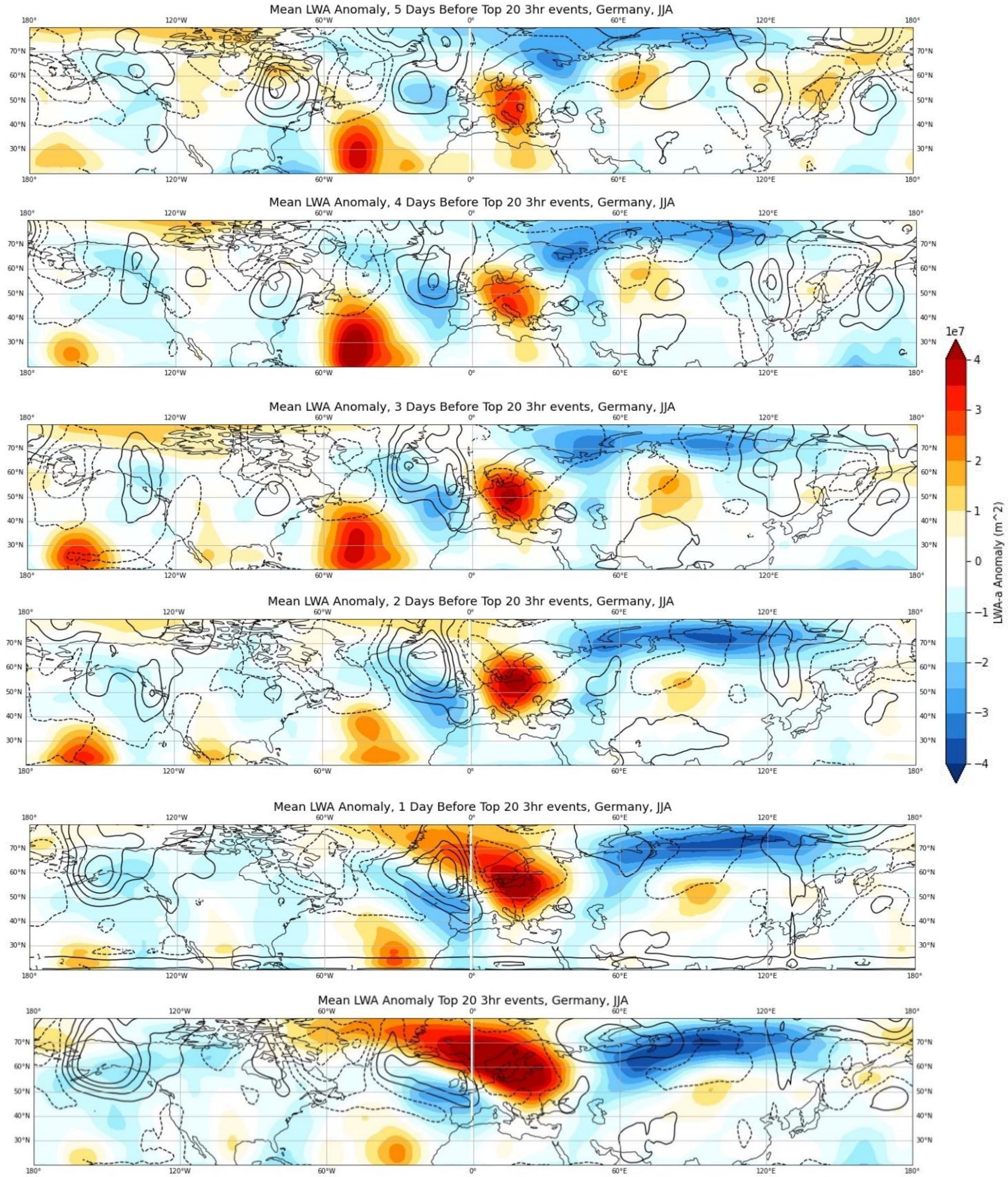

Figure 5.4: Composites of LWA component anomalies on the days prior to the top 20 3hr events in Germany.

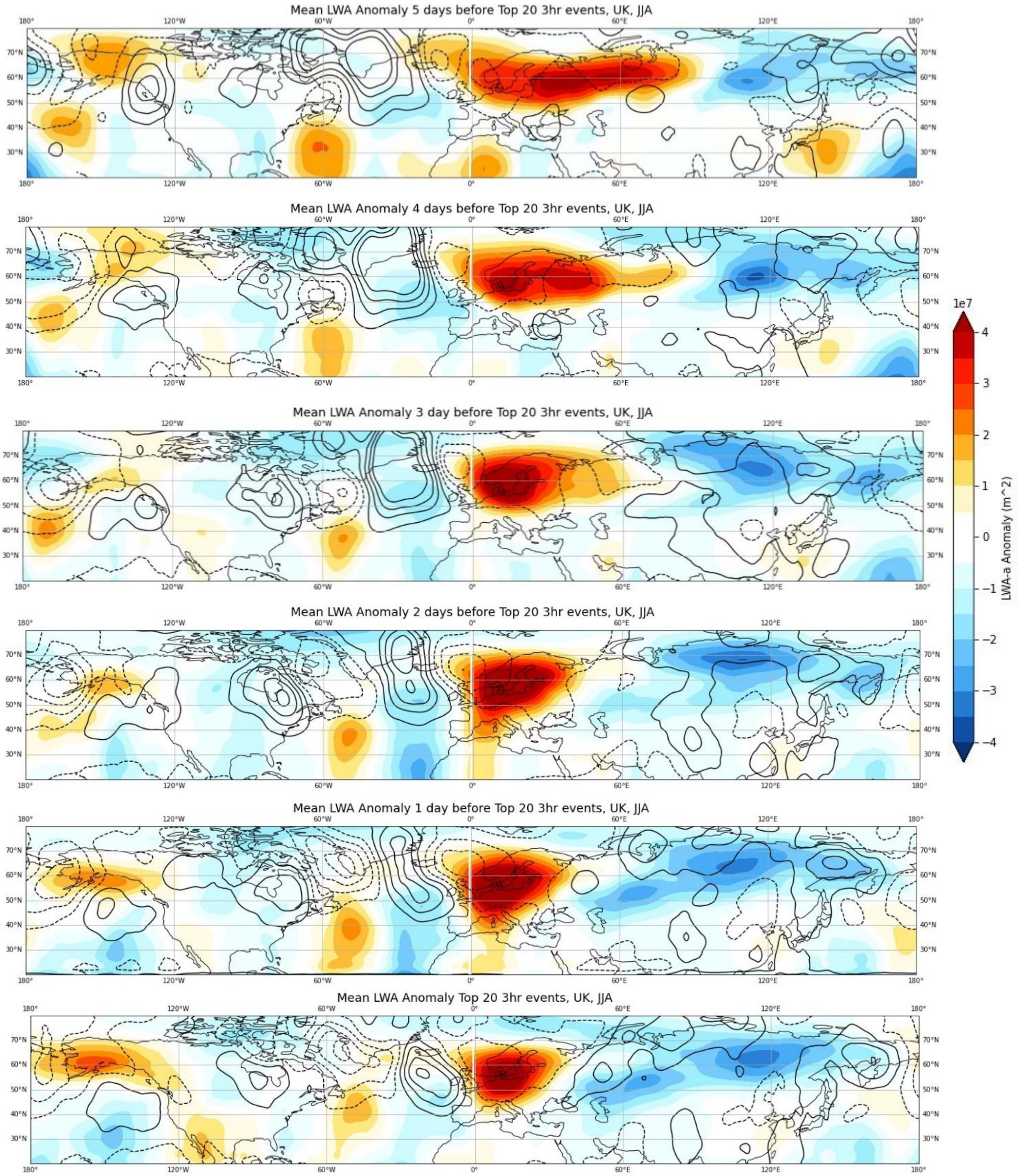

Figure 5.5: Composites of LWA component anomalies on days prior to the top 20 3hr events in the UK.

5.3.8 Comparison of z500 and LWA Composites on top 20 3hr Rainfall Event Days

The z500 anomalies on the days with top20 3hr events in the UK and Germany were calculated to compare to the LWA results and to examine if the possible 'double wave' seen in the LWA plots were visible in the z500 too, and thus more likely to be a physical signal and not an artefact of the

LWA methodology. The standardised z500 anomalies were used to make it easier to see areas where anomalies are climatologically weaker (Figure 5.12).

The standardised z500 anomaly composite of the top 20 events in Germany has a strong positive anomaly over Scandinavia and the Baltics, with an extended negative anomaly just to the west of the UK. These anomalies are part of a wave train which stretches NE from the mid Atlantic to northern Russia. There is also a strong negative anomaly over Alaska, which appears to be part of a second wave train, reaching from central Russia around the pole towards Greenland. For days with extremes in the UK the z500 anomalies show a similar spatial pattern to the LWA, with a strong positive geopotential height anomaly over Scandinavia and a negative anomaly to the west of the UK (Figure 5.12). There is also a positive z500 anomaly over Alaska. There is a clear wave train in the z500 stretching from south of Alaska, across America and around to the UK. There also appears to be a second, higher latitude wave stretching from eastern Russia around the pole to the UK.

In both the Germany and UK composites in Figure 5.12 there is a strong positive anomaly over Scandinavia and a negative anomaly to the west of the UK, and these anomalies appear to be part of a wave train, however, the way in which these anomalies end up in these locations appears to be different – as shown by the opposite sign of the anomalies over Alaska. Additionally, in both cases there are potentially two Rossby waves that converge over Europe. Therefore, does the positive-negative pair over Europe occur due to this being a preferred phase for Rossby waves at this latitude? Or does the potential second wave in each case meet the first wave and interact with it to force the waves to be in the same phase over Europe? These are questions that are outside the scope of this thesis but would be very interesting for future research to consider.

The LWA analysis has a slight advantage over using z500 as these plots show more detail around the cyclonic and anticyclonic anomalies associated with the extreme rainfall events. However, the fact that both methods show such similar results is supportive of our hypothesis that there is a large-scale circulation link to (at least some of) the extreme sub-daily events, and that the positive and negative anomalies over Europe that were linked to the events in Chapter 4 are part of a much larger wave train, rather than just being individual anomalies.

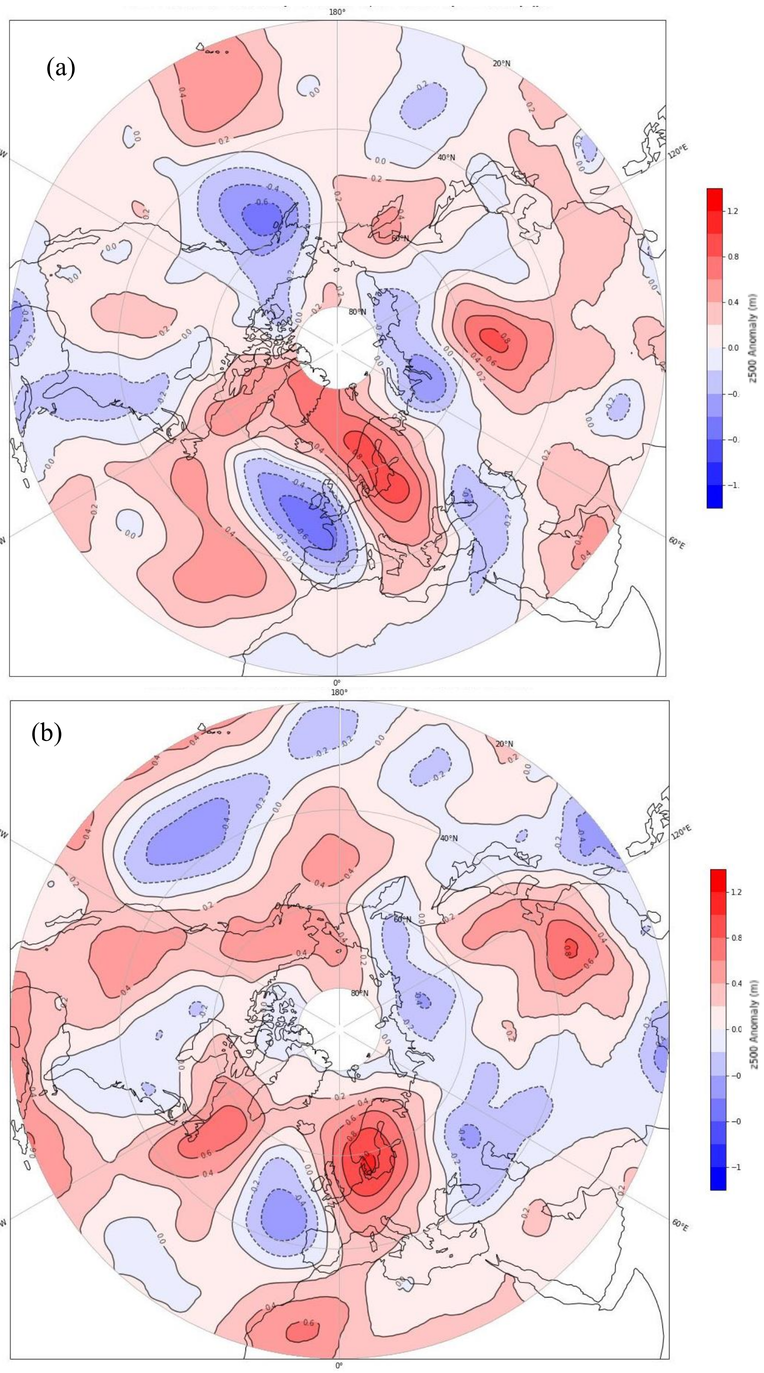

Figure 5.6: Composites of the z500 standardised anomalies on the top 20 3hr rainfall event days in a) Germany and b) the UK

5.3.9 Meridional wind anomalies on event days

There are many different ways to examine Rossby waves, so to further investigate the wave trains seen in the LWA results, the v300 has been used as a third method to look at the Rossby wave patterns on days with extreme 3hr events. The v300 anomaly indicates locations with anomalous northerly or southerly winds, showing regions with cyclonic or anticyclonic activity.

The v300 anomalies composite for the top20 3hr event days in Germany and the UK are presented in Figure 5.13. The v300 anomaly composite for the top20 events in Germany has a clear wave train that stretches from Alaska to central Russia. There is a strong southerly wind anomaly over the North Sea and northern Germany, with a northerly anomaly to the east and another to the west, creating an anticyclonic flow anomaly over Scandinavia and a cyclonic flow anomaly to the west of the UK. The UK v300 composite also has a very clear wave train, stretching from the west Pacific across the USA and Atlantic to Scandinavia. The resultant pattern produces a southerly wind anomaly over the UK, with a northerly anomaly over the Baltic Sea. This indicates anticyclonic motion to the east of the UK and cyclonic motion to the west. These locations of the anticyclonic and cyclonic activity agree with the patterns seen in the LWA and z500 anomalies. The composites of v300 on event days for the UK and Germany show a very similar large-scale pattern to the LWA composites, further indicating that these patterns are a legitimate feature associated with the sub-daily rainfall extremes. The only discrepancy between the two methods is that the strong anticyclonic anomaly over Alaska in the UK LWA composite does not appear in the v300 composite for the UK, instead there is a cyclonic anomaly just to the south of Alaska.

The significance of anomalies in the v300 composite plots was tested using a 1000 run seasonal bootstrap against all summer days from 1979-2016 for the UK and 1996-2016 for Germany, taking the mean of 20 days each time, to determine the 95th and 5th percentile levels. For both case studies the wave train is significant at the 90% confidence interval, particularly the southerly anomaly over the UK and the northerly anomalies either side of this (see Appendix Figure C.5). This result indicates the wave train is not a common pattern and that there is an association between this pattern and the occurrence of 3hr rainfall extremes.

Each day from the composite was also plotted individually as for the LWA results (Figures 5.6 and 5.7). The v300 anomalies consistently show the presence of a wave train for 3hr extreme rainfall events in both Germany (Figure 5.14) and the UK (Figure 5.15). For Germany, 16 of the 20 days have a southerly v300 anomaly over or just to the north of the country and 14 of these days have a wave train reaching from the US to Europe. For the UK, 15 of 20 days have a wave train and ~10 days have a southerly anomaly over the UK with a northerly anomaly over the Baltic. Based on these results there is perhaps a slightly stronger link between this ridge-trough pairing and the wave train for sub-daily rainfall extremes in Germany than for those in in the UK.

The standard deviation of the composites was also plotted and is shown in Figure C.6. The variability within the composite in locations which are related to the wave train is high, but this is to be expected as the wave train will not occur in the exact same location for each event and not all of the extreme events are associated with a wave train. Figures 5.6 and 5.7 show this.

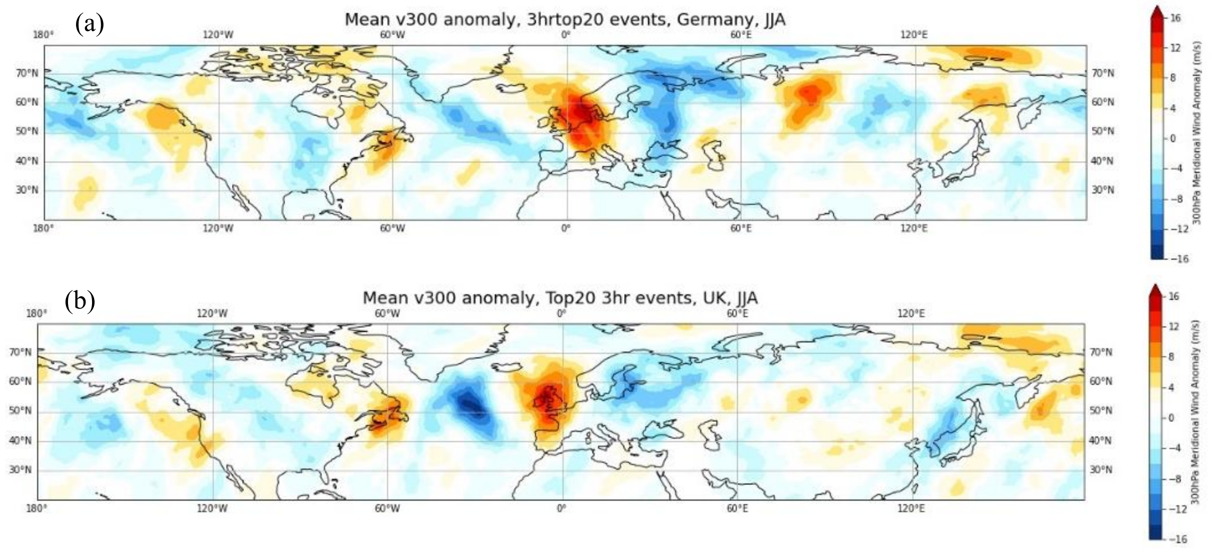

Figure 5.7: Composites of mean v300 anomalies on top 20 3hr event days for a) Germany and b) the UK

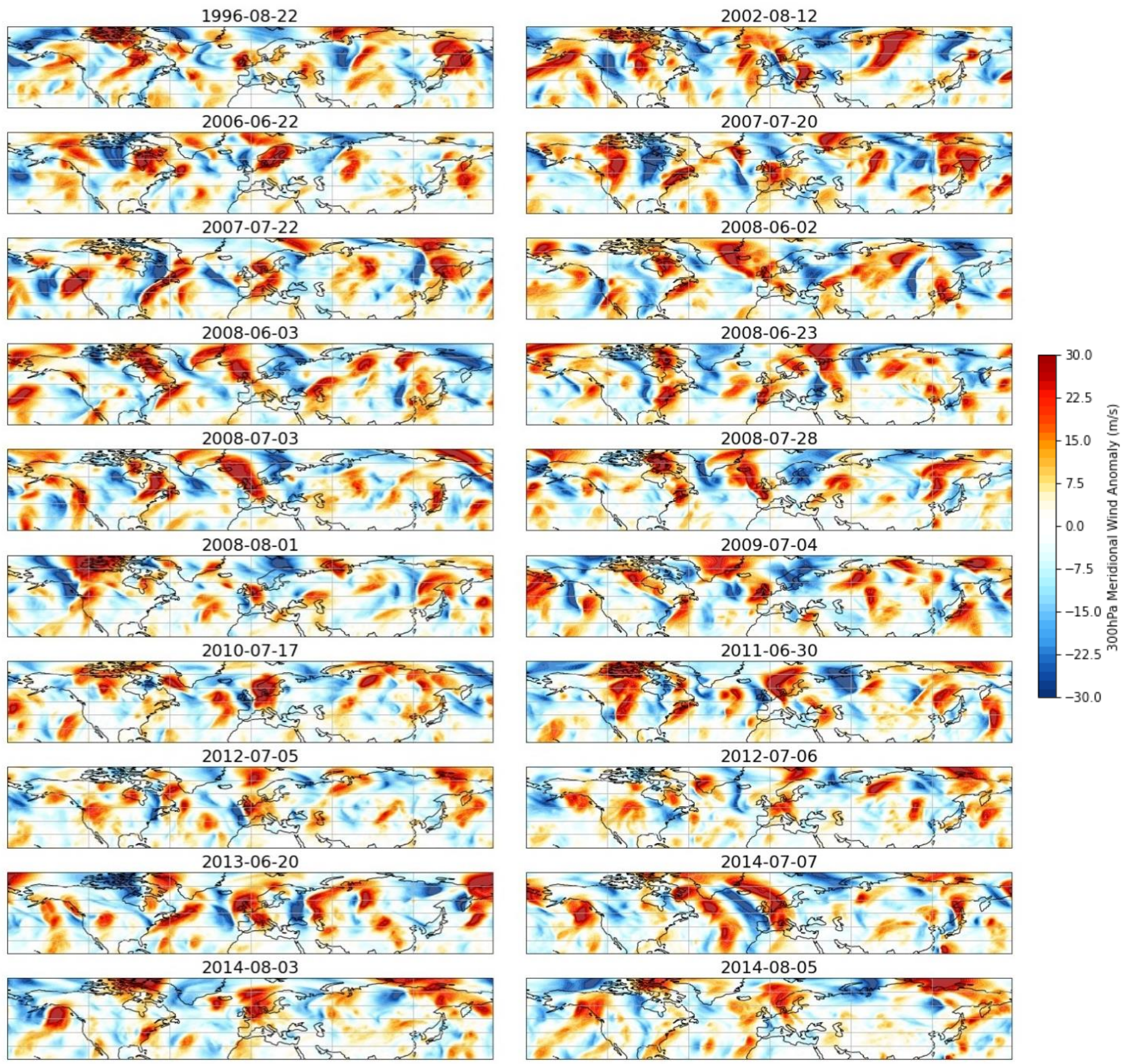

Figure 5.8: Individual day composites of the v300 anomalies present on top 20 3hr event days in Germany.

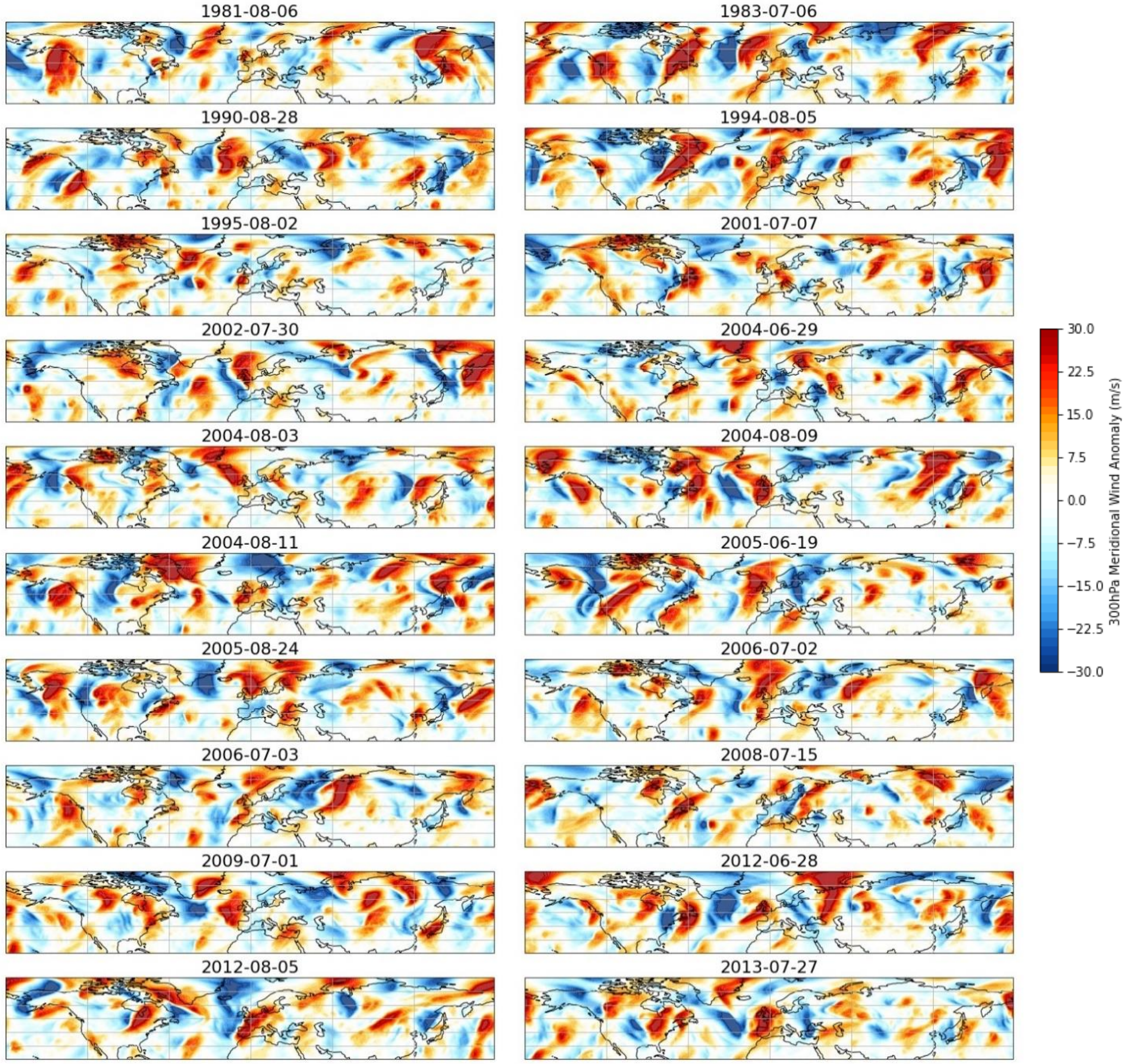

Figure 5.9: Individual day composites of the v300 anomalies present on top 20 3hr event days in the UK.

5.3.10 Evolution of meridional wind anomalies on days before the extreme events

Examining the evolution of the v300 anomalies composites on the days leading up to the extreme events further indicates a level of stationarity to the Rossby waves, supporting the result from Section 5.3.9 and extending this further temporally. The LWA anomalies did not show a clear wave train beyond 5 days before the 3hr events, however the v300 anomalies do. The v300 anomalies on days surrounding Germany top 20 3hr events are shown in Figure 5.16. From 7 days before the 3hr event there is a wave train which stretches from Alaska to Europe, which continues to strengthen from 6 days before the 3hr events. From 5 days before, there is a southerly wind anomaly over the UK and a northerly anomaly to the west, with a strong southerly anomaly over eastern Canada. This wave train remains very stationary until 2 days before the 3hr event, with the ridges and troughs staying in approximately the same location while the wave energy moves downstream towards the UK. Over this time a northerly wind anomaly develops over eastern

Europe, indicating the development of a ridge here. The day before the 3hr event, the wave trains appear to move slightly eastwards, with the negative v300 anomaly previously far to the west of the UK moving to just off the coast of Portugal, while the positive anomaly that was over the UK is now slightly further east over the North Sea and increased in strength. On the day of the 3hr event, the anomalies are in approximately the same position as they were on the day before. However, on the day after the events these anomalies begin to weaken, with the anomalies upstream decreasing in both size and amplitude and by 3 days after the 3hr event the composite indicates only a southerly anomaly over the UK remaining. Again, these results indicate a strong level of stationarity to the waves associated with these 3hr rainfall extremes, with the phases remaining in consistent locations from 6 days before the extreme event until 2 days afterwards, as the group velocity moves downstream.

The evolution of v300 anomalies on days before the top20 3hr events over the UK show a very similar pattern of development (Figure 5.17). From 7 days before, a wave train reaching from Alaska towards Europe can be identified, although it is very weak over the Atlantic. At 4 days before, this wave train extends to just west of Ireland with a strong southerly wind anomaly there, and a northerly anomaly to the west. By 2 days before the 3hr event, the composite anomaly between Canada and the UK has again strengthened but remains in the same location, and a northerly wind anomaly has developed over Scandinavia. At 1 day before the 3hr event, the anomalies remain in roughly the same location having travelled slightly eastwards, with a small increase in strength. On the day of the 3hr extreme, the southerly wind anomaly that was just west of the UK is now over the UK, as the whole wave train has shifted slightly to the east. The day after the 3hr event, the anomalies are still present in the same locations but have already weakened and by 3 days after, the wave train over the Atlantic has broken down and only a very weak southerly anomaly remains near the UK. Through the plots of the v300 anomalies on days before the 3hr events, it is possible to see the wave train developing and the phases then becoming relatively stationary around 5 and 4 days before the events in the Germany and the UK respectively. The phase velocity remains approximately zero while the group velocity moves downstream, increasing the amplitude of the anomalies over the UK and Scandinavia. The wave then breaks down rapidly after the day with 3hr extremes. The wave associated with the 3hr events in Germany appears to build earlier and break down more slowly than the wave associated with 3hr events in the UK.

The 3hr extreme rainfall in both Germany and the UK appears to be associated with waves which remain relatively stationary for ~6 days and develop an anomalous ridge (block) over Scandinavia and a trough to the west. Six days is similar to the time period required by Wills *et al.* (2019) and

Wolf *et al.* (2018) in their studies of QSWs. It is interesting to note that the wave train present on the days leading up to the 3hr extremes in the UK has 3 whole waves (peak and trough) in 180^{o} while for Germany there are ~2.5/3 waves in 180^{o}, indicating the presence of a wavenumber 6 and wavenumber 5/6 pattern respectively on these days. The wavenumber 5 and wavenumber 6 patterns has previously been linked with heatwaves and rainfall extremes in Europe in several studies (Blackburn *et al.*, 2008; Petoukhov *et al.*, 2013; Kornhuber *et al.*, 2020; Tuel and Martius, 2022). This will be discussed further in Section 5.4.

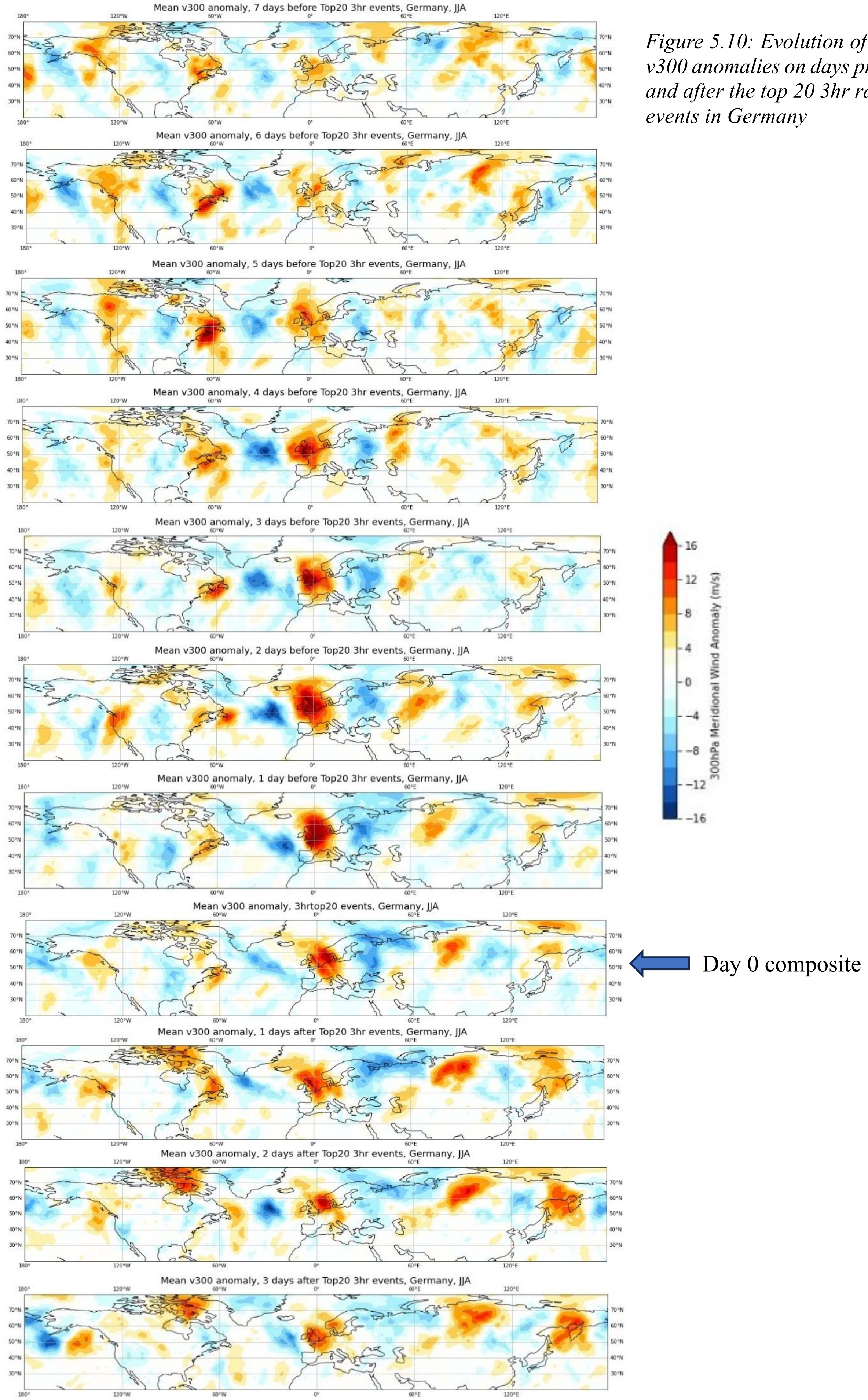

Figure 5.10: Evolution of mean v300 anomalies on days prior to and after the top 20 3hr rainfall events in Germany

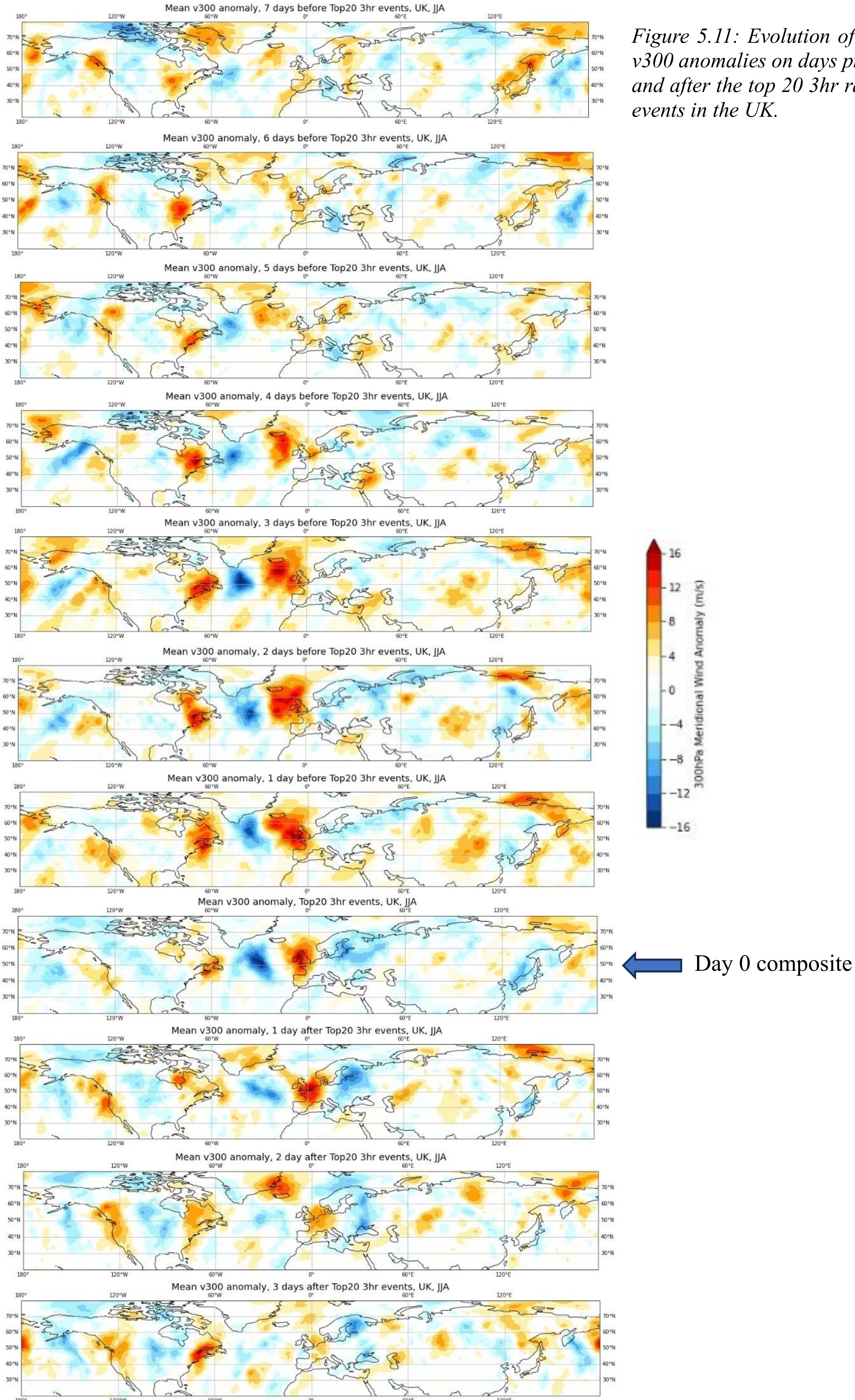

Figure 5.11: Evolution of mean v300 anomalies on days prior to and after the top 20 3hr rainfall events in the UK.

5.3.11 Temperature anomalies, Rossby waves and extreme rainfall events

The discovery in Sauter *et al.* (2022) that heatwaves in Australia are often broken with a period of short-duration intense rainfall was rapidly followed by the finding that this sequence of events occurs more often in the mid-latitudes than elsewhere (Sauter *et al.*, 2023). It has also been shown that a substantial portion of (sub-daily) temperature extremes in Europe are related to atmospheric blocking (Pfahl and Wernli, 2012a). Therefore, given the presence of a strong blocking anomaly on a high proportion of the days leading up to the extreme rainfall events investigated here, it seems plausible there may be a link between the blocking anomaly and extreme rainfall relationship observed here and high temperatures due to the persistent blocking anomaly remaining over the region for several days prior to the events (Figure 5.16 & 5.17).

The normalised temperature anomaly at the gauge recoding a top20 3hr rainfall event was calculated for the 6 days prior to and the 3 days after the event. The results of this analysis for Germany are shown in Figure 5.18. The mean normalised anomaly shows an increase in temperature from 3 days before the event, which peaks on the day before the event and then rapidly decreases to be close to 0 by the day after the event. The individual events (grey lines) show a lot of variation around the mean, however, there is in most cases an increase in the normalised temperature from ~3 days before the event, with a sharp decrease in temperature from the day before or the day of the 3hr rainfall event. The composite maps in Appendix Figure C.7 show the mean change in temperature across Europe on the days surrounding the 3hr rainfall event. These maps show there is a positive temperature anomaly over Germany (and to the north and west) 4 days before the 3hr extreme rainfall, which increases in strength over the following days, up to a maximum of 6K the day before the rainfall event. On the day of the 3hr event there is a decrease in the temperature anomaly over Germany and the day after the events the anomaly is <1K and continues to decrease in the following days.

The graph of normalised temperature change at gauges with 3hr events in the UK (Figure 5.19) show a similar trend of increasing temperatures on the days before the extreme rainfall, followed by a sharp decrease from the day before or the day of the event. The mean normalised temperature anomaly remains above 1 standard deviation for 2 days before the event. There is more variation in the individual event temperature changes for the UK than for Germany, which agrees with the previous findings that fewer events in the UK showed the wave train and strong southerly v300 wind anomaly on the day of event (Section 5.3.9). We would therefore expect a less strong blocking-high temperature-rainfall link here. The composite maps in this case (Appendix Figure C.8) again show a positive temperature anomaly over the UK and for areas to the west and south from 4 days before the 3hr rainfall event, with the anomaly increasing to a maximum of 4K on the day before the event. In this case, the highest temperature anomaly is reached on the day of the 3hr events, with a 5K anomaly over the Low Countries and a 4K anomaly over the southern UK. The day after event the temperature anomaly over the UK drops to 2K and continues to decrease in the days after this.

We are not looking to define a heatwave in this instance, only to identify whether there is a temperature change on the days surrounding the extreme rainfall and therefore a plausible link between the dynamical and thermodynamical drivers of these events. The composite normalised temperature anomaly for 3 days before (Germany) and 2 days before (UK) a top20 3hr event is more than 1 standard deviation above the mean, indicating that temperatures are unusually high for several days before the 3hr extreme rainfall events. These high temperatures are followed by a sharp drop in temperature on the day before or the day of the 3hr rainfall event in most cases, indicating that the extreme rainfall occurs at the end of the 'heatwave', as expected from Sauter *et al.* (2022, 2023). In both cases, the composite maps of the temperature anomaly (Appendix Figure C.7 and C.8) show that the highest temperatures are co-located with the area of blocking anomalies identified in Figures 5.16 and 5.17, thereby following the conclusions in Pfahl and Wernli (2012) that atmospheric blocking is the main cause of the temperature anomalies.

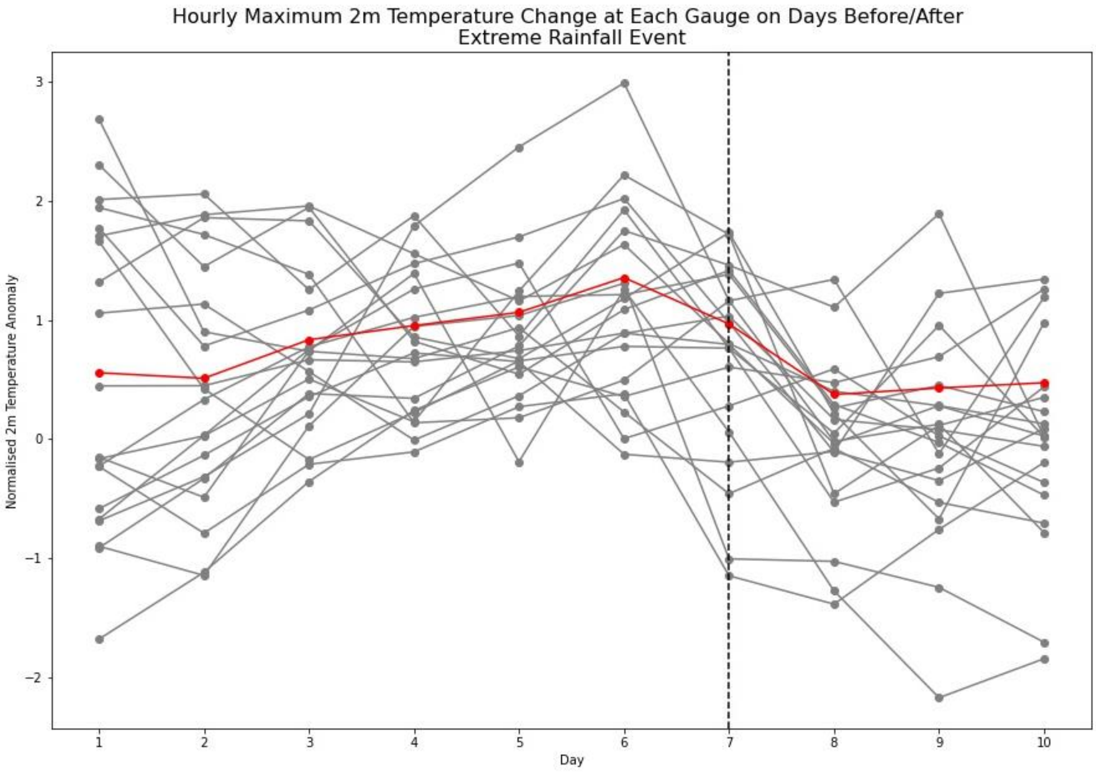

Figure 5.12 Change in normalised daily maximum hourly 2m Temperature anomaly on days before and after extreme rainfall event at each gauge recording a 3hr top 20 rainfall event in Germany (grey). The mean temperature change is shown in red. Dashed line indicates day of event.

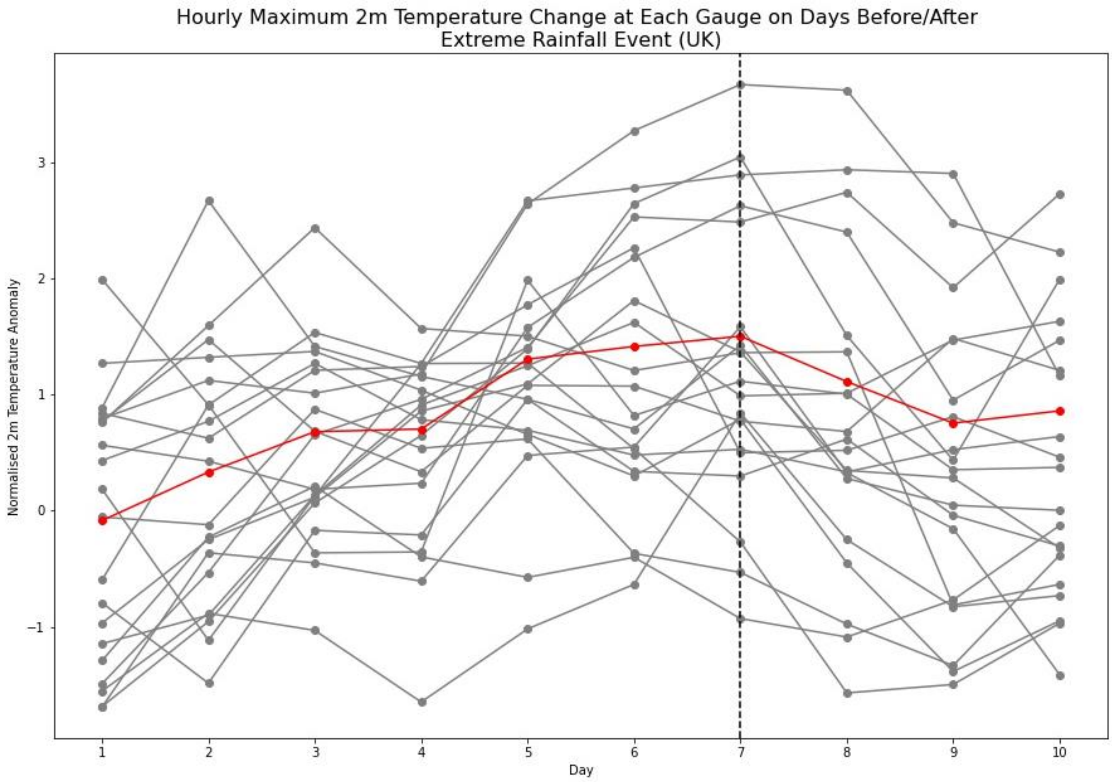

Figure 5.13: Change in normalised daily maximum hourly 2m Temperature anomaly on days before and after extreme rainfall event at each gauge recording a 3hr top20 rainfall event in the UK (grey). The mean temperature change is shown in red. Dashed line indicates day of event.

5.4 Discussion

This chapter has identified connections between large-scale Rossby wave activity and conditions associated with sub-daily rainfall extremes in Germany and the UK. While the metrics used here are not capable of showing the local-scale conditions leading to the extreme rainfall, they provide an indication of the large-scale flow features which may be associated with conditions conducive to extreme sub-daily rainfall events. These large-scale circulation features have previously only been used to look at connections with long-duration weather extremes (days to weeks time-scale). Studying the connections between these very large-scale features and extreme weather on short timescales is a novel way of looking at the potential dynamical drivers of these sub-daily extremes.

5.4.1 Using the LWA as an indicator of dynamical drivers of sub-daily rainfall extremes

An investigation into Rossby wave patterns on days with top20 3hr events in Germany and the UK using the LWA has revealed a relatively consistent wave pattern occurring on event days. Using the cyclonic and anticyclonic components of the LWA separately has provided a clearer picture of the location and amplitude of different activity anomalies and highlighted the presence of a strong anticyclonic anomaly to the east and cyclonic anomaly to the west in both cases, which echoes the results from the z500 analysis in Chapter 4. This indicates that the LWA is capable of diagnosing the large-scale conditions associated with high impact events not just at daily and longer timescales (Chen *et al.*, 2015; Huang and Nakamura, 2016) but also at sub-daily timescales. As seen in Figure

5.4, there is a stronger association between LWA anomalies and 3hr rainfall extremes than for 24hr rainfall extremes, which are produced from a simple strong positive cyclonic anomaly over the rainfall region, compared to the complex and hemispheric wave pattern associated with 3hr extremes.

The appearance of wave structures within the LWA anomalies for 3hr extremes is a key feature of interest. There is a clear wave train within the cyclonic anomaly in each case study, with this wave train appearing to be confined to higher latitudes. The anticyclonic anomalies display a wave pattern at lower latitudes in each case, which then appears to then couple with the cyclonic wave train over western Europe. However, this apparent 'double wave' is very hard to quantify for several reasons. Firstly, the LWA is calculated on the z500 contours. The z500 gradient changes with latitude, essentially reflecting the location of the jet stream. Due to the way LWA is calculated this means that if the point of interest is to the south of a jet, the cyclonic activity will be stronger as the z500 gradient is stronger to the north. If the point of interest is to the north of a jet, the anticyclonic activty will be stronger as the z500 gradient is stronger to the south. Therefore, the location of the LWA-a and LWA-c anomalies on each day with top 20 3hr extreme events depends on where the jets were located on those days. Thus the 'double wave' may be just an artefact of the method for calculating the LWA or it may in fact be reflecting the presence of a wave on each of the polar and subtropical jets on these days. Secondly, when examining the composite plots of the LWA based on the z500 climatology (Appendix Figure C.1) there is less clear evidence of the lower latitude cyclonic wave. There is also no sign of a second wave in the v300 plots (Figure 5.13). A double wave is harder to spot in the standardised z500 composite plots (Figure 5.12) however, in the UK plot a very high latitude wave and a lower latitude wave are visible and it is feasible that the Germany plot shows a wave originating in the sub-tropics reaching to Europe and meeting with a separate high latitude wave.

Therefore, there are several possible explanations; firstly, the double wave may be representative of the fact the LWA picks up wave activity at different latitudes depending on the jets and is therefore simply showing different pathways for the waves on the day of events, indicating that different pathways can lead to the same outcome of having an increased likelihood of a 3hr extreme. Using lagged composites means it is not possible to identify distinct dynamical pathways which lead to an event, instead creating a composite of multiple possible outcomes (Dorrington *et al.*, 2023). Secondly, using the LWA, the overall peaks/troughs of the Rossby wave pattern appear in the same locations as in the v300 plots. Therefore, the LWA may be showing areas with anomalies which have a large latitudinal extent, appearing in both the cyclonic and anticyclonic activity as the negative phase of the opposite activity. Finally, it is possible that the presence of two waves is a legitimate feature that is most strongly picked up in the LWA and only weakly observed in the z500 parameter. It would be of great interest to further investigate this phenomenon and try to diagnose the presence of two waves on the days leading up to the 3hr extreme rainfall events which then meet over the region of interest just before the events occur, not least due to the increased predictability this would provide for the rainfall extremes. However, such an in-depth analysis is outside the scope of this thesis and therefore the ‘double wave’ remains as an open question.

The weaker climatological LWA activity in summer months suggests the stationary wave over Scandinavia at this time is weaker (Martineau *et al.*, 2017). Martineau *et al.* (2017) identified that extreme LWA-a and LWA-c wave events were characterised by transient geopotential height anomalies aligning with stationary waves, with constructive interference leading to enhanced wave activity. Therefore, it would require even greater constructive interference between the stationary wave and the transient wave to produce a large-amplitude positive anomaly in summer, as seen in the event composites here. This further indicates the significance of the wave pattern present on the 3hr extreme rainfall event days.

The key features of the large-scale circulation on the extreme rainfall days are found in results from all the methods of investigating Rossby waves used here, namely anticyclonic activity over Scandinavia and cyclonic activity to the west of the UK and the presence of an upstream wave train. Using the LWA allowed for the initial identification of a wave train associated with the 3hr rainfall extremes and comparison with the z500 anomalies, while the v300 parameter also indicates there is a level of stationarity to the wave train. The fact these waves are apparent in multiple metrics of Rossby wave activity shows this result is not sensitive to the exact diagnostic used. Some of these features have already been linked to sub-daily rainfall extremes and some have previously only been associated with long-duration weather extremes. This will be discussed further in the following sections.

5.4.2 Blocking over Scandinavia

Both the LWA composites and the v300 composites indicate a clear anticyclonic anomaly over Scandinavia/the North Sea, which increases in strength in the days leading up to the 3hr extreme events (Figures 5.10/5.11 and Figures 5.17/5.18). This is accompanied by a cyclonic anomaly to the west, which appears to strengthen over time in the v300 but the LWA plots do not show the strengthening as clearly.

The anticyclonic anomaly over Scandinavia has appeared in every method of looking at the large-scale atmospheric circulation associated with sub-daily rainfall extremes used in this thesis. As identified in other studies investigating links between extreme short-duration rainfall and large-scale circulations in Europe, the presence of a blocking ridge over the Scandinavian region has been linked to extreme short-duration (daily and sub-daily) rainfall in western Europe due to decreased stability and increased moisture in the area from the advection of warm and moist air masses from the south and southwest along the western side of the block (Piper *et al.*, 2016; Weder *et al.*, 2017; Lenggenhager and Martius, 2019; Mohr *et al.*, 2019, 2020; Barton *et al.*, 2022). The blocking can result in increased odds of precipitation in the areas to the north and south of the block due to the increased atmospheric instability and the increased likelihood of formation of cut-off low systems upstream of the block, as happened over central Europe in July 2021 contributing to the devastating floods there (Lenggenhager and Martius, 2019; Kreienkamp *et al.*, 2021; Barton *et al.*, 2022). The results here indicate that this blocking anomaly is in fact part of a much larger wave train. Strong, localised blocking regimes are frequently associated with persistent periods of extreme weather (e.g. heatwaves) and these blocking anticyclones can often be part of a much larger pattern (Kautz *et al.*, 2022), which may be associated with a longitudinally extended QSW (Wolf *et al.*, 2018). However, here the results show a strong association between the blocking regime and associated wave train and sub-daily rainfall extremes, which has not previously been found in the literature.

5.4.3 The quasi-stationary wave train in v300

The apparent stationarity of the wave train seen in the wave metrics on the days leading up to 3hr extreme rainfall in the UK and Germany is a very interesting feature. Quasi-stationary waves have received an increasing amount of attention in recent years, particularly in connection to extreme weather events (Coumou *et al.*, 2014; Screen and Simmonds, 2014; Wolf *et al.*, 2018). Screen and Simmonds (2014) found a strong link between highly amplified planetary waves and temperature extremes which was strongest on 5 to 14 day timescales. They also found a strong link between these waves and long-duration rainfall extremes, however, their results showed this relationship weakened for timescales of less than 12 days. The authors suggest this is due to rainfall variability being more closely related to synoptic- or local-scale drivers on short timescales while rainfall on longer timescales has a stronger link to the large-scale circulation. The results shown here appear to refute this, indicating there is a strong link between anomalous wave amplitudes and short-duration extreme rainfall events. It is also worth noting that Allan *et al.* (2019) identified a slow eastward movement of large-scale weather patterns in the days preceding 3hr rainfall extremes in the UK, with extremes in northwest England and Wales in particular associated with slow eastward movement of negative pressure anomalies to the west and positive anomalies to the northeast. While the authors do not diagnose this as being connected to a much larger-scale pattern, this pattern has cyclonic/anticyclonic anomalies in positions similar to the slow-moving wave identified as associated with extreme events over the UK in Sections 5.3.7 and 5.3.10.

Wolf *et al.* (2018) show that the 30 most extreme 7-day total precipitation events in Europe in JJA are connected with a very strong QSW (exceeding the 99th percentile), with a large-scale trough over central Europe, indicating connection between these waves, similar in location and phase speed to the ones identified in this thesis, and longer-duration extreme rainfall in Europe. When looking at the QSWs associated with extreme temperature events, Wolf *et al.* (2018) note that strong QSW amplitudes develop around 5 days before the 7-day extreme events, which agrees with the wave evolution time period observed here. They also show that the amplitude of QSWs tends to peak in the storm track exit regions over Europe, which is where Tuel and Martius (2022) found temporally compounding daily rainfall extremes were associated with hemispheric wave-like patterns (although they could not diagnose if these patterns were due to QSWs or recurrent Rossby wave packets). Finally, Blackburn *et al.* (2008) found that for each of the June-July 2007 extreme daily rainfall events in England, there was a persistent upper-level trough over the region which barely moved from the two days preceding each rainfall event. These troughs were all part of an almost stationary hemispheric wave pattern with wavenumber ~6. These studies provide evidence of a link between QSWs and extreme rainfall events in Europe of daily and longer duration. Therefore, it is not unreasonable for the apparent link between a quasi-stationary wave and sub-daily extreme rainfall shown here to be a potential dynamical driver of these extremes.

5.4.4 The wave 5/7 pattern

Rossby waves with a wavenumber of 5 or 7 have been increasingly identified as being associated with extreme weather events in recent years (Petoukhov *et al.*, 2013; Kornhuber *et al.*, 2019, 2020; Tuel and Martius, 2022). This may in part be due to the discovery of Coumou *et al.* (2014) that there has been a statistically significant increase in the frequency of high-amplitude QSWs with the wave numbers 7 and 8 since 2000. However, as mentioned above, Screen and Simmonds (2014) showed that extreme temperature events in particular are strongly connected to highly amplified Rossby waves, with the additional proviso of wavenumbers 5 and 7 having the greatest number of strongly positive wave amplitude anomalies.

Kornhuber *et al.* (2019) identified the concurrent extreme heat and rainfall events (lasting for >= 2 days) that occurred in summer 2018 across the northern hemisphere were associated with a recurrent wave-7 pattern in the upper atmosphere. They go on to show that this pattern was also present during several past extreme weather events including the extreme heatwaves of 2003 and 2015. Similarly, Kornhuber *et al.* (2020) found that Rossby waves with wavenumber 5 and 7 have a preferred phase position and produce recurrent circulation patterns in summer, which are associated with increased probability of simultaneous heat extremes across the northern midlatitudes. Additionally, Petoukhov *et al.* (2013) showed that northern hemisphere midlatitude quasistationary meridional velocity during several heatwaves was characterised by unusual high-amplitude wave patterns with wave numbers 6, 7 or 8. Tuel and Martius (2022) found a trough over western Europe with a ridge to the east and amplified flow over Europe with a hemispheric wave pattern of ~5 was associated with temporally clustered daily rainfall extremes in autumn. Therefore, our results from the v300 anomalies composites on days with 3hr rainfall extremes of a wavenumber ~ 5 or 6 pattern on the days with top20 3hr extremes in Germany (Figure 5.13a) and a wavenumber ~6 pattern on days with top20 3hr extremes in the UK (Figure 5.13b) appears consistent with previous findings for longer duration extremes. Comparison of these plots with Figure 2 in Kornhuber *et al.* (2020) indicates the v300 anomalies on the Germany events composite occur in roughly the same locations as the anomalies in the Wave 5 plot (Figure 2a), while the v300 anomalies in the UK composite occur in similar locations to the Wave 7 plot (Figure 2c). The difference in the wavenumber despite the similar location of the waves peaks/troughs in the UK composite may be due to the wave in our plot breaking down downstream of Europe while the wave in the Kornhuber *et al.* (2020) plot remains consistent. However, the finding that wavenumbers 5-7 appear to be related to sub-daily rainfall extremes is still of great interest given the aforementioned results showing these high wave numbers are strongly associated with extreme weather. This result indicates that there may be a dynamical link between this large-scale pattern and the development of local scale conditions which are conducive to sub-daily rainfall extremes.

5.4.5 Large-scale circulation links to sub-daily rainfall extremes

The results here are based on just 20 extreme rainfall events. This is a very limited sample of events, however, we wanted to investigate just the most intense events as these have the most potential for impact. Adding more events will mean that less extreme periods are included and the consistent connection to the large-scale circulation decreases (as in Figure 5.5). Despite selecting the two regions with most dense gauge coverage, there is still an inherent issue with using gauge data, as short-duration extreme events on small spatial scales can be missed (Lengfeld *et al.*, 2020). Additionally, the short record period in Germany (1996-2015) means there is a smaller sample of extreme events there, although this is to some extent moderated by the dense gauge network in Germany. However, gauge-data provides more reliable estimates of extreme event intensity compared to gridded or reanalysis data (Reder *et al.*, 2022) and gave us a limited number of events to work with in this initial investigation.

We have shown in this chapter and in Chapter 4 that the presence of a blocking high over Scandinavia/the Baltic Sea is very important for sub-daily rainfall extremes over Europe. This result could have significant implications for the forecasting of these short-duration events. The connection of blocking to hemispheric dynamics in this chapter could help provide more skillful predictions of blocking variability, and subsequently more skillful probabilistic forecasts of the associated impacts on varying timescales (Kautz *et al.*, 2022). However, there is currently a lack of studies investigating the predictability of rainfall extremes in connection with blocking (Kautz *et al.*, 2022). Additionally, blocking is still a challenge for numerical weather prediction models to accurately forecast and the blocking frequency in European regions is often underestimated (Ferranti *et al.*, 2015; Quinting and Vitart, 2019). There is also the potential for projected weakening of the zonal flow to result in an increase in the wave number that becomes stationary in the future i.e. making stationary waves with wavenumber >5 more likely (Hoskins and Woollings, 2015).

The analysis of temperature changes on the days surrounding the top20 3hr events revealed what appears to be a relatively consistent link between (some of) the extreme rainfall events in Germany and the UK and high surface temperatures generated as a result of upper-level blocking. Sauter *et al.,* (2023) found the likelihood of hourly extreme rainfall after a heatwave was three to four times higher than climatological hourly extreme rainfall likelihood in central Europe and one to two times higher over the UK. The high temperature-extreme rainfall link here also appears to be stronger for Germany than for the UK. Sauter *et al.,* (2023) also found that hourly extreme rainfall is more likely compared to climatology even when only considering 'dry' heatwaves (<1 mm rainfall in the 3 days preceding heatwave termination) and thus they propose the rainfall is not solely convection driven but that synoptic-scale drivers such as fronts or cyclones also play a role. Based on the results in 5.3.11, it is plausible that the eastward movement of the upper-level trough identified to the west of the region in each case provides a dynamical driving force behind the generation of extremes (e.g. through initiating upper-level ascent).

Therefore, a potential storyline for these events is proposed whereby: a QSW train develops in the northern hemisphere and results in a ridge over central/eastern Europe with a trough to the west. The ridge and trough remain relatively stationary over several days, and as a result heat begins to build up beneath the (blocking) ridge. During this time the southerly airflow along the western edge of the ridge draws warm moist air up from the south. Eventually, the block (and associated subsidence) moves to the east and the trough moves over/close to the region previously occupied by the block. This could result in further warm-air advection in the lower troposphere, increasing available moisture and large-scale ascent/lifting motions in the mid-troposphere. Thus, as the wave train moves east after remaining stationary for several days, this dynamic ascent, combined with the moist air potentially already in the region from warm-air advection around the block and high surface temperatures, gives a conditionally unstable environment with available moisture and large-scale ascent, ergo a prime environment for intense rainfall generation. This provides a consistent storyline from the dynamical drivers influencing the thermodynamical drivers which then trigger the rainfall. The strength of the resulting rainfall likely depends on the level of meso-scale convective organisation, as well as on the link between the large-scale dynamics and convective scale dynamics (Qin *et al.*, 2022). This apparent relationship between the Rossby waves, blocking and rainfall extremes also has implications for understanding future changes in extreme rainfall. The impact of climate change on both the persistence and strength of the Rossby waves (Mann *et al.*, 2017), and subsequent related impacts on the persistence and strength of blocking could both influence the future occurrence of sub-daily rainfall extremes.

While the extreme rainfall events themselves will be triggered by much smaller scale local conditions, the apparent link with the more forecastable large-scale conditions examined here would be very useful for longer lead-time forecasting and also in climate modelling of future changes in extreme event occurrence (Merino *et al.*, 2016; Mastrantonas *et al.*, 2022a; Chan *et al.*, 2023). This investigation has shown that atmospheric dynamics on hemispheric scales can be identified as driving forces in the development of local sub-daily rainfall extremes. Knowing that there is a link between sub-daily extremes and a large-scale block which may be part of a wavenumber 5 or wavenumber 6 Rossby wave could help to identify periods with increased likelihood of having extreme events much further in advance. Forecast lead times are generally 10 days for an atmospheric pattern such as blocking (Lavers *et al.*, 2014; Baker *et al.*, 2018), while for small-scale sub-daily extreme rainfall events they are a maximum of 1 day (P. Davies, Met Office Chief Meteorologist, *Personal Communication*). Therefore, knowing that a large-scale (blocking) pattern conducive to extremes will occur 5 days ahead is very useful for forecasters and provides a warning for a potential higher risk of extremes with enough time to implement mitigating action (Flack *et al.*, 2019).

There is recent evidence that land-atmosphere interactions and increased aridity in mid-latitude regions such as North America and Europe may result in an enhanced amplification of circumglobal QSW events during boreal summer (Teng and Branstator, 2019). Combined with potential future changes in northern hemisphere stationary Rossby waves with climate change (Wills *et al.*, 2019) and the potential increase in wavenumber of stationary waves (Hoskins and Woollings, 2015), the large-scale dynamical driving forces of 3hr rainfall extremes identified here are likely to undergo changes with global warming. Therefore, further research into the links between these dynamical drivers and the rainfall extremes are required to better understand how the extreme event characteristics may be affected by climate change.

5.5 Conclusions

This chapter has investigated the large-scale dynamical drivers of extreme 3hr rainfall events by using different proxies of Rossby wave activity to assess the conditions on days with the most extreme observed events in the UK and Germany. This analysis has found a surprisingly strong and consistent spatiotemporal connection between Rossby waves and the occurrence of sub-daily rainfall extremes in Europe. The key results of this analysis are as follows:

- The LWA provides more detail than z500 on the spatial location and amplitude of the Rossby wave activity and has indicated that the anomalies identified over Europe are associated with wave trains. However, the v300 anomalies show most clearly how the wave train develops on the days leading up to the 3hr extreme rainfall events.
- All the methods of examining Rossby waves show a strong anticyclonic anomaly over Scandinavia and a strong cyclonic anomaly to the west of the UK on the days with extreme sub-daily rainfall in both Germany and the UK. This pattern supports the findings in Chapter 4 of a trough over western Europe and a ridge over Scandinavia being key large-scale circulation patterns linked to 3hr rainfall extremes.
- Using the Rossby wave proxies has shown that this trough-ridge pattern is part of a large-scale wave train. The wave train appears to build up beginning from 5/6 days before the event and then breaks down 1-2 days after the rainfall event has occurred. Additionally, this wave train has aspects of quasistationary, meaning an increased level of predictability, which could help to increase the lead time of forecasts of these rainfall events.
- There is a connection between the strongest 3hr rainfall events and high temperatures, with the rainfall being associated with a sharp decrease in temperature, preceded by several days with above-average temperatures. This forms a coherent link with the large scale dynamics, resulting in a persistent high pressure anomaly to the east of the country of interest, and resulting in a build-up of temperatures there, while strong southerly airflow occurs to the west. As the wave train moves east, extreme rainfall occurs in an environment conducive to intense rainfall due to this combination of dynamical and thermodynamical factors.

The discovery of a wave train, and particularly a relatively quasi-stationary wave train, associated with 3hr rainfall extremes has potentially significant implications for the forecasting of these events. The v300 parameter is widely used in the analysis of mid-latitude weather extremes and can also be used in forecast models. The results of this initial investigation suggest addition of the LWA parameter may provide another tool for identifying large-scale features associated with an increased risk of sub-daily extremes. As far as we are aware this is the first time the potential links between Rossby waves and sub-daily rainfall extremes have been investigated in the literature.

Given the localised nature of these extremes, assuming the majority are convective in origin, it is surprising to find any link to the large-scale dynamics, let alone a potential QSW connection. The next steps in this research would be to repeat this analysis using a dataset with a longer record of sub-daily rainfall (especially in Germany) to determine if there are other cases where this wave train is associated with the most intense short-duration rainfall extremes to give a more robust indication of the extent to which having this wave train increases the likelihood of sub-daily rainfall extremes.

Chapter 6
Conclusions

6.1 Summary of Results

This thesis has explored the climatology and dynamical drivers of sub-daily rainfall extremes in western Europe. The research aims and objectives set out in Chapter 1 were justified by the review of literature surrounding existing climatologies of extreme rainfall in Europe and the current state of knowledge regarding the dynamical drivers of mid-latitude sub-daily rainfall extremes presented in Chapter 2. This literature review showed the need for a set of rainfall indices specifically for sub-daily timescales, to allow the creation of a climatology of sub-daily rainfall extremes on a continental scale. The recent development of the GSDR-I dataset of sub-daily extreme rainfall indices meant that it was possible to do this for the first time (Pritchard *et al.*, 2023). The literature review also highlighted the comparative lack of knowledge around the large-scale dynamical drivers of sub-daily rainfall extremes, despite this being a crucial component of forecasts of these events.

Chapter 3 introduced the rainfall data used throughout the thesis. The observational gauge-based GSDR dataset (Lewis *et al.*, 2019) provides a robust timeseries that has undergone multiple quality control checks. However, the use of this dataset does come with the large caveat of spatial coverage. Even in the most densely gauged areas (e.g. the UK with 1900 gauges recording hourly rainfall), the gauges only provide point coverage and therefore it is possible that short-duration extremes will be missed by the gauge network. For example the rainfall associated with the Coverack Flood in Cornwall in July 2017 was entirely missed by rain gauges (Flack *et al.*, 2019). This limitation must therefore be taken into account when drawing conclusions from gauge-based results with the understanding that many localised extreme events may be missed (Lengfeld *et al.,* 2020). However, the use of long gauge records, combined with the likelihood of storms moving across a region and thereby reaching at least one gauge in regions with higher spatial coverage, increases the probability of having a representative record of events.

The GSDR data was the basis for the GSDR-I dataset, which was calculated as part of the INTENSE project, with the seasonal indices being developed specifically for this climatology, alongside an additional diurnal cycle index. This chapter represents the first time the GSDR-I has been analysed for western Europe, with the resulting climatology being the first of its kind for this region. An earlier study by Lakatos *et al.* (2021) using an early version of the GSDR-I focussed on the Pannonian basin region in the east.

The climatological analysis revealed that the most intense and frequent 3hr extremes occur in southern Europe, with the strongest of these occurring in autumn, while northern and central regions have lower intensity events that occur most frequently in summer. The 3hr extremes were often the main source of rainfall on that day, indicating they occur either as individual storms or as a strong peak in a longer duration storm. The differences in the temporal and spatial patterns of 3hr and 24hr rainfall extremes revealed by the indices provides evidence that these extremes should be considered separately in design of heavy-rainfall management systems. Finally, the comparison of indices between different Koppen-Geiger climate zones indicated the potential utility of a climate-zone-based set of indices for flood risk planning in ungauged areas and for assessment of future changes in flood risk under climate change. For countries which were either not part of or only have a small representation in the original GSDR dataset, the discussion of indices by climate regions in this chapter provides a first order understanding of the sub-daily rainfall characteristics and flash-flood hazard faced in different areas of Europe. This chapter therefore satisfactorily resolves the first key objective set out in Chapter 1 by providing a climatology of sub-daily rainfall extremes for Europe.

Chapter 4 introduced the Met Office MO30 WP classification, which was used as the first order determination of potential links between large-scale dynamics and sub-daily rainfall extremes. As this thesis is focussed on large-scale, rather than mesoscale, dynamical drivers of the rainfall extremes, it made sense to begin the analysis with a set of synoptic-scale weather patterns already shown to be of use in forecasting periods with increased risk of extreme rainfall in Europe (Richardson *et al.*, 2020). Analysing the connections between these WPs and 3hr extremes gave an initial indication of study feasibility. The results from this research identified a link between the occurrence of certain WPs and the increased frequency of 3hr extremes in several regions of Europe. For most regions investigated in western Europe, over 50% of 3hr ≥40 mm events occurred under just 5 WPs, indicating that a relatively limited set of dynamical conditions are associated with the 3hr extremes. A small selection of the MO30 patterns were repeatedly associated with a high proportion of 3hr extremes. These are WPs 1, 2, 5, 6 and 11, with at least two of these patterns being within the top 5 patterns contributing to 3hr rainfall extremes in each of the countries investigated. Other WPs never contributed to extreme events, including WPs 4 and 9. The probability of a 3hr extreme event occurring, given a certain WP, was also assessed. While all WPs most strongly associated with the occurrence of extremes had an extreme event probability higher than expected from random chance, only a few had a probability above 0.2. However, given the localised nature of 3hr extremes and their relatively rare occurrence, a 20% chance of having a 3hr extreme rainfall event given a particular WP is still of significant value to forecasting. This section of Chapter 4 resolves the third objective from Chapter 1 of assessing the relationships between the MO30 WPs and 3hr rainfall extremes. This chapter also expands the current literature on sub-daily extreme rainfall connections to WPs beyond just Germany (Weder *et al.*, 2017; Brieber and Hoy, 2019; Haacke and Paton, 2021) and the Netherlands (Manola *et al.*, 2019) to now cover the wider western Europe region.

To further investigate the links between large-scale dynamical drivers and 3hr rainfall extremes, z500 anomalies on days with WPs 1, 2, 5, 6 and 11 and extreme rainfall were calculated. These results show the tropospheric conditions influencing mesoscale and lower-level conditions, as flow at 500 hPa may advect warm, moist air into a region and drive dynamical ascent from positive vorticity advection, providing one or two of the ingredients required for convective activity (moisture, lifting and instability) (Doswell *et al.*, 1996). These z500 anomalies indicated that, in many cases, there was an upper-level trough present over western Europe, which resulted in a southerly or south-westerly flow over the region of interest. This was often accompanied by a ridge over eastern Europe, particularly Scandinavia or the Baltic Sea, generating a further southerly flow component, bringing more warm, moist air to the region along its western flank. Notably, the z500 patterns were very similar between the different regions, indicating that similar large-scale dynamics favour 3hr rainfall extremes in different regions of Europe, in agreement with results from Dorrington *et al.* (2023). Comparison of z500 anomalies on WP days with 3hr extreme rainfall compared to WP days without extreme rainfall revealed significant differences in the spatial pattern and amplitude of anomalies. The analysis suggested that identification of these WPs in forecasts of z500 would provide an indication of an increased risk of the region of interest experiencing sub-daily extremes. This section of Chapter 4 therefore satisfies objective 4 from Chapter 1, by analysing how upper-level atmospheric circulation differs between days with and without extreme sub-daily rainfall.

The results of this chapter have shown that there are strong links between synoptic-scale dynamics and sub-daily rainfall extremes across Europe. The operational WPs provide some information about the dynamical drivers of 3hr rainfall extremes; however, the z500 anomalies can be used to further refine this, providing a clearer understanding of the large-scale circulation patterns that are associated with conditions which lead to an increased probability of 3hr extreme events. As previously discussed, Richardson *et al.* (2020) showed how the MO30 WPs could be used to provide advance warning of periods with higher risk of fluvial flooding due to heavy rainfall occurrence. Wilkinson and Neal (2021) proved the WP methodology could provide a signal of thunderstorm occurrence several days before the event, based on probabilistic forecasts from ECMWF ensembles. It is therefore feasible that such a method could be adjusted to work for probabilistic forecasts of sub-daily rainfall extremes, based on the results shown in this thesis. In particular, if the MO30 WPs were used in combination with forecasts of z500 anomalies it would be possible to identify periods when different regions of western Europe might expect a higher risk of sub-daily rainfall extremes occurring and thus potential flash flooding.

Chapter 5 extended the investigation of dynamical drivers to the very large-scale, providing an assessment of the connections between Rossby wave patterns and sub-daily rainfall extremes. The Local Finite Amplitude Wave Activity (LWA) metric of Huang and Nakamura (2016) was used, initially as an indicator of the location and amplitude of anomalous Rossby waves on days which had an extreme 3hr rainfall event. For the purposes of this chapter, a subset of 40 3hr extremes was used, representing the 20 most intense events recorded in each of the UK and Germany. Analysis of the LWA pattern composites on these days showed very clearly that a particular organisation of the waves was strongly associated with events in each country. This pattern includes a strong positive anticyclonic activity anomaly over Scandinavia in both cases, with a strong positive cyclonic activity anomaly over the UK for events in Germany and a similar anomaly to the west of Ireland for events in the UK, echoing the pattern seen in the z500 anomalies in Chapter 4. This configuration of the anomalies was shown to be (visually) distinct from the pattern present on days with the top 20 most intense 24hr events in each country, suggesting that the pattern seen in the 3hr composites is specifically linked to extremes of this shorter duration. A further feature of interest in these composites is the presence of a wave pattern which appears to extend from eastern Russia around to Europe at high latitudes, with a possible second wave at lower latitudes extending from the mid-Pacific towards Europe. Examination of the LWA on each of the top 20 days individually showed that most days featured a pattern similar to that seen in the composite, thereby confirming that the pattern was not a result of just one or two days with very high amplitude anomalies in these locations. The development of the LWA wave pattern on the days prior to the 3hr extreme rainfall event was then investigated, revealing a signal of wave energy moving downstream towards Europe. This indicates an element of predictability to the LWA pattern present on the 3hr extreme rainfall days that could be useful for forecasting.

To further investigate the wave train on days leading up to 3hr rainfall extremes, the v300 parameter was used as a proxy for Rossby wave activity. Composites of v300 on the top 20 event days for each case study showed a very clear wave train reaching from the western Pacific to Scandinavia, with southerly wind anomalies over the North Sea/UK and northerly anomalies either side of this, indicating cyclonic and anticyclonic motion in the same locations as the LWA. The development of the v300 anomalies on days leading up to the 3hr rainfall extremes showed some stationarity in the wave, with peaks and troughs remaining in approximately the same locations while the wave energy moved downstream. After the 3hr rainfall events, the wave rapidly broke down and appeared to have dissipated by 2-3 days afterwards. These waves had wavenumbers ~6 and ~5 or 6 for the UK and Germany respectively. The presence of a QSW with a high wavenumber on the days of and prior to sub-daily rainfall extremes echoes previous findings for longer duration rainfall events (Wolf *et al.*, 2018; Kornhuber *et al.*, 2019) and strongly suggests the very strongest 3hr rainfall extremes have a connection to these large-scale dynamics which could be utilised in forecast models. The fifth objective of Chapter 1 is therefore satisfactorily resolved by chapter 5. The linkage of 3hr rainfall extremes to these QSWs prompted the investigation of the temperatures on days surrounding the extreme rainfall, resulting in the identification of a rise in temperature several days before the events followed by a sharp drop in temperature the day before or the day of the 3hr extremes. This result ties into the observational findings from Sauter *et al.* (2023), using the same GSDR dataset, that sub-daily rainfall extremes are more likely to occur at the end of a heatwave in midlatitude regions.

The combination of results from Chapter 4 and Chapter 5 provides a range of predictable atmospheric conditions with a connection to 3hr rainfall extremes. This predictability could have important implications for the advance warning of flash flooding, not just through using the WPs as previously mentioned but through identification of hemispheric patterns that are linked to extreme rainfall. As Oertel *et al.* (2023) showed for the 2021 Pacific Northwest Heatwave, the identification of a linked system of dynamical precursors leading up to the extreme weather event can greatly help in the accurate prediction of such events at longer- lead-times. The connection of forecasts of these dynamical drivers to potential extreme rainfall events could allow improved warnings of flash flooding on timescales which allow flood risk management action to be taken (Pappenberger *et al.*, 2015).

The discovery in Chapter 5 that the atmospheric circulation patterns associated with the most intense 3hr rainfall extremes in both the UK and Germany had a significant anticyclonic anomaly over Scandinavia suggests that it is the presence of this ridge in combination with a trough over western Europe which is important for the very strongest 3hr rainfall extremes. Similarly, the finding from Chapter 4 that WPs 1, 2, 5 and 6, which the z500 analysis showed all involve a high-pressure ridge to the east (and a trough to the west), are most strongly associated with 3hr rainfall extremes across western Europe indicates that this ridge often plays an important role as a dynamical driver of these extremes. This pattern of a trough to the west and a ridge to the east was found to be associated with 3hr rainfall extremes for all the different methods used in this thesis. This consistency therefore provides confidence in the findings here; namely that extreme sub-daily rainfall in western Europe often occurs when an upstream trough moves towards a blocking system which has been in place over eastern Europe for several days. This finding links together the dynamical (QSW train resulting in blocking and large scale ascent driven by upper-level trough) and thermodynamical (high surface temperature due to blocking) drivers, which together generate the conditions required for strong convective activity to take place (Doswell, 1987; Doswell *et al.*, 1996). While other studies have investigated these atmospheric features individually as important for the generation of rainfall extremes or thunderstorms, no study has so far (to the author's knowledge) focussed on the combination of these features in driving sub-daily extreme rainfall.

The proposed increase in sub-daily rainfall extremes frequency and intensity due to climate change influences on thermodynamic drivers is well accepted and proven through numerous studies (Trenberth *et al.*, 2003; Chan *et al.*, 2014; Kendon *et al.*, 2014; O'Gorman, 2015; Lenderink *et al.*, 2017a). However, as mentioned in Chapter 2, the influence of climate change on sub-daily extremes through changes in dynamical drivers has so far received less research attention. It is currently still unknown how changes to large-scale circulation dynamics will influence the intensification of short-duration rainfall extremes (Fowler, et al., 2021). A large-scale shift in circulation patterns might lead to a change in jet stream and storm track positioning over Europe, or move moisture sources enough to affect the regional-scale response (Cohen *et al.*, 2014; Shaw *et al.*, 2016) . Changes in the large-scale dynamics could also affect where the rainfall extremes occur most frequently in mid-latitudes (Shaw *et al.*, 2016). Changes in mean circulation can influence the mean precipitation change, as shown in de Vries *et al.*, (2022) where change in the mean circulation over western Europe, with the development of a high pressure centre west of Ireland results in extensive drying to the east. However, this does not necessarily apply to rainfall extremes.

Individually, the dynamical drivers investigated in this thesis have been shown to be impacted in different ways by climate change. It has been suggested that there will be a decrease in blocking frequency in Europe in the future (Hoskins and Woollings, 2015; Rousi *et al.*, 2021) but the confidence in this assertion is limited by the model skill in accurately representing blocking (even in the present climate) (Ferranti *et al.*, 2015; Hoskins and Woollings, 2015). This possible decrease in future blocking frequency may be moderated by the potential increase in the waviness of the jet streams, as Arctic amplification leads to a weaker jet and therefore stronger waves (Francis and Vavrus, 2012). However, there is again a lack of confidence in the model representation of this feature and a general consensus on the impact of Artic amplification on the jet stream has yet to be reached (Blackport and Screen, 2020; White *et al.*, 2022). It has also recently been suggested that a warmer Arctic will lead to an increase in double-jet flow regimes over Europe and amplified circumglobal wave patterns, which have been linked to an increase in heatwaves through the formation and/or maintenance of blocking anticyclones in the low-wind region between the jets

(Rousi *et al.*, 2022). The potential future changes in stationary Rossby waves may also play a role (Hoskins and Woollings, 2015; Wills *et al.*, 2019). Given the links identified in this thesis between blocking systems, Rossby waves and 3hr rainfall extremes, there are thus many mechanisms through which climate change may impact the dynamical drivers and therefore lead to changes in future sub-daily rainfall extremes, although a consistent understanding of the climate change impacts on these drivers is yet to be reached.

6.2 Results in the context of the existing literature and operational practice

The results presented in this thesis are important steps in the identification of large-scale dynamical drivers of sub-daily rainfall extremes. The repeated appearance of a blocking ridge over the Scandinavian region, with an upstream trough or a cut-off low over western Europe, in all methods used here to examine dynamics associated with 3hr rainfall extremes, is in agreement with several other studies investigating the large-scale conditions associated with intense rainfall in Europe (Piper *et al.*, 2016, 2019; Weder *et al.*, 2017; Allan *et al.*, 2019; Champion *et al.*, 2019; Lenggenhager and Martius, 2019; Mohr *et al.*, 2019, 2020; Haacke and Paton, 2021; Tuel and Martius, 2022). However, this is the first time such a study has been carried out specifically for sub-daily rainfall extremes in regions of Europe outside of the UK and Germany. This thesis thereby provides further evidence of dynamical conditions which could be of benefit to medium range forecasting of these sub-daily extreme events and the extra insight to be gained from considering sub-daily extremes from a larger-scale perspective.

The potential for using forecasts of atmospheric variables as precursors to predicting the occurrence of rainfall extremes beyond the short-range of forecasts associated with weather conditions has recently become a point of research focus (Lavers *et al.*, 2014, 2016; Mastrantonas *et al.*, 2022b; Dorrington *et al.*, 2023). The findings here that using both the MSLP based WPs and the z500 anomalies together provides a clearer picture of the dynamical drivers than using just the WPs agrees with Mastrantonas *et al.* (2021) who showed clustering based on a combination of SLP and z500 led to the highest association of (daily) extreme rainfall events with the atmospheric clusters compared with a range of other variables. The benefit of using a combination of several atmospheric variables including a surface variable and a tropospheric variable in weather patterns for identifying drivers of short-duration rainfall has been shown in several studies (Weder *et al.*, 2017; Allan *et al.*, 2019; Champion *et al.*, 2019). Additionally, as Richardson *et al.* (2020) and Wilkinson and Neal (2021) have already shown, the MO30 WPs can be used to improve the medium-range forecasting of fluvial flood risk from intense daily rainfall and the occurrence of thunderstorms respectively. The analysis here indicates the potential applicability of both WPs and tropospheric variables for similar improvements to medium-range forecasting of sub-daily rainfall extremes and subsequent flash flood warnings.

Several studies have indicated that the predictive skill of rainfall conditioned on large-scale dynamics is lower in summer, although these studies have only examined daily and longer rainfall events, and not necessarily the most extreme thresholds (Richardson *et al.*, 2020; Dorrington *et al.*, 2023). While the predictive skill may be lower in summer, this does not mean that using large-scale dynamics as predictors of summertime short-duration extremes is without benefit. Indeed, the results in Chapter 5 for the most intense 3hr events have shown there are dynamical precursors visible 4 to 6 days before the events. This is similar to Allan *et al.* (2019) who found precursor signals for the heaviest 200 3hr summer rainfall events in the UK were visible in SLP and 200hPa geopotential height variables 4 days before the events occurred and beyond the 3 days found by Dorrington *et al.* (2023) when using geopotential height, wind and vapour transport variables as precursors for daily extremes in Europe. Given that medium range forecasts have a 3-14 day lead time (Lavers *et al.*, 2014), a 5 or 6-day lead time for the dynamical drivers observed here would still be very useful predictors. A significant proportion of the most intense 3hr events in both Germany and the UK occur under a persistent Rossby wave pattern, with the wave train developing several days before the extreme events, then remaining quasistationary, before breaking down in the days after the rainfall event. To the authors knowledge, such a strong link between Rossby wave dynamics and sub-daily rainfall in Europe has never been identified before, although several studies have found a similar situation for longer-duration rainfall extremes (de Vries, 2021; Barton *et al.*, 2022; Tuel *et al.*, 2022). This analysis therefore builds on previous knowledge and provides evidence that this is a valid research area requiring more attention from the community. In particular, the differences in the dynamical situation leading to sub-daily compared to daily rainfall extremes is an area requiring further investigation to improve forecasts of the former. The potential link to heatwaves identified at the end of Chapter 5 may play a part in this, as initially identified in Sauter *et al.* (2023).

The variables of WPs, z500 anomalies and v300 anomalies examined here have all been used previously (either individually or in combination) in studies investigating the drivers of, and potential ways to improve the forecasting of (daily) rainfall extremes in Europe (Blackburn *et al.*, 2008; Martius *et al.*, 2008; Merino *et al.*, 2016; Toreti *et al.*, 2016; Weder *et al.*, 2017; Richardson *et al.*, 2020; Grazzini *et al.*, 2021; Barton *et al.*, 2022; Mastrantonas *et al.*, 2022b; Tuel and Martius, 2022; Dorrington *et al.*, 2023). This thesis therefore provides an initial step towards the same attention, and potential subsequent improvement in forecasting, being directed towards the dynamical drivers of sub-daily extremes. This is a highly necessary move for the research community to make, as the improvement of medium-range forecasts of flash-flood inducing rainfall is critical to reducing the economic and social consequences of such events (Pappenberger *et al.*, 2015).

Finally, Chapter 3 provides the first climatology of sub-daily rainfall extremes for western Europe. While the methods used here were not novel, the information provided is new and of benefit to both the hydrological and climate modelling communities and may be easily replicated in other regions where data becomes available. This gauge-based climatology could be used to validate satellite or radar-based extreme rainfall climatologies, similar to the evaluation of precipitation diurnal cycles in model and reanalysis products performed by (Watters *et al.*, 2021) using the observation based IMERG product. Alternatively, the gauge data could be combined with radar and/or satellite data to create a merged sub-daily rainfall dataset as has already been done for the UK (Yu *et al*., 2020). Additionally, Ban *et al.* (2021) have already shown how indices of sub-daily rainfall can be used to validate high-resolution convection-permitting climate model simulations. The results from Chapter 3, in addition to the open-source portions of the GSDR-I dataset available online, allow this validation to be performed for climate model simulations across much of western Europe. Furthermore, having a climatology of sub-daily rainfall extremes against which to compare projections of future short-duration rainfall would allow flood practitioners to determine which regions are at risk of experiencing potential flood-inducing weather conditions. The comparison of 3hr with 24hr extreme rainfall indices possible with this dataset is of particular use for assessing the type of flood management scheme required in different areas, due to their differing impacts (Hurford *et al.*, 2012; Dale, 2021).

6.3 Future work

As part of the investigation of synoptic scale drivers of sub-daily extremes carried out in this thesis, a preliminary investigation of the influence of Cut-Off Lows (COLs) on 3hr extremes in Germany and the UK was performed,. This analysis utilised a dataset of COLs kindly provided by Dr Andreas Prien (NCAR) after discussion with the author and supervisors about the best methods for calculating COL occurrence. This investigation was inspired by the results of Barbero *et al.* (2019b) which showed that COLs contribute substantially to the occurrence of 1hr annual and seasonal rainfall maxima in the US. The preliminary results showed a variable monthly frequency of COLs over Europe in summer (JJA), with the highest frequency generally in June. The proportion of all 3hr n-largest (using an n=1 threshold) events in each country that occurred within 500 km and 12 hours of a COL centre for 1996-2015 in Germany and 1979-2015 in the UK was calculated (Appendix Figure D.1 and D.2). While both countries show an unexpectedly high proportion of the events can be associated with a COL (between 10 and 40% for most gauges in the UK and 5-30% in Germany), there is no clear spatial pattern to the results. This lack of pattern is thought to be due to a combination of the short gauge records available and the apparent lack of consistency between gauges recording the same rainfall events. Therefore, due to time constraints this analysis was not continued. However, it would be a very useful endeavour to repeat this analysis using a gridded observational dataset or reanalysis data to increase the spatial and temporal resolution of the rainfall data. This would allow an assessment of the importance of COLs for sub-daily rainfall extremes in Europe, which could then be linked to the occurrence of individual WPs.

In this thesis 3hr rainfall totals are used to investigate the links with large-scale atmospheric dynamics. An investigation of the dynamical situations associated with 1hr rainfall extremes in the UK has been performed by P. Davies of the Met Office and has identified a 4-stage process whereby short-duration extremes are generated due to the interaction of a Rex Vortex (or Cut-off low) with an Omega block. This work has been accepted for publication and builds on the findings of Barbero *et al*. (2019) of the importance of COL and jet stream events for producing 1hr extremes in the US and also supports the initial investigation detailed above, finding COL to be associated with 3hr extremes in the UK. Another piece of future work in this area would be to examine the atmospheric conditions present on the day(s) before the recorded rainfall event in more detail, using both the WPs and z500 analysis. Both the sequencing of the WPs linked with extremes and the persistence of the WPs over previous days would be useful features to investigate in more detail. The conditions on the days before the rainfall may prove to be more relevant from a short-term forecast perspective than the conditions on the day of the event.

Further to this, investigation of case studies of the evolution of Rossby wave patterns for individual extreme rainfall events would provide further detail on how these patterns develop, grow and then break down and where exactly in the process the extreme rainfall occurs. Work on this will be carried out as part of the development of Chapter 5 into a paper, alongside ensuring the extreme rainfall events used do not occur over midnight and that events are sufficiently far apart temporally to be part of separate Rossby wave trains.

The UK Flood Forecasting Centre (FFC) provides county-level river, surface water, coastal and groundwater flood risk information to government and core responders in England and Wales. The service aims to issue warnings with a lead time of ~3-5 days, supported by a flood outlook service which provides information on flood risk for 6 to 30 days ahead (Flood Forecasting Centre, 2022). For medium to long range forecasting of river and coastal flooding the FFC have two WP-based forecast tools already in operation. Both of these tools use the probabilistic predictions of the daily MO30 pattern from the Decider tool, which takes forecast daily SLP fields from an ensemble forecasting model (such as ECMWF-EPS) and assigns the fields to the closest-matching WP using the sum-of-squared differences (Neal *et al.*, 2016). The Coastal Decider tool highlights periods when UK coastal sites may be at increased risk of flooding (Neal *et al.*, 2018) while the Fluvial Decider provides regionalised warnings of periods with a higher likelihood of extreme daily rainfall and hence higher potential fluvial flood risk (Richardson *et al.*, 2020). The recent development of a new 'multi-model' ensemble based version of Decider will help to improve the flood risk assessment in the outlook (6-30 days) period and aid in the early identification of the potential for extreme events (Flood Forecasting Centre, 2022). These tools mean the forecasting team can rapidly assess the predicted WPs and any associated potential hydro-meteorological impacts which may follow. Based on these current forecast tools, there is arguably space for another tool which provides longer-term probabilistic projections of periods with potential for extreme sub-daily rainfall, and therefore flash flooding, in the UK, with the possibility of development for regions further afield too. Work on developing such an operational tool is on-going in collaboration with the FFC, funded by a Knowledge Transfer Bursary from Newcastle University which was awarded to the author. Part of this work will include assessing the 'hit/miss rate' of the flood forecast based on the Decider WP forecast as part of the verification process, which may lead to the development of a set of WPs more tailored towards short-duration rainfall extremes.

The GSDR data could potentially be used to develop depth-duration-frequency (DDF) curves for the UK (and other regions of Europe where this data is available) and fit a DDF model to the sub-daily extremes to predict extreme values for given return periods. The GSDR records are relatively short however, so this would not allow for a proper characterisation of the local climatology. Additionally, due to the short records, regionalisation would likely be required and therefore the quality of the DDF models would depend on how well the data could be regionalised – which in the majority of countries with GSDR data would limit the reliability of the model due to the sparse nature of the gauge networks (Guerreiro *et al.*, 2017).

Another driver of sub-daily extremes which could be utilised as a potential forecasting tool is the integrated water vapour transport (IVT) associated with the events. This variable has been used in several studies recently as a feature with greater potential predictability than the rainfall itself (Lavers *et al.*, 2014). The ECMWF extreme forecast index (EFI) of the IVT was categorically proven to be more useful in predicting extreme rainfall in western Europe from 2 weeks ahead during NAO positive phases, providing earlier awareness of upcoming winter rainfall extremes (Lavers *et al.*, 2016). Grazzini *et al.* (2021) used IVT to help diagnose daily extremes in northern Italy and their connection to Rossby wave packets. Similarly, both Tuel and Martius (2022) and de Vries (2021) use IVT as part of their assessment of synoptic scale conditions associated with (temporally clustered) daily extremes. Finally, Champion *et al.* (2019) and Allan *et al.* (2019) both use horizontal water vapour transport variables as indicators of the synoptic scale conditions associated with extreme 3hr rainfall in the UK. Therefore, it would be useful for both forecasting applications and improving the understanding of dynamical drivers for future work to study the water vapour transport associated with the 3hr extremes under each WP, alongside the z500 anomalies. Such analysis could also help in further diagnosing the connections between the sub-daily rainfall extremes and Rossby waves (de Vries, 2021).

The WP-extreme rainfall connections found here could be used in the analysis of future changes in the frequency of extremes under climate change. Pope *et al.* (2022) examined the future changes in frequency and persistence of the MO30 WPs under two ensemble climate models and both RCP2.6 and RCP8.5 for the period 2071-2099 compared to the historical period. They found for the summer under both scenarios that WPs 1, 2, 5, 6, 10 and 11 show an increase in frequency, with a larger increase in the higher emission scenario. These same patterns also all show an increase in persistence in summer. Therefore, the WPs most strongly associated with a high frequency of 3hr rainfall extremes across western Europe in this thesis are all projected to increase in their frequency and persistence under future climate change. This finding indicates that future work should focus on a more detailed assessment of what these changes in WPs might mean for future flash flood risk in Europe. Additionally, Rau *et al.* (2020) used a statistical downscaling method based on circulation patterns to develop projections of extreme hourly rainfall over the UK under future climate change. The links identified here between the MO30 and 3hr extremes could be utilised for such analysis in the UK and western Europe.

References

(GDV), G. I. A. (2021) *2021 the costliest year of natural catastrophes in Germany*.

Adri Buishand, T. and Brandsma, T. (1997) ‘Comparison of circulation classification schemes for predicting temperature and precipitation in The Netherlands’, *International Journal of Climatology*, 17(8), pp. 875–889. doi: 10.1002/(sici)1097-0088(19970630)17:8<875::aid-joc164>3.0.co;2-c.

Alderman, K., Turner, L. R. and Tong, S. (2012) ‘Floods and human health: A systematic review’, *Environment International*. Elsevier B.V., 47, pp. 37–47. doi: 10.1016/j.envint.2012.06.003.

Alexander, L. V. *et al.* (2006) ‘Global observed changes in daily climate extremes of temperature and precipitation’, *Journal of Geophysical Research Atmospheres*, 111(5), pp. 1–22. doi: 10.1029/2005JD006290.

Alexander, L. V *et al.* (2019) ‘On the use of indices to study extreme precipitation on sub-daily and daily timescales’, *Environmental Research Letters*. IOP Publishing, 14(12), p. 125008. doi: 10.1088/1748-9326/ab51b6.

Ali, H. *et al.* (2021a) ‘Consistent Large-Scale Response of Hourly Extreme Precipitation to Temperature Variation Over Land’, *Geophysical Research Letters*, 48(4). doi: 10.1029/2020GL090317.

Ali, H., Peleg, N. and Fowler, H. J. (2021b) ‘Global Scaling of Rainfall With Dewpoint Temperature Reveals Considerable Ocean-Land Difference’, *Geophysical Research Letters*, 48(15), pp. 1–11. doi: 10.1029/2021GL093798.

Ali, S. M., Martius, O. and Röthlisberger, M. (2021c) ‘Recurrent Rossby Wave Packets Modulate the Persistence of Dry and Wet Spells Across the Globe’, *Geophysical Research Letters*, 48(5), pp. 1–11. doi: 10.1029/2020GL091452.

Allan, R. and Liu, C. (2021) ‘Global-scale changes in Earth’s energy budget and implications for the water cycle’, *EGU General Assembly 2021 (online)*, EGU21-1335. Available at: https://doi.org/10.5194/egusphere-egu21-1335.

Allan, R. P., Blenkinsop, S., Fowler, H. J. and Champion, A. J. (2019) ‘Atmospheric precursors for intense summer rainfall over the United Kingdom’, *International Journal of Climatology*, (November 2019), pp. 1–19. doi: 10.1002/joc.6431.

Allan, R. P., Lavers, D. A. and Champion, A. J. (2016) ‘Diagnosing links between atmospheric moisture and extreme daily precipitation over the UK’, *International Journal of Climatology*, 36(9), pp. 3191–3206. doi: 10.1002/joc.4547.

Archer, D. R. and Fowler, H. J. (2018) ‘Characterising flash flood response to intense rainfall and impacts using historical information and gauged data in Britain’, *Journal of Flood Risk Management*, 11, pp. S121–S133. doi: 10.1111/jfr3.12187.

Arnbjerg-Nielsen, K., Leonardsen, L. and Madsen, H. (2015) ‘Evaluating adaptation options for urban flooding based on new high-end emission scenario regional climate model simulations’, *Climate Research*, 64(1), pp. 73–84. doi: 10.3354/cr01299.

Avanzi, F. *et al.* (2015) ‘Orographic signature on extreme precipitation of short durations’, *Journal of Hydrometeorology*, 16(1), pp. 278–294. doi: 10.1175/JHM-D-14-0063.1.

Baker, L. H., Shaffrey, L. C. and Scaife, A. A. (2018) ‘Improved seasonal prediction of UK regional precipitation using atmospheric circulation’, *International Journal of Climatology*, 38(December 2017), pp. e437–e453. doi: 10.1002/joc.5382.

Ban, N. *et al.* (2021) 'The first multi-model ensemble of regional climate simulations at kilometer-scale resolution, part I: evaluation of precipitation', *Climate Dynamics*. Springer Berlin Heidelberg, 57(1–2), pp. 275–302. doi: 10.1007/s00382-021-05708-w.

Barbero, R. *et al.* (2019a) 'A synthesis of hourly and daily precipitation extremes in different climatic regions', *Weather and Climate Extremes*. Elsevier B.V., 26, p. 100219. doi: 10.1016/j.wace.2019.100219.

Barbero, R., Abatzoglou, J. T. and Fowler, H. J. (2019b) 'Contribution of large-scale midlatitude disturbances to hourly precipitation extremes in the United States', *Climate Dynamics*. Springer Berlin Heidelberg, 52(1–2), pp. 197–208. doi: 10.1007/s00382-018-4123-5.

Barbero, R., Fowler, H. J., Lenderink, G. and Blenkinsop, S. (2017) 'Is the intensification of precipitation extremes with global warming better detected at hourly than daily resolutions?', *Geophysical Research Letters*, 44(2), pp. 974–983. doi: 10.1002/2016GL071917.

Barbero, R., Westra, S., Lenderink, G. and Fowler, H. J. (2018) 'Temperature-extreme precipitation scaling: a two-way causality?', *International Journal of Climatology*, 38(December 2017), pp. e1274–e1279. doi: 10.1002/joc.5370.

Bárdossy, A. and Caspary, H. J. (1990) 'Detection of climate change in Europe by analyzing European atmospheric circulation patterns from 1881 to 1989', *Theoretical and Applied Climatology*, 42(3), pp. 155–167. doi: 10.1007/BF00866871.

Barredo, I. (2007) 'Major flood disasters in Europe : 1950 – 2005', *Natrual Hazards*, 42, pp. 125–148. doi: 10.1007/s11069-006-9065-2.

Barton, Y. *et al.* (2016) 'Clustering of regional-scale extreme precipitation events in southern Switzerland', *Monthly Weather Review*, 144(1), pp. 347–369. doi: 10.1175/MWR-D-15-0205.1.

Barton, Y. *et al.* (2022) 'On the temporal clustering of European extreme precipitation events and its relationship to persistent and transient large-scale atmospheric drivers', *Weather and Climate Extremes*. Elsevier B.V., 38(February), p. 100518. doi: 10.1016/j.wace.2022.100518.

Beck, H. E. *et al.* (2018) 'Present and future köppen-geiger climate classification maps at 1-km resolution', *Scientific Data*. The Author(s), 5, pp. 1–12. doi: 10.1038/sdata.2018.214.

Beck, H. E. *et al.* (2020) 'PPDIST, global 0.1° daily and 3-hourly precipitation probability distribution climatologies for 1979–2018', *Scientific Data*, 7(1), pp. 1–12. doi: 10.1038/s41597-020-00631-x.

Beniston, M. *et al.* (2007) 'Future extreme events in European climate: An exploration of regional climate model projections', *Climatic Change*, 81(SUPPL. 1), pp. 71–95. doi: 10.1007/s10584-006-9226-z.

Beranová, R., Kyselý, J. and Hanel, M. (2018) 'Characteristics of sub-daily precipitation extremes in observed data and regional climate model simulations', *Theoretical and Applied Climatology*. Theoretical and Applied Climatology, 132(1–2), pp. 515–527. doi: 10.1007/s00704-017-2102-0.

Blackburn, M., Methven, J. and Roberts, N. (2008) 'Large-scale context for the UK floods in summer 2007', *Weather*, 63(9), pp. 280–288. doi: 10.1002/wea.322.

Blackport, R. and Screen, J. A. (2020) 'Insignificant effect of Arctic amplification on the amplitude of midlatitude atmospheric waves', *Science Advances*, 6(8), pp. 1–10. doi: 10.1126/sciadv.aay2880.

Blenkinsop, S. *et al.* (2015) 'Temperature influences on intense UK hourly precipitation and dependency on large-scale circulation', *Environmental Research Letters*. IOP Publishing, 10(5). doi: 10.1088/1748-9326/10/5/054021.

Blenkinsop, S. *et al.* (2018) 'The INTENSE project: using observations and models to understand the past, present and future of sub-daily rainfall extremes', *Advances in Science and Research*, 15, pp. 117–126. doi: 10.5194/asr-15-117-2018.

Blenkinsop, S., Lewis, E., Chan, S. C. and Fowler, H. J. (2017) 'Quality-control of an hourly rainfall dataset and climatology of extremes for the UK', *International Journal of Climatology*, 37(2), pp. 722–740. doi: 10.1002/joc.4735.

Boers, N. *et al.* (2019) 'Complex networks reveal global pattern of extreme-rainfall teleconnections', *Nature*. Springer US, 566(7744), pp. 373–377. doi: 10.1038/s41586-018-0872-x.

Borga, M. *et al.* (2014) 'Hydrogeomorphic response to extreme rainfall in headwater systems: Flash floods and debris flows', *Journal of Hydrology*. Elsevier B.V., 518(PB), pp. 194–205. doi: 10.1016/j.jhydrol.2014.05.022.

Branstator, G. (2002) 'Circumglobal teleconnections, the jet stream waveguide, and the North Atlantic Oscillation', *Journal of Climate*, 15(14), pp. 1893–1910. doi: 10.1175/1520-0442(2002)015<1893:CTTJSW>2.0.CO;2.

Breugem, A. J., Wesseling, J. G., Oostindie, K. and Ritsema, C. J. (2020) 'Meteorological aspects of heavy precipitation in relation to floods – An overview', *Earth-Science Reviews*. Elsevier, 204(March), p. 103171. doi: 10.1016/j.earscirev.2020.103171.

Brieber, A. and Hoy, A. (2019) 'Statistical analysis of very high-resolution precipitation data and relation to atmospheric circulation in Central Germany', *Advances in Science and Research*, 16(2011), pp. 69–73. doi: 10.5194/asr-16-69-2019.

Di Capua, G. *et al.* (2020) 'Dominant patterns of interaction between the tropics and mid-latitudes in boreal summer: causal relationships and the role of timescales', *Weather and Climate Dynamics*, 1(2), pp. 519–539. doi: 10.5194/wcd-1-519-2020.

Cassano, J. J., Uotila, P. and Lynch, A. (2006) 'Changes in synoptic weather patterns in the polar regions in the twentieth and twenty-first centuries, Part 1: Arctic', *International Journal of Climatology*, 26(8), pp. 1027–1049. doi: 10.1002/joc.1306.

Catto, J. L. and Pfahl, S. (2013) 'The importance of fronts for extreme precipitation', *Journal of Geophysical Research Atmospheres*, 118(19), pp. 10791–10801. doi: 10.1002/jgrd.50852.

Centre, F. F. (2022) *Flood Forecasting Centre: Annual Review 2021 to 2022*. Available at: https://www.gov.uk/government/publications/flood-forecasting-centre-annual-review-2021-to-2022.

Champion, A. J., Allan, R. P. and Lavers, D. A. (2015) 'Atmospheric rivers do not explain UK summer extreme rainfall', *Journal of Geophysical Research*, 120(14), pp. 6731–6741. doi: 10.1002/2014JD022863.

Champion, A. J., Blenkinsop, S., Li, X. F. and Fowler, H. J. (2019) 'Synoptic-Scale Precursors of Extreme U.K. Summer 3-Hourly Rainfall', *Journal of Geophysical Research: Atmospheres*, 124(8), pp. 4477–4489. doi: 10.1029/2018JD029664.

Chan, S. C. *et al.* (2014) 'Projected increases in summer and winter UK sub-daily precipitation extremes from high-resolution regional climate models'. IOP Publishing. doi: 10.1088/1748-9326/9/8/084019.

Chan, S. C. *et al.* (2018a) 'Large-scale predictors for extreme hourly precipitation events in convection-permitting climate simulations', *Journal of Climate*, 31(6), pp. 2115–2131. doi: 10.1175/JCLI-D-17-0404.1.

Chan, S. C. *et al.* (2020a) ‘Europe-wide precipitation projections at convection permitting scale with the Unified Model’, *Climate Dynamics*. Springer Berlin Heidelberg, 55(3–4), pp. 409–428. doi: 10.1007/s00382-020-05192-8.

Chan, S. C. *et al.* (2020b) ‘Europe-wide precipitation projections at convection permitting scale with the Unified Model - Supplementary’, *Climate Dynamics*, (accepted), pp. 1–23.

Chan, S. C. *et al.* (2023) ‘Large-scale dynamics moderate impact-relevant changes to organised convective storms’, *Communications Earth and Environment*. Springer US, 4(1), pp. 1–10. doi: 10.1038/s43247-022-00669-2.

Chan, S. C., Kahana, R., Kendon, E. J. and Fowler, H. J. (2018b) ‘Projected changes in extreme precipitation over Scotland and Northern England using a high - resolution regional climate model’, *Climate Dynamics*. Springer Berlin Heidelberg, 51(9), pp. 3559–3577. doi: 10.1007/s00382-018-4096-4.

Chen, G., Lu, J., Alex Burrows, D. and Ruby Leung, L. (2015) ‘Local finite-amplitude wave activity as an objective diagnostic of midlatitude extreme weather’, *Geophysical Research Letters*, 42(24), pp. 10952–10960. doi: 10.1002/2015GL066959.

Cioffi, F., Lall, U., Rus, E. and Krishnamurthy, C. K. B. (2015) ‘Space-time structure of extreme precipitation in Europe over the last century’, *International Journal of Climatology*, 35(8), pp. 1749–1760. doi: 10.1002/joc.4116.

Cipolla, G., Francipane, A. and Noto, L. V. (2020) ‘Classification of Extreme Rainfall for a Mediterranean Region by Means of Atmospheric Circulation Patterns and Reanalysis Data’, *Water Resources Management*. Water Resources Management, 34(10), pp. 3219–3235. doi: 10.1007/s11269-020-02609-1.

Clark, M. R. and Webb, J. D. C. (2013) ‘A severe hailstorm across the English Midlands on 28 June 2012’, *Weather*, 68(11), pp. 284–291. doi: 10.1002/wea.2162.

Cohen, J. *et al.* (2014) ‘Recent Arctic amplification and extreme mid-latitude weather’, *Nature Geoscience*. Nature Publishing Group, 7(9), pp. 627–637. doi: 10.1038/ngeo2234.

Coles, S. (2001) *An Introduction to Statistical Modeling of Extreme Values*. 3rd edn. Springer.

Cotterill, D. F., Pope, J. O. and Stott, P. A. (2023) ‘Future extension of the UK summer and its impact on autumn precipitation’, *Climate Dynamics*. Springer Berlin Heidelberg, 60(5), pp. 1801–1814. doi: 10.1007/s00382-022-06403-0.

Coumou, D. *et al.* (2014) ‘Quasi-resonant circulation regimes and hemispheric synchronization of extreme weather in boreal summer’, *Proceedings of the National Academy of Sciences of the United States of America*, 111(34), pp. 12331–12336. doi: 10.1073/pnas.1412797111.

Cresswell-Clay, N., Ummenhofer, C.C., Thatcher, D.L. *et al.* (2022) 'Twentieth-century Azores High expansion unprecedented in the past 1,200 years', *Nature Geoscience*. 15, pp. 548–553. doi: 10.1038/s41561-022-00971-w

Dale, M. *et al.* (2017) ‘New climate change rainfall estimates for sustainable drainage’, *Proceedings of the Institution of Civil Engineers: Engineering Sustainability*, 170(4), pp. 214–224. doi: 10.1680/jensu.15.00030.

Dale, M. (2021) ‘Managing the effects of extreme sub-daily rainfall and flash floods - A practitioner’s perspective’, *Philosophical Transactions of the Royal Society A: Mathematical, Physical and Engineering Sciences*, 379(2195). doi: 10.1098/rsta.2019.0550.

Darwish, M. M. *et al.* (2020) ‘New hourly extreme precipitation regions and regional annual probability estimates for the UK’, *International Journal of Climatology*, 41(1), pp. 582–600. doi:

10.1002/joc.6639.

Darwish, M. M., Fowler, H. J., Blenkinsop, S. and Tye, M. R. (2018) 'A regional frequency analysis of UK sub-daily extreme precipitation and assessment of their seasonality', *International Journal of Climatology*, 38(13), pp. 4758–4776. doi: 10.1002/joc.5694.

Dawson, R. J. . *et al.* (2016) *UK Climate Change Risk Assessment Evidence Report: Chapter 4 - Infrastructure*, *UK Climate Change Risk Assessment Evidence Report*. doi: http://dx.doi.org/10.1016/B978-0-12-420217-7.00004-3.

Dee, D. P. *et al.* (2011) 'The ERA-Interim reanalysis: Configuration and performance of the data assimilation system', *Quarterly Journal of the Royal Meteorological Society*, 137(656), pp. 553–597. doi: 10.1002/qj.828.

Delden, A. Van (2001) 'The synoptic setting of thunderstorms in western Europe', pp. 89–110.

Dietzsch, F. *et al.* (2017) 'A global ETCCDI-based precipitation climatology from satellite and rain gauge measurements', *Climate*, 5(1). doi: 10.3390/cli5010009.

Doe, B. R. K. (2004) 'Extreme Precipitation and Runoff Induced Flash Flooding at Boscastle, Cornwall, UK - 16 August 2004', *Journal of Meteorology*, 29(293).

Donat, M. G. *et al.* (2013a) 'Global land-based datasets for monitoring climatic extremes', *Bulletin of the American Meteorological Society*, 94(7), pp. 997–1006. doi: 10.1175/BAMS-D-12-00109.1.

Donat, M. G. *et al.* (2013b) 'Updated analyses of temperature and precipitation extreme indices since the beginning of the twentieth century: The HadEX2 dataset', *Journal of Geophysical Research Atmospheres*, 118(5), pp. 2098–2118. doi: 10.1002/jgrd.50150.

Donat, M. G., Leckebusch, G. C., Pinto, J. G. and Ulbrich, U. (2010) 'European storminess and associated circulation weather types: Future changes deduced from a multi-model ensemble of GCM simulations', *Climate Research*, 42(1), pp. 27–43. doi: 10.3354/cr00853.

Dorrington, J. *et al.* (2023) 'Domino: A new framework for the automated identification of weather event precursors, demonstrated for European extreme rainfall', *Quarterly Journal of the Royal Meteorological Society*. Available at: http://arxiv.org/abs/2306.16787.

Doswell, C. A. (1987) 'The Dsitinction between Large-Scale and Mesoscale Contribution to Severe Convection: A Case Study Example', *Weather and Forecasting*, 2(March 1987).

Doswell, C. A., Brooks, H. E. and Maddox, R. A. (1996) 'Flash Flood Forecasting : An Ingredients-Based Methodology', *Weather and Forecasting*, 11(December 96), pp. 560–581.

Drobinski, P. *et al.* (2018) 'Scaling precipitation extremes with temperature in the Mediterranean: past climate assessment and projection in anthropogenic scenarios', *Climate Dynamics*, 51(3), pp. 1237–1257. doi: 10.1007/s00382-016-3083-x.

E.B. Wilson (1927) 'Probable inference, the law of succession, and statistical inference', *Journal of the American Statistical Association*, 22(158), pp. 209–2012. doi: 10.1080/01621459.1927.10502953.

Essex, J. (2018) *Coverack Flood Incident Review; Technical Report*. Available at: http://www.cornwall.gov.uk/media/32471292/coverack-flood-incident-review-technical-summary-report-2017s6474_v20-mar-2018.pdf (accessed on 25th October 2020).

Fereday, D., Chadwick, R., Knight, J. and Scaife, A. A. (2018) 'Atmospheric dynamics is the largest source of uncertainty in future winter European rainfall', *Journal of Climate*, 31(3), pp. 963–977. doi: 10.1175/JCLI-D-17-0048.1.

Ferranti, L., Corti, S. and Janousek, M. (2015) 'Flow-dependent verification of the ECMWF ensemble over the Euro-Atlantic sector', *Quarterly Journal of the Royal Meteorological Society*, 141(688), pp. 916–924. doi: 10.1002/qj.2411.

Ferranti, L., Magnusson, L., Vitart, F. and Richardson, D. S. (2018) 'How far in advance can we predict changes in large-scale flow leading to severe cold conditions over Europe?', *Quarterly Journal of the Royal Meteorological Society*, 144(715), pp. 1788–1802. doi: 10.1002/qj.3341.

Flack, D. L. A. *et al.* (2019) 'Recommendations for improving integration in national end-to-end flood forecasting systems: An overview of the FFIR (Flooding From Intense Rainfall) programme', *Water (Switzerland)*, 11(4). doi: 10.3390/w11040725.

Formetta, G. *et al.* (2022) 'Differential orographic impact on sub-hourly, hourly, and daily extreme precipitation', *Advances in Water Resources*. Elsevier Ltd, 159(November 2021), p. 104085. doi: 10.1016/j.advwatres.2021.104085.

Förster, K. and Thiele, L. B. (2020) 'Variations in sub-daily precipitation at centennial scale', *npj Climate and Atmospheric Science*. Springer US, 3(1). doi: 10.1038/s41612-020-0117-1.

Fowler, H. J. *et al.* (2021a) 'Anthropogenic intensification of short-duration rainfall extremes', *Nature Reviews Earth & Environment*. Springer US, 2(2), pp. 107–122. doi: 10.1038/s43017-020-00128-6.

Fowler, H. J. *et al.* (2021b) 'Towards advancing scientific knowledge of climate change impacts on short-duration rainfall extremes', *Philosophical Transactions of the Royal Society A: Mathematical, Physical and Engineering Sciences*, 379(2195). doi: 10.1098/rsta.2019.0542.

Fowler, H. J. and Kilsby, C. G. (2002) 'Precipitation and the North Atlantic Oscillation: A study of climatic variability in Northern England', *International Journal of Climatology*, 22(7), pp. 843–866. doi: 10.1002/joc.765.

Fowler, H. J., Wasko, C. and Prein, A. F. (2021c) 'Intensification of short-duration rainfall extremes and implications for flood risk: Current state of the art and future directions', *Philosophical Transactions of the Royal Society A: Mathematical, Physical and Engineering Sciences*, 379(2195). doi: 10.1098/rsta.2019.0541.

Fragkoulidis, G. and Wirth, V. (2020) 'Local rossby wave packet amplitude, phase speed, and group velocity: Seasonal variability and their role in temperature extremes', *Journal of Climate*, 33(20), pp. 8767–8787. doi: 10.1175/JCLI-D-19-0377.1.

Fragkoulidis, G., Wirth, V., Bossmann, P. and Fink, A. H. (2018) 'Linking Northern Hemisphere temperature extremes to Rossby wave packets', *Quarterly Journal of the Royal Meteorological Society*, 144(January), pp. 553–566. doi: 10.1002/qj.3228.

Francis, J. A. and Vavrus, S. J. (2012) 'Evidence linking Arctic amplification to extreme weather in mid-latitudes', *Geophysical Research Letters*, 39(6), pp. 1–6. doi: 10.1029/2012GL051000.

G. W. Platzman (1968) 'The Rossby Wave', *Quarterly Journal of the Royal Meteorological Society*, 94(401), pp. 225–248.

Gaume, E. *et al.* (2009) 'A compilation of data on European flash floods', *Journal of Hydrology*, 367(1–2), pp. 70–78. doi: 10.1016/j.jhydrol.2008.12.028.

Gaume, E. *et al.* (2016) 'Mediterranean extreme floods and flash floods (Sub-chapter 1.3.4)', in Allenvi (ed.) *The Mediterranean Region under Climate Change*, pp. 133–144.

Gelbrecht, M., Boers, N. and Kurths, J. (2018) 'Phase coherence between precipitation in South America and Rossby waves', *Science Advances*, 4(12), pp. 1–10. doi: 10.1126/sciadv.aau3191.

Ghinassi, P., Fragkoulidis, G. and Wirth, V. (2018) ‘Local finite-amplitude wave activity as a diagnostic for Rossby Wave Packets’, *Monthly Weather Review*, 146(12), pp. 4099–4114. doi: 10.1175/MWR-D-18-0068.1.

Giannakaki, P. and Martius, O. (2016) ‘Synoptic-scale flow structures associated with extreme precipitation events in northern Switzerland’, *International Journal of Climatology*, 36(6), pp. 2497–2515. doi: 10.1002/joc.4508.

Giorgi, F. *et al.* (2016) ‘Enhanced summer convective rainfall at Alpine high elevations in response to climate warming’, *Nature Geoscience*, 9(8), pp. 584–589. doi: 10.1038/ngeo2761.

Graf, M., Kossmann, M., Trusilova, K. and Mühlbacher, G. (2016) ‘Identification and climatology of alpine pumping from a regional climate simulation’, *Frontiers in Earth Science*, 4(February), pp. 1–11. doi: 10.3389/feart.2016.00005.

Grams, C. M. *et al.* (2014) ‘Atmospheric processes triggering the central European floods in June 2013’, *Natural Hazards and Earth System Sciences*, 14(7), pp. 1691–1702. doi: 10.5194/nhess-14-1691-2014.

Grams, C. M. and Blumer, S. R. (2015) ‘European high-impact weather caused by the downstream response to the extratropical transition of North Atlantic Hurricane Katia (2011)’, *Geophysical Research Letters*, 42(20), pp. 8738–8748. doi: 10.1002/2015GL066253.

Grazzini, F. *et al.* (2021) ‘Extreme precipitation events over northern Italy. Part II: Dynamical precursors’, *Quarterly Journal of the Royal Meteorological Society*, 147(735), pp. 1237–1257. doi: 10.1002/qj.3969.

Grimm, A. M. and Tedeschi, R. G. (2009) ‘ENSO and extreme rainfall events in South America’, *Journal of Climate*, 22(7), pp. 1589–1609. doi: 10.1175/2008JCLI2429.1.

Guerreiro, S. B. *et al.* (2018) ‘Detection of continental-scale intensification of hourly rainfall extremes’, *Nature Climate Change*. Springer US, 8(9), pp. 803–807. doi: 10.1038/s41558-018-0245-3.

Guerreiro, S. B., Glenis, V., Dawson, R. J. and Kilsby, C. (2017) ‘Pluvial flooding in European cities-A continental approach to urban flood modelling’, *Water (Switzerland)*, 9(4). doi: 10.3390/w9040296.

Guimares Nobre, G., Jongman, B., Aerts, J. and Ward, P. J. (2017) ‘The role of climate variability in extreme floods in Europe’, *Environmental Research Letters*, 12(8). doi: 10.1088/1748-9326/aa7c22.

Haacke, N. and Paton, E. N. (2021) ‘Analysis of diurnal, seasonal, and annual distribution of urban sub-hourly to hourly rainfall extremes in Germany’, *Hydrology Research*, 52(2), pp. 478–491. doi: 10.2166/nh.2021.181.

Hardwick Jones, R., Westra, S. and Sharma, A. (2010) ‘Observed relationships between extreme sub-daily precipitation, surface temperature, and relative humidity’, *Geophysical Research Letters*, 37(22), pp. 1–5. doi: 10.1029/2010GL045081.

Hawkins, E. and Sutton, R. (2011) ‘The potential to narrow uncertainty in projections of regional precipitation change’, *Climate Dynamics*, 37(1), pp. 407–418. doi: 10.1007/s00382-010-0810-6.

Hidalgo-Muñoz, J. M. *et al.* (2011) ‘Trends of extreme precipitation and associated synoptic patterns over the southern Iberian Peninsula’, *Journal of Hydrology*, 409(1–2), pp. 497–511. doi: 10.1016/j.jhydrol.2011.08.049.

Hirata, F. E. and Grimm, A. M. (2016) ‘The role of synoptic and intraseasonal anomalies in the life cycle of summer rainfall extremes over South America’, *Climate Dynamics*. Springer Berlin

Heidelberg, 46(9–10), pp. 3041–3055. doi: 10.1007/s00382-015-2751-6.

Hoffmann, P. and Schlünzen, K. H. (2013) 'Weather pattern classification to represent the urban heat island in present and future climate', *Journal of Applied Meteorology and Climatology*, 52(12), pp. 2699–2714. doi: 10.1175/JAMC-D-12-065.1.

Hoskins, B. and Woollings, T. (2015) 'Persistent Extratropical Regimes and Climate Extremes', *Current Climate Change Reports*, 1(3), pp. 115–124. doi: 10.1007/s40641-015-0020-8.

Hosseinzadehtalaei, P., Tabari, H. and Willems, P. (2020) 'Satellite-based data driven quantification of pluvial floods over Europe under future climatic and socioeconomic changes', *Science of the Total Environment*. Elsevier B.V, p. 100632. doi: 10.1016/j.neubiorev.2019.07.019.

Hoy, A., Schucknecht, A., Sepp, M. and Matschullat, J. (2014) 'Large-scale synoptic types and their impact on European precipitation', *Theoretical and Applied Climatology*, 116(1–2), pp. 19–35. doi: 10.1007/s00704-013-0897-x.

Huang, C. S. Y. and Nakamura, N. (2016) 'Local finite-amplitude wave activity as a diagnostic of anomalous weather events', *Journal of the Atmospheric Sciences*, 73(1), pp. 211–229. doi: 10.1175/JAS-D-15-0194.1.

Hurford, A. P., Parker, D. J., Priest, S. J. and Lumbroso, D. M. (2012) 'Validating the return period of rainfall thresholds used for Extreme Rainfall Alerts by linking rainfall intensities with observed surface water flood events', *Journal of Flood Risk Management*, 5(2), pp. 134–142. doi: 10.1111/j.1753-318X.2012.01133.x.

Huth, R. *et al.* (2008) 'Classifications of atmospheric circulation patterns: Recent advances and applications', *Annals of the New York Academy of Sciences*, 1146, pp. 105–152. doi: 10.1196/annals.1446.019.

Insua-Costa, D., Lemus-Cánovas, M., Miguez-Macho, G. and Llasat, M. C. (2021) 'Climatology and ranking of hazardous precipitation events in the western Mediterranean area', *Atmospheric Research*, 255(May 2020). doi: 10.1016/j.atmosres.2021.105521.

IPCC (2022) 'Key Risks Across Sectors and Regions', *IPCC WGII Sixth Assessment Report*, pp. 20–22.

Jaagus, J., Briede, A., Rimkus, E. and Remm, K. (2010) 'Precipitation pattern in the Baltic countries under the influence of large-scale atmospheric circulation and local landscape factors', *International Journal of Climatology*, 30(5), pp. 705–720. doi: 10.1002/joc.1929.

Jacobeit, J., Rathmann, J., Philipp, A. and Jones, P. D. (2009) 'Central European precipitation and temperature extremes in relation to large-scale atmospheric circulation types', *Meteorologische Zeitschrift*, 18(4), pp. 397–410. doi: 10.1127/0941-2948/2009/0390.

Jaroszweski, D. *et al.* (2021) 'The Third UK Climate Change Risk Assessment Technical Report'.

Jenkinson, A. F. and Collison, F. P. (1977) 'An initial climatology of gales over the North Sea', *Synoptic Climatology Branch Memorandum No.62*, Meteorolog.

Jeong, J. H. *et al.* (2011) 'Diurnal cycle of precipitation amount and frequency in Sweden: Observation versus model simulation', *Tellus, Series A: Dynamic Meteorology and Oceanography*, 63(4), pp. 664–674. doi: 10.1111/j.1600-0870.2011.00517.x.

Jiang, Q. *et al.* (2019) 'Evaluation of satellite-based products for extreme rainfall estimations in eastern coastal areas of China', *Journal of Integrative Environmental Sciences*, 16(1), pp. 191–207.

Jones, P. D., Harpham, C. and Briffa, K. R. (2013) 'Lamb weather types derived from reanalysis products', 1139(April 2012), pp. 1129–1139. doi: 10.1002/joc.3498.

Kahraman, A., Kendon, E. J., Chan, S. C. and Fowler, H. J. (2021) 'Quasi-Stationary Intense Rainstorms Spread Across Europe Under Climate Change', *Geophysical Research Letters*, 48(13), pp. 1–11. doi: 10.1029/2020GL092361.

Kahraman, A., Kendon, E. J., Fowler, H. J. and Wilkinson, J. M. (2022) 'Contrasting future lightning stories across Europe', *Environmental Research Letters*, 17(114023). doi: 10.1088/1748-9326/ac9b78.

Kam, P. M. *et al.* (2021) 'Global warming and population change both heighten future risk of human displacement due to river floods', *Environmental Research Letters*, 16(4). doi: 10.1088/1748-9326/abd26c.

Kautz, L.-A. *et al.* (2022) 'Atmospheric blocking and weather extremes over the Euro-Atlantic sector – a review', *Weather and Climate Dynamics*, 3(1), pp. 305–336. doi: 10.5194/wcd-3-305-2022.

Kendon, E. J. *et al.* (2014) 'Heavier summer downpours with climate change revealed by weather forecast resolution model', *Nature Climate Change*, 4(7), pp. 570–576. doi: 10.1038/nclimate2258.

Kendon, E. J., Blenkinsop, S. and Fowler, H. J. (2018) 'When will we detect changes in short-duration precipitation extremes?', *Journal of Climate*, 31(7), pp. 2945–2964. doi: 10.1175/JCLI-D-17-0435.1.

Klein Tank, A. M. G. *et al.* (2002) 'Daily dataset of 20th-century surface air temperature and precipitation series for the European Climate Assessment', *International Journal of Climatology*, 22(12), pp. 1441–1453. doi: 10.1002/joc.773.

Klein Tank, A. M. G. and Können, G. P. (2003) 'Trends in Indices of daily temperature and precipitation extremes in Europe, 1946-99', *Journal of Climate*, 16(22), pp. 3665–3680. doi: 10.1175/1520-0442(2003)016<3665:TIIODT>2.0.CO;2.

Kornhuber, K. *et al.* (2017) 'Summertime planetary wave resonance in the Northern and Southern hemispheres', *Journal of Climate*, 30(16), pp. 6133–6150. doi: 10.1175/JCLI-D-16-0703.1.

Kornhuber, K. *et al.* (2019) 'Extreme weather events in early summer 2018 connected by a recurrent hemispheric wave-7 pattern', *Environmental Research Letters*. IOP Publishing, 14(5). doi: 10.1088/1748-9326/ab13bf.

Kornhuber, K. *et al.* (2020) 'Amplified Rossby waves enhance risk of concurrent heatwaves in major breadbasket regions', *Nature Climate Change*. Springer US, 10(1), pp. 48–53. doi: 10.1038/s41558-019-0637-z.

Kreienkamp, F. *et al.* (2021) 'Rapid attribution of heavy rainfall events leading to the severe flooding in Western Europe during July 2021', *World Weather Attribution*, 13(July), p. 18. Available at: https://www.meteo.be/fr/infos/actualite/ce-que-lon-sait-sur-les-pluies-.

Krichak, S. O., Breitgand, J. S., Gualdi, S. and Feldstein, S. B. (2014) 'Teleconnection-extreme precipitation relationships over the Mediterranean region', *Theoretical and Applied Climatology*, 117(3–4), pp. 679–692. doi: 10.1007/s00704-013-1036-4.

Kučerová, M., Beck, C., Philipp, A. and Huth, R. (2017) 'Trends in frequency and persistence of atmospheric circulation types over Europe derived from a multitude of classifications', *International Journal of Climatology*, 37(5), pp. 2502–2521. doi: 10.1002/joc.4861.

Kundzewicz, Z. W. *et al.* (2014) 'flood risk and climate change: global and regional perspectives', *Hydrological Sciences Journal*. Taylor & Francis, 59(1), pp. 1–28. doi:

10.1080/02626667.2013.857411.

Kundzewicz, Z. W., Radziejewski, M. and Pińskwar, I. (2006) ‘Precipitation extremes in the changing climate of Europe’, *Climate Research*, 31(1), pp. 51–58. doi: 10.3354/cr031051.

Lakatos, M. *et al.* (2021) ‘Analysis of Sub-Daily Precipitation for the PannEx Region’, *Atmosphere*, 12(838), pp. 1–18.

Lamb, H. (1972) ‘British Isles weather types and a register of the daily sequence of circulation patterns 1861-1971’, *Geophysical Memoirs*, 116, p. 85.

Larsen, A. N. *et al.* (2009) ‘Potential future increase in extreme one-hour precipitation events over Europe due to climate change’, *Water Science and Technology*, 60(9), pp. 2205–2216. doi: 10.2166/wst.2009.650.

Lavers, D. A. *et al.* (2018) ‘Earlier awareness of extreme winter precipitation across the western Iberian Peninsula’, *Meteorological Applications*, 25(4), pp. 622–628. doi: 10.1002/met.1727.

Lavers, D. A., Pappenberger, F., Richardson, D. S. and Zsoter, E. (2016) ‘ECMWF Extreme Forecast Index for water vapor transport: A forecast tool for atmospheric rivers and extreme precipitation’, *Geophysical Research Letters*, 43(22), pp. 11,852-11,858. doi: 10.1002/2016GL071320.

Lavers, D. A., Pappenberger, F. and Zsoter, E. (2014) ‘Extending medium-range predictability of extreme hydrological events in Europe’, *Nature Communications*. Nature Publishing Group, 5. doi: 10.1038/ncomms6382.

Lavers, D. A. and Villarini, G. (2013) ‘The nexus between atmospheric rivers and extreme precipitation across Europe’, *Geophysical Research Letters*, 40(12), pp. 3259–3264. doi: 10.1002/grl.50636.

Lenderink, G. *et al.* (2019) ‘Systematic increases in the thermodynamic response of hourly precipitation extremes in an idealized warming experiment with a convection-permitting climate model’, *Environmental Research Letters*, 14(7). doi: 10.1088/1748-9326/ab214a.

Lenderink, G., Barbero, R., Loriaux, J. M. and Fowler, H. J. (2017a) ‘Super-Clausius-Clapeyron scaling of extreme hourly convective precipitation and its relation to large-scale atmospheric conditions’, *Journal of Climate*, 30(15), pp. 6037–6052. doi: 10.1175/JCLI-D-16-0808.1.

Lenderink, G., Barbero, R., Loriaux, J. M. and Fowler, H. J. (2017b) ‘Super-Clausius-Clapeyron scaling of extreme hourly convective precipitation and its relation to large-scale atmospheric conditions’, *Journal of Climate*, 30(15), pp. 6037–6052. doi: 10.1175/JCLI-D-16-0808.1.

Lenderink, G. and Fowler, H. J. (2017a) ‘Hydroclimate: Understanding rainfall extremes’, *Nature Climate Change*. Nature Publishing Group, 7(6), pp. 391–393. doi: 10.1038/nclimate3305.

Lenderink, G. and Fowler, H. J. (2017b) ‘Hydroclimate: Understanding rainfall extremes’, *Nature Climate Change*. Nature Publishing Group, 7(6), pp. 391–393. doi: 10.1038/nclimate3305.

Lenderink, G. and Van Meijgaard, E. (2008) ‘Increase in hourly precipitation extremes beyond expectations from temperature changes’, *Nature Geoscience*, 1(8), pp. 511–514. doi: 10.1038/ngeo262.

Lenderink, G. and Van Meijgaard, E. (2010) ‘Linking increases in hourly precipitation extremes to atmospheric temperature and moisture changes’, *Environmental Research Letters*, 5(2). doi: 10.1088/1748-9326/5/2/025208.

Lengfeld, K. *et al.* (2019) ‘Characteristic spatial extent of hourly and daily precipitation events in Germany derived from 16 years of radar data’, *Meteorologische Zeitschrift*, 28(5), pp. 363–378.

doi: 10.1127/metz/2019/0964.

Lengfeld, K. *et al.* (2020) 'Use of radar data for characterizing extreme precipitation at fine scales and short durations', *Environmental Research Letters*, 15(8). doi: 10.1088/1748-9326/ab98b4.

Lenggenhager, S. and Martius, O. (2019) 'Atmospheric blocks modulate the odds of heavy precipitation events in Europe', *Climate Dynamics*. Springer Berlin Heidelberg, 53(7–8), pp. 4155–4171. doi: 10.1007/s00382-019-04779-0.

Lewis, E. *et al.* (2019) 'GSDR: A global sub-daily rainfall dataset', *Journal of Climate*, 32(15), pp. 4715–4729. doi: 10.1175/JCLI-D-18-0143.1.

Lewis, E. *et al.* (2021) 'Quality control of a global hourly rainfall dataset', *Environmental Modelling & Software*. Elsevier Ltd, 144(August), p. 105169. doi: 10.1016/j.envsoft.2021.105169.

Lewis, M. W. and Gray, S. L. (2010) 'Categorisation of synoptic environments associated with mesoscale convective systems over the UK', *Atmospheric Research*. Elsevier B.V., 97(1–2), pp. 194–213. doi: 10.1016/j.atmosres.2010.04.001.

Li, C. *et al.* (2019) 'Larger Increases in More Extreme Local Precipitation Events as Climate Warms', *Geophysical Research Letters*, 46(12), pp. 6885–6891. doi: 10.1029/2019GL082908.

Lledo, L., Thomas, H., Schrottle, J. and Forbes, R. (2023) *Scale-dependent verification of precipitation and cloudiness at ECMWF*. Available at: https://www.ecmwf.int/en/newsletter/174/earth-system-science/scale-dependent-verification-precipitation-and-cloudiness.

Lorenzo, M. N., Ramos, A. M., Taboada, J. J. and Gimeno, L. (2011) 'Changes in present and future circulation types frequency in northwest Iberian Peninsula', *PLoS ONE*, 6(1). doi: 10.1371/journal.pone.0016201.

Luo, Y. *et al.* (2016) 'Synoptic situations of extreme hourly precipitation over China', *Journal of Climate*, 29(24), pp. 8703–8719. doi: 10.1175/JCLI-D-16-0057.1.

Łupikasza, E. B., Hänsel, S. and Matschullat, J. (2011) 'Regional and seasonal variability of extreme precipitation trends in southern Poland and central-eastern Germany 1951-2006', *International Journal of Climatology*, 31(15), pp. 2249–2271. doi: 10.1002/joc.2229.

Malby, A. R. *et al.* (2007) 'Long-term variations in orographic rainfall: Analysis and implications for upland catchments', *Hydrological Sciences Journal*, 52(2), pp. 276–291. doi: 10.1623/hysj.52.2.276.

Mann, M. E. *et al.* (2017) 'Influence of Anthropogenic Climate Change on Planetary Wave Resonance and Extreme Weather Events', *Scientific Reports*. Nature Publishing Group, 7(February). doi: 10.1038/srep45242.

Manola, I., Steeneveld, G. J., Uijlenhoet, R. and Holtslag, A. A. M. (2019) 'Analysis of urban rainfall from hourly to seasonal scales using high-resolution radar observations in the Netherlands', *International Journal of Climatology*, 40(2), pp. 822–840. doi: 10.1002/joc.6241.

Maraun, D., Osborn, T. J. and Rust, H. W. (2011) 'The influence of synoptic airflow on UK daily precipitation extremes. Part I: Observed spatio-temporal relationships', *Climate Dynamics*, 36(1), pp. 261–275. doi: 10.1007/s00382-009-0710-9.

Marchi, L., Borga, M., Preciso, E. and Gaume, E. (2010) 'Characterisation of selected extreme flash floods in Europe and implications for flood risk management', *Journal of Hydrology*. Elsevier B.V., 394(1–2), pp. 118–133. doi: 10.1016/j.jhydrol.2010.07.017.

Marra, F., Armon, M., Borga, M. and Morin, E. (2021) 'Orographic Effect on Extreme

Precipitation Statistics Peaks at Hourly Time Scales', *Geophysical Research Letters*, 48(5), pp. 1–9. doi: 10.1029/2020GL091498.

Marra, F., Armon, M. and Morin, E. (2022) 'Coastal and orographic effects on extreme precipitation revealed by weather radar observations', *Hydrology and Earth System Sciences*, 26(5), pp. 1439–1458. doi: 10.5194/hess-26-1439-2022.

Martineau, P., Chen, G. and Burrows, D. A. (2017) 'Wave events: Climatology, trends, and relationship to Northern Hemisphere winter blocking and weather extremes', *Journal of Climate*, 30(15), pp. 5675–5697. doi: 10.1175/JCLI-D-16-0692.1.

Martínez-Casasnovas, J. A., Ramos, M. C. and Ribes-Dasi, M. (2002) 'Soil erosion caused by extreme rainfall events: Mapping and quantification in agricultural plots from very detailed digital elevation models', *Geoderma*, 105(1–2), pp. 125–140. doi: 10.1016/S0016-7061(01)00096-9.

Martius, O., Schwierz, C. and Davies, H. C. (2008) 'Far-upstream precursors of heavy precipitation events on the Alpine south-side', *Quarterly Journal of the Royal Meteorological Society*, 134, pp. 417–428. doi: 10.1002/qj.229.

Mastrantonas, N. *et al.* (2021) 'Extreme precipitation events in the Mediterranean: Spatiotemporal characteristics and connection to large-scale atmospheric flow patterns', *Int. J. Climatology*, (December 2020), pp. 1–19. doi: 10.1002/joc.6985.

Mastrantonas, N. *et al.* (2022a) 'Forecasting extreme precipitation in the central Mediterranean: Changes in predictors' strength with prediction lead time', *Meteorological Applications*, 29(6), pp. 1–17. doi: 10.1002/met.2101.

Mastrantonas, N., Magnusson, L., Pappenberger, F. and Matschullat, J. (2022b) 'What do large-scale patterns teach us about extreme precipitation over the Mediterranean at medium- and extended-range forecasts?', *Quarterly Journal of the Royal Meteorological Society*, 148(743), pp. 875–890. doi: 10.1002/qj.4236.

Mazzoglio, P., Butera, I., Alvioli, M. and Claps, P. (2022) 'The role of morphology in the spatial distribution of short-duration rainfall extremes in Italy', *Hydrology and Earth System Sciences*, 26(6), pp. 1659–1672. doi: 10.5194/hess-26-1659-2022.

Merino, A. *et al.* (2016) 'Large-scale patterns of daily precipitation extremes on the Iberian Peninsula', *International Journal of Climatology*, 36(11), pp. 3873–3891. doi: 10.1002/joc.4601.

Meyer, J. *et al.* (2022) 'Atmospheric conditions favouring extreme precipitation and flash floods in temperate regions of Europe', *Hydrology and Earth System Sciences*, 26(23), pp. 6163–6183. doi: 10.5194/hess-26-6163-2022.

Minářová, J. *et al.* (2017) 'Duration, rarity, affected area, and weather types associated with extreme precipitation in the Ore Mountains (Erzgebirge) region, Central Europe', *International Journal of Climatology*, 37(12), pp. 4463–4477. doi: 10.1002/joc.5100.

Moberg, A. *et al.* (2006) 'Indices for daily temperature and precipitation extremes in Europe analyzed for the period 1901-2000', *Journal of Geophysical Research Atmospheres*, 111(22). doi: 10.1029/2006JD007103.

Mohr, S. *et al.* (2020) 'The role of large-scale dynamics in an exceptional sequence of severe thunderstorms in Europe May–June 2018', *Weather and Climate Dynamics*, 1(2), pp. 325–348. doi: 10.5194/wcd-1-325-2020.

Mohr, S., Wandel, J., Lenggenhager, S. and Martius, O. (2019) 'Relationship between atmospheric blocking and warm-season thunderstorms over western and central Europe', *Quarterly Journal of the Royal Meteorological Society*, 145(724), pp. 3040–3056. doi: 10.1002/qj.3603.

Moron, V. *et al.* (2019) 'Weather types and hourly to multiday rainfall characteristics in tropical Australia', *Journal of Climate*, 32(13). doi: 10.1175/JCLI-D-18-0384.1.

Morris, R. M. (1986) 'The Spanish plume - testing the forecaster's nerve', *Meteorological Magazine*, 115, pp. 349–357.

Murphy, J. M. *et al.* (2018) 'UKCP18 Land Projections: Science Report', 2018(November), pp. 1–191. doi: https://www.metoffice.gov.uk/pub/data/weather/uk/ukcp18/science-reports/UKCP18-Land-report.pdf.

Nakamura, N. and Huang, C. S. Y. (2018) 'Atmospheric blocking as a traffic jam in the jet stream', *Science*, 361, pp. 42–47.

Nakamura, N. and Zhu, D. (2010) 'Finite-amplitude wave activity and diffusive flux of potential vorticity in eddy-mean flow interaction', *Journal of the Atmospheric Sciences*, 67(9), pp. 2701–2716. doi: 10.1175/2010JAS3432.1.

Neal, R. *et al.* (2018) 'Use of probabilistic medium- to long-range weather-pattern forecasts for identifying periods with an increased likelihood of coastal flooding around the UK', *Meteorological Applications*, 25(4), pp. 534–547. doi: 10.1002/met.1719.

Neal, R., Fereday, D., Crocker, R. and Comer, R. E. (2016) 'A flexible approach to defining weather patterns and their application in weather forecasting over Europe', *Meteorological Applications*, 23(3), pp. 389–400. doi: 10.1002/met.1563.

Nie, J., Sobel, A. H., D.A., S. and S., W. (2018) 'Dynamic amplification of extreme precipitation sensitivity', *Proceedings of the National Academy of Sciences of the United States of America*, 115, pp. 9467–9472.

Nieto, R. *et al.* (2006) 'Interannual variability of cut-off low systems over the European sector: The role of blocking and the Northern Hemisphere circulation modes', *Meteorology and Atmospheric Physics*, 96(1–2), pp. 85–101. doi: 10.1007/s00703-006-0222-7.

O'Gorman, P. A. (2015) 'Precipitation Extremes Under Climate Change', *Current Climate Change Reports*, 1(2), pp. 49–59. doi: 10.1007/s40641-015-0009-3.

Oertel, A. *et al.* (2023) 'Everything Hits at Once: How Remote Rainfall Matters for the Prediction of the 2021 North American Heat Wave', *Geophysical Research Letters*, 50(3). doi: 10.1029/2022GL100958.

Olsson, J. *et al.* (2022) 'Sub-daily rainfall extremes in the Nordic–Baltic region', *Hydrology Research*, 53(6), pp. 807–824. doi: 10.2166/nh.2022.119.

Otero, N., Sillmann, J. and Butler, T. (2018) 'Assessment of an extended version of the Jenkinson–Collison classification on CMIP5 models over Europe', *Climate Dynamics*. Springer Berlin Heidelberg, 50(5–6), pp. 1559–1579. doi: 10.1007/s00382-017-3705-y.

Oueslati, B., Yiou, P. and Jézéquel, A. (2019) 'Revisiting the dynamic and thermodynamic processes driving the record-breaking January 2014 precipitation in the southern UK', *Scientific Reports*, 9(1), pp. 1–7. doi: 10.1038/s41598-019-39306-y.

Panziera, L., Gabella, M., Germann, U. and Martius, O. (2018) 'A 12-year radar-based climatology of daily and sub-daily extreme precipitation over the Swiss Alps', *International Journal of Climatology*, 38(10), pp. 3749–3769. doi: 10.1002/joc.5528.

Pappenberger, F. *et al.* (2015) 'The monetary benefit of early flood warnings in Europe', *Environmental Science and Policy*. Elsevier Ltd, 51, pp. 278–291. doi: 10.1016/j.envsci.2015.04.016.

Pattison, I. and Lane, S. N. (2012) 'The relationship between Lamb weather types and long-term changes in flood frequency, River Eden, UK', *International Journal of Climatology*, 32(13), pp. 1971–1989. doi: 10.1002/joc.2415.

Paulat, M., Frei, C., Hagen, M. and Wernli, H. (2008) 'A gridded dataset of hourly precipitation in Germany: Its construction, climatology and application', *Meteorologische Zeitschrift*, 17(6), pp. 719–732. doi: 10.1127/0941-2948/2008/0332.

Peterson, T. C. and Manton, M. J. (2008) 'Monitoring changes in climate extremes: A tale of international collaboration', *Bulletin of the American Meteorological Society*, 89(9), pp. 1266–1271. doi: 10.1175/2008BAMS2501.1.

Petoukhov, V., Rahmstorf, S., Petri, S. and Schellnhuber, H. J. (2013) 'Quasiresonant amplification of planetary waves and recent Northern Hemisphere weather extremes', *PNAS*, 110(14), pp. 5336–5341. doi: 10.1073/pnas.1222000110/-/DCSupplemental.www.pnas.org/cgi/doi/10.1073/pnas.1222000110.

Pfahl, S. (2014) 'Characterising the relationship between weather extremes in Europe and synoptic circulation features', *Natural Hazards and Earth System Sciences*, 14(6), pp. 1461–1475. doi: 10.5194/nhess-14-1461-2014.

Pfahl, S., O'Gorman, P. A. and Fischer, E. M. (2017) 'Understanding the regional pattern of projected future changes in extreme precipitation', *Nature Climate Change*, 7(6), pp. 423–427. doi: 10.1038/nclimate3287.

Pfahl, S. and Wernli, H. (2012a) 'Quantifying the relevance of atmospheric blocking for co-located temperature extremes in the Northern Hemisphere on (sub-)daily time scales', *Geophysical Research Letters*, 39(12), pp. 1–6. doi: 10.1029/2012GL052261.

Pfahl, S. and Wernli, H. (2012b) 'Quantifying the relevance of cyclones for precipitation extremes', *Journal of Climate*, 25(19), pp. 6770–6780. doi: 10.1175/JCLI-D-11-00705.1.

Piper, D. *et al.* (2016) 'Exceptional sequence of severe thunderstorms and related flash floods in May and June 2016 in Germany - Part 1: Meteorological background', *Natural Hazards and Earth System Sciences*, 16(12), pp. 2835–2850. doi: 10.5194/nhess-16-2835-2016.

Piper, D. A., Kunz, M., Allen, J. T. and Mohr, S. (2019) 'Investigation of the temporal variability of thunderstorms in central and western Europe and the relation to large-scale flow and teleconnection patterns', *Quarterly Journal of the Royal Meteorological Society*, 145(725), pp. 3644–3666. doi: 10.1002/qj.3647.

Piper, D. and Kunz, M. (2017) 'Spatiotemporal variability of lightning activity in Europe and the relation to the North Atlantic Oscillation teleconnection pattern', *Natural Hazards and Earth System Sciences*, 17(8), pp. 1319–1336. doi: 10.5194/nhess-17-1319-2017.

Pitt, M. (2008) *The Pitt Review: Learning lessons from the 2007 floods*.

Pizarro, R. *et al.* (2012) 'Latitudinal Analysis of Rainfall Intensity and Mean Annual Precipitation in Chile', *Chilean journal of agricultural research*, 72(2), pp. 252–261. doi: 10.4067/s0718-58392012000200014.

Planchon, O., Quénol, H., Dupont, N. and Corgne, S. (2009) 'Application of the Hess-Brezowsky classification to the identification of weather patterns causing heavy winter rainfall in Brittany (France)', *Natural Hazards and Earth System Science*, 9(4), pp. 1161–1173. doi: 10.5194/nhess-9-1161-2009.

Pope, J. O. *et al.* (2022) 'Investigation of future climate change over the British Isles using weather patterns', *Climate Dynamics*. Springer Berlin Heidelberg, 58(9–10), pp. 2405–2419. doi:

10.1007/s00382-021-06031-0.

Poschlod, B., Ludwig, R. and Sillmann, J. (2021) ‘Ten-year return levels of sub-daily extreme precipitation over Europe’, *Earth System Science Data*, 13(3), pp. 983–1003. doi: 10.5194/essd-13-983-2021.

Prein, A. F., Mooney, P. A. and Done, J. M. (no date) ‘The Multi-Scale Interactions of Atmospheric Phenomenon in Extreme and Mean Precipitation’, *Earth’s Future*.

Pritchard, D. *et al.* (2023) ‘GSDR-I: An Observation-Based Dataset of Global Sub-Daily Precipitation Indices’, *Scientific Data*. Springer US, pp. 1–13. doi: 10.1038/s41597-023-02238-4.

Pritchard, D. *et al.* (no date) ‘GSDR-I: An Observation-Based Dataset of Global Sub-Daily Precipitation Indices’, *Scientific Data*.

Púčik, T., Groenemeijer, P., Rỳva, D. and Kolář, M. (2015) ‘Proximity soundings of severe and nonsevere thunderstorms in central Europe’, *Monthly Weather Review*, 143(12), pp. 4805–4821. doi: 10.1175/MWR-D-15-0104.1.

Qin, H. *et al.* (2022) ‘Climate change attribution of the 2021 Henan extreme precipitation: Impacts of convective organization’, *Science China Earth Sciences*, 65(10), pp. 1837–1846. doi: 10.1007/s11430-022-9953-0.

Quinting, J. F. and Vitart, F. (2019) ‘Representation of Synoptic-Scale Rossby Wave Packets and Blocking in the S2S Prediction Project Database’, *Geophysical Research Letters*, 46(2), pp. 1070–1078. doi: 10.1029/2018GL081381.

Randel, W. J. (1988) ‘The seasonal evolution of planetary waves in the Southern Hemispehre stratosphere and troposphere’, *Quarterly Journal of the Royal Meteorological Society*, 114, pp. 1385–1409. doi: 10.1002/qj.49711448403.

Rau, M., He, Y., Goodess, C. and Bardossy, A. (2020) ‘Statistical downscaling to project extreme hourly precipitation over the United Kingdom’, *Int. J. Climatology*, 40, pp. 1805–1823. doi: 10.1002/joc.6302.

Reder, A. *et al.* (2022) ‘Characterizing extreme values of precipitation at very high resolution: An experiment over twenty European cities’, *Weather and Climate Extremes*. Elsevier B.V., 35, p. 100407. doi: 10.1016/j.wace.2022.100407.

Restrepo-Posada, P. J. and Eagleson, P. S. (1982) ‘Identification of independent rainstorms’, *Journal of Hydrology*, 55(1–4), pp. 303–319. doi: 10.1016/0022-1694(82)90136-6.

Rex, D. F. (1950) ‘Blocking action in the middle troposphere and its effect upon regional climate’, *Tellus*, 2, pp. 275–301.

Richardson, D. *et al.* (2020) ‘Linking weather patterns to regional extreme precipitation for highlighting potential flood events in medium- to long-range forecasts’, *Meteorological Applications*, 27(4), pp. 1–17. doi: 10.1002/met.1931.

Richardson, D., Fowler, H. J., Kilsby, C. G. and Neal, R. (2018) ‘A new precipitation and drought climatology based on weather patterns’, *International Journal of Climatology*, 38(2), pp. 630–648. doi: 10.1002/joc.5199.

Riemann-Campe, K., Fraedrich, K. and Lunkeit, F. (2009) ‘Global climatology of Convective Available Potential Energy (CAPE) and Convective Inhibition (CIN) in ERA-40 reanalysis’, *Atmospheric Research*. Elsevier B.V., 93(1–3), pp. 534–545. doi: 10.1016/j.atmosres.2008.09.037.

Röthlisberger, M. *et al.* (2019) ‘Recurrent synoptic-scale Rossby wave patterns and their effect on the persistence of cold and hot spells', *Journal of Climate*, 32(11), pp. 3207–3226. doi: 10.1175/JCLI-D-18-0664.1.

Röthlisberger, M., Martius, O. and Wernli, H. (2016a) 'An algorithm for identifying the initiation of synoptic-scale Rossby waves on potential vorticity waveguides', *Quarterly Journal of the Royal Meteorological Society*, 142(695), pp. 889–900. doi: 10.1002/qj.2690.

Röthlisberger, M., Pfahl, S. and Martius, O. (2016b) 'Regional-scale jet waviness modulates the occurrence of midlatitude weather extremes', *Geophysical Research Letters*, 43(20), pp. 10,989-10,997. doi: 10.1002/2016GL070944.

Rousi, E. *et al.* (2022) 'Accelerated western European heatwave trends linked to more-persistent double jets over Eurasia', *Nature Communications*. doi: 10.1038/s41467-022-31432-y.

Rousi, E., Selten, F., Rhamstorf, S. and Coumou, D. (2021) 'Changes in north atlantic atmospheric circulation in a warmer climate favor winter flooding and summer drought over europe', *Journal of Climate*, 34(6), pp. 2277–2295. doi: 10.1175/JCLI-D-20-0311.1.

Ruff, F. and Pfahl, S. (2022) 'What distinguishes 100-year precipitation extremes over Central European river catchments from more moderate extreme events ?', (October), pp. 1–29.

Rybka, H. *et al.* (2022) 'Convection-permitting climate simulations with COSMO-CLM for Germany: Analysis of present and future daily and sub-daily extreme precipitation', *Meteorologische Zeitschrift*. doi: 10.1127/metz/2022/1147.

Santos, M., Santos, J. A. and Fragoso, M. (2017) 'Atmospheric driving mechanisms of flash floods in Portugal', *International Journal of Climatology*, 37(March), pp. 671–680. doi: 10.1002/joc.5030.

Sauter, C. *et al.* (2023) 'Compound extreme hourly rainfall preconditioned by heatwaves most likely in the mid-latitudes', *Weather and Climate Extremes*. Elsevier B.V., 40(February), p. 100563. doi: 10.1016/j.wace.2023.100563.

Sauter, C., White, C. J., Fowler, H. J. and Westra, S. (2022) 'Temporally compounding heatwave–heavy rainfall events in Australia', *International Journal of Climatology*, 43(2), pp. 1050–1061. doi: 10.1002/joc.7872.

Sayers, P. . *et al.* (2020) 'Third UK Climate Change Risk Assessment (CCRA3) Future flood risk Main Report Final Report prepared for the Committee on Climate Change, UK', (July). Available at: www.sayersandpartners.co.uk.

Schär, C. *et al.* (2016) 'Percentile indices for assessing changes in heavy precipitation events', *Climatic Change*. Climatic Change, pp. 201–216. doi: 10.1007/s10584-016-1669-2.

Schroeer, K., Kirchengast, G. and Sungmin, O. (2018) 'Strong Dependence of Extreme Convective Precipitation Intensities on Gauge Network Density', *Geophysical Research Letters*, 45(16), pp. 8253–8263. doi: 10.1029/2018GL077994.

Schubert, S., Wang, H. and Suarez, M. (2011) 'Warm season subseasonal variability and climate extremes in the northern hemisphere: The role of stationary Rossby waves', *Journal of Climate*, 24(18), pp. 4773–4792. doi: 10.1175/JCLI-D-10-05035.1.

Scoccimarro, E. *et al.* (2015) 'Projected changes in intense precipitation over Europe at the daily and subdaily time scales', *Journal of Climate*, 28(15), pp. 6193–6203. doi: 10.1175/JCLI-D-14-00779.1.

Screen, J. A. and Simmonds, I. (2014) 'Amplified mid-latitude planetary waves favour particular regional weather extremes', *Nature Climate Change*, 4(8), pp. 704–709. doi: 10.1038/nclimate2271.

Seneviratne, S. I. *et al.* (2021) ‘Weather and Climate Extreme Events in a Changing Climate (Chapter 11)’, in Masson-Delmotte, V., Zhai, P., Pirani, A., Connors, S.L., Péan, C., Berger, S., Caud, N., Chen, Y., et al (ed.) *IPCC 2021: Climate Change 2021: The Physical Science Basis. Contribution of Working Group I to the Sixth Assessment Report of the Intergovernmental Panel on Climate Change.* Cambridge, UK and New York, USA: Cambridge University Press, pp. 1513–1766.

Sharma, A., Wasko, C. and Lettenmaier, D. P. (2018) ‘If Precipitation Extremes Are Increasing , Why Aren’t Floods ?’, *Water Resources Research*, 54, pp. 8545–8551. doi: 10.1029/2018WR023749.

Shaw, T. A. *et al.* (2016) ‘Storm track processes and the opposing influences of climate change’, *Nature Geoscience*, 9(9), pp. 656–664. doi: 10.1038/ngeo2783.

Shepherd, T. G. (2014) ‘Atmospheric circulation as a source of uncertainty in climate change projections’, *Nature Geoscience*. Nature Publishing Group, 7(10), pp. 703–708. doi: 10.1038/NGEO2253.

Sibley, A. (2012) ‘Thunderstorms from a Spanish Plume event on 28 June 2011’, *Weather*, 67(6), pp. 143–146. doi: 10.1002/wea.1928.

Smith, D. M., Scaife, A. A. and Kirtman, B. P. (2012) ‘What is the current state of scientific knowledge with regard to seasonal and decadal forecasting?’, *Environmental Research Letters*, 7(1).

Smith, P. J. *et al.* (2016) ‘On the Operational Implementation of the European Flood Awareness System (EFAS)’, in Adams, T. E. and Pagano, T. C. (eds) *Flood Forecasting: A Global Perspective*. Academic Press, pp. 313–348.

Špitalar, M. *et al.* (2014) ‘Analysis of flash flood parameters and human impacts in the US from 2006 to 2012’, *Journal of Hydrology*, 519(PA), pp. 863–870. doi: 10.1016/j.jhydrol.2014.07.004.

Stefanicki, G., Talkner, P. and Weber, R. O. (1998) ‘Frequency changes of weather types in the Alpine region since 1945’, *Theoretical and Applied Climatology*, 60(1–4), pp. 47–61. doi: 10.1007/s007040050033.

Sukovich, E. M. *et al.* (2014) ‘Extreme quantitative precipitation forecast performance at the weather prediction center from 2001 to 2011’, *Weather and Forecasting*, 29(4), pp. 894–911. doi: 10.1175/WAF-D-13-00061.1.

Taszarek, M. *et al.* (2019) ‘A climatology of thunderstorms across Europe from a synthesis of multiple data sources’, *Journal of Climate*, 32(6), pp. 1813–1837. doi: 10.1175/JCLI-D-18-0372.1.

Teng, H. and Branstator, G. (2019) ‘Amplification of Waveguide Teleconnections in the Boreal Summer’, *Current Climate Change Reports*, 5(4), pp. 421–432. doi: 10.1007/s40641-019-00150-x.

Toreti, A. *et al.* (2010) ‘Characterisation of extreme winter precipitation in mediterranean coastal sites and associated anomalous atmospheric circulation patterns’, *Natural Hazards and Earth System Science*, 10(5), pp. 1037–1050. doi: 10.5194/nhess-10-1037-2010.

Toreti, A., Giannakaki, P. and Martius, O. (2016) ‘Precipitation extremes in the Mediterranean region and associated upper-level synoptic-scale flow structures’, *Climate Dynamics*. Springer Berlin Heidelberg, 47(5–6), pp. 1925–1941. doi: 10.1007/s00382-015-2942-1.

Trenberth, K. E., Dai, A., Rasmussen, R. M. and Parsons, D. B. (2003) ‘The changing character of precipitation’, *Bulletin of the American Meteorological Society*, 84(9), pp. 1205-1217+1161.

doi: 10.1175/BAMS-84-9-1205.

Tu, M., de Laat, P. J. M., Hall, M. J. and de Wit, M. J. M. (2005) ‘Precipitation variability in the Meuse basin in relation to atmospheric circulation’, *Water Science and Technology*, 51(5), pp. 5–14. doi: 10.2166/wst.2005.0096.

Tuel, A. *et al.* (2022) ‘Large-Scale Drivers of Persistent Extreme Weather During Early Summer 2021 in Europe’, *Geophysical Research Letters*, 49(18), pp. 1–11. doi: 10.1029/2022GL099624.

Tuel, A. and Martius, O. (2022) ‘Subseasonal Temporal Clustering of Extreme Precipitation in the Northern Hemisphere: Regionalization and Physical Drivers’, *Journal of Climate*, 35(11), pp. 3537–3555. doi: 10.1175/JCLI-D-21-0562.1.

UKMO (2022) *Climate Zones*, *Weather and Climate*. Available at: https://www.metoffice.gov.uk/weather/climate/climate-explained/climate-zones.

Ulbrich, U. *et al.* (2003) ‘The central European floods of August 2002: Part 1 – Rainfall periods and flood development’, *Weather*, 58(10), pp. 371–377. doi: 10.1256/wea.61.03A.

Villalobos-Herrera, R. *et al.* (2024) ‘Towards new UK design rainfall profiles’, *Journal of Flood Risk Management*, 17(1).

Villalobos-Herrera, R., Blenkinsop, S., Guerreiro, S. and Fowler, H. J. (2023) ‘The creation and climatology of a large independent rainfall event database for Great Britain’, *International Journal of Climatology*.

de Vries, A. J. (2021) ‘A global climatological perspective on the importance of Rossby wave breaking and intense moisture transport for extreme precipitation events’, *Weather and Climate Dynamics*, 2(1), pp. 129–161. doi: 10.5194/wcd-2-129-2021.

de Vries, H., Lenderink, G., van der Wiel, K. and van Meijgaard, E. (2022) ‘Quantifying the role of the large-scale circulation on European summer precipitation change’, *Climate Dynamics*. Springer Berlin Heidelberg, 59(9–10), pp. 2871–2886. doi: 10.1007/s00382-022-06250-z.

Wasko, C., Lu, W. T. and Mehrotra, R. (2018) ‘Relationship of extreme precipitation, dry-bulb temperature, and dew point temperature across Australia’, *Environmental Research Letters*, 13(7). doi: 10.1088/1748-9326/aad135.

Watters, D., Battaglia, A. and Allan, R. P. (2021) ‘The Diurnal Cycle of Precipitation according to Multiple Decades of Global Satellite Observations, Three CMIP6 Models and the ECMWF Reanalysis’, *Journal of Climate*, 34(12), pp. 5063–5080.

Weder, C., Müller, G. and Brümmer, B. (2017) ‘Precipitation extremes on time scales from minute to month measured at the Hamburg Weather Mast 1997-2014 and their relation to synoptic weather types’, *Meteorologische Zeitschrift*, 26(5), pp. 507–524. doi: 10.1127/metz/2017/0812.

Werner, P. C., Gerstengarbe, F. W. and Wechsung, F. (2008) ‘Großwetterlagen and precipitation trends in the Elbe river catchment’, *Meteorologische Zeitschrift*, 17(1), pp. 61–66. doi: 10.1127/0941-2948/2008/0263.

Werner, P. and Gerstengarbe, F.-W. (2010) ‘Catalogue of European Grosswetterlagen’, *PIK (Potsdam Institute for Climate Impact Research) report*, 7(119).

Westra, S. *et al.* (2014) ‘Future changes to the intensity and frequency of short-duration extreme rainfall’, *Reviews of Geophysics*, 52(3), pp. 522–555. doi: 10.1002/2014RG000464.

White, R. H. (2019) ‘Detecting Waveguides for Atmospheric Planetary Waves: Connections to Extreme Weather Events’, *NCAR Technical Notes*. doi: 10.5065/y82j-f154.

White, R. H., Kornhuber, K., Martius, O. and Wirth, V. (2022) 'From Atmospheric Waves to Heatwaves: A waveguide perspective for understanding and predicting concurrent, persistent and extreme extratropical weather', *Bulletin of the American Meteorological Society*, 103(March 2022), pp. E923–E935.

White, R. H., Wallace, J. M. and Battisti, D. S. (2021) 'Revisiting the Role of Mountains in the Northern Hemisphere Winter Atmospheric Circulation', *Journal of the Atmospheric Sciences*, pp. 2221–2235. doi: 10.1175/jas-d-20-0300.1.

Whitford, A. C., Blenkinsop, S., Pritchard, D. and Fowler, H. J. (2023) 'A gauge-based sub-daily extreme rainfall climatology for western Europe', *Weather and Climate Extremes*. Elsevier B.V., 41(February), p. 100585. doi: 10.1016/j.wace.2023.100585.

Wibig, J. (1999) 'Precipitation in Europe in relation to circulation patterns at the 500 hPa level', *International Journal of Climatology*, 19(3), pp. 253–269. doi: 10.1002/(SICI)1097-0088(19990315)19:3<253::AID-JOC366>3.0.CO;2-0.

Wilkinson, J. M. and Neal, R. (2021) 'Exploring relationships between weather patterns and observed lightning activity for Britain and Ireland', (April), pp. 2772–2795. doi: 10.1002/qj.4099.

Willems, P. (2013) 'Multidecadal oscillatory behaviour of rainfall extremes in Europe', *Climatic Change*, 120(4), pp. 931–944. doi: 10.1007/s10584-013-0837-x.

Wills, R. C. J., White, R. H. and Levine, X. J. (2019) 'Northern Hemisphere Stationary Waves in a Changing Climate', *Current Climate Change Reports*. Current Climate Change Reports, 5(4), pp. 372–389. doi: 10.1007/s40641-019-00147-6.

Wirth, V., Riemer, M., Chang, E. K. M. and Martius, O. (2018) 'Rossby wave packets on the midlatitude waveguide-A review', *Monthly Weather Review*, 146(7), pp. 1965–2001. doi: 10.1175/MWR-D-16-0483.1.

Wolf, G., Brayshaw, D. J., Klingaman, N. P. and Czaja, A. (2018) 'Quasi-stationary waves and their impact on European weather and extreme events', *Quarterly Journal of the Royal Meteorological Society*, 144(717), pp. 2431–2448. doi: 10.1002/qj.3310.

Xiao, C., Yuan, W. and Yu, R. (2018) 'Diurnal cycle of rainfall in amount, frequency, intensity, duration, and the seasonality over the UK', *International Journal of Climatology*, 38(13), pp. 4967–4978. doi: 10.1002/joc.5790.

Xu, P. *et al.* (2021) 'Amplified Waveguide Teleconnections Along the Polar Front Jet Favor Summer Temperature Extremes Over Northern Eurasia', *Geophysical Research Letters*, 48(13), pp. 1–9. doi: 10.1029/2021GL093735.

Yu, J., Li, X-F., Lewis ,E., Blenkinsop, S., Fowler, H.J. (2020) 'UKGrsHP: a UK high-resolution gauge-radar-satellite merged hourly precipitation analysis dataset', Climate Dynamics, 54, pp.2919-2904. doi: 10.1007/s00382-020-05144-2.

Zhang, X. *et al.* (2017) 'Complexity in estimating past and future extreme short-duration rainfall', *Nature Geoscience*, 10(4), pp. 255–259. doi: 10.1038/ngeo2911.

Appendices

Appendix A: Supporting information for Chapter 3

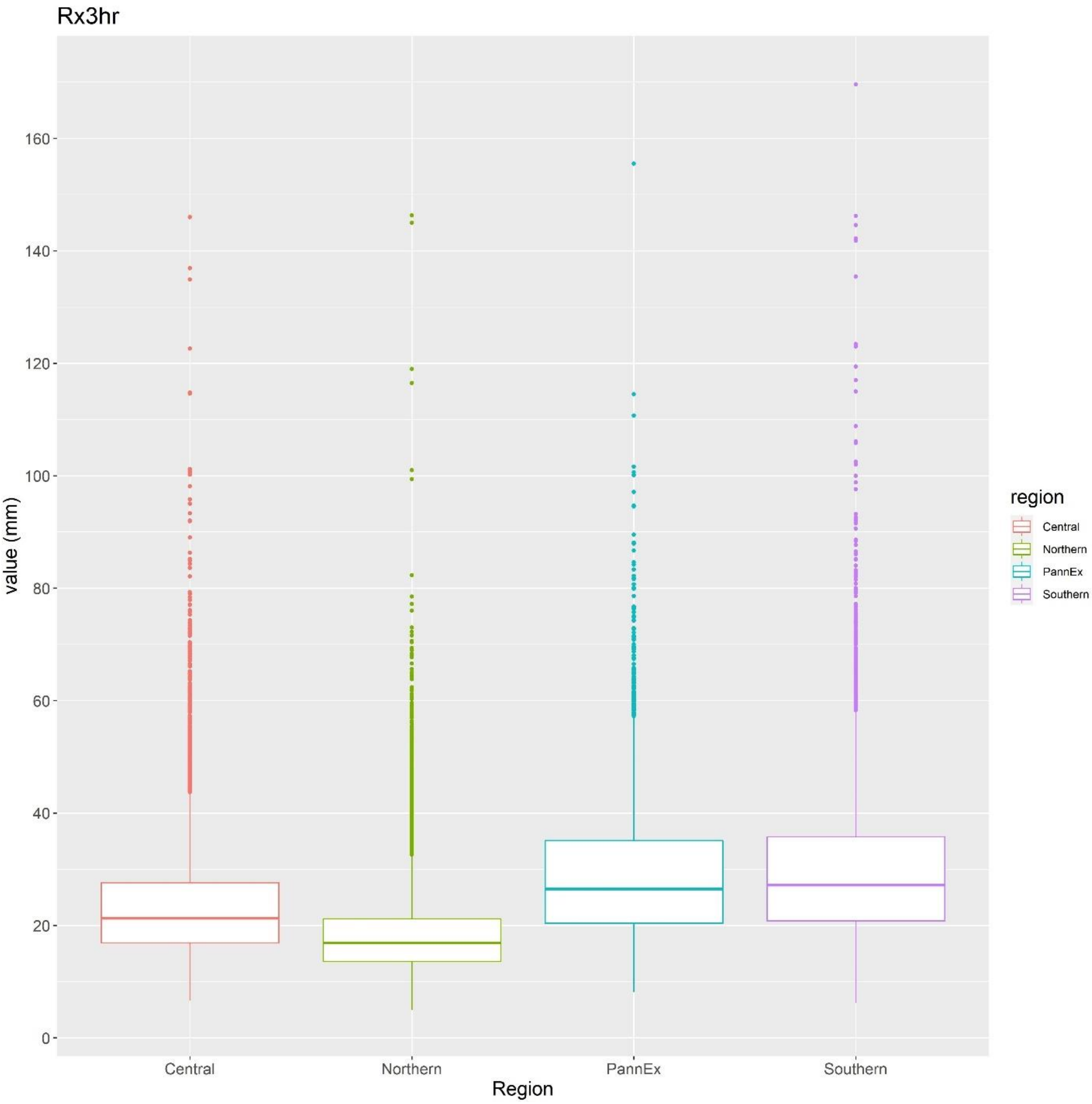

Figure A.1: Rx3hr boxplots by region. The boxplots consist of the Rx3hr value for each year of record at each gauge in the region. The number of gauges in each region is given in black.

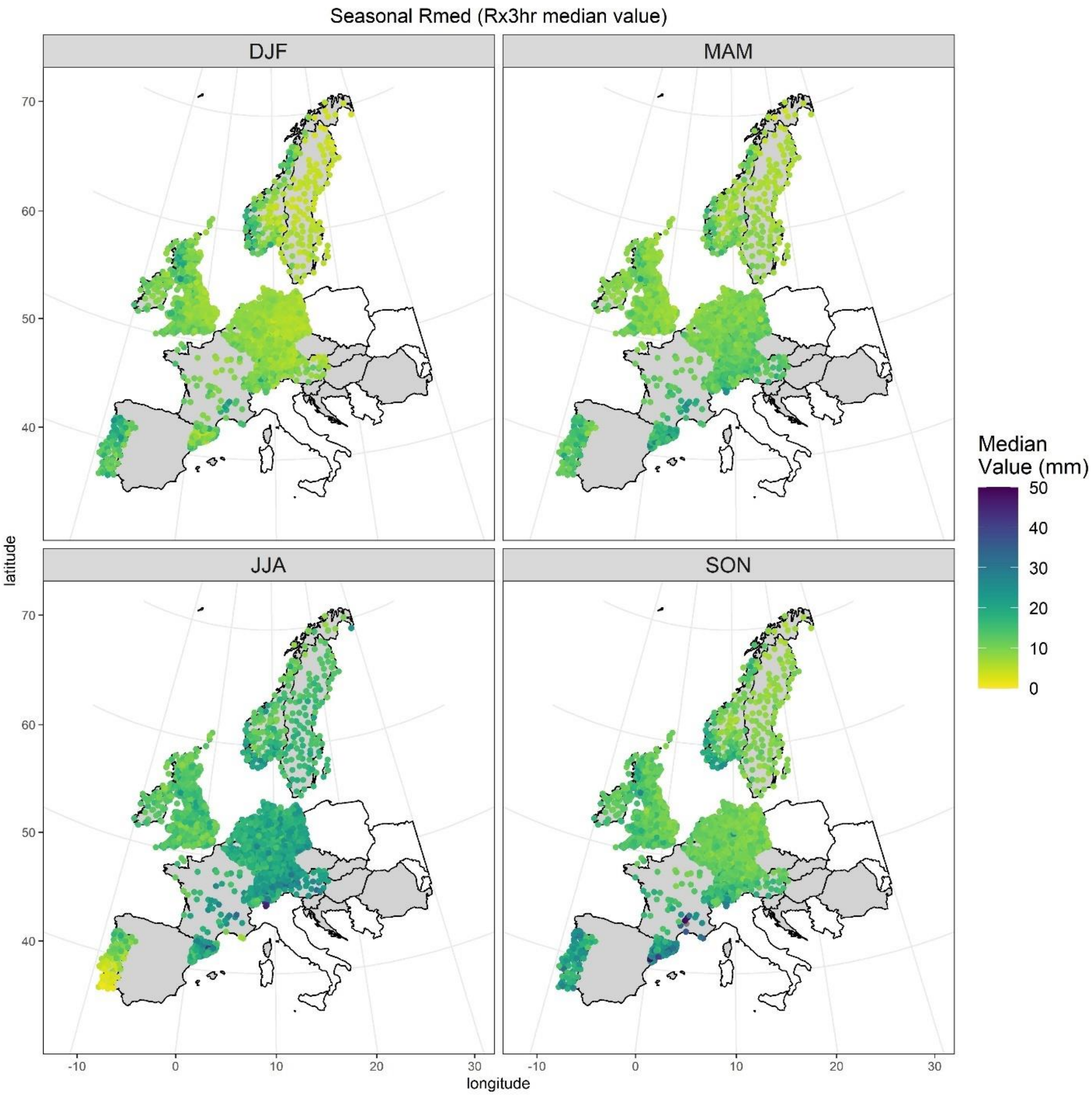

Figure A.2: The seasonal Rx3hr median value. Note the Pannonian Basin region does not have seasonal level data available.

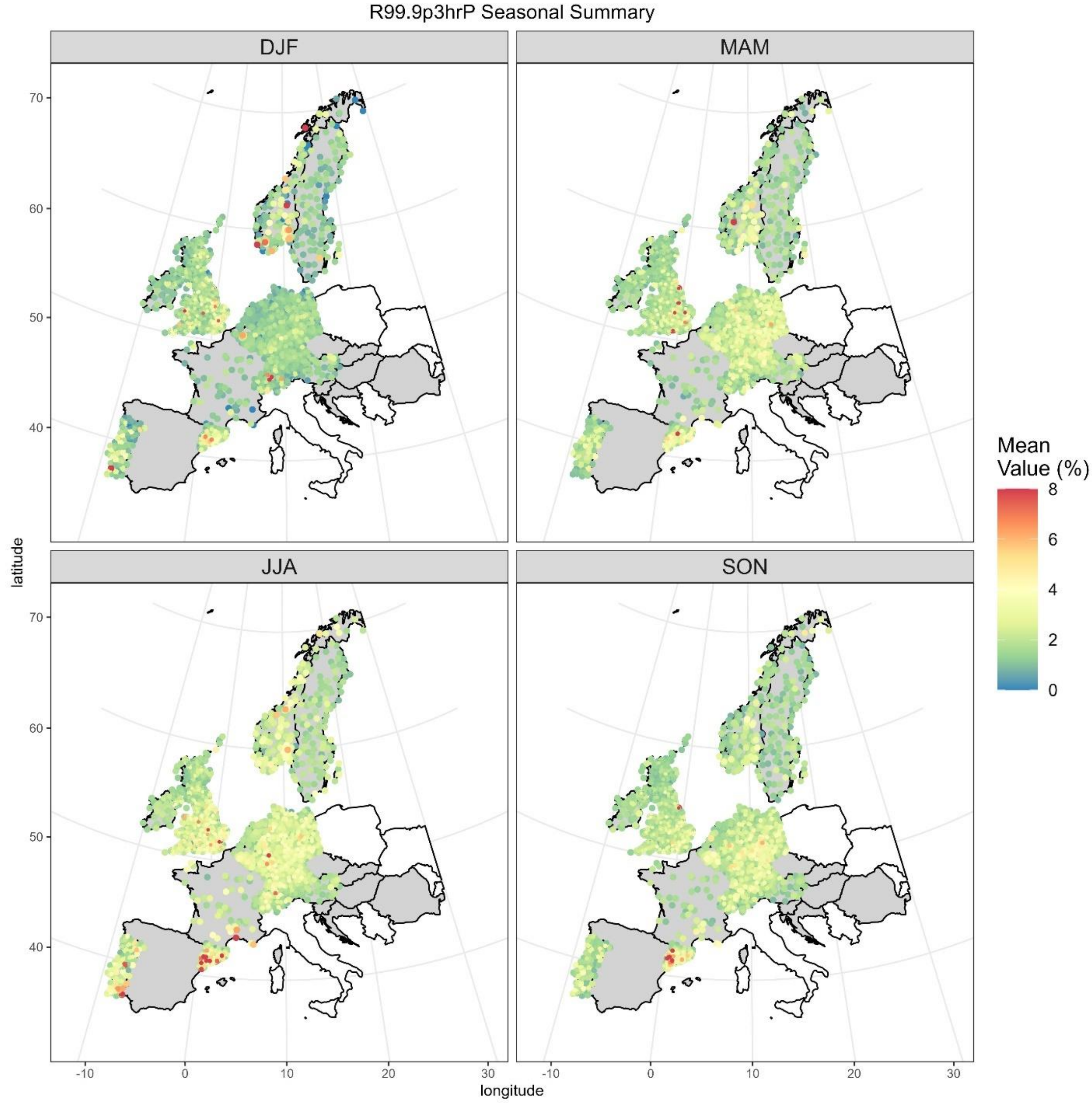

Figure A.3: The seasonal mean contribution from 3hr events above the 99.9th percentile at each gauge.

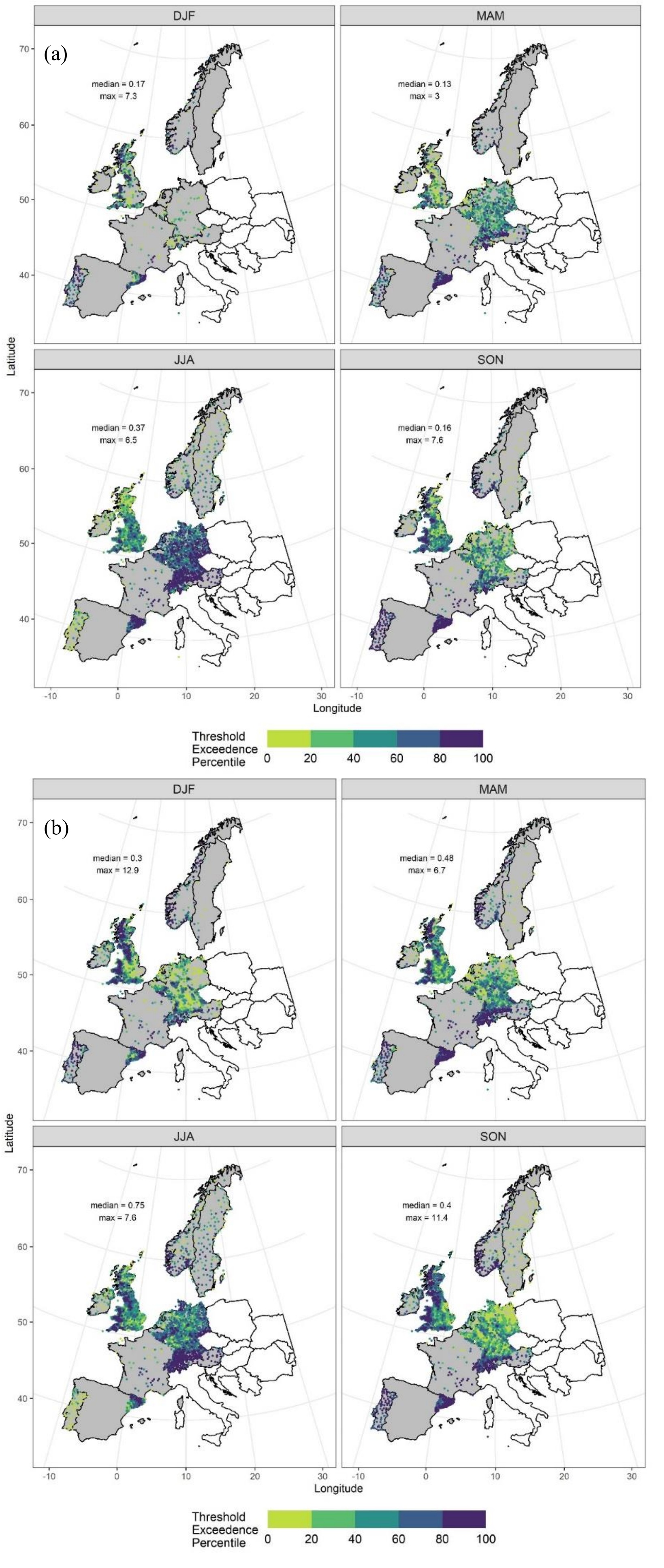

Figure A.4: Seasonal mean frequency over threshold for a) 3-hour 20mm events and b) 24-hour 30mm events. The colours represent which percentile the gauge result lies in for that season. E.g. Dark blue means the R99.9pHhr value at that gauge lies between the 80th and 100th percentile for that season.

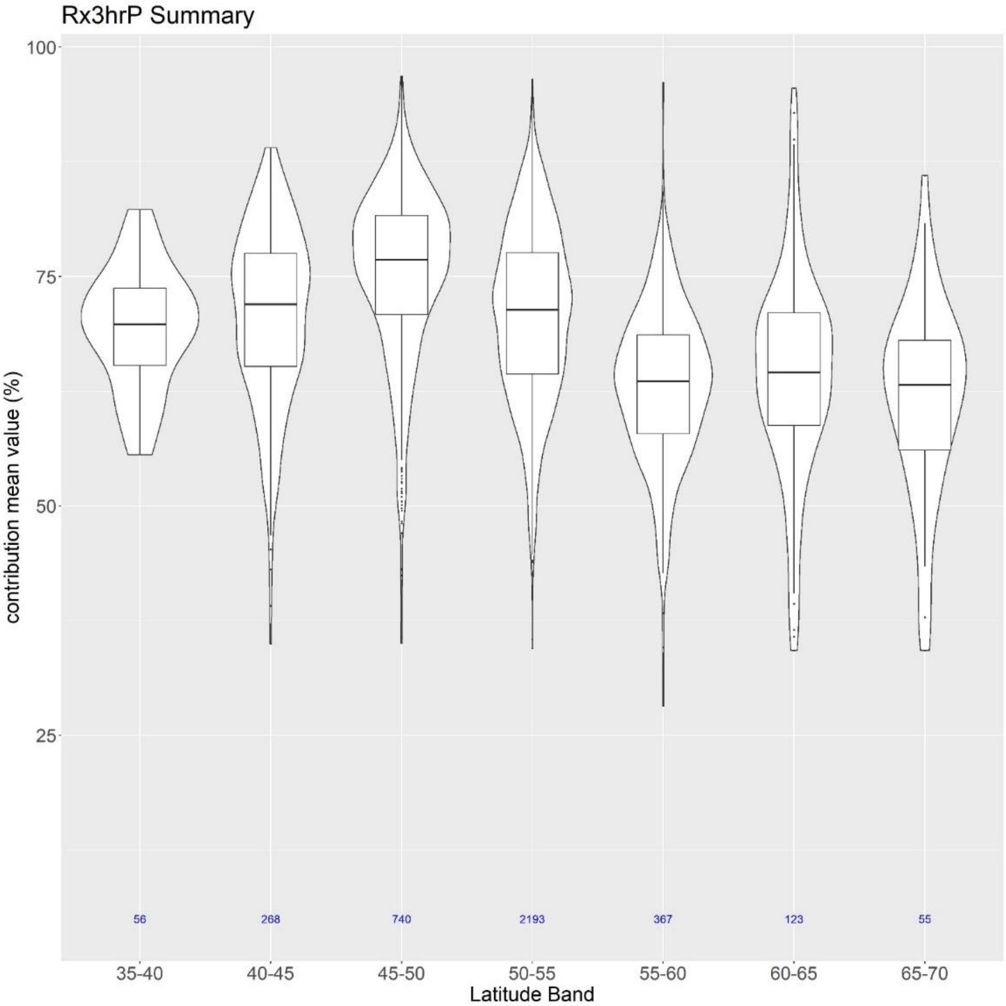

Figure A.5: Mean contribution of the Rx3hr event to rainfall on the day of occurrence by latitude band.

Appendix B: Supporting information for Chapter 4

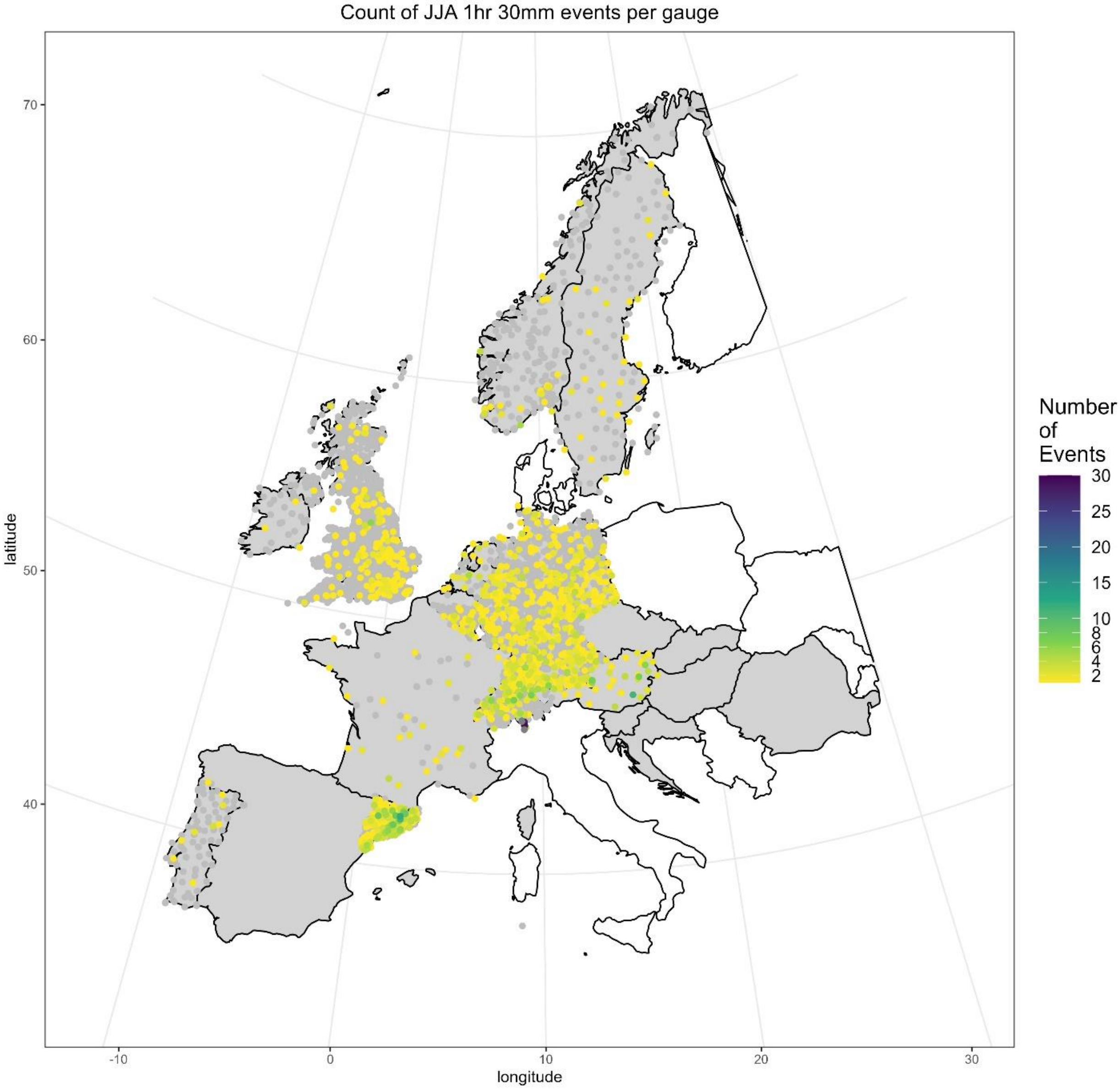

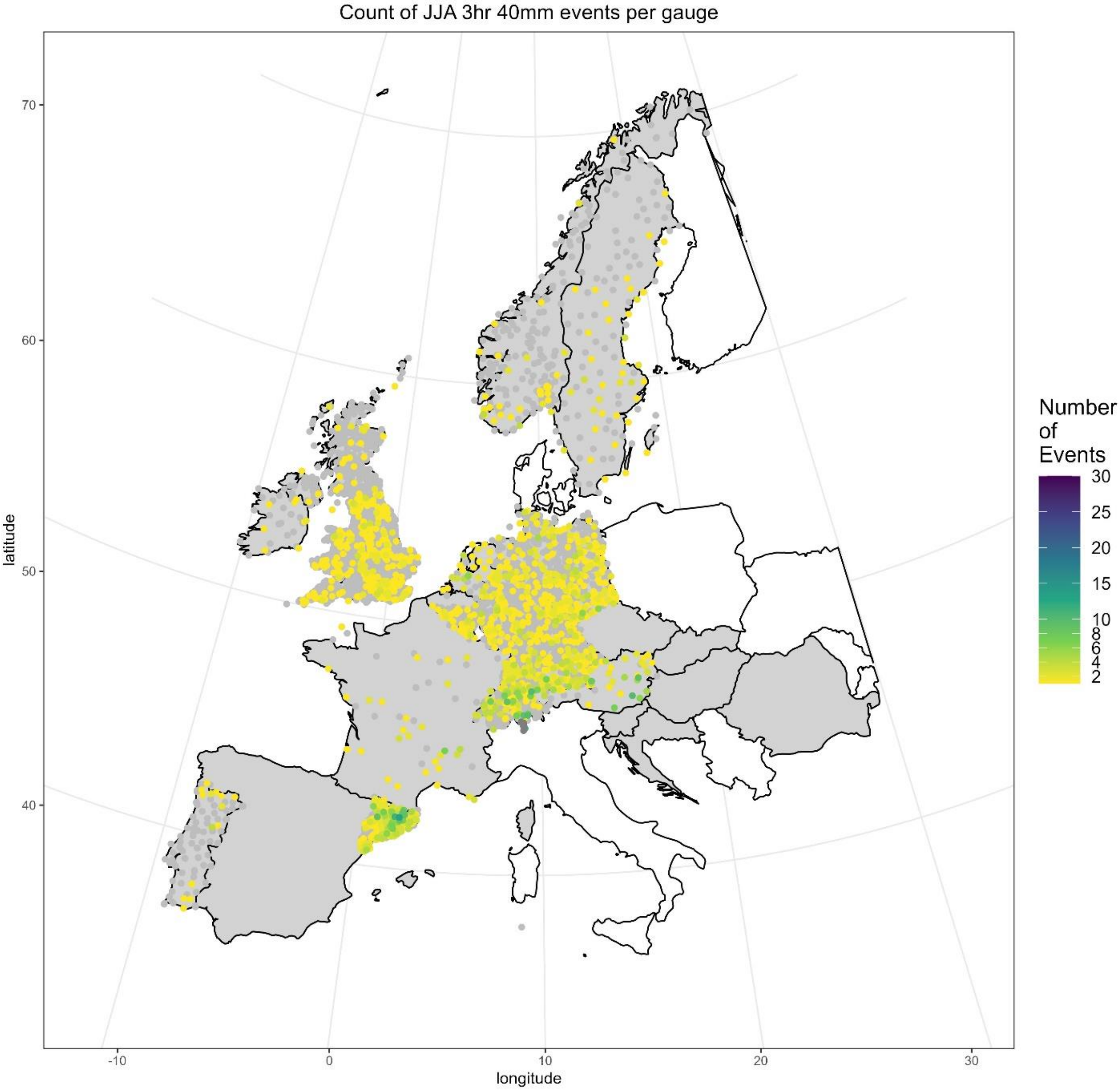

Figure B.1: Comparison of the total number of a) 1hr ≥30mm events per gauge and b) 3hr ≥40mm events per gauge in summer in western Europe.

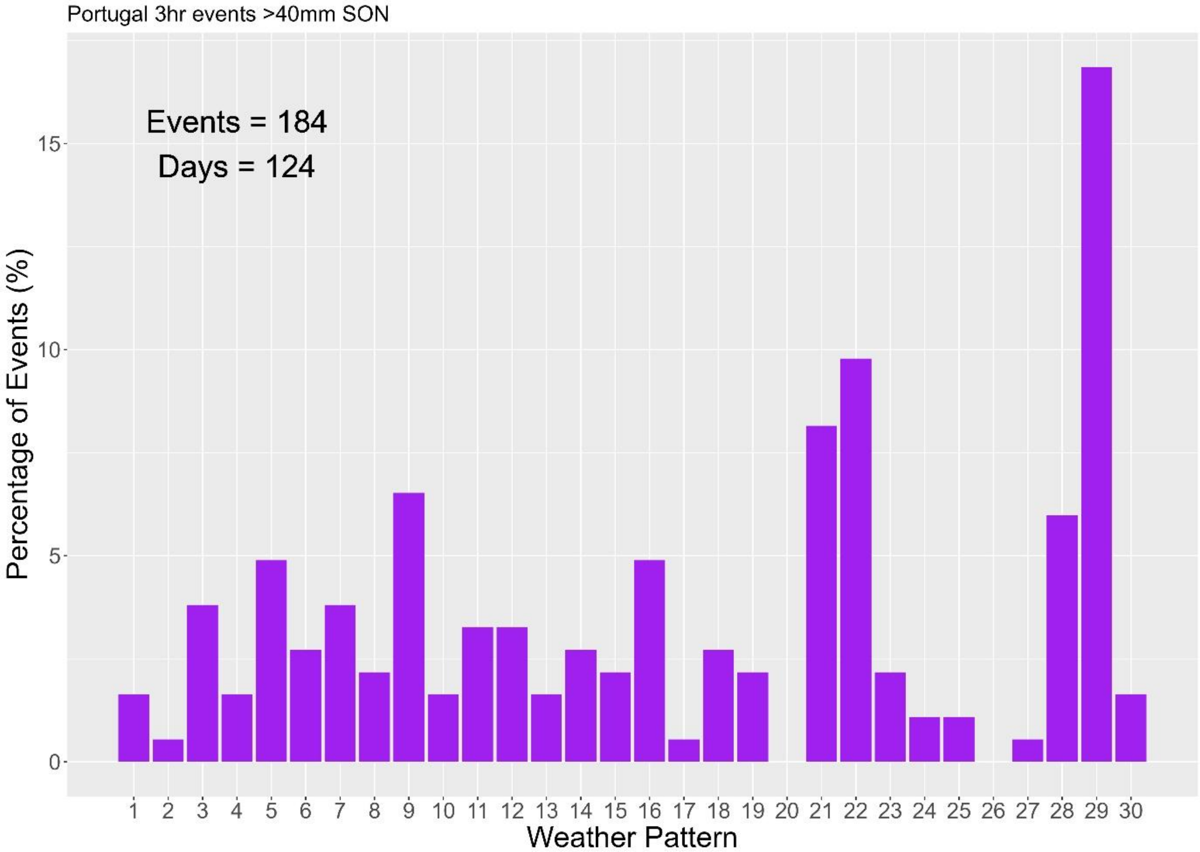

Figure B.2: MO30 WPs associated with 3hr 40mm events in Portugal in Autumn. Proportion of all events which occur under each WP given as %. The number of events and the number of days with events over the threshold are given in the top left corner of the panel.

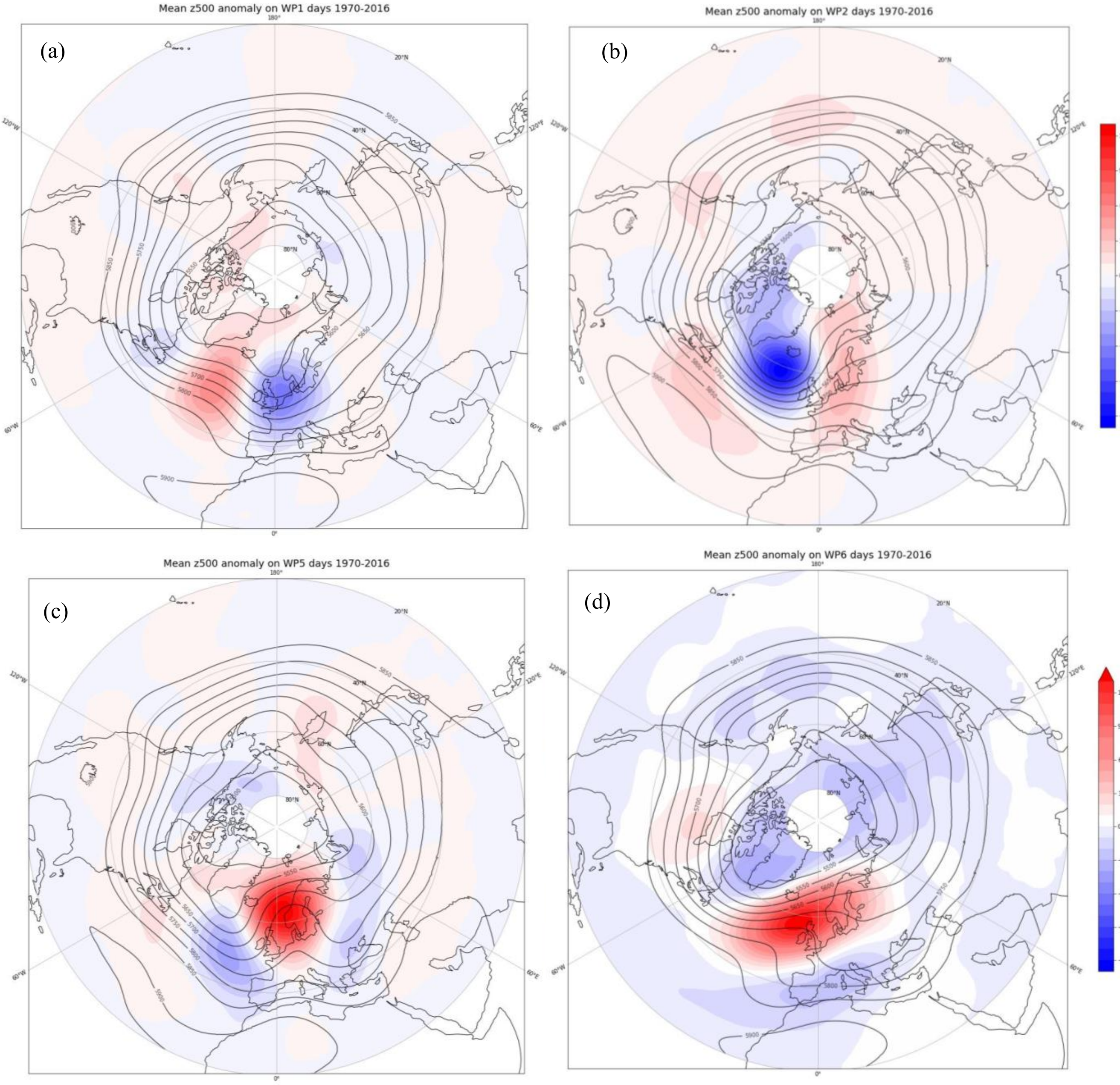

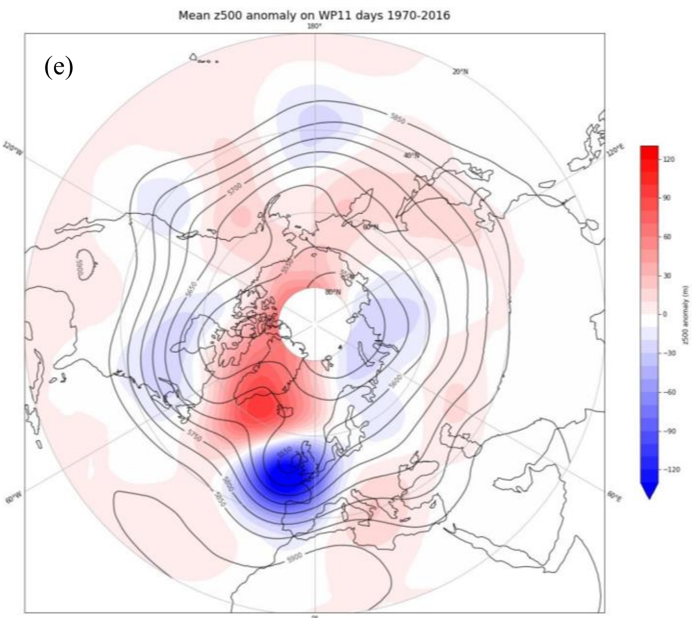

Figure B.3: z500 composite anomaly maps for all JJA days (1970-2016) with a) WP1, b) WP2, c) WP5, d) WP6, e) WP11. z500 anomalies in colour and mean z500 in black contours(m).

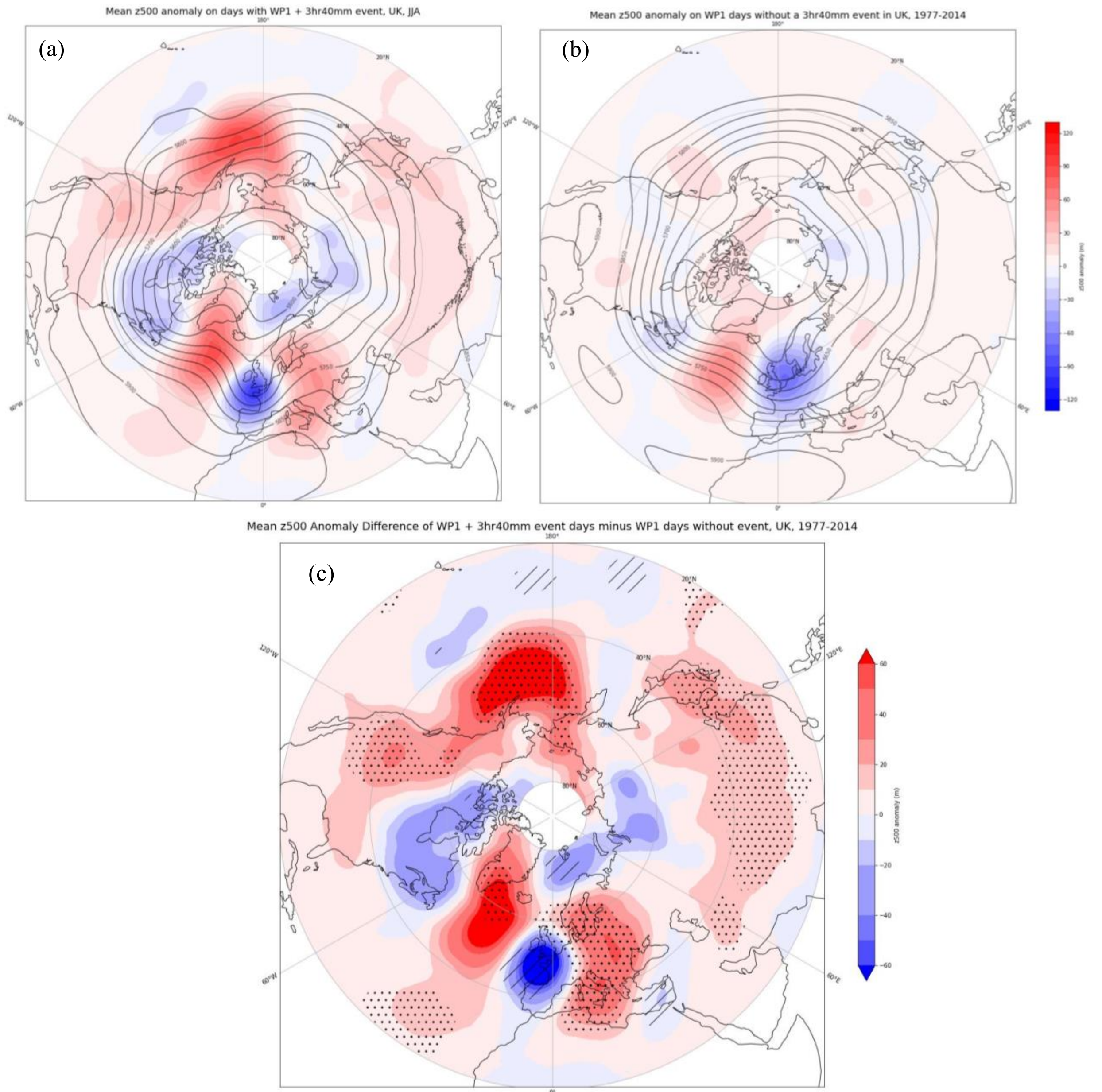

Figure B.4: Results of significance testing of the z500 anomalies on event days. a) the mean z500 anomalies on days with WP1 + 3hr40mm event in the UK. b) mean z500 anomalies on days with WP6 and no extreme even in the UK. The colours are z500 anomaly (m) and black contours mean z500(m.) c) The difference between a) and b). Colours are the mean z500 anomaly difference between (a) and (b) and the stippling shows areas where the mean z500 anomaly on event days (from (a)) are above the 95th percentile (dots) and below the 5th percentile (hashes) limits from the bootstrap of all WP1 days without an event (b).

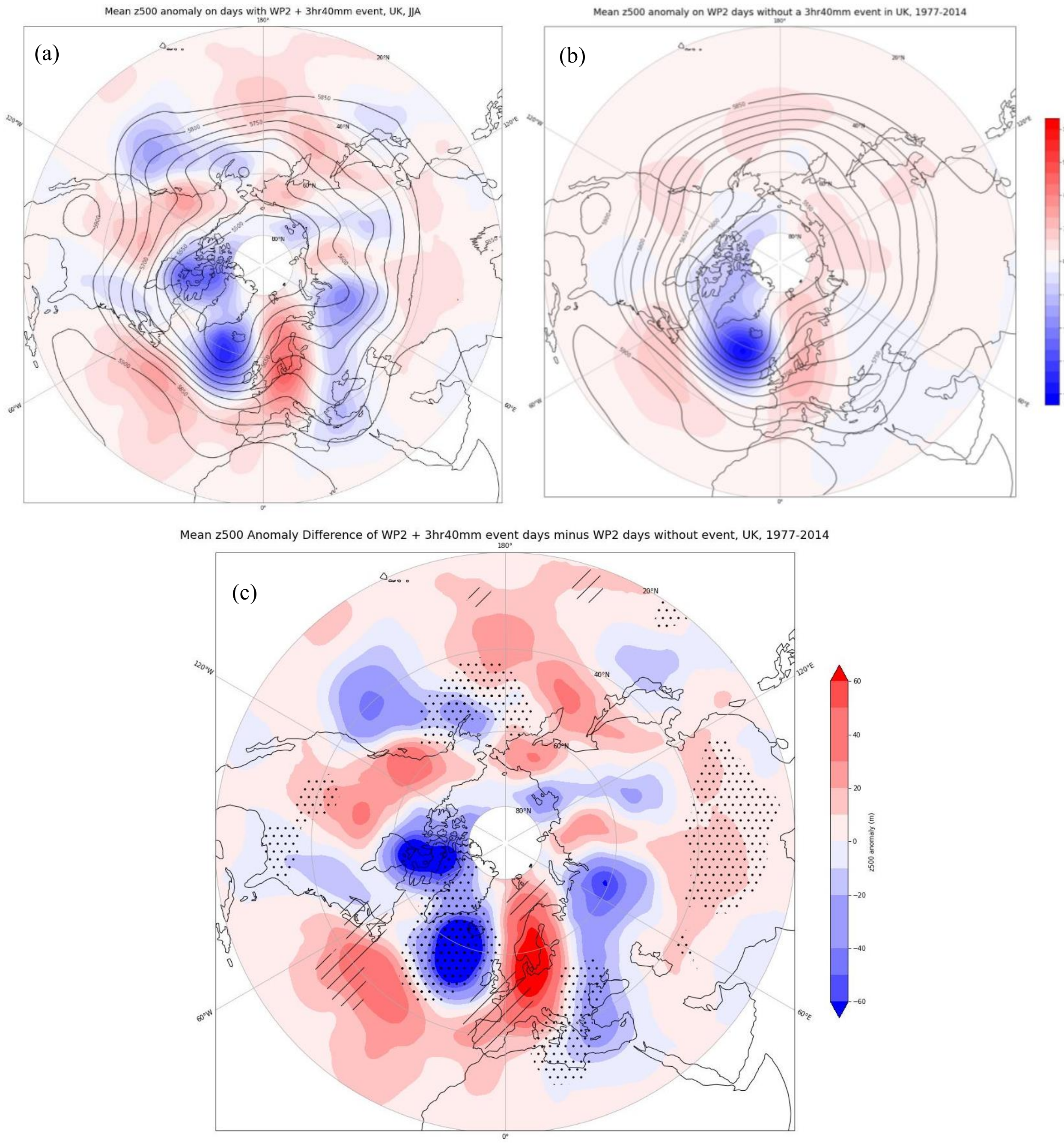

Figure B.5: Results of significance testing of the z500 anomalies on event days. a) the mean z500 anomalies on days with WP2 + 3hr40mm event in the UK. b) mean z500 anomalies on days with WP2 and no extreme even in the UK. The colours are z500 anomaly (m) and black contours mean z500(m.) c) The difference between a) and b). Colours are the mean z500 anomaly difference between (a) and (b) and the stippling shows areas where the mean z500 anomaly on event days (from (a)) are above the 95th percentile (dots) and below the 5th percentile (hashes) limits from the bootstrap of all WP2 days without an event (b).

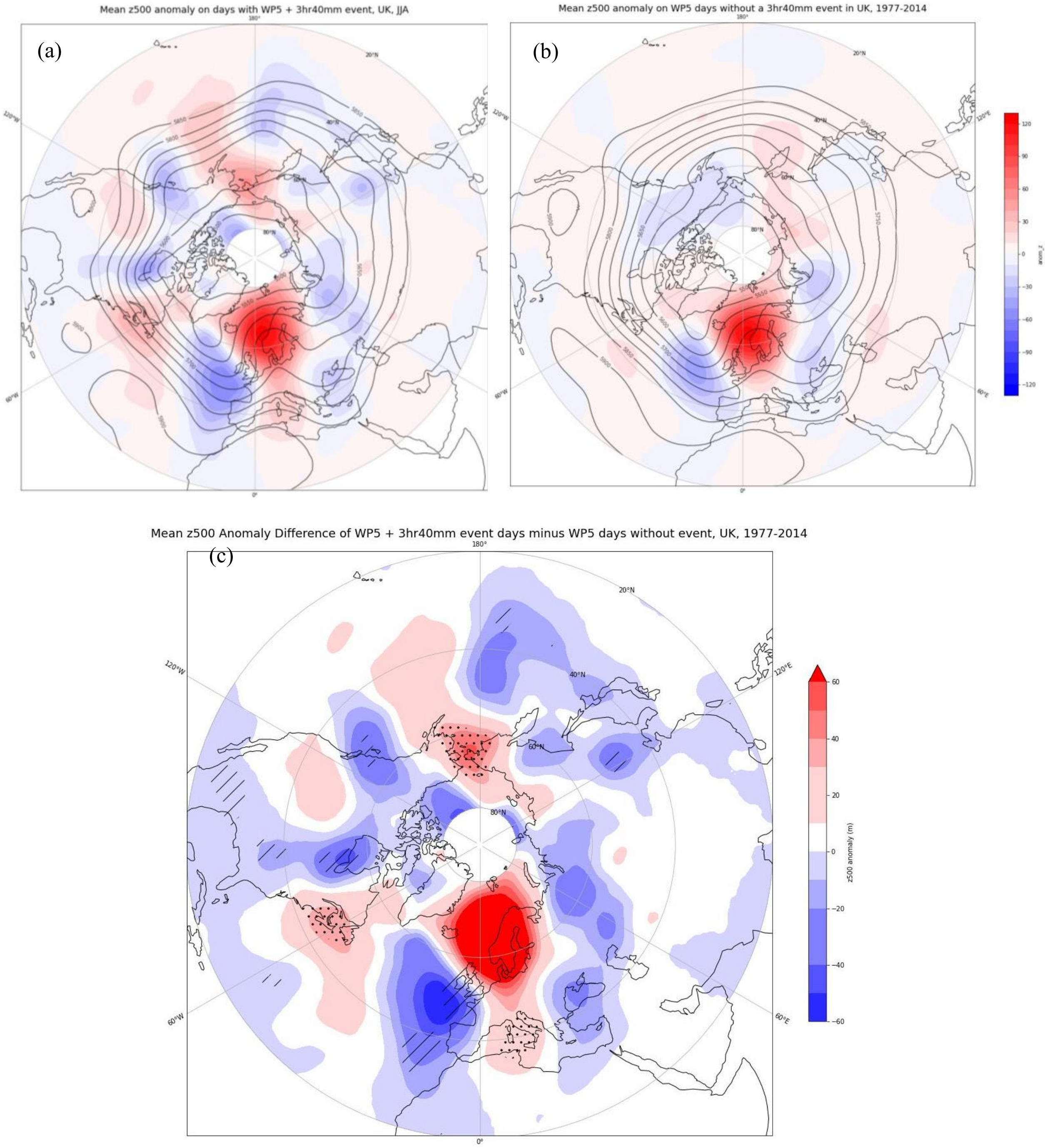

Figure B.6: Results of significance testing of the z500 anomalies on event days. a) the mean z500 anomalies on days with WP5 + 3hr40mm event in the UK. b) mean z500 anomalies on days with WP5 and no extreme even in the UK. The colours are z500 anomaly (m) and black contours mean z500(m.) c) The difference between a) and b). Colours are the mean z500 anomaly difference between (a) and (b) and the stippling shows areas where the mean z500 anomaly on event days (from (a)) are above the 95th percentile (dots) and below the 5th percentile (hashes) limits from the bootstrap of all WP5 days without an event (b).

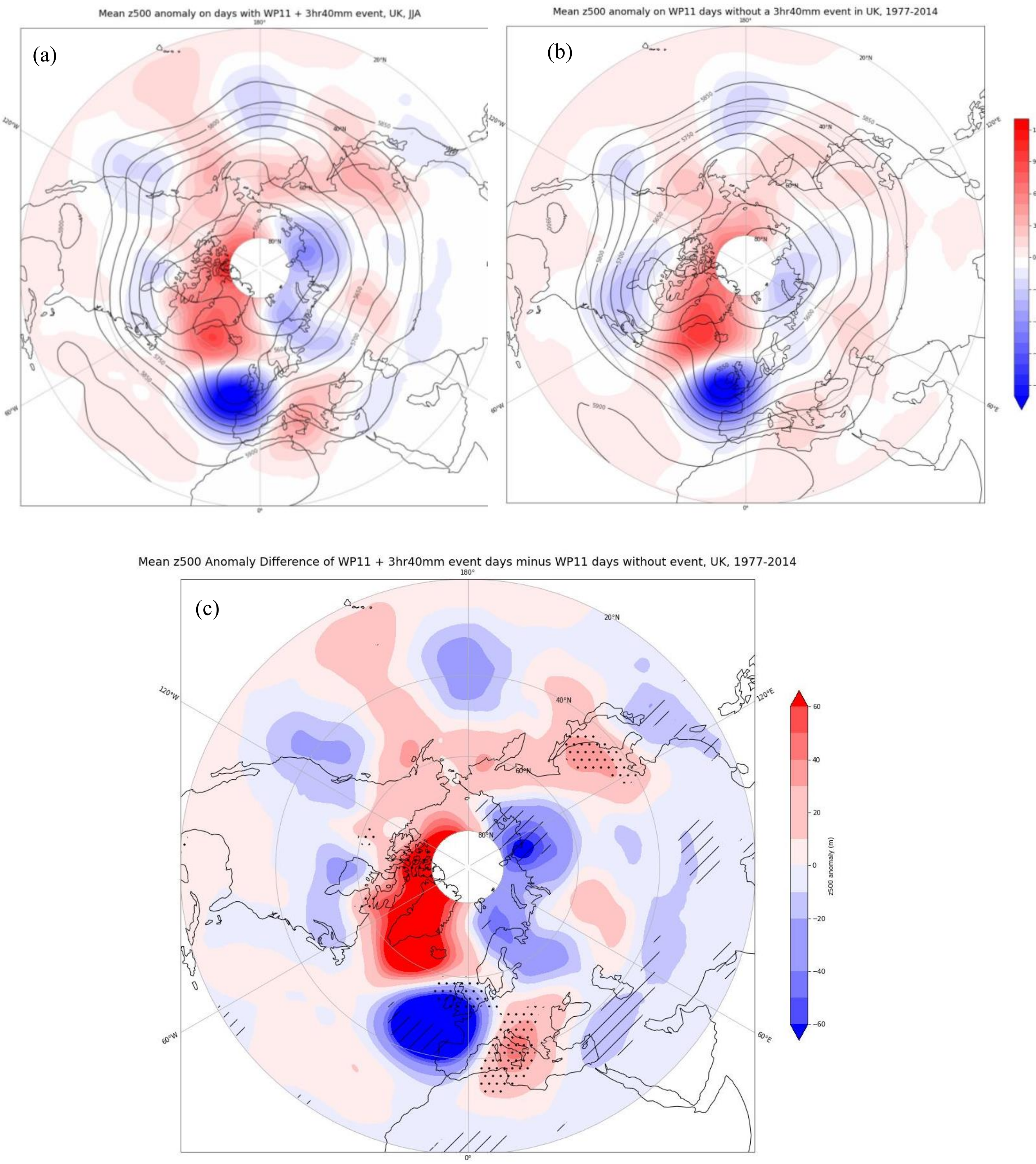

Figure B.7: Results of significance testing of the z500 anomalies on event days. a) the mean z500 anomalies on days with WP11 + 3hr40mm event in the UK. b) mean z500 anomalies on days with WP11 and no extreme even in the UK. The colours are z500 anomaly (m) and black contours mean z500(m.) c) The difference between a) and b). Colours are the mean z500 anomaly difference between (a) and (b) and the stippling shows areas where the mean z500 anomaly on event days (from (a)) are above the 95th percentile (dots) and below the 5th percentile (hashes) limits from the bootstrap of all WP11 days without an event (b).

Appendix C: Supporting information for Chapter 5

(a)

(b)

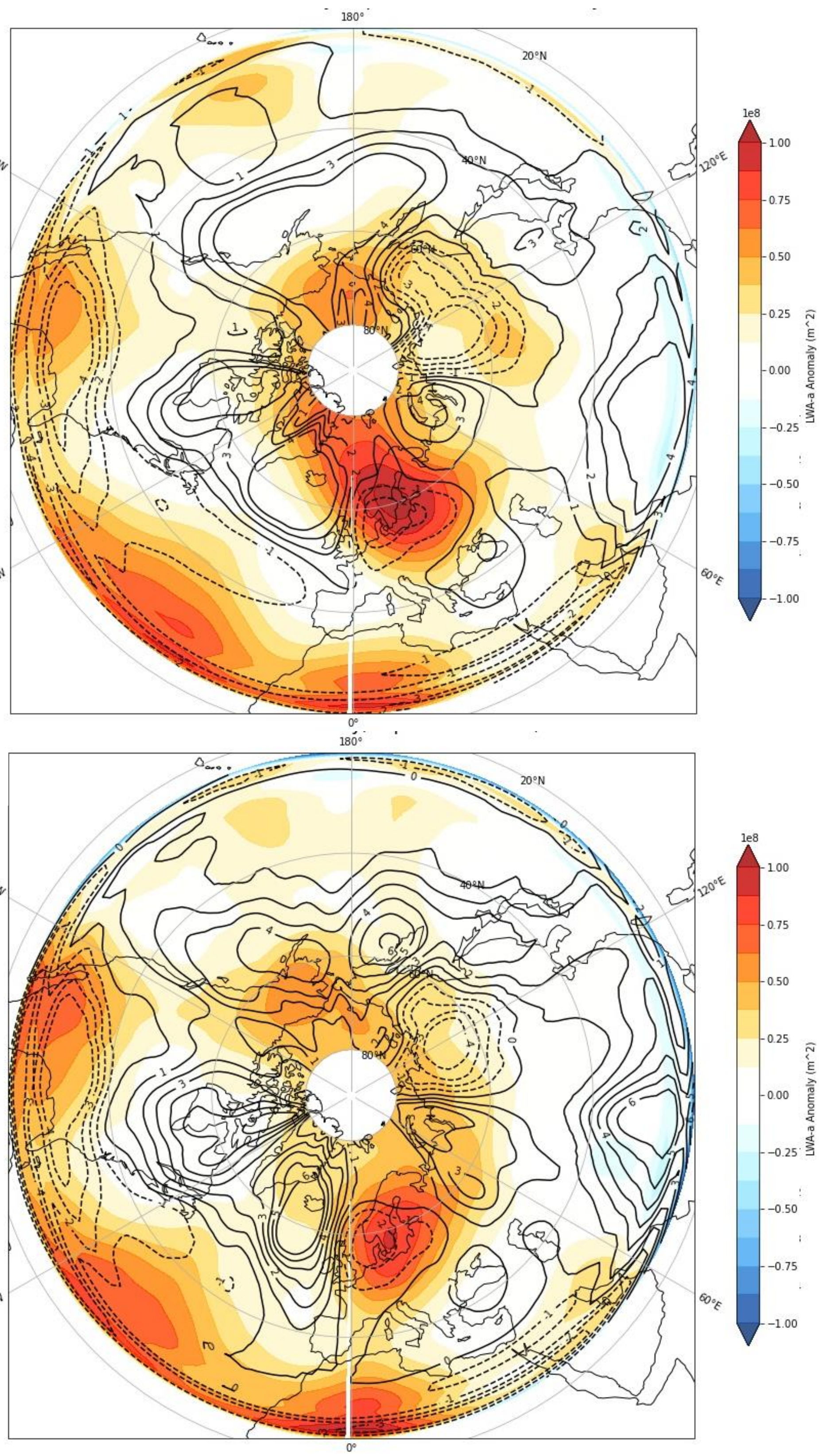

Figure C.1: Composites of mean LWA cyclonic and anticyclonic anomalies for the LWA calculated on the z500 climatology. a) top 20 3hr rainfall events in Germany. b) top 20 3hr rainfall events in UK.

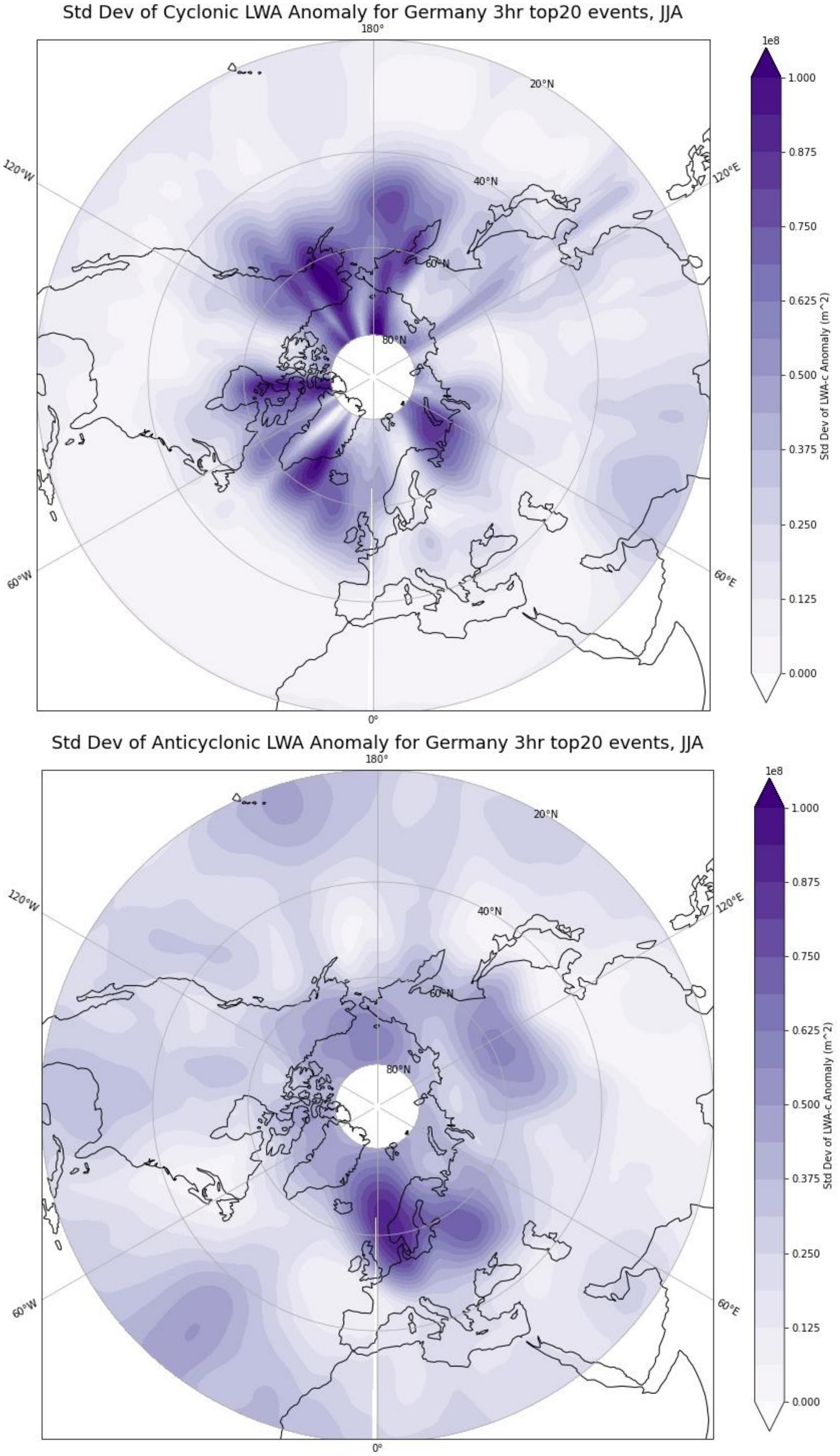

Figure C.2a: Standard deviation of LWA cyclonic and anticyclonic anomalies on the top 20 3hr event days for Germany

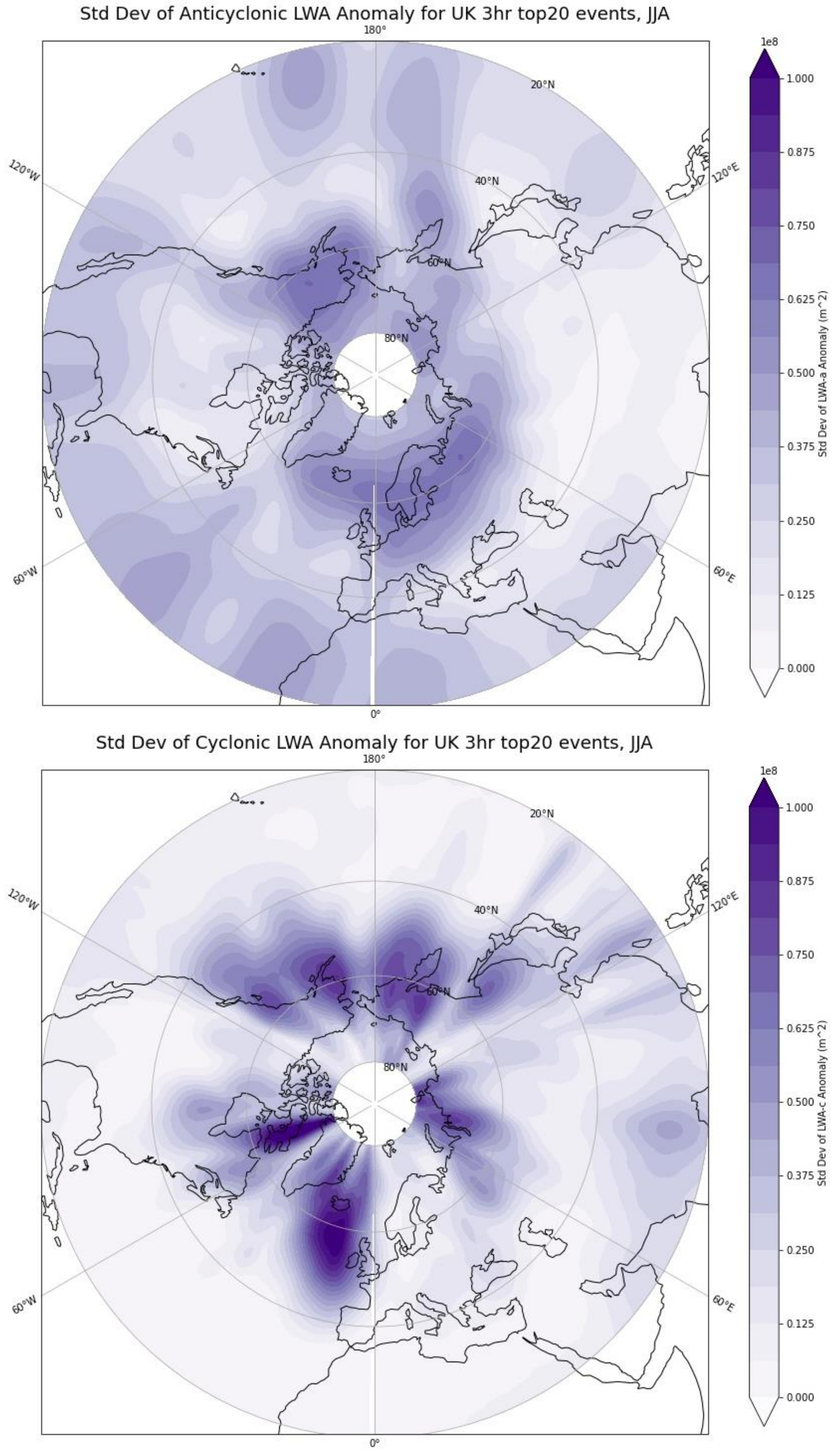

Figure C.2b: Standard deviation of LWA cyclonic and anticyclonic anomalies on the top 20 3hr event days for the UK

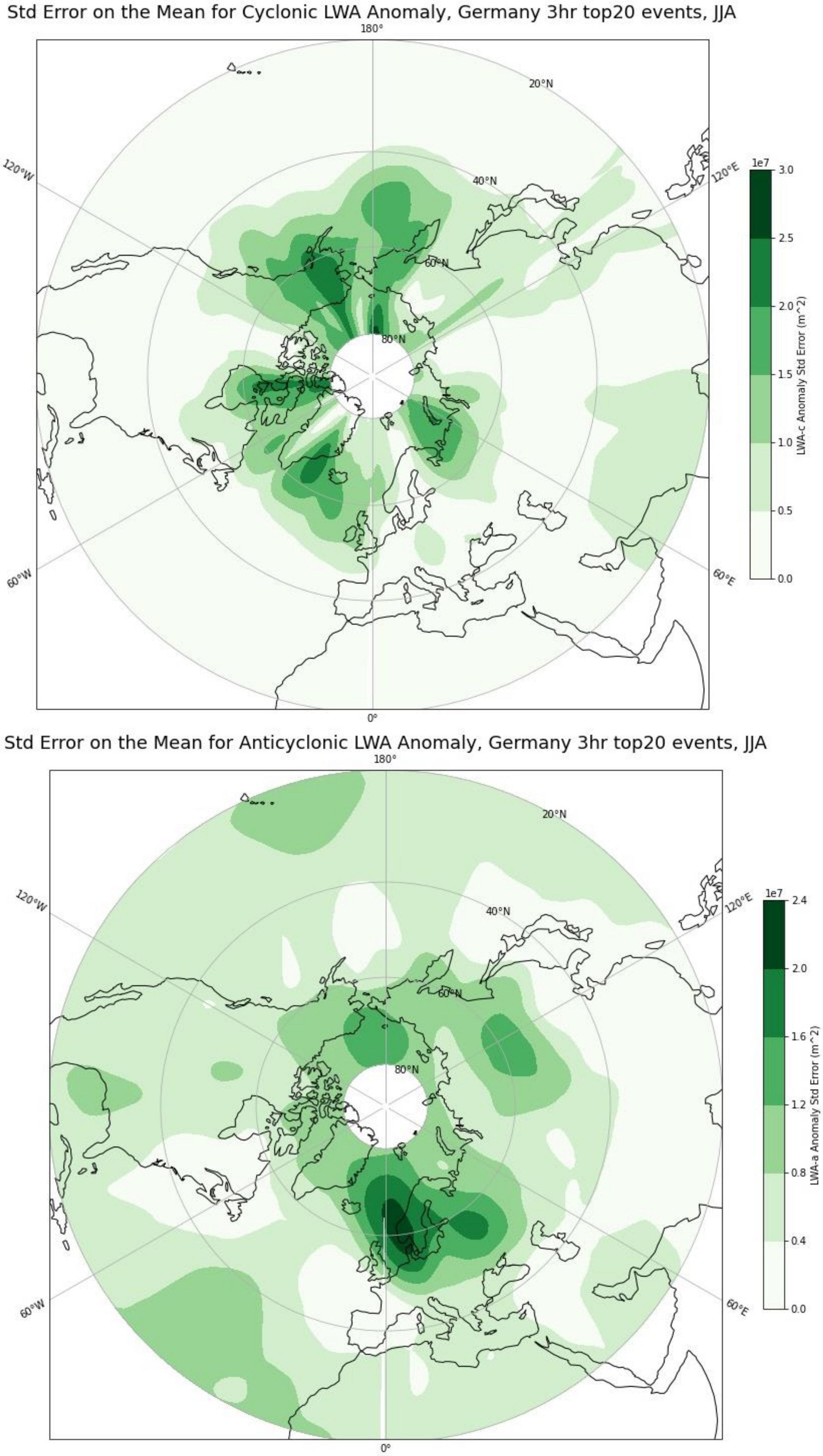

Figure C.3a: Standard error on the mean for LWA cyclonic and anticyclonic anomalies on top 20 3hr event days for Germany

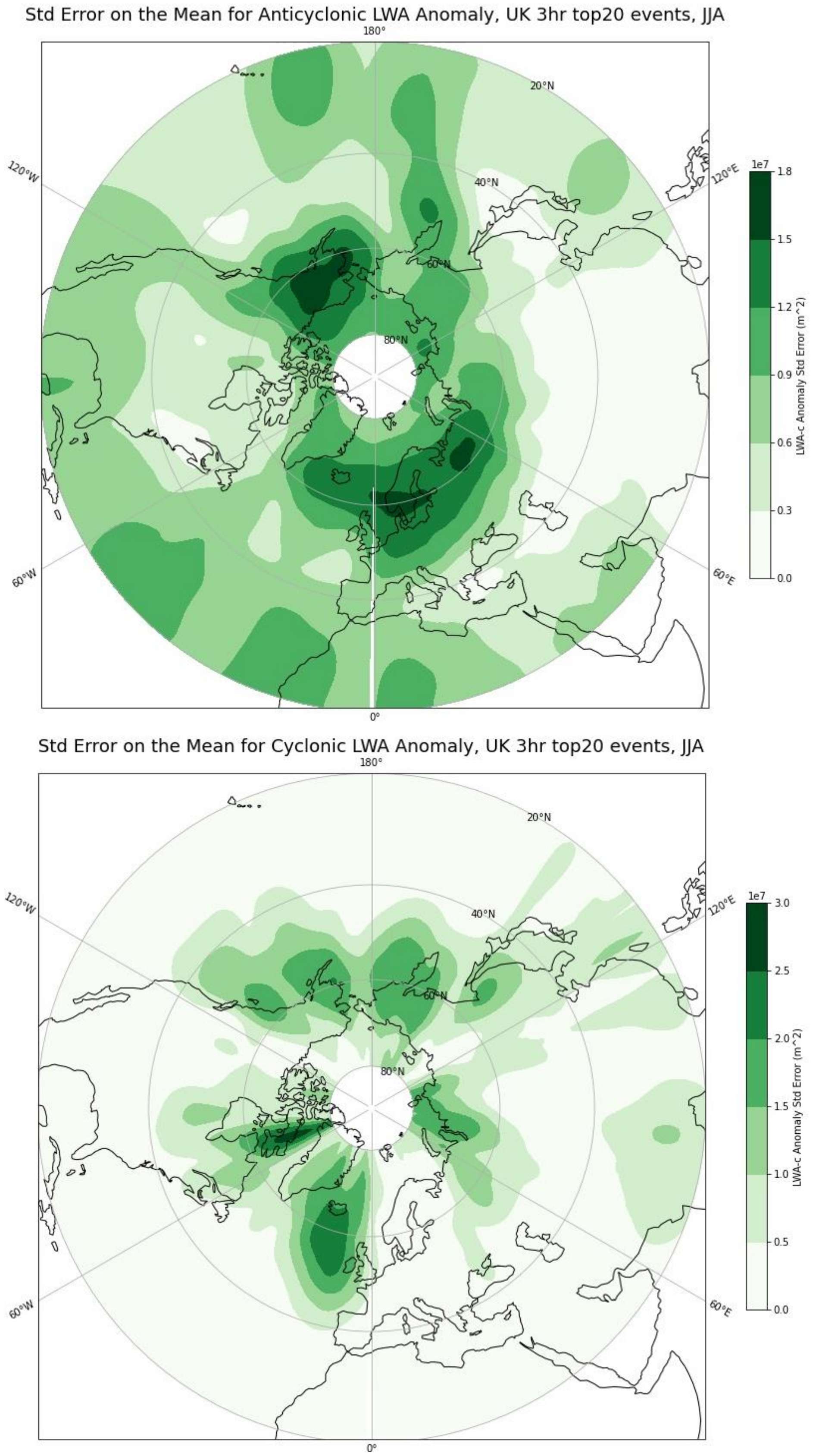

Figure C.3b: Standard error on the mean for LWA cyclonic and anticyclonic anomalies on top 20 3hr event days for the UK

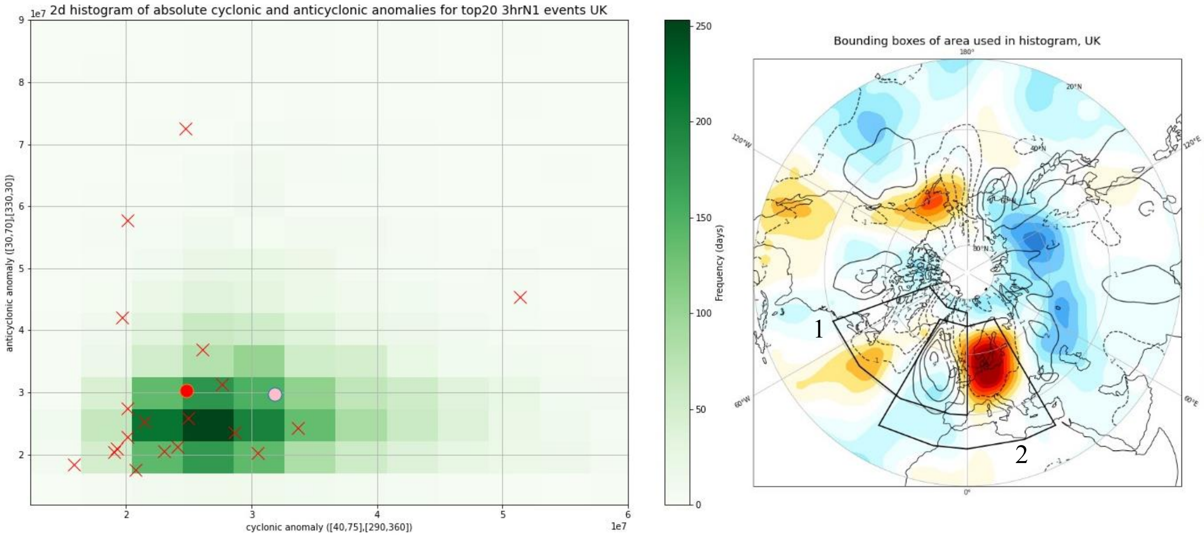

Figure C.4: Histogram of the absolute amplitude of anticyclonic and cyclonic activity anomalies on UK top 20 3hr days (red crosses) compared to all JJA days. Mean of all JJA days shown by pink circle, mean of all top20 3hr days shown by red circle. The bounding boxes used to calculate anomalies within are for cyclonic (box 1) and anticyclonic (box 2) anomalies.

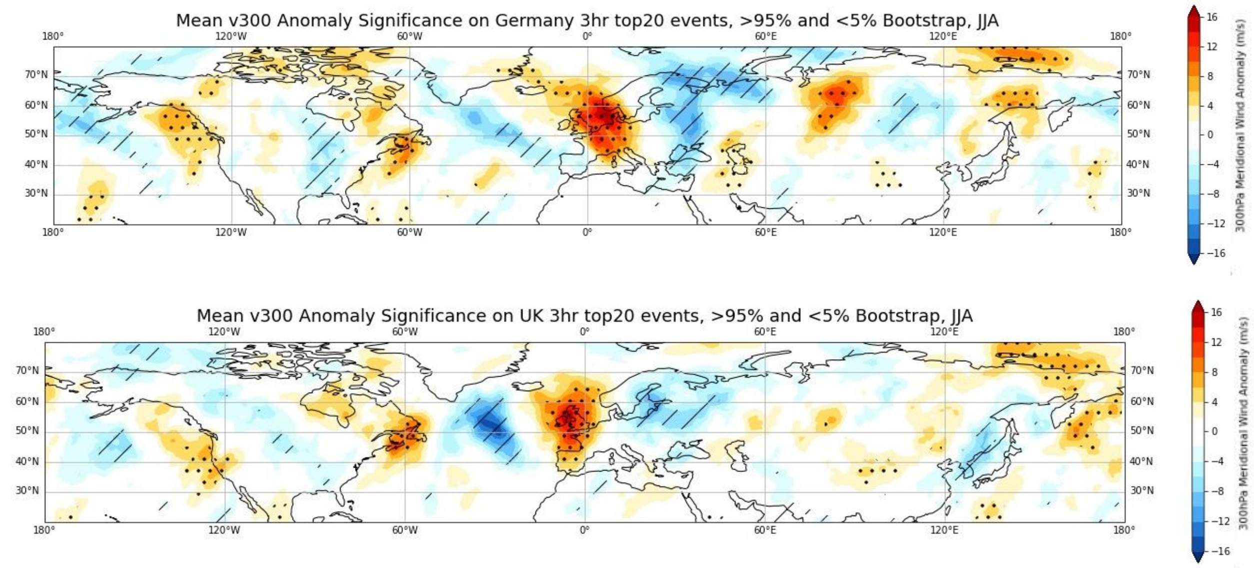

Figure C.5: Bootstrapped significance of the mean v300 anomalies on top 20 3hr event days in a) Germany and b) the UK. Stippling shows regions with anomalies above the 95th percentile level. Hashes show regions with anomalies below the 5th percentile.

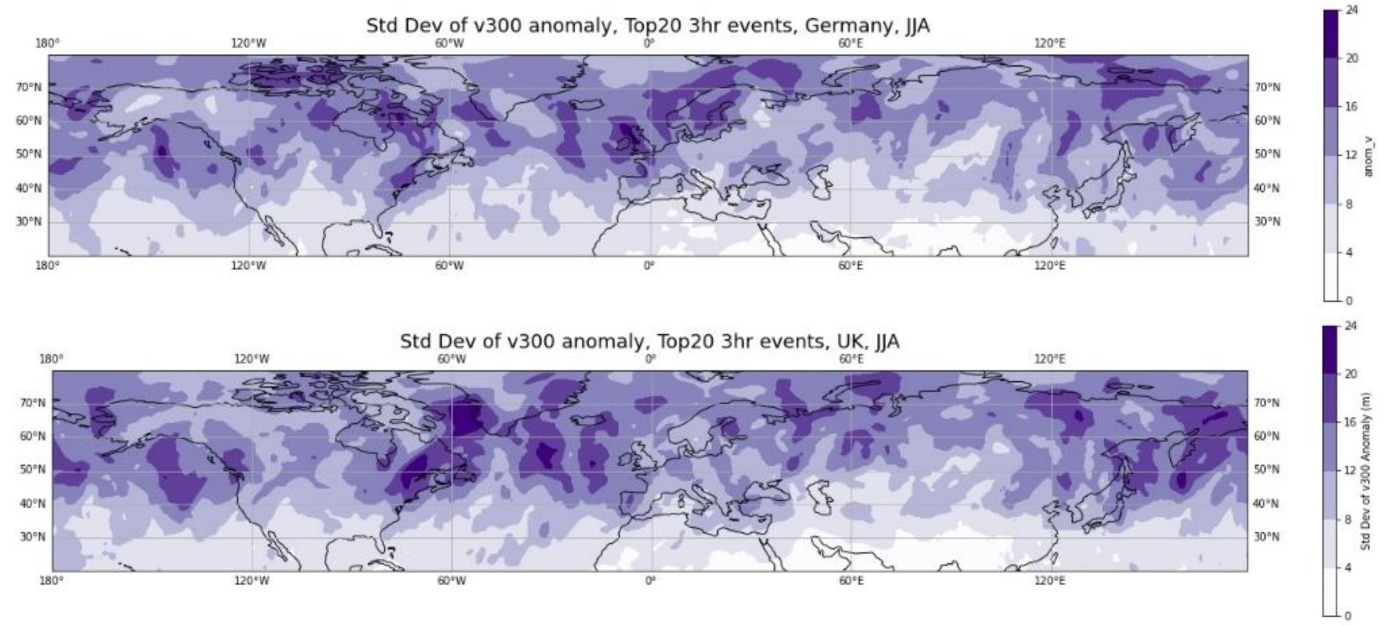

Figure C.6: Standard deviation of v300 anomalies on top20 3hr event days in Germany and UK

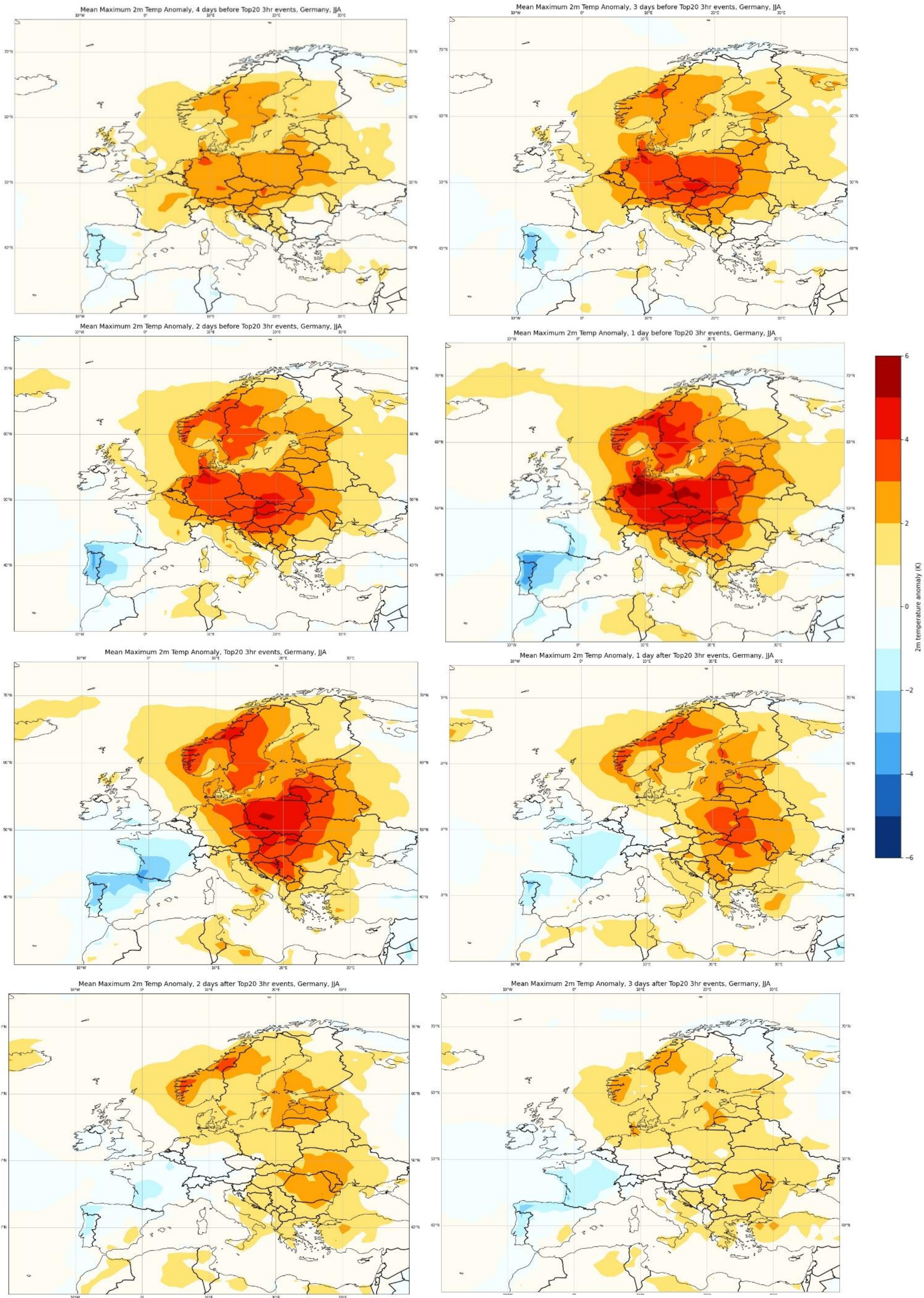

Figure C.7: Composite maps of mean temperature anomaly on days surrounding top 20 3hr rainfall events in Germany. Starting from 4 days before the rainfall events.

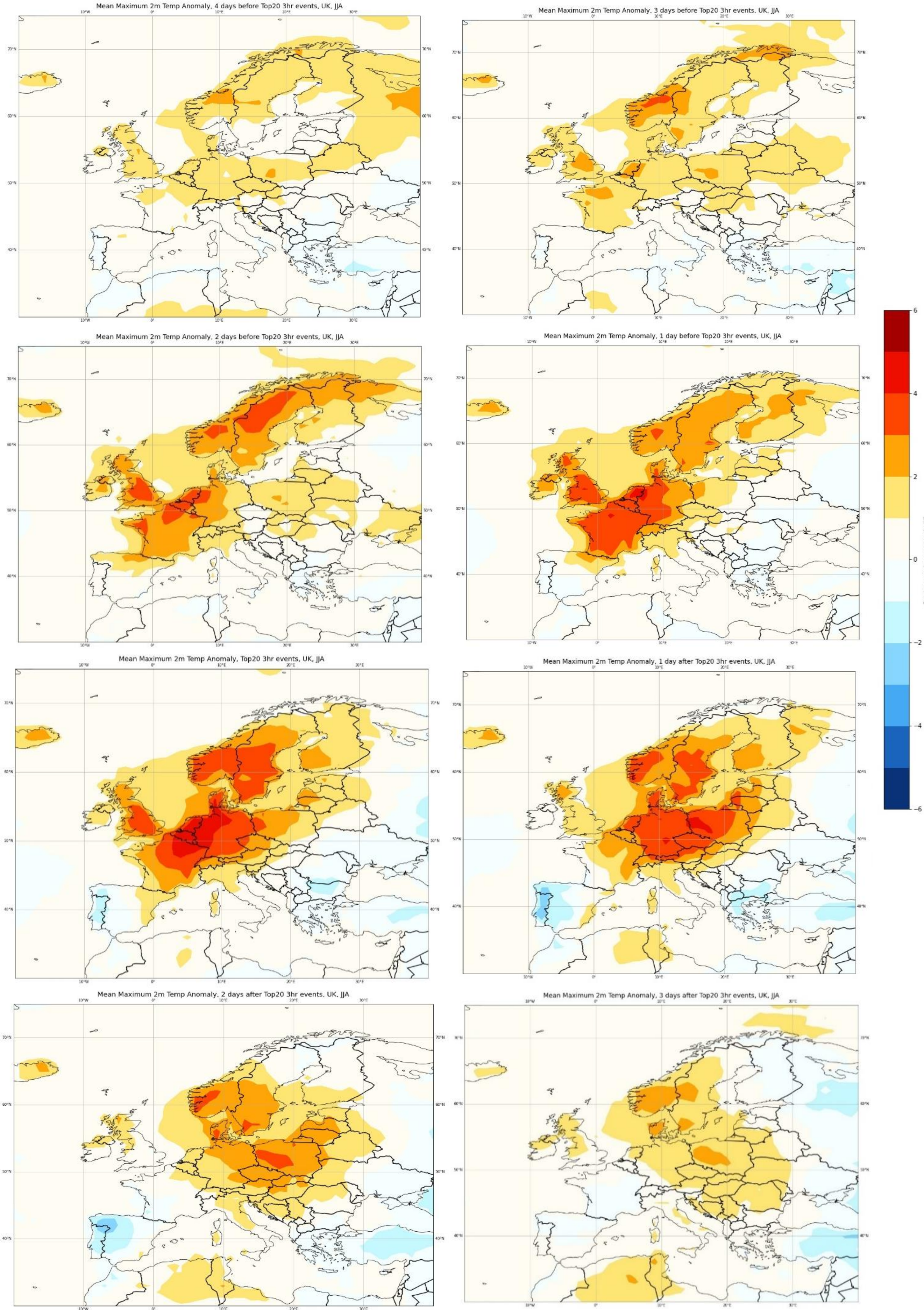

Figure C.8: Composite maps of mean temperature anomaly on days surrounding top 20 3hr rainfall events in the UK. Starting from 4 days before the rainfall events.

Appendix D: Supporting information for Chapter 6

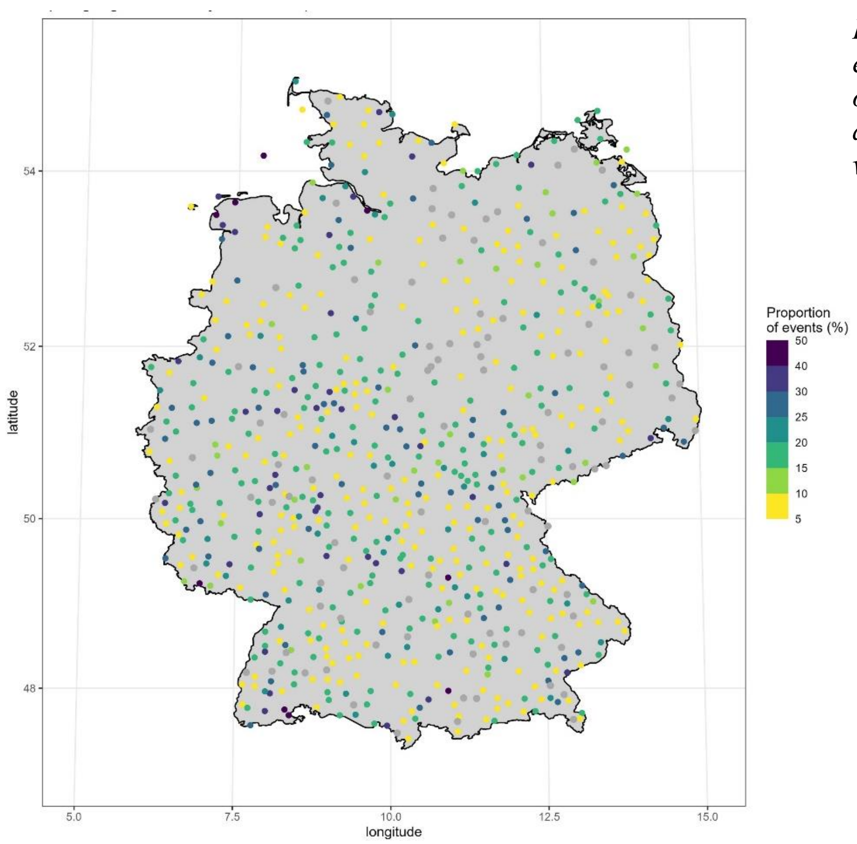

Figure D.1: Proportion of 3hr n-1 events that occurred within 500km of a COL centre in Germany during JJA 1996-2015.For gauges with >10 years of record only.

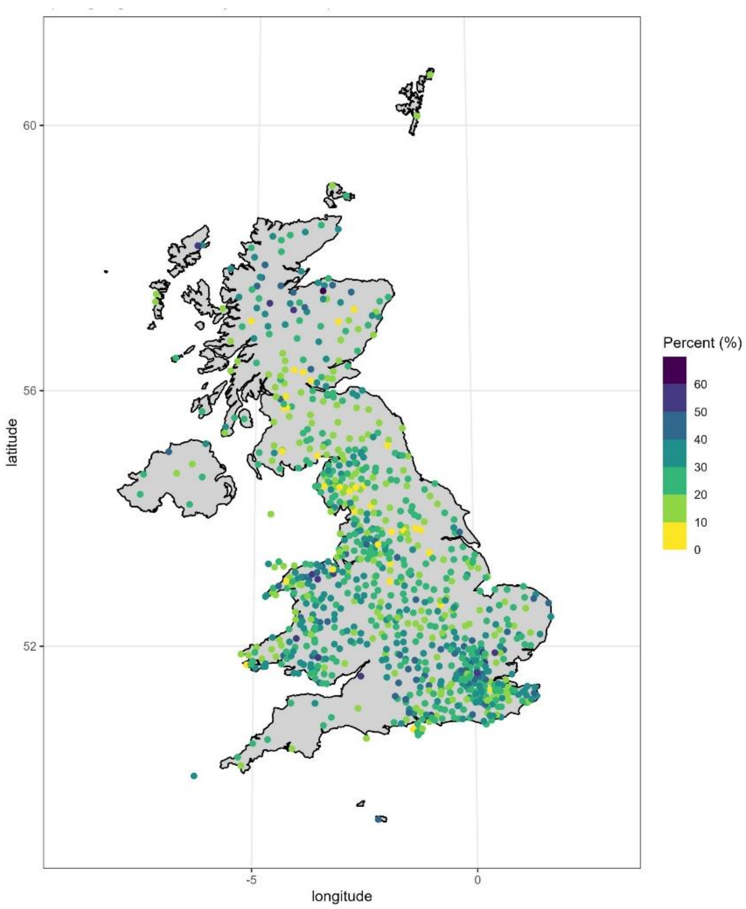

Figure D.2: Proportion of 3hr n-1 events that occurred within 500km of a COL centre in the UK during JJA 1979-2015. For gauges with >15 years of data only.